# New advances in our understanding of the control and functions of brown adipose tissue thermogenesis

**Rajaa Sebaa**

**Thesis submitted to the**

**Faculty of Graduate and Postdoctoral Studies**

**in partial fulfillment of the requirements for the**

**Doctorate in Philosophy degree in Biochemistry**

**Department of Biochemistry, Microbiology and Immunology**

**Biochemistry Graduate Program**

**Faculty of Medicine**

**University of Ottawa**

**ABSTRACT**

Brown adipose tissue (BAT) generates heat in a process referred to as non-shivering thermogenesis (NST). The process is dependent on the proton leak activity of uncoupling protein1 (UCP1), a protein found in the mitochondrial inner membrane. Physiologically, NST is activated by environmental cold, and to a lesser extent, diet. NST is an energetically costly process, and thus activated BAT consumes remarkable amounts of fatty acids and glucose, which positively influences systemic metabolism. Studies in mice have shown that defective BAT activity can contribute to the development of obesity, and increased BAT activity can protect against obesity. In humans, amounts of BAT are highest in newborns, and atrophy with age. BAT is also a secretory organ that releases 'batokines' and other signaling molecules, some of which are in small extracellular vesicels (sEV). The latter may act on BAT itself in a autocrine fashion, or on other tissues in an endocrine fashion, which may also contribute to the systemic effect of BAT activity. The overall aim of my Ph.D. thesis was to elucidate molecular mechanisms controlling BAT activity and its regulatory effects on other tissues/cells.

In my first project, the deacetylation control of BAT activity was studied in mice. Mitochondrial deacetylation is mainly mediated by Sirtuin 3 (SIRT3). Previous studies showed that cold increases the transcript level of SIRT3 in BAT, and that fasted *Sirt3* knockout (*Sirt3*KO) mice are cold intolerant, suggesting a potential thermoregulatory role of SIRT3. However, the molecular mechanisms by which SIRT3 regulates BAT thermogenesis are not fully understood. Here, we examined functional links between SIRT3 and UCP1. To study this, wild-type (WT) and *Sirt3*KO mice were used to perform physiological, molecular, and proteomic analyses of BAT when it is activated by cold or by the β3-adrenergic agonist, CL316,243. Our findings indicated

that the absence of SIRT3 in *ad libitum* fed mice led to impaired use of BAT lipid droplets, defective thermoregulation and decreased BAT mitochondrial respiration, without affecting the expression of UCP1. Label-free mass spectrometry revealed that the absence of SIRT3 increased the acetylation status of several BAT mitochondrial proteins including UCP1 and proteins involved in crucial pathways upstream of UCP1, such as the complexes of the electron transport chain (ETC) and acylcarnitine/fatty acid oxidation (FAO) metabolism. Therefore, we next examined the effect of hyperacetylated sites found in those BAT mitochondrial proteins on their functions. Mutagenesis work conducted in a cellular model revealed that SIRT3-regulated acetylation sites on UCP1 did not impact proton leak respiration when UCP1 was activated. However, analysis of acylcarnitines in the blood showed that the absence of SIRT3 resulted in a decrease in the levels of selected medium-chain and long-chain acylcarnitines. Additionally, functional analysis of ETC complexes in BAT mitochondria demonstrated that the absence of SIRT3 decreased the activities of complex I and complex II (CI and CII), which could impair the production of proton motive force, required for the activity of UCP1. Altogether our results indicate that SIRT3 regulates BAT thermogenesis indirectly by targeting proteins involved in crucial pathways upstream of UCP1.

In my second project, we studied the metabolic response of BAT to hypoxia in naked mole rats (NMRs). NMRs are exceptionally tolerant to hypoxic environments; during acute hypoxia their body temperature is decreased nearly to the ambient temperature. The underlying mechanisms of these observations are not well understood. We hypothesized that BAT activity in NMRs is decreased during hypoxia. To study this, NMRs were exposed to normoxia (21% $O_2$/1hr), hypoxia (7% $O_2$/1hr), or hypoxia followed by recovery (21% $O_2$/1hr). Thermal imaging,

body temperature measurements, thermogenic protein and overall protein ubiquitination levels, and mitochondrial morphology analyses of BAT were conducted. In addition, the level of thermogenic proteins in iBAT from different species of mole rats were examined under normoxic or hypoxic conditions for comparative and evolutionary analyses. Our results illustrated that during acute hypoxia, NMRs had rapidly decreased their body temperature close to the ambient temperature. Also, thermal imaging showed that heat produced in interscapular BAT region in hypoxic NMRs was decreased regardless of the degree to which BAT was activated. Western blotting analysis revealed that levels of UCP1 and selected ETC proteins were markedly decreased in hypoxic NMRs. Also, UCP1 was decreased in some, but not all other species of mole rats that were studied. To probe possible mechanisms of these marked acute decreases in mitochondrial proteins, levels of ubiquitinated proteins in BAT were examined and found to be increased by hypoxia. Consistently, ultrastructural analyses of BAT by electron microscopy indicated abnormal mitochondrial morphology in BAT of hypoxic NMRs, including abnormal cristae and jagged membranes suggesting that mitophagy events may be induced during hypoxia. Further investigations are needed to examine the potential role of proteasome-mediated degradation or mitophagy mechanisms in BAT during hypoxia. Our results reveal that hypoxia diminished BAT thermogenesis in NMRs, at least in part, by targeting mitochondrial thermogenesis related proteins and by altering mitochondrial morphology.

In my third project, the metabolic effects of BAT-derived sEV on skeletal muscle (SkM) cells were investigated. BAT releases sEV and its activation increases the release of sEV. However, the roles of activated BAT-derived sEV are not well understood. Generally, sEV are involved in interorgan communication and contain regulatory moleculaes that can be taken by recipient

tissues or cells to regulate their functions. During cold exposure, BAT and skeletal muscle (SkM) produce NST and shivering, respectively, to maintain controlled body temperature. Defects in the thermogenic function in one of the tissue leads to increase the heat production in the other tissues, suggesting cross-talk mechanisms between BAT and SkM. Given the role of sEV, we questioned whether activated BAT-derived sEV effect the function of SkM cells. Thus, we investigate the metabolic effects of sEV released from acutely activated BAT, *in vivo* or *in vitro*, on SkM myoblast bioenergetics. Our findings demonstrated that BAT releases sEV and its acute activation does not significantly impact the size and concentration of sEV released in mouse plasma or conditioned medium. Surprisingly, bioenergetics analyses illustrated that neither plasma sEV from CL316,243-injected mice nor sEV from conditioned medium of CL316,243-treated BAT explants had impacts on C2C12 myoblasts bioenergetics following one day of treatment. To conclude, our findings demonstrate that sEV released from acutely activated BAT do not influence the bioenergetics of C2C12 myoblasts under normal metabolic conditions. Further investigations are needed to examine the effects of BAT-derived sEV on SkM cells under different metabolic conditions or time-frames.

Overall, the findings reported in this thesis expand our understanding of the control of BAT and its systemic roles in thermoregulatory metabolism, which is important in the field of metabolic physiology.

**ACKNOWLEDGMENT**

Foremost, I want to thank Allah for his many blessings including this great opportunity to completing my Ph.D thesis. He helped me to successfully go through this PhD journey and to overcome obstacles that I went through. Thanks to Allah to make the completion of this thesis possible.

The first person whom I would like to thank is my PhD supervisor Dr. Mary-Ellen Harper, whom I owe an immense debt of gratitude. Dr. Harper, you have been the real inspiration in my scientific research life and my role-model whom I would like to emulate in my career. Thank you very much for believing in me and accepting me in your mitochondrial lab. Being in your lab has given me many advantages, not only being experienced and trained with great scientific machines, but it has also given me more knowledge in the field of mitochondrial bioenergetics. We have had a lot of great discussions with smart and brilliant lab mates and collaborators. Thank you very much for all your help, support, guidance, motivation, and enthusiasm. You have taught me how to be an independent PhD candidate and research investigator. I would like to say that I am grateful to be under your supervision and mentorship. Without you, this work would not be possible.

I would like to thank my thesis advisory committee members Dr. Michael Downey and Dr. Alexander Sorisky for guiding me through these years of my PhD and by providing me with helpful suggestions and advice. All your support and constructive criticism are much appreciated.

Thanks to all the previous and current lab members of the Harper's lab for being there when I had those cheerful and disappointing moments during my PhD journey. Thank you all for your support and help. It has been a blessing working with you all.

I would like to give special thanks to Shaqra University, the Ministry of Higher Education in Saudi Arabia and the Saudi Cultural Bureau for giving me the great opportunity to study in Canada and providing me with the financial and health support throughout my PhD studies.

I would like to dedicate my thesis to all my lovely family members including my grandma Hamdaah, my parents Braik and Ghaliah, my sisters Areej, Bashair, Tasneem and Aryam, my brothers Abdulaziz, Mohammed and Abdulmajeed, and my nephews Anas and Raed. You all always motivate me to pursue my Ph.D degree and stand by my side during the difficult times during this journey. Without you all, my PhD studies would be difficult. Thank you all from the bottom of my heart for supporting and motivating me.

Last but not least, I would like also to dedicate my thesis to my friends Abir, Saeedah, Haya, Randa, Lulu, Walaa, Abi, Lenah and Nedaa. Without your support, my path would have been way more difficult. I apologize for the sake of brevity, I would like to thank all of my friends who have given me their continued support, love, encouragement, and understanding.

This following thesis is dedicated to all of you.

**LIST OF CONTENTS**

**LIST OF ABBREVIATIONS**

| | |
|---|---|
| WHO | World Health Organization |
| BMI | Body mass index |
| WHR | Waist-to-hip ratio |
| WC | Waist circumference |
| DEXA | Dual Energy X-ray absorptiometry |
| BMR | Basal metabolic rate |
| CT | Computerized Tomography |
| MRI | Magnetic Resonance Imaging |
| T2D | Type 2 diabetes mellitus |
| CVD | Cardiovascular diseases |
| BED | Binge-eating disorder |
| SNPs | Single nucleotide polymorphisms |
| PPAR-γ | Peroxisome proliferator activated receptor-γ |
| PPAR-α | Peroxisome proliferator activated receptor-α |
| LPL | Lipoprotein lipase |
| LEPR | Leptin receptor |
| MAOA | Monoamine oxidase A |
| PON1 | Paraoxonase 1 |
| PON2 | Paraoxonase 2 |
| ATs | Adipose tissues |
| β3-AR | β3-Adrenergic receptor |
| WAT | White adipose tissue |
| MSCs | Mesenchymal stem cells |
| Myf5 | Myogenic factor 5 |
| BAT | Brown adipose tissue |
| SkM | Skeletal muscle |
| NST | Non shivering thermogenesis |
| vWAT | Visceral WAT |
| sWAT | Subcutaneous WAT |
| eWAT | Epididymal white adipose tissue |
| iBAT | Interscapular brown adipose tissue |
| TGs | Triglycerides |
| AdipoQ | Adiponectin |
| ATGL | Adipose triglyceride lipase |
| HSL | Hormone sensitive lipase |
| FFAs | Free fatty acids |
| GLUT4 | Glucose transporter 4 |
| PM | Plasma membrane |
| DNL | *de novo* Lipogenesis |
| TNF-*α* | Tumor necrosis factor |
| IL-6 | Interleukin-6 |
| MCP1 | Monocyte chemotactic protein-1 |

| | |
|---|---|
| PAI-1 | Plasminogen activator inhibitor-1 |
| NGF | Nerve growth factor |
| VEGF | Vascular endothelial growth factor |
| 12,13-diHOME | 12,13-dihydroxy-9Z-octadecenoic acid |
| PET-CT | Positron emission tomography computerized tomography |
| FGF21 | Fibroblast growth factor 21 |
| NRG4 | Neuregulin 4 |
| NiAc | Nicotinic acid |
| ROS | Reactive oxygen species |
| TCA | Tricarboxylic acid |
| SD | Succinate dehydrogenase |
| MOM | Mitochondrial outer membrane |
| MIM | Mitochondrial inner membrane |
| OPA1 | Optic atrophy 1 |
| MICOS | Mitochondrial contact site and cristae organizing system |
| Mfn1 | Mitofusins 1 |
| Mfn2 | Mitofusins 2 |
| Drp1 | Dynamin related protein 1 |
| OXPHOS | Oxidative phosphorylation |
| ETC | Electron transport chain |
| UCP1 | Uncoupling protein1 |
| CI | Complex I |
| CII | Complex II |
| CIII | Complex III |
| CIV | Complex IV |
| CV | Complex V |
| PMF | Proton motive force |
| PNs | Purine nucleotides |
| SNS | Sympathetic nervous system |
| GPCR | G-protein coupled receptor |
| NE | Norepinephrine |
| AC | Adenylyl cyclase |
| GC | Guanylyl cyclase |
| cAMP | Cyclic adenosine monophosphate |
| PKA | Protein kinase A |
| PKG | Protein kinase G |
| T4 | Thyroxine |
| T3 | Triiodothyronine |
| ChREBP | Carbohydrate response element binding protein |
| ANP | Atrial natriuretic peptide |
| BNP | Ventricular natriuretic peptide |
| NPs | Natriuretic peptides |
| NPRA | Atriuretic peptide receptor A |
| NPRC | Catriuretic peptide receptor C |

| | |
|---|---|
| cGMP | Cyclic guanosine monophosphate |
| MAPK | Mitogen activated protein kinase |
| TSK | Tsukushi |
| SLRP | Small leucine-rich proteoglycan |
| PGC1-α | Peroxisome proliferator-activated receptor gamma coactivator 1-alpha |
| FNDC5 | Fibronectin type III domain- containing protein 5 |
| BAIBA | β-aminoisobutyric acid |
| Metrnl | Meteorin-like |
| TCA | Tricarboxylic acid |
| CREB | cAMP response element binding protein |
| CRE | cAMP response element |
| ATF2 | Activating transcription factor 2 |
| mTORC1 | Mammalian target of rapamycin complex 1 |
| MitoQ | Mitochondria-targeted antioxidant |
| LXRα | Liver X receptor α |
| RIP140 | Receptor interacting protein 140 |
| PTMs | Post translation modifications |
| SIRT5 | Sirtuin 5 |
| SIRT3 | Sirtuin 3 |
| SIRT4 | Sirtuin 4 |
| FAO | Fatty acid oxidation |
| KAT | Lysine acetyltransferase |
| WT | Wild-type |
| KO | Knock-out |
| CLAMS | Comprehensive lab animal monitoring system |
| H&E | Hematoxylin and Eosin |
| PLC | Palmitoyl-L-carnitine |
| G3P | Glycerol-3-phosphate |
| GDP | Guanosine-5'-diphosphate |
| HRR | High resolution respirometry |
| OCR | Oxygen consumption rate |
| ECAR | Extracellular acidification rate |
| VO2 | Volume of oxygen consumption |
| TCA | Tricarboxylic acid |
| CACT | Carnitine acylcarnitine translocase |
| ROS | Reactive oxygen spices |
| $T_b$ | Body temperature |
| $T_a$ | Ambient temperature |
| FLIR | Forward looking infrared |
| RFID | Radio frequency identification |
| NMRs | Naked mole rats |
| CHM | *Cryptomys hottentotus mahali* |
| CHP | *Cryptomys hottentotus pretoria* |
| GC | *Georychus capensis* |

| | |
|---|---|
| CHH | *Cryptomys hottentotus hottentotus* |
| UPS | Ubiquitin-proteasome system |
| PGAM5 | Phosphoglycerate mutase family member 5 |
| sEV | Small extracellular vesicles |

**LIST OF FIGURES**

**CHAPTER 1: GENERAL INTRODUCTION**



**CHAPTER 2: SIRT3 CONTROLS BROWN FAT THERMOGENESIS BY DEACETYLATION REGULATION OF PATHWAYS UPSTREAM OF UCP1**



**CHAPTER 3: ACUTE HYPOXIA DIMINISHES BROWN FAT THERMOGENESIS IN NAKED MOLE-RAT BY DECREASING MITOCHONDRIAL CONTENT AND THERMOGENIC PROTEIN EXPRESSION**



**CHAPTER 4: SMALL EXTRACELLULAR VESICLES RELEASED FROM ACUTELY ACTIVATED BROWN ADIPOSE TISSUE DO NOT IMPACT C2C12 MYOBLAST BIOENERGETICS**

**CHAPTER 6: APPENDIX**

**6.1 SUPPLEMENTARY FIGURES FOR CHAPTER 2**



**6.2 SUPPLEMENTARY FIGURES FOR CHAPTER 3**

# CHAPTER 1: GENERAL INTRODUCTION

## 1.1 THE ENERGY

### 1.1.1 THE ENERGY SOURCE: FOOD

Food is a fundamental requirement for all mammals including humans because it has essential nutrients needed for the basic performance and function of the human body. Specifically, food nutrients are involved in several important biological roles. First, they are used to build and maintain all the tissues and organs. Second, they regulate the biochemical reactions that take place in the body tissues and organs. Third, they provide energy to support energy-demanding reactions, and additional energy that can be stored for subsequent use (Kohlmeier, 2003). These are needed for healthy physiological processes during normal or stressful conditions. Despite the necessity of food, the current effortless access to highly palatable foods and reduced physical activities in developing and developed countries often leads to the disruption of the energy balance in the human body, which leads eventually to the development of metabolic disease: obesity.

### 1.1.2 THE DISRUPTION OF ENERGY BALANCE AND OBESITY

Energy transduction in the human body obeys the first law of thermodynamics of energy conservation, which states that energy cannot be created or destroyed, but is converted from one form to another (Walsh, 2013). To maintain whole body energy balance, the amount of dietary energy intake should be equal to the expended energy (Hill et al., 2012). However, if the intake energy is greater than the expended energy, this results in the disruption of energy balance. As a consequence, the remaining energy is stored mainly in the adipose tissues (ATs),

and leads to an increase in body mass, which if it continues chronically, it can lead to obesity (Hill and Commerford, 1996; Spiegelman and Flier, 2001).

## 1. 2 OBESITY

### 1.2.1 OBESITY DEFINITION AND ITS ASSESSMENT MODES

Recently, obesity was pronounced as a disease by the Canadian and American Medical Associations and the World Health Organization (WHO) (James, 2008; Pollack, 2013; Rich, 2105), and is defined as an abnormal accumulation of fat within the human body. In the clinical field, there are several assessment approaches used to classify the level and severity of obesity. The most common measurement, which is the body mass index (BMI), is traditionally used to assess obesity based on the individual's weight (in kg) divided by the individual's height (in $m^2$). An individual is considered overweight or obese when their BMI is between 25-29.9 $kg/m^2$ or ≥ $30kg/m^2$, respectively (Jensen et al., 2014). However, the BMI approach has some limitations due to the following reasons. First, it does not consider other factors such as age, sex, or muscle mass, which may affect the interpretation of the individual's BMI. Second, BMI only measures body weight, but does not accurately measure the body fat mass/distribution. Therefore, other means were developed for the measurements of fat mass/distribution. One of these means is waist-to-hip ratio (WHR), which is a measure of relative central abdominal obesity. Another approach is waist circumference (WC), which has also been suggested to be used as a anthropometric tool for measuring central abdominal obesity in clinical practice (Hu, 2008; Lau et al., 2007). WC is used as a risk predictor of obesity-related metabolic complications when women and men have greater than 35 inches and 40 inches, respectively (Wang et al., 2005). Additional modes of measurement have also evolved to allow precise measurement of abdominal/central and overall

adiposity, including Dual Energy X-ray Absorptiometry (DEXA), Computerized Tomography (CT) and Magnetic Resonance Imaging (MRI)(Hu, 2008).

### 1.2.2 PREVALENCE OF OBESITY

According to the WHO, the global prevalence of obesity nearly tripled between 1975 and 2016 (World Health Organization, 2018). Based on the most recent population statistics, in 2016, there are more than 1.9 billion overweight adults around the world, 650 million of whom are considered obese (World Health Organization, 2018). A study done by Kelly *et al.* estimated that 57.8% of the world's adults population could be overweight or obese by the year 2030 if this trend of increased weight gain/obesity continues (Kelly et al., 2008). In 2018, recent statistics done on the population of Canada showed that 63.1% of Canadians whose age are 18-year-old or older were obese or overweight (Statistics Canada, 2019). The prevalence of obesity around the world is greater in women than in men (Ng et al., 2014). In 2014, it was reported that more than half a billion adults were considered to be obese, representing 11% of men and 15% of women. In addition, the prevalence of obesity can be different dependent on the geographical regions. For example, the population of United States of America has the highest prevalence of obesity (27% of the population), whereas the population of South-East Asia has the lowest prevalence of obesity (5% of the population) (Organisation mondiale de la santé, 2014). Moreover, obesity prevalence-related studies illustrated that the increased rate of obesity is positively correlated with age. For instanse, in most countries, the proportion of obese individuals increases from mid to late adulthood (Haslam and James, 2005). Notably, being overweight or obese causes a higher percentage of deaths worldwide compared with being underweight (World

Health Organization, 2018). All these studies indicate that the progression of overweight/obesity has alarmingly increased internationally in different groups of people with different genders, races and ages.

### 1.2.3 COMORBIDITIES OF OBESITY

The increased rate of obesity has become a major health issue that can threaten people's lives. Obesity negatively impacts the normal physiological functions of the body, which can ultimately lead to death. It has been reported that there is a positive association between obesity and an increased rate of mortality between 2- to 3- fold (Adams et al., 2006). Furthermore, a study of 1.46 million white adults illustrated that mortality is positively correlated with being overweight and obese (de Gonzalez et al., 2010). Other recent work established the association of weight gain and obesity with an increased all-cause mortality in Asia, Australia and New Zealand, Europe, and North America (Global BMI Mortality Collaboration et al., 2016).

With regard to the impact of obesity on other body systems, obesity increases the risk for other metabolic diseases. Obesity is a major risk factor for type 2 diabetes mellitus (T2D), as it can disturb the uptake and metabolism of glucose, particularly in skeletal muscle, *i.e*., insulin resistance (Chan et al., 1994; Colditz et al., 1995; DeFronzo et al., 2015; Guh et al., 2009; Menke et al., 2014). Other comorbidities of obesity include cardiovascular diseases (CVD) (including hypertension, and stroke) and dyslipidemia (Klop et al., 2013; Manson et al., 1990, 1995; Willett et al., 1995). Several cancer types have also been positively associated with obesity (Apovian, 2016; Bray et al., 2016, 2017a; Garfinkel, 1985; Guh et al., 2009; Khaodhiar et al., 1999). Additional diseases and disorders associated with obesity include sleep apnea, osteoarthritis,

hyperuricemia, gall bladder disease, infertility, polycystic ovary syndrome and reproductive hormonal imbalances (Andersen, 1992; Felson, 1995; Guh et al., 2009; Khaodhiar et al., 1999; Partinen, 1995; Soulez et al., 1996). Moreover, it has been reported that there is a positive association between obesity and mood disorders, such as depression, and this positive association can lead to the development of binge-eating disorder (BED) (Khaodhiar et al., 1999; de Zwaan, 2001). The energy disruption, obesity and comorbidities associated with obesity are summarized in Figure 1.1.

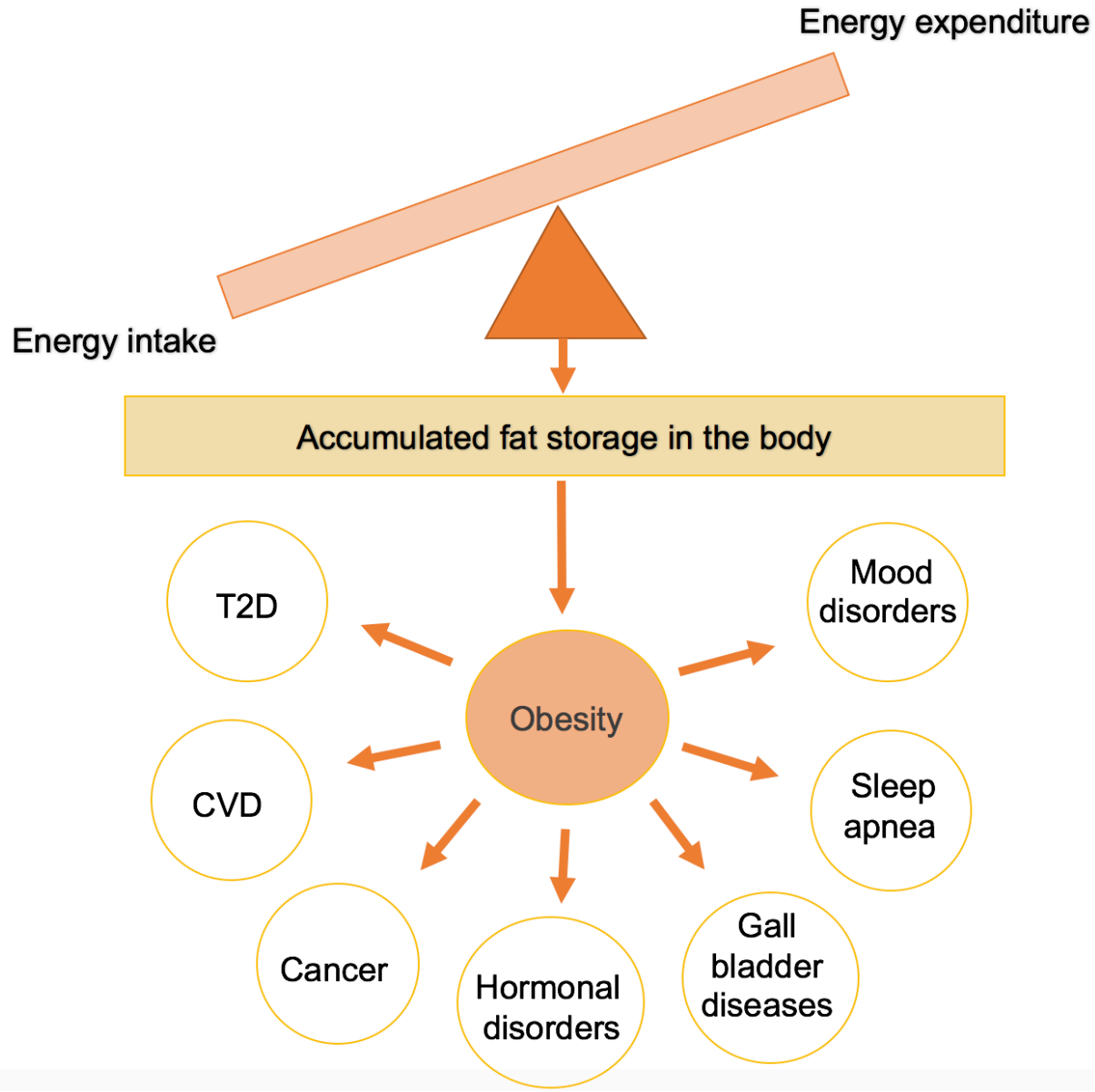


**Figure 1.1: Illustrative diagram of energy balance disruption, *i.e.*, a positive energy balance, which leads to obesity and obesity associated diseases.**

### 1.2.4 OBESITY AND ITS LEADING FACTORS

Obesity is a complex disease that can be caused by myriad factors. These factors can be classified as non-genetic or genetic. The following sections elaborate on the involvement of these factors in the progression of obesity.

#### 1.2.4.1 OBESITY AND NON-GENETIC FACTORS

Many studies have discussed numerous non-genetic factors that can contribute to the development of obesity, including endocrine disorders (Bougnères et al., 2008; Reinehr et al., 2007; Scerif et al., 2011), gut microbiome (Angelakis et al., 2012; Burcelin, 2012; Jess, 2014; Taber et al., 2013; Turta and Rautava, 2016), environmental factors, such as exposure to endocrine-altering toxins (Carwile and Michels, 2011; Trasande et al., 2012; Warner et al., 2014), socioeconomic factors (Bray et al., 2016, 2017b; Wang, 2001), lifestyle factors, such as high-fat and high-carbohydrate diets (Bray et al., 2016, 2017a), and physical inactivity (ten Hacken, 2009; Pietiläinen et al., 2008) and reduced sleep (Jiang et al., 2009; Wang et al., 2017) .

This section mainly describes the relationship between obesity and changes in the lifestyle of the modern world. Two of the most common causes of obesity are overeating and lack of exercise. Regarding overeating, several studies have demonstrated a positive association, in both young and old adults, between an increased BMI and the increased rate of fast food consumption, as well as the frequency of restaurant visits (Duffey et al., 2007; Jeffery and French, 1998; Jeffery et al., 2006; Pereira et al., 2005). Moreover, a questionnaire-based study revealed that weight gain is positively associated with an increase of total energy intake in women between the ages of 20-45 years (French et al., 2000). It has been thought that the composition of a diet can be involved in the development of obesity. For example, diets that include high fats

or carbohydrates without fiber can lead to obesity (Bray et al., 2016, 2017b). Other studies have shown that consuming sugar-sweetened beverages also leads to obesity (Taber et al., 2013). Recently, Hall *et al.* have reported that eating ultra-processed food for two weeks leads to increased energy intake, body weight and carbohydrate and fat consumption (Hall et al., 2019).

In addition to overeating, physical inactivity can be an important factor that contributes to weight gain/obesity. Various studies have evaluated the effects of physical inactivity on body weight. For instance, a population-based prospective study was conducted in the USA on men and women between the ages of 18-30 years. Over the course of seven years, a decrease in the physical activities was associated with weight gain in both genders (Lewis et al., 1997). Moreover, other follow up studies conducted on youth demonstrated a positive association between lack of exercise, and increased BMI and skinfold thickness in females (Kimm et al., 2005). Another study was done on a Finnish population during their transition period from adolescence into adulthood to examine the effect of being inactive on body weight. The study indicated that there is a significantly increased association between lack of activity with being overweight in males, as well as with obesity in men and women, and with severe abdominal obesity in women (Tammelin et al., 2004). In addition, other studies have focused on the effects of time spent watching television or playing video games/electronic devices on weight gain/obesity. These studies showed that childhood obesity is positively correlated with increased time spent on television or video games (Dietz and Gortmaker, 1985). Furthermore, it has been reported that children who have no access to electronic entertainment devices within their bedrooms have improved sleep duration and quality, which are known to impact weight gain (Chen et al., 2008; Dube et al., 2017). A study performed on adults demonstrated that men who spent more than

three hours/day watching television had a predisposition to developing obesity compared to men who spent one hour/day watching television (Tucker and Friedman, 1989).

In conclusion, these studies collectively confirm the involvement of increased food intake and decreased physical activity in the development of weight gain/obesity.

#### 1.2.4.2 OBESITY AND GENETIC FACTORS

Numerous studies have reported that obesity can be strongly influenced by genetic factors. In most cases the effects are polygenic, and there are over 500 genetic loci associated with obesity (Loos, 2018). However, in rare cases, there are single gene mutations that lead to obesity, as is the case in Prader-Willi syndrome, Bardet-Biedl syndrome, Alström syndrome and Cohen syndrome (Budisteanu et al., 2010; Butler, 2011; Marshall et al., 2011; Suspitsin and Imyanitov, 2016).

Furthermore, obesity is associated with single nucleotide polymorphisms (SNPs), which are single position nucleotide changes in DNA. SNPs can occur in some genes encodong proteins needed for the regulation of the body composition. Examples of these proteins are peroxisome proliferator activated receptor-γ (PPAR-γ), lipoprotein lipase (LPL*),* leptin receptor (LEPR)*,* monoamine oxidase A (MAOA) and paraoxonase 1 (PON1) and paraoxonase 2 (PON2), which can regulate adipocyte differentiation, triglyceride metabolism, leptin levels, monoamine levels, and low-density lipoprotein oxidation, respectively (Camps et al., 2009; Fuemmeler et al., 2008; Spiegelman et al., 1997; Wang and Eckel, 2009; Yang and Barouch, 2007). Importantly, genetic studies conducted in humans demonstrated that mutations in genes that control the function of ATs can be associated with obesity (Arner and Hoffstedt, 1999; Cassard-Doulcier et al., 1996;

Fumeron et al., 1996; Oppert et al., 1994; Strosberg, 1997). Examples of these genes include mutations in the β3-adrenergic receptor (β3-AR) and uncoupling protein 1 (UCP1), which play important roles in non-shivering thermogenesis, which takes place in brown adipose tissue (BAT). It has been reported that the substitution mutation of (Trp64Arg) in the β3-AR leads to an impaired function of the receptor in human fat cells (Arner and Hoffstedt, 1999; Umekawa et al., 1999). In addition, the polymorphism of Trp64Arg of the β3-AR was found in individuals characterized with obesity from different populations (Arner and Hoffstedt, 1999; Kadowaki et al., 1995; Kim-Motoyama et al., 1997; Strosberg, 1997), and it was associated with decreases in the basal metabolic rate (BMR) in obese Finns (Sipiläinen et al., 1997). Another thermogenic gene that is also associated with obesity encods for UCP1, exclusively expressed in BAT, where it uncouples respiration from ATP production in mitochondria and dissipates energy in the form of heat (Cannon and Nedergaard, 2004). Various studies conducted in Québec families and Eastern Asian populations have demonstrated different polymorphisms of A3826G, A1766G and Ala64Thr of UCP1 gene that are associated with dysregulated fat metabolism, weight gain and resistence to weight loss on a low-calorie diet, and obesity and diabetes (Cassard-Doulcier et al., 1996; Fumeron et al., 1996; Oppert et al., 1994; Shin et al., 2005; Soo Kim et al., 2005). Interestingly, it has been reported that obese individuals who have a combination of both mutations A3826G in UCP1 and Trp64Arg in *β3-AR* have an additive effect on weight gain that is faster than that in individuals without mutations or with only one mutation (Fogelholm et al., 1998).

Furthermore, epigenetics can play an integral role in the development of obesity. Epigenetics are defined as DNA methylation and histones modification events that result in

changes in gene expression without affecting the sequence of DNA (Herrera et al., 2011). Epigenetics can be developed *in utero* and early life, and can be affected by the maternal nutrition (Lee, 2015). Numerous studies have examined the effect of *in utero* under-nutrition and over-nutrition on the metabolism of the offspring and their susceptibility to developing chronic diseases including obesity in their adulthood. It has been illustarated that there is a U-shaped relationship between maternal malnutrition, either undernutrition or overnutrition, and the development of obesity in adulthood of the offspring (Grattan, 2008). According to the Barker theory, known as the fetal origins hypothesis, initiated based on observations during the Dutch hunger winter (1944-1945), it was proposed that the fetal adaptation to *in utero* undernutrition can cause altered metabolism and physiology in the offspring in adulthood (Barker, 1997; Roseboom et al., 2001). Moreover, it has been shown that a poor maternal diet in early pregnancy can lead to abdominal obesity in women at age of 50 years (Ravelli et al., 1999). Another study in rats showed that maternal undernutrition during pregnancy may result in obesity in the adult offspring (Vickers et al., 2000). Moreover, a research study conducted in our lab has examined the effects of *in utero* undernutrition on the metabolism of the offspring in mice. Briefly, offspring from undernourished dams showed impaired metabolic physiology in skeletal muscle (SkM) and increased adiposity (Beauchamp et al., 2015a). Also, another study conducted in our lab illustrated that *in utero* undernutriton in mice can led to impared cardiac respiration in adult offspring (Beauchamp et al., 2015b). Not only *in utero* undernutrition can predispose offspring to metabolic diseases, but also prepregnancy and *in utero* overnutrition can also affect the health of offspring. Another study conducted in our lab elucidated that maternal overnutrition-induced obesity in mice can lead to metabolic diseases in the the offsprings, in

which they showed alterations in the mitochondrial function of red gastrocnemius muscle such as increased mitochondrial leak respiration and reduced reactive oxygen species (ROS) in response to palmitoyl carnitine (McMurray et al., 2019).

To sum up, research demonstrates the involvement of many complex non-genetic and genetic factors in the development of obesity. Of particular relevance to this thesis, some of these genetic mutations associated with obesity occur in genes that control the function of BAT.

### 1.2.5 Treatment and Prevention

Adipose tissue loss is the main goal in the treatment of obesity. Treating obesity can reduce the mortality and morbidity associated with obesity (Jensen et al., 2014). As obesity is a chronic disease that is caused by the complex interplay of many factors, the many contributing factors should be considered in the selection of suitable treatments for obesity (Eckel et al., 2014; Garvey et al., 2014; Jensen et al., 2014). With the greater understanding of this disease, many different treatment approaches have been developed; there are three main treatment options: 1) lifestyle modifications, including diet and exercise; 2) pharmacotherapy; and 3) bariatric surgery.

Despite the available therapeutic options to treat obesity and its associated morbidities, the prevalence of obesity has not been changed substantially, and for that reason there is an increasing body of experimental studies conducted on mice and humans with the hopes of developing more effective strategies to treat obesity.

## 1.3 ADIPOSE TISSUES

Physiologically, ATs are involved in the regulation of whole-body metabolism homeostasis. There are three major classifications of ATs, including white adipose tissue (WAT), BAT and beige adipose tissue. Structurally, ATs are composed of adipocytes and other cell types such as stromovascular cells, immune cells and preadipocytes (Kershaw and Flier, 2004). The three types of AT are considerably distinct from each other in terms of their physiological functions, developmental origins, cellular structures, and anatomical locations (Choe et al., 2016; Harms and Seale, 2013; de Jong et al., 2015; Nedergaard et al., 2007, 2011; Seale et al., 2008; Villarroya et al., 2017). This is summarized in Figures 1.2 and Figure 1.3. The subsequent sections will focus on the different types of ATs.

### 1.3.1 WHITE ADIPOSE TISSUE

WAT is the most predominant type of AT in the body. It is metabolically less active compared to other ATs and acts mainly as an energy storing tissue. Due to the previous reasons, WAT has a low density of blood vessels and nerves (Lim et al., 2013). Also, white adipocytes from WAT have a distinct appearance compared to brown and beige adipocytes. White adipocytes are spherical cells containing a central large lipid droplet that takes up much of the space within the cytoplasm, and there are few mitochondria (Sanchez-Gurmaches et al., 2016). White adipocytes are originally derived from multipotent mesenchymal stem cells (MSCs). Based on cell lineage tracing studies, white adipocytes arise from distinct lineages that do not express a myogenic transcriptional marker called myogenic factor 5 (Myf5) (Seale et al., 2008). In terms of the anatomical location of WAT, there are two major types classified as visceral WAT (vWAT), which

is localized in the abdominal cavity and subcutaneous WAT(sWAT), which is found underneath the skin (Choe et al., 2016; Park et al., 2014). Also, WAT can be classified based on its distribution in the body. For example, android WAT is mainly located in the upper part of the body while gynoid WAT is found in the lower part of the body (Esteve Ràfols, 2014). Examples of vWAT and sWAT in rodents and humans are summarized in Figure 1.3.

As mentioned above, the main function of WAT is to store excess dietary energy, in the form of triglycerides (TGs). WAT is metabolically flexible, and responds to changes in the energy balance status of the body. For instance, during fasting, WAT is stimulated by noradrenaline, which in turn activate lipases such as adipose triglyceride lipase (ATGL) and hormone sensitive lipase (HSL). These lipases hydrolase lipid droplets releasing into the circulation free fatty acids (FFAs), which are used by other tissues such as liver, skeletal muscle, and BAT to meet their metabolic needs (Braun et al., 2018; Harmelen et al., 1997; Rosen and Spiegelman, 2014; Schweiger et al., 2006). However, following meals, the level of glucose in the circulation is elevated causing an induction of insulin release. Then, insulin negatively affects the lipolysis actions of ATGL and HSL, positively increases the uptake of glucose through glucose transporter 4 (GLUT4) and induces *de novo* lipogenesis (DNL) to package the excess energy as lipid droplets. Consequently, WAT expands its mass to accommodate excess nutrients and energy (Chakrabarti et al., 2013; Claus et al., 2005; Herman et al., 2012). This metabolic expanding feature of WAT can be achieved by two ways, increasing the size of adipocytes *i.e.,* by hypertrophy or by recruiting new adipocytes *i.e.,* hyperplasia. The plasticity of WAT protects several tissues such liver, skeletal muscle, and heart from lipotoxicity that could impair their functions (Longo et al., 2019). In addition, WAT functions as a thermal insulator in the body (Carrillo et al., 2018).

Moreover, WAT has been considered as an a ctive endocrine organ releasing adipokines such as leptin, whose discovery was followed by that of adiponectin (Scherer et al., 1995; Zhang et al., 1994). Indeed, WAT releases several adipokines that act as signaling and regulatory molecules, and permit communication with distant organs to regulate their functions (Frühbeck et al., 2001; Rajala and Scherer, 2003; Trayhurn and Beattie, 2001; Trayhurn and Wood, 2004). For instance, WAT secretes some adipokines *e.g.,* leptin, adiponectin (AdipoQ); cytokines *e.g.,* tumor necrosis factor (TNF-$\boldsymbol{\alpha}$), interleukin 6 (IL-6); chemokines *e.g.,* monocyte chemotactic protein-1 (MCP1); acute phase proteins *e.g.,* plasminogen activator inhibitor-1 (PAI-1); inflammation-related adipokines *e.g.,* nerve growth factor (NGF) and vascular endothelial growth factor (VEGF) (Trayhurn, 2005).

### 1.3.2 BROWN ADIPOSE TISSUE

BAT is a thermogenic tissue that exists abundantly in hibernating animals and rodents. It was thought that in humans BAT exists only in babies; however radiological imaging of BAT in human adults by using the positron emission tomography computerized tomography (PET-CT) electron microscopy and immunostaining analyses revealed that human adults actually have significant functional BAT (Cypess et al., 2009; Hany et al., 2002; van Marken Lichtenbelt et al., 2009; Virtanen et al., 2009; Zingaretti et al., 2009). In terms of the anatomical locations, BAT of mice is mainly found in the interscapular, axillary and perirenal depots, and in humans, BAT is predominantly located in the supraclavicular and paravertebral depots (Choe et al., 2016). As speculated previously, the physiological importance of the anatomical location of BAT is to function as a internal heating source that is supported by many blood vessels, and when BAT is

activated, it becomes as an active metabolic heater that provides heat directly to the bloodstream to heat vital tissues, ensuring proper function of these tissues in cold enviroments (Sacks and Symonds, 2013). Anatomical locations of BAT in mice and humans are described in Figure 1.3.

In contrast to WAT, BAT burns stored energy and produces heat through a process called non shivering thermogenesis (NST) as a defense mechanism against cold environments (Foster and Frydman, 1978, 1979; Himms-Hagen, 1985; Nedergaard et al., 2011; Smith and Horwitz, 1969). BAT thermogenesis is mainly under the control of the sympathetic nervous system (SNS), which releases norepinephrine (NE) to bind to β3-AR on brown adipocytes resulting in signaling cascades needed for the activation of BAT as detailed below in section 1.5.1. There are several stimuli that can induce BAT thermogenesis such as cold exposure or diet or a pharmacological agent, *e.g.* a β3-AR agonist like CL316,243 (Cannon and Nedergaard, 2004; von Essen et al., 2017; Himms-Hagen, 1990). When BAT is activated, it subsequently increases its thermogenic capacity through BAT hyperplasia, which can further enhance BAT thermogenesis (Bukowiecki et al., 1982; Fukano et al., 2016). The control mechanisms of BAT activation will be discussed in details below in section 1.5.

To support its function, BAT is richly innervated with sympathetic nerves to ensure sufficient sympathetic control and stimulation (Contreras et al., 2015). The effect of experimental BAT denervation on thermogenesis has been well studied and published work has shown that denervation of BAT can lead to impaired thermogenesis, increased body fat mass, and decreased whole-body energy expenditure (Dulloo and Miller, 1984; Fischer et al., 2018; Rothwell and Stock, 1984; Vaughan and Bartness, 2012). Moreover, BAT is highly vascularized with blood vessels to

provide sufficient nutrient and oxygen supply for its metabolic demands, and to allow rapid efflux of the heat into the blood circulation (Contreras et al., 2015). Little is known about the effect of insufficient amount of oxygen, hypoxia, on BAT and its thermogenic function. However, it is known that hypoxia reduces whole-body temperature in mice and humans (Kottke and Phalen, 1948). In rodent studies, Shimizu *et al.* have shown that obesity reduces the density of the vascular capillaries in BAT and induces hypoxia in this tissue, which can lead to BAT whitening and dysfunction (Shimizu et al., 2014). Moreover, hypoxia has an inhibitory effect on the central and neural feedback pathways involved in shivering thermogenesis in squirrels (Tattersall and Milsom, 2009). A mouse study showed that a combination of chronic hypoxia and cold exposure led to decreased NE-induced respiration compared with control mice (Beaudry and McClelland, 2010). To our knowledge, no study has examined the effect of acute hypoxia on BAT thermogenesis and the molecular mechanisms involved. In order to better understand how BAT responds to acute hypoxia, we examined the effects of acute hypoxia on BAT thermogenesis in a unique mammalian species called the naked mole rat (NMR), which is exceptionally hypoxia tolerant. Chapter 3 describes this study.

BAT is mainly composed of brown adipocytes that contain multiple multilocular cytoplasmic lipid droplets. Furthermore, brown adipocytes are highly enriched with mitochondria, which in turn have a high amount of UCP1 at approximately 10% of mitochondrial protein (Busiello et al., 2015; Cannon and Nedergaard, 2004; Nicholls, 2006). UCP 1 is a member of the uncoupling protein family, which has five known members, all of which are found exclusively in the mitochondrial inner membrane (Demine et al., 2019). Also uncoupling protein 3 (UCP3) was found to expressed in BAT but at levels approximately 400 times less compared to

UCP1 (Hilse et al., 2016). UCP1 is the main mediator of NST and mice lacking UCP1 are cold intolerent and have blunted oxygen consumption after treatment with CL316,243 (Enerbäck et al., 1997).

In addition to its thermogenic role, BAT can release regulatory molecules called batokines that have beneficial impacts on BAT itself (autocrine effect) and on other tissues (paracrine and endocrine effects). Examples of these regulatory molecules include fibroblast growth factor 21 (FGF21), neuregulin 4 (NRG4), and vascular endothelia growth factor (VEGF), myostatin, and 12,13-dihydroxy-9Z-octadecenoic acid (12,13-diHOME) (Hondares et al., 2011; Kong et al., 2018; Lagercrantz et al., 1998; Stanford et al., 2018; Wang et al., 2014).

Notably, BAT can also release small extracellular vesicles (sEV) and BAT activation increases the release of sEV (Chen et al., 2016). sEV are involved in cellular signaling and interorgan communication; their size is less than 200 nm (Théry et al., 2018); are formed through a regulated process; and contain cargo carrying bioactive molecules, including proteins, nucleic acids and lipids (Akers et al., 2013; Ostrowski et al., 2010; Raposo and Stoorvogel, 2013). Published work by Chen *et al.* has shown that microRNA-92a packaged in sEV is inversely correlated with activated BAT in mice and humans and can be used as a biomarker of BAT activity (Chen et al., 2016). The biological effects of sEV derived from BAT on other tissues/cells has not been fully explored. To date, one study, conducted by Thomou *et al.,* showed that BAT releases sEV containing microRNAs that are taken up by the liver and regulate gene expression (Thomou et al., 2017). Further investigation is required to have a better understanding of the functional roles of BAT-derived sEV on other tissues/cells. Chapter 4 will focus on the metabolic effects of BAT-derived sEV on skeletal muscle cell bioenergetics.

BAT has been suggested as having therapeutic potential to treat obesity for the following reasons. First, as mentioned above, it was firmly evident that functional BAT does exist in adult humans (not only in infants). BAT is more active in healthy lean individuals than in obese individuals (Cypess et al., 2009; van Marken Lichtenbelt et al., 2009; Nedergaard et al., 2007; Virtanen et al., 2009). Second, in rodents and humans, activated BAT utilizes remarkable amounts of energy substrates such as fats and carbohydrates, resulting in increased whole-body energy expenditure (Abreu-Vieira et al., 2015; Saito, 2013). Recognition of the metabolic role of BAT in energy metabolism and the potential of BAT as a treatment for obesity propels researchers to conduct further studies on this tissue in order to understand how it is regulated. In this thesis, chapters 2 and 3 will focus on the regulation of BAT activity.

### 1.3.3. BEIGE ADIPOSE TISSUE

Beige adipose tissue is composed of inducible brown-like adipocytes. These cells possess thermogenic capacity in response to some environmental and metabolic stressors such as chronic cold exposure, exercise, and the long-term administration of adrenergic agonists (Himms-Hagen et al., 2000; Kajimura et al., 2015). Beige adipocytes are found as clusters of cells emerging sporadically within WAT depots. Once they are induced, they cause changes in the colour of WAT through a process called browning of WAT; the beige colour is as a result of mitochondriogenesis (Ghorbani and Himms-Hagen, 1997; Young et al., 1984). The developmental origin of beige adipocytes is sophisticated. Several studies reportd that beige adipocytes can be derived from lineages that do not express Myf5 (Sanchez-Gurmaches et al., 2012; Seale et al., 2008), as illustrated in Figure1.2. However, other studies have shown that some beige adipocytes can be

derived from Myf5 expressing precursors or from smooth muscle (Long et al., 2014; Sanchez-Gurmaches et al., 2012). The formation of beige adipocytes is still debated and different theories have been proposed. Briefly, beige adipocytes can be developed from the *de novo* differentiation of beige adipocyte precursors, from pre-existing mature beige adipocytes, or from white adipocyte transdifferentiation (Kajimura et al., 2015). Generally, when beige adipocytes are induced, they exhibit morphological features seen in classic brown adipocytes such as many small lipid droplets and condensed mitochondria containing high amounts of UCP1 (Cousin et al., 1992; Ghorbani and Himms-Hagen, 1997; Ikeda et al., 2018).

Animal studies illustrated that the thermogenic capacity of beige adipocytes is mainly independent of UCP1 function. It has been observed that cold exposed UCP1-deficient mice have higher respiration in inguinal WAT compared with wild type mice or UCP1 deficient mice housed at thermoneutrality (Ukropec et al., 2006). Moreover, UCP1 deficient mice that were chronically treated with β3-adrenergic agonist exhibited increased metabolic rate, body temperature and respiration in WAT depots. All of these observations indicate that there are UCP1 independent thermogenic mechanisms occurring in WAT in response to thermogenic stimuli (Granneman et al., 2003). Examples of these mechanisms include futile creatine pathways (Kazak et al., 2015), which were shown to play important roles in the regulation of whole-body energy homeostasis and UCP1 independent thermogenesis. However, a recent study demonstrated that there are two types of beige adipocytes that have UCP1 or not. It was shown that UCP1 positive beige adipocytes actually possess two thermogenic mechanisms, which are UCP1-dependent or creatine-driven (Bertholet et al., 2017).

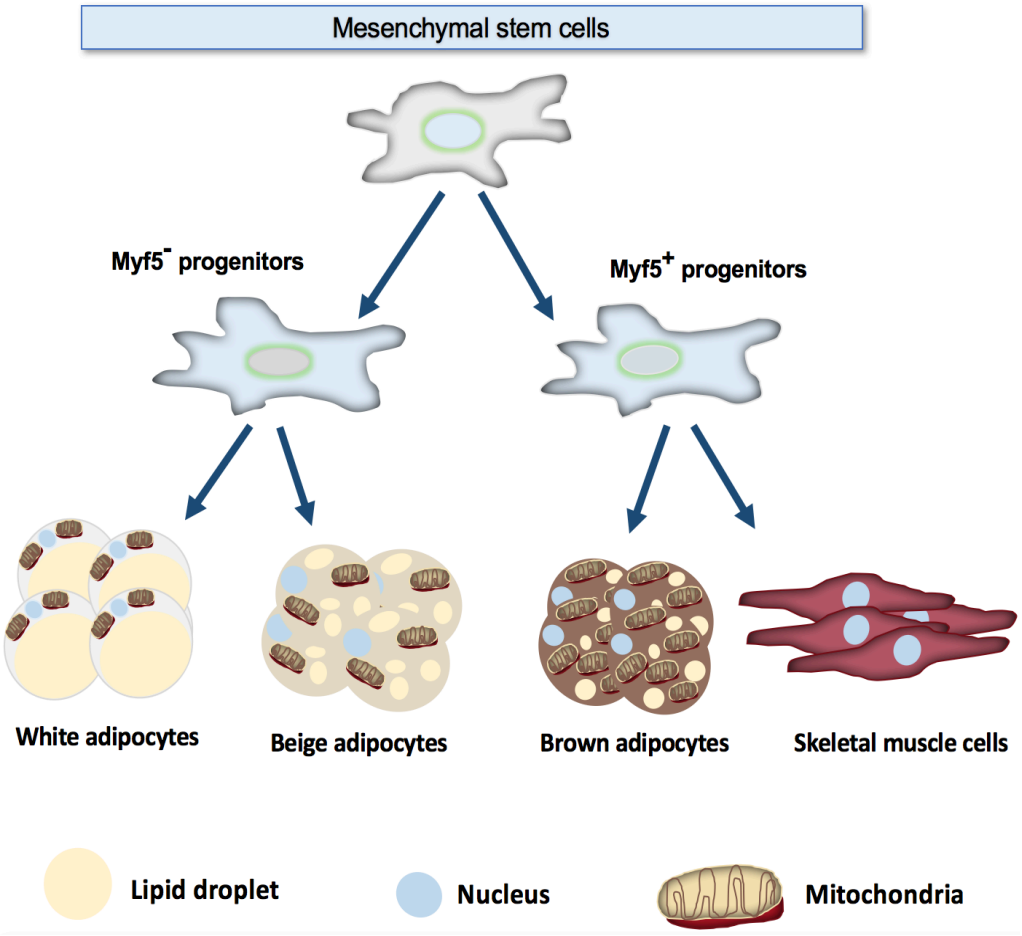


**Figure 1.2: The developmental origin and cellular structure of different adipocytes.**

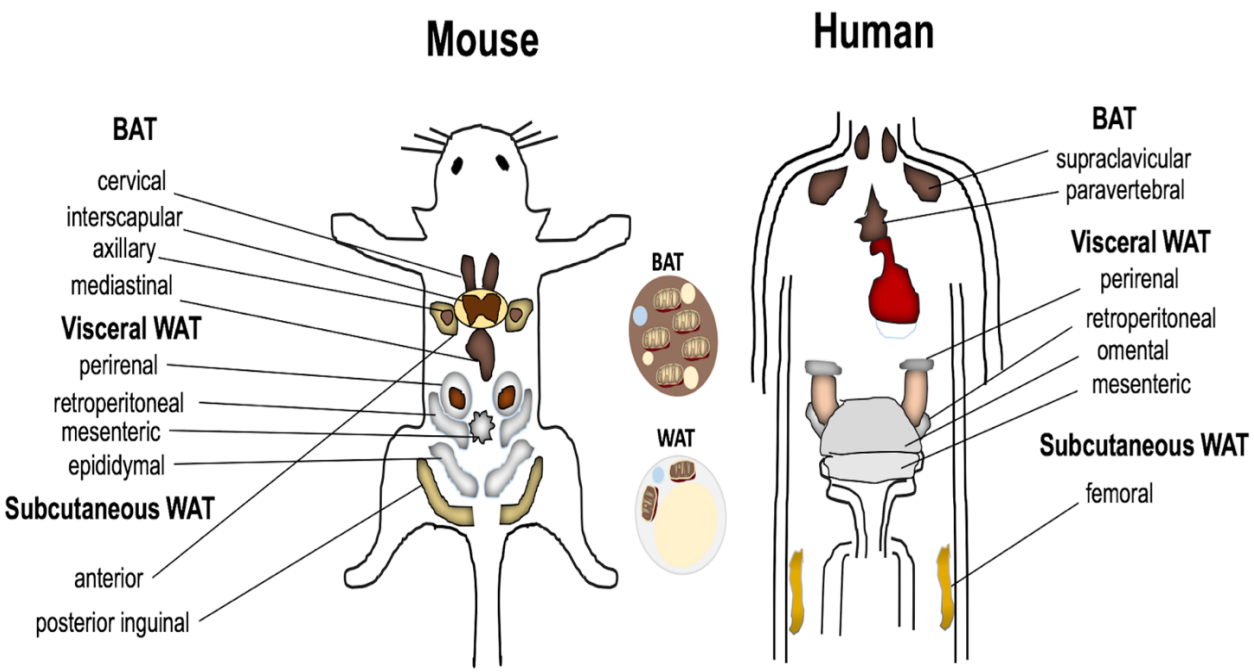


**Figure1.3: Anatomical locations of ATs in mice and humans, modified from (Choe et al., 2016).**

## 1.4 BAT THERMOGENESIS

### 1.4.1 BAT FUEL UTILIZATION AND THERMOGENESIS

As mentioned above, activated BAT utilizes glucose and fatty acids from the circulation, and its own stores of fatty acids, to meet its metabolic needs for thermogenesis. During cold exposure, the activities of metabolic pathways are upregulated including the uptake and oxidation of glucose; the uptake and oxidation of FAs and *de novo* lipogenesis (Yu et al., 2002). It is known that FFAs are the primary energy source for BAT during its activation. As described below in section 1.5.1, adrenergic activation of BAT thermogenesis induces the release of FFAs from intracellular TGs in lipid droplets through lipolysis. Also, in response to cold, the level of plasma TG-rich lipoproteins is decreased via the action of lipoprotein lipase (LPL) that releases FFAs to be taken up by cells through the fatty acid transporter, CD36 (Bartelt et al., 2011). Internalized FFAs are reesterified for fatty acid oxidation (FAO) or are stored as lipid droplets (Bartelt et al., 2011). Gene expression studies have demonstrated that glucose metabolism related genes are considerably upregulated in BAT during cold exposure (Hao et al., 2015). Cold exposure increases the expression of glucose transporters 1 and 4 (Glut1 and Glut4) (Bartelt et al., 2011). Moreover, adrenergic stimulation of brown adipocytes induces the expression of Glut1 and the translocation to the plasma membrane (PM) of Glut4 (Olsen et al., 2014; Shimizu et al., 1998). Despite the up-regulation of glucose metabolism related genes and glucose transporters, glucose oxidation is somewhat restricted because glucose flux is directed to the pentose phosphate pathway, which provides reducing equivalents in the form of NAPDH for *de novo* fatty acid synthesis. Moreover, glucose is used to synthesize glycerol to support *de novo* lipid synthesis (Hao et al., 2015). Therefore, it is considered that glucose is not a main energy substrate for BAT

thermogenesis, but it is largely needed for lipogenesis. To evaluate the contribution of intracellular TG pools to BAT thermogenesis *in vivo,* a study was conducted on rats in which adipocyte TG lipolysis was inhibited by using nicotinic acid (NiAc). The data revealed that the skin temperature of interscapular BAT was decreased by 90% after acute cold and by 71% after cold acclimation. Consistently, the increased oxidative metabolism in BAT was blunted in acute (84%) and chronic (73%) cold exposure. Published data also show that intracellular TG pools are major thermogenic substrates (Labbé et al., 2015). Although, the molecular mechanisms that orchestrate these metabolic pathways are not fully clear.

During BAT activation, TG lipid droplets will be hydrolyzed by specific enzymes. After being hydrolyzed, the released FFAs are used for UCP1 activation and to support the β-oxidation pathway. This will be explained in section 1.5.1.

### 1.4.2 BAT MITOCHONDRIAL BIOENERGETICS

Mitochondria are very dynamic organelles within cells. Functionally, they are considered as the powerhouses of the cells because of their main function, generating ATP by oxidative phosphorylation. However, in brown adipocytes their main function is heat production. Also, mitochondria play essential roles in various cellular processes such as metabolism, calcium signaling, apoptosis, and ROS generation and detoxification (Duchen, 2004; Tzameli, 2012). Notably, tissues that have high energy demands have many mitochondria, such as the heart, skeletal muscle, and BAT (Farmer, 2008; Marín-García and Goldenthal, 2002). In BAT mitochondria, energy is released as heat instead of being captured in the form of ATP (Cannon and Nedergaard, 2004).

Our understanding of the structure of mitochondria has been advanced through the use of many different experimental approaches including live cell imaging, electron microscopy and mitochondrial sub-fractionation analyses (Frey et al., 2006; Jakobs, 2006; Pallotti and Lenaz, 2001). Morphologically, mitochondria are composed of two double membranes, the mitochondrial outer membrane (MOM) and the mitochondrial inner membrane (MIM), which both have a high amount of phospholipid such as cardiolipin and a low level of cholesterol to ensure efficient mitochondrial function (Mileykovskaya et al., 2005; Simbeni et al., 1991; Sustarsic et al., 2018). In terms of the structural differences between these two mitochondrial membranes, MOM separates mitochondria from the cytoplasm and it is highly permeable, allowing molecules less than 6 kilodalton (kDa) to freely diffuse through membrane proteins called porins. In comparison to the MOM, MIM separates mitochondrial matrix from the mitochondrial intermembrane space, and it is selectively impermeable to most ions and small molecules. Also, MIM has a much larger surface area than MOM due its folds, called cristae (Cooper, 2000). Cristae are very dynamic structures whose formation can be affected by some nutritional and metabolic conditions such as starvation (Patten et al., 2014). The formation of the cristae is dependent mainly on two master proteins called optic atrophy 1 (OPA1) and mitochondrial contact site and cristae organizing system (MICOS) complex and this has an impact on mitochondrial respiration (Frezza et al., 2006; Pfanner et al., 2014).

Mitochondria constantly undergo fission and fusion to maintain healthy functioning of this organelle. The regulatory mechanisms that control mitochondrial fission and fusion are complex and not fully understood. However, there are important mitochondrial proteins needed for the control of fission and fusion. For instance, mitofusins1 and 2 (Mfn1 and Mfn2) are located

in MOM, and OPA1 is located in MIM, and these proteins are essential for mitochondria fusion. On the contrary, dynamin related protein 1 (Drp1) plays an important role in mitochondrial fission (van der Bliek et al., 2013; Shaw and Nunnari, 2002). Interestingly, mitochondrial fission is a fundamental regulator of cold-induced BAT thermogenesis and energy expenditure in mice (Park et al., 2019; Wikstrom et al., 2014).

Uncoupled respiration in BAT mitochondria is also supported by the action of proteins found upstream of UCP1 such as proteins in the electron transport chain (ETC) (Cannon and Nedergaard, 2004). There are over 80 proteins in the four complexes of the ETC. The multiprotein complexes are NADH dehydrogenase or complex 1 (CI), succinate dehydrogenase or complex II (CII), cytochrome oxidoreductase or complex III (CIII), and cytochrome c oxidase or complex IV (CIV). During oxidation reactions taking a place in the mitochondrial matrix, reducing equivalent (electron) carriers such NADH + H and FADH2 shuttle electrons to the ETC. While the electrons move through the ETC until the final electron acceptor, oxygen, protons are pumped to the intermembrane space from CI, CIII and CIV, generating a proton motive force (PMF). The PMF drives proton back to the mitochondrial matrix through UCP1; heat does not emanate from UCP1 itself, but from all of the upstream oxidation reactions that are active when UCP1 is stimulated (Cannon and Nedergaard, 2004; Lodish et al., 2000).

As electrons move through the ETC complexes, some can escape and associate with molecular oxygen to form ROS. ROS such as superoxide are mainly formed at CI and CIII in the ETC and can be converted to other forms of ROS such as hydrogen peroxide (Murphy, 2009). Depending on the level and duration of ROS levels, there can be oxidative damage or beneficial effects (*e.g.*, signaling) in cells (Sarangarajan et al., 2017). In regard to BAT thermogenesis, it has

been shown that ROS can augment UCP1 dependent thermogenic respiration (Chouchani et al., 2016), as detailed below in section 1.5.4.1.

## 1.5 THE CONTROL OF BAT THERMOGENESIS

BAT function can be controlled at different levels, acutely and chronically. The subsequent sections will focus on the various known levels of control of BAT thermogenesis.

### 1.5.1 BAT THERMOGENESIS UNDER THE CONTROL OF SYMPATHETIC NERVOUS SYSTEM

The SNS is the predominant signaling pathway that induces BAT thermogenesis. Released NE mainly activates β3-AR, the most abundant adrenergic receptor (AR) on the plasma membrane of brown adipocytes in rodents (Cannon and Nedergaard, 2004; Lafontan and Berlan, 1993). Several isoforms of AR are expressed on the plasma membrane of adipocytes including α1-AR, α2-AR, β1-AR, β2-AR, and β3-AR but their physiological roles vary, depending on the fat depot and the animal species (Lafontan and Berlan, 1993). All of these receptors belong to the G-protein coupled receptor (GPCR) family. Several studies have demonstrated the importance of β3-AR in thermogenesis, energy expenditure, and weight loss. β3-AR is found on brown and white adipocytes. The activation of this receptor leads to heat production in brown adipocytes and lipolysis in white adipocytes. Since the discovery of β3-AR and its activators, this receptor has gained a lot of attention due to its ability to induce lipolysis and NST (Arch, 2002). Another reason for the great interest in this AR is related to the fact that the β3-AR is almost exclusively expressed in these adipose tissues (and not in the heart, for example). Thus the idea of developing β3-AR-selective agonists for the potential treatment of obesity attracted wide attention. The other

adrenergic receptors are not involved in BAT thermogenesis; however, β1-AR is required for the development and proliferation of brown adipocytes, which is needed to recruit BAT during chronic induction of thermogenesis (Bronnikov et al., 1992, 1999; Lafontan and Berlan, 1993).

In response to cold or excessive food intake, SNS releases NE as a neurotransmitter that acts on brown adipocytes to activate signaling pathways (Cannon and Nedergaard, 2004; Leblanc et al., 1982; Zhang and Bi, 2015). In detail, NE binds to β3-AR on brown adipocytes and this binding results in the activation of canonical AR–Gs–adenylyl cyclase (AC)-cyclic adenosine monophosphate (cAMP)- protein kinase A (PKA) signaling pathway. The activation of the latter pathway leads eventually to the lipolysis of the intracellular lipid droplets. As a result, FFAs are released from the lipid droplets to serve as direct UCP1 activators and as oxidative substrates used in FAO. While FFAs act as direct UCP1 activators, specifically long forms of FFAs, which directly bind to UCP1 releasing its purine nucleotide inhibition. Purine nucleotides (PNs) can compete with FFAs to inhibit UCP1 activity in a simple competitive mechanism (Cannon and Nedergaard, 2004; Fedorenko et al., 2012; Himms-Hagen, 1985; Shabalina et al., 2004). These mechanisms are depicted in Figure 1.4.

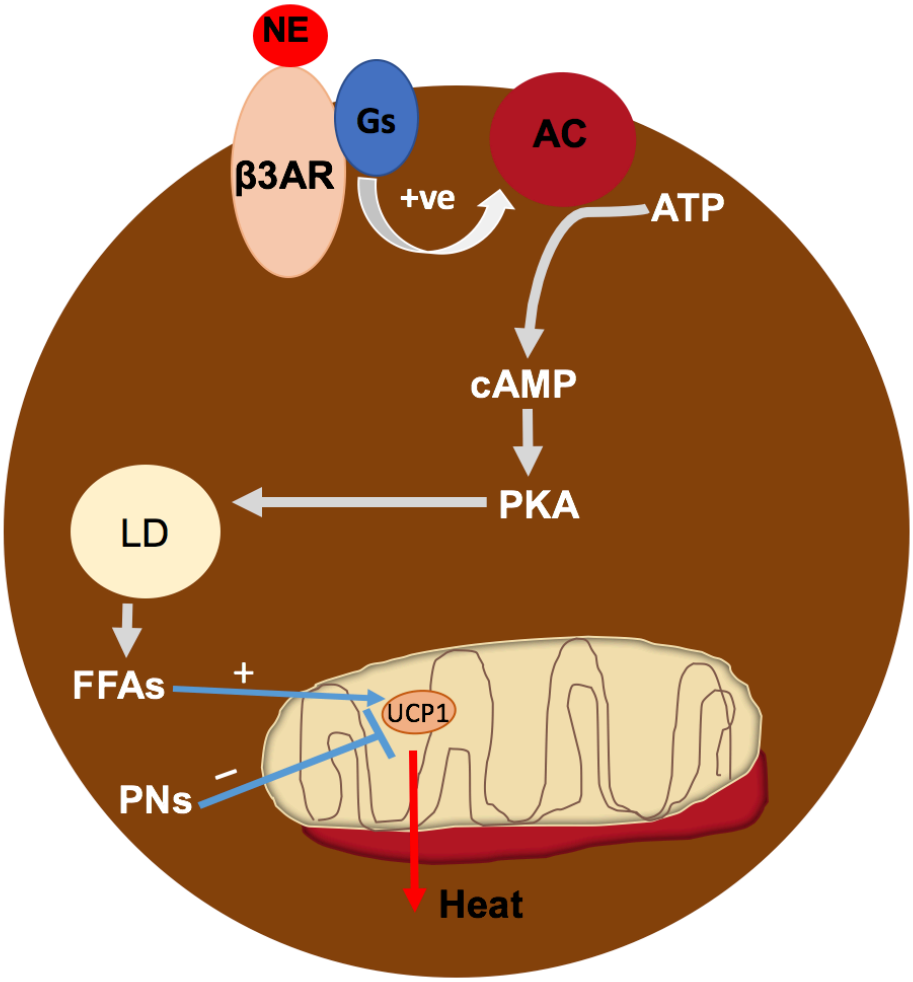


**Figure1.4: Adrenergic activation of BAT thermogenesis, modified from (Cannon and Nedergaard, 2004).**

### 1.5.2 FACTORS RELEASED BY VARIOUS TISSUES CONTROL BAT ACTIVITY

Although the SNS is known as the main regulator of BAT thermogenesis, there is a growing body of research demonstrating how BAT thermogenesis can be augmented acutely and chronically through additional mechanisms. BAT thermogenesis can be induced by various other molecules released from other organs. Moreover, these molecules can act on the recruitment and/or the activity of BAT and some of these molecules are able to induce the browning of WAT. In the following section, the focus is on some of these released factors from the thyroid gland, heart, liver, and skeletal muscles.

#### 1.5.2.1 THYROID GLAND DERIVED REGULATORS OF BAT ACTIVITY

The thyroid is a butterfly-shaped gland located in the neck secreting hormones that can regulate body functions such as development, growth, and metabolism. The thyroid gland produces thyroxine (T4), a prohormone, and triiodothyronine (T3), the active hormone form. It is known that the increased activity of thyroid derived hormones promotes energy expenditure and metabolism (Brent, 2012; Oetting and Yen, 2007). Studies conducted in mice examined the effect of hypothyroidism, reduced levels of thyroid hormones, or hyperthyroidism, increased levels of thyroid hormones, on WAT browning and BAT activity (Weiner et al., 2016). They found that mice with either hypothyroidism or hyperthyroidism have increased thermogenic genes expression in WAT and induced browning of WAT. Interestingly, BAT activity was reduced in hypothyroid mice and activated in hyperthyroid mice (Weiner et al., 2016). Mechanistically, thyroid hormones activate BAT by acting on their receptors, thyroid hormone receptors (TRs), in brown adipocytes or in hypothalamic neurons (Weiner et al., 2017). T3 can activate BAT thermogenesis and WAT browning through its action in the ventromedial nucleus

of the hypothalamus (VMH) (López et al., 2010; Martínez-Sánchez et al., 2016). T3 reduces AMP-activated protein kinase (AMPK) pathways in the VMH, which decreases ceramide-induced endoplasmic reticulum (ER) stress, which in turn activates BAT thermogenesis (Martínez-Sánchez et al., 2017). In addition, thyroid hormones bind to their receptors (TR-β) in brown adipocytes to activate nuclear dependent signaling pathways that induce expression of thermogenic genes including UCP1 (Cioffi et al., 2018). Recently, a study has demonstrated that T3 can induce the expression of UCP1 in brown adipocytes through the action of the transcription factor named carbohydrate-response element-binding protein (ChREBP), which binds to the UCP1 gene promoter (Katz et al., 2017). In this study, it was also shown that knockdown of ChREBP leads to a decrease in the expression of UCP1 and respiration in brown adipocytes treated with T3 (Katz et al., 2017).

#### 1.5.2.2 HEART-DERIVED REGULATORS OF BAT ACTIVITY

The heart can regulate the thermogenic capacity and related genes of brown and white adipocytes through its endocrine factors called atrial natriuretic peptide (ANP) and ventricular natriuretic peptide (BNP). It has been reported that the levels of these natriuretic peptides is increased in response to some stressors such as cardiac wall stress, hypoxia, cold exposure and exercise (Gruden et al., 2014). The action of these natriuretic peptides (NPs) on brown and white adipocytes is dependent on their binding to their receptors on adipocytes called natriuretic peptide receptor A (NPRA) and natriuretic peptide receptor C (NPRC) (Chinkers et al., 1989; Waldman et al., 1984). A study conducted by Collins' group showed that mice exposed to cold for 6 hours had elevated circulating plasma level of BNP and increased transcript levels of ANP

and BNP in the heart. Moreover, mice injected with BNP or human adipocytes treated with BNP had increased expression of BAT specific thermogenic genes including UCP1, PPAR-γ, peroxisome proliferator activated receptor-γ coactivator1-α (PGC1-α) and induced mitochondrial biogenesis and respiration (Bordicchia et al., 2012). They also proposed a model wherein the activation of NPRA induces the activation of guanylyl cyclase(GC)-cyclic guanosine monophosphate (cGMP)-protein kinase G (PKG) signaling pathways, which leads to lipolysis and increases the expression of thermogenic proteins to promote thermogenesis (Bordicchia et al., 2012). They also showed that mammalian target of rapamycin complex 1 (mTORC1) activation is needed for the increase in the expression of UCP1 in beige adipocytes as a part of WAT browning and thermogenesis (Liu et al., 2018).

#### 1.5.2.3 LIVER-DERIVED REGULATORS OF BAT ACTIVITY

The liver is a dynamic, organized and multifunctional organ that is composed of a heterogeneous population of cells. It is involved in fundamental biological mechanisms such as the metabolism of dietary nutrients supplied by the portal vein, the regulation of blood volume, the support of immune system, and the secretion of hormones (Bechmann et al., 2012; Gordillo et al., 2015; Gruppuso and Sanders, 2016; Hijmans et al., 2014; Rui, 2014; Trefts et al., 2015, 2017). Several studies have demonstrated the regulatory role of hepatic hormones on different tissues involved in the regulation of whole-body energy homestasis including BAT. In particular, a hormone secreted mainly by the liver named fibroblast growth factor 21 (FGF21) has been shown to regulate neonatal BAT thermogenesis (Hondares et al., 2010). A study conducted on neonatal mice examined the abundance and involvement of FGF21 in the regulation of BAT

thermogenesis needed at birth. In this study, it was found that the gene expression in the liver and plasma level of FGF21 are dramatically elevated in response to suckling. The induction of the hepatic FGF21 requires the action of the transcriptional factor, peroxisome proliferator activated receptor-α (PPAR-α). Also, the neonatal mice that were injected with FGF21 exhibited enhanced body temperature and increased expression of thermogenic genes in BAT compared with controls. Moreover, a similar response (uncoupled respiration) was observed in brown adipocytes treated with FGF21 *in vitro*. These findings demonstrated the importance of FGF21 in the activation of BAT (Hondares et al., 2010).

Recently, a study conducted in mice discovered a hepatic suppressor of BAT thermogenesis called Tsukushi (TSK) (Wang et al., 2019b). It was initially discovered in the chick lens in 2004 and identified as an extracellular signaling molecule that belongs to small leucine-rich proteoglycan (SLRP) family. Since its discovery it has been reported that TSK interacts with several signaling pathways to regulate numerous developmental processes (Ohta, 2014; Ohta et al., 2004). TSK can modulate BAT thermogenesis by acting on sympathetic signaling in BAT. In their study, it was shown that the level of TSK was dramatically enriched in the liver compared to other tissues under conditions in which BAT activity and energy expenditure were enhanced. Also, TSK deficient mice showed elevated body temperature, resistance to high-fat-diet induced obesity, induced adrenergic activation, and increased thermogenic machinery and energy expenditure. To conclude, TSK released by the liver in response to increased energy expenditure, can negatively impact the activity of BAT by suppressing its sympathetic activation (Wang et al., 2019b).

### 1.5.2.4 SKELETAL MUSCLE-DERIVED REGULATOR OF BAT THERMOGENESIS

Skeletal muscles (SkM) and BAT have strong cellular and functional links. As mentioned above, parenchymal cells in SkM and BAT are derived from the same progenitor, MyF5 containing precursors (Seale et al., 2008). Also, SkM and BAT generates shivering and NST thermogenesis, respectively for integrated responses to a cold environment (Golozoubova et al., 2001). During exercise, SkM is a highly metabolic tissue, utilizing energy-rich molecules and releasing myokines that positively impact other tissues. A particular exercise-induced myokine that has beneficial effects on the browning of WAT and thermogenesis is termed irisin, and it is a cleavage product of a membrane bound protein named fibronectin type III domain 5 (FNDC5)(Boström et al., 2012). Spiegelman's group discovered this exercise-induced myokine and demonstrated that it is able to induce beige adipocytes in WAT of mice. The elevated level of irisin is dependent on the action of the co-transcriptional factor, PGC1-α (Boström et al., 2012). After the discovery of irisin, additional studies conducted by the same group and by others have identified other examples of exercise-induced myokines such as β-aminoisobutyric acid (BAIBA) and meteorin-like (Metrnl) that lead to increased browning of WAT and thermogenesis (Rao et al., 2014; Roberts et al., 2014).

Recently, Chouchani's group discovered that the metabolite, succinate, can be released by shivering muscle during acute cold exposure, and can induce BAT thermogenesis (Mills et al., 2018). Succinate is an intermediate product in the tricarboxylic acid (TCA) cycle and can be oxidized by its mitochondrial enzyme succinate dehydrogenase (SDH). In their study, they demonstrate that succinate is avidly taken up by BAT during acute cold exposure and has a stimulatory effect on BAT activity. Moreover the administration of succinate in mice was able to

boost whole-body oxygen consumption and BAT thermogenesis. These mechanisms were shown to be UCP1 dependent since the metabolic and thermogenic effects of succinate were not observed in UCP1 deficient mice Brown adipocytes treated with succinate had increased mitochondrial uncoupled respiration. Succinate-induced respiration in brown adipocytes was decreased by either the inhibitor of SDH (malonate) or the inhibitor of electron transfer between SDH and the ubiquinone pool (atpenin A5). To sum up, they discovered unexpected thermogenic role of succinate in BAT thermogenesis independent of β-adrenergic stimulation during acute cold exposure in which succinate oxidation by SDH drives ROS production and BAT thermogenesis (Mills et al., 2018).

### 1.5.3 TRANSCRIPTIONAL CONTROL OF BAT THERMOGENESIS

In response to adrenergic stimulation of BAT, gene transcriptional events are induced to promote the expression of thermogenic genes such as UCP1 and other BAT specific mitochondrial genes that are needed to control thermogenesis. As described above, BAT thermogenic stimuli such as NE or CL316,243 bind to the β3-AR on brown adipocytes resulting in an increased level of cAMP, which activates PKA in the cytoplasm. Activated PKA phosphorylates and activates transcriptional factors directly or indirectly through other signaling pathways, including p38 mitogen activated protein kinase (MAPK) and mTORC1. Activated PKA phosphorylates directly a transcriptional factor called cAMP response element binding protein (CREB), which binds to its identified binding sites on the DNA sequences called cAMP response element (CRE) to promote the transcription of PGC1-$\alpha$, which coactivates nuclear receptor proteins such as PPAR-γ (Wicksteed and Dickson, 2017). Moreover, activated PKA phosphorylates p38MAPK, which in turn phosphorylates and

activates the transcription factor called activating transcription factor 2 (ATF2) and coactivator PGC1-α. In addition, it has been shown that activated PKA phosphorylates and activates the mTORC1, which leads eventually to promote the gene expression of PPAR-α. The induction of all of the previously mentioned nuclear transcriptional factors and coactivators stimulates the expression of UCP1 (Barbera et al., 2001; Liu et al., 2016; Shi and Collins, 2017). On the other hand, to suppress the expression of UCP1 gene, liver X receptor-α (LXRα) binds to its ligand called receptor-interacting protein 140 (RIP140) to form a RIP14-LXRα complex, that competes with PPAR-γ from the enhancer of UCP1 gene. RIP140 binds to PGC1-α to inhibit its transcriptional activity on the UCP1 promoter acting as a suppressor of UCP1 gene expression (Collins et al., 2010; Wang et al., 2008).

### 1.5.4 POST-TRANSLATIONAL CONTROL OF BAT THERMOGENESIS

Post-translational modifications (PTMs) are alterations of proteins through attaching functional chemical groups to the amino acid sequences, and these modifications commonly result in changes in the activity of the proteins (Walsh et al., 2005). PTMs events can occur enzymatically or non-enzymatically, and take a place either with protein translation process or concomitant with translation (Walsh et al., 2005). The following section will focus on the recent studies that have demonstrated different PTMs that affect UCP1 induced thermogenesis.

#### 1.5.4.1 ROS AND SULFENYLATION CONTROL OF BAT THERMOGENESIS

Chouchani *et al* demonstrated that UCP1-dependent thermogenesis in mice are supported by mitochondrial ROS (Chouchani et al., 2016). In their *in vivo* studies, they showed that pharmacological inhibition of mitochondrial ROS with the administration of the

mitochondria-targeted antioxidant (MitoQ) to cold acclimated or CL316,243 mice resulted in reduced body temperature, energy expenditure and UCP1-dependent thermogenesis. During thermogenesis, mitochondrial ROS production resulted in a more oxidized redox state in BAT, and increased levels of protein sulfenic acids. Specifically, cysteine253 of UCP1 was identified in the sulfenylated form. Whereas, mutation of this cysteine causes decreased UCP1-dependent respiration following the addition of the ATP synthase inhibitor, oligomycin, and subsequent NE stimulation in brown adipocytes. In conclusion, BAT thermogenesis is supported by mitochondrial ROS, which promote cysteine sulfenylation and augmented UCP1 activity (Chouchani et al., 2016).

#### 1.5.4.2 SUCCINYLATION CONTROL OF BAT THERMOGENESIS

Recently, Kahn's group demonstrated the importance of succinylation control of BAT thermogenesis (Wang et al., 2019a). Succinylation is mainly mediated by sirtuin 5 (SIRT5), which belongs to the Sirtuins family. SIRT5 also plays roles in mitochondrial demalonylation and glutarylation (Hirschey and Zhao, 2015; Kumar and Lombard, 2018; Park et al., 2013; Tan et al., 2014). In their study, they analyzed BAT mitochondrial function and morphology in a BAT-specific knockout of Sirt5 in mice. Their data revealed that the absence of SIRT5 in BAT results in increased levels of protein succinylation and malonylation. In addition, they found that SIRT5 targets lysine sites in UCP1 and other BAT mitochondrial proteins, such as glutamate dehydrogenase and succinate dehydrogenase, and that the activity of these proteins in BAT of SIRT5KO was decreased. Importantly, the mutation of lysine succinylation sites in UCP1 decreased UCP1 stability and function. Cumulative evidence from their work illustrated that the absence of SIRT5 in BAT results in defective BAT mitochondrial function and metabolic inflexibility. Their findings

support the overall conclusion that succinylation of BAT mitochondrial proteins including UCP1 plays an important role in BAT thermogenesis (Wang et al., 2019a).

Previous studies have explained the regulatory effects of PTM on UCP1-mediated thermogenesis although the importance of other types of PTMs needs to be explored. Therefore, we studied the effect of mitochondrial deacetylation on UCP1-mediated respiration and BAT thermogenesis, as detailed in Chapter 2.

## 1.6 PROJECT RATIONALES, OBJECTIVES AND HYPOTHESES

The overall goals of my doctoral research are to elucidate molecular mechanisms that control BAT activation and thermogenesis and to study the effects of sEV released by BAT. Investigations were conducted in different animal and cellular models as detailed below. Specific rationales, objectives and hypotheses as follows:

**Rationale 1**: Several studies demonstrated that mitochondrial deacetylation mediated by sirtuin3 (SIRT3), a mitochondrial $NAD^+$-dependent deacetylase, is an important post-translational modification mechanism that targets and regulates the activity of numerous mitochondrial proteins (Hirschey et al., 2010, 2011; Jing et al., 2013). Importantly, mice lacking SIRT3 were previously shown to be cold intolerant when fasted (Hirschey et al., 2010). Moreover, the transcript level of SIRT3 in BAT is increased upon cold exposure (Shi et al., 2005). Previous findings thus suggested that SIRT3 may play a role in BAT thermoregulation. However, no study as yet had focused on a direct functional link between SIRT3 and UCP1.

**Objective:** To investigate if the absence of SIRT3 impacts BAT thermogenesis in mice, and if there is a functional relationship between SIRT3 and UCP1.

**Hypothesis**: SIRT3 controls BAT thermogenesis by deacetylating and enhancing the function of UCP1 and/or its upstream proteins.

**Rationale 2:** Oxygen supply is essential for BAT thermogenesis to ensure sufficient ETC activity. Previous studies in various mammalian species showed that hypoxia causes decreases in body temperature (DiPasquale et al., 2015; Gautier et al., 1987; Gordon and Fogelson, 1991; Kottke and Phalen, 1948). The underlying mechanisms of the hypoxic inhibition of body temperature are not fully understood. Based on the previous observations, it is suggested that hypoxia may affect

the function of BAT since it is an avid consumer of oxygen when active. For a better understanding of how hypoxia affects BAT function, we studied naked mole rats (NMRs), (*Heterocephalus glaber*) during acute hypoxia because of their remarkable ability to survive under hypoxic conditions compared to other mammals. NMRs are highly unusual in that they are able to tolerate minutes of complete anoxia, hours at 3% $O_2$, and days to weeks at 8% $O_2$ (Chung et al., 2016; Pamenter et al., 2015, 2018; Park et al., 2017).

**Objective:** To examine the thermogenic effect of acute hypoxia on BAT thermogenesis in NMRs *in vivo*, and the metabolic effect of acute hypoxia on BAT thermogenesis related proteins.

**Hypothesis:** Acute hypoxia decreases the function of BAT, at least in part, by targeting the degradation of thermogenic proteins, resulting in a decrease in body temperature.

**Rationale 3:** Activated BAT releases sEV whose biological roles are poorly understood (Chen et al., 2016). Generally, sEV are involved in interorgan communication and can be taken up by other cells and tissues regulating their functions (Raposo and Stoorvogel, 2013). BAT and SkM are functionally linked. While BAT is responsible for NST, SkM generates heat through shivering thermogenesis during cold exposure (Golozoubova et al., 2001). BAT and SkM are complimentary in their functions. If BAT or SkM have defects in their thermogenic functions, one tissue can compensate to some extent for the defect in the other (Bal et al., 2017; Golozoubova et al., 2001), suggesting cross-talk mechanisms between SkM and BAT. Therefore, we speculated that acutely activated BAT-derived sEV can regulate the bioenergetics of skeletal muscle cells.

**Objective:** To study the effects of activated BAT derived sEV on C2C12 myoblast bioenergetics.

**Hypothesis:** Acutely activated BAT-derived sEV modulate the bioenergetics of C2C12 myoblasts.

## 1.7 REFERENCES


Abreu-Vieira, G., Xiao, C., Gavrilova, O., and Reitman, M.L. (2015). Integration of body temperature into the analysis of energy expenditure in the mouse. Mol. Metab. *4*, 461–470.

Adams, K.F., Schatzkin, A., Harris, T.B., Kipnis, V., Mouw, T., Ballard-Barbash, R., Hollenbeck, A., and Leitzmann, M.F. (2006). Overweight, obesity, and mortality in a large prospective cohort of persons 50 to 71 years old. N. Engl. J. Med. *355*, 763–778.

Akers, J.C., Gonda, D., Kim, R., Carter, B.S., and Chen, C.C. (2013). Biogenesis of extracellular vesicles (EV): exosomes, microvesicles, retrovirus-like vesicles, and apoptotic bodies. J. Neurooncol. *113*, 1–11.

Andersen, T. (1992). Liver and gallbladder disease before and after very-low-calorie diets. Am. J. Clin. Nutr. *56*, 235S-239S.

Angelakis, E., Armougom, F., Million, M., and Raoult, D. (2012). The relationship between gut microbiota and weight gain in humans. Future Microbiol. *7*, 91–109.

Apovian, C.M. (2016). Obesity: definition, comorbidities, causes, and burden. Am. J. Manag. Care *22*, s176-185.

Arch, J.R.S. (2002). beta(3)-Adrenoceptor agonists: potential, pitfalls and progress. Eur. J. Pharmacol. *440*, 99–107.

Arner, P., and Hoffstedt, J. (1999). Adrenoceptor genes in human obesity. J. Intern. Med. *245*, 667–672.

Barbera, M.J., Schluter, A., Pedraza, N., Iglesias, R., Villarroya, F., and Giralt, M. (2001). Peroxisome proliferator-activated receptor alpha activates transcription of the brown fat uncoupling protein-1 gene. A link between regulation of the thermogenic and lipid oxidation pathways in the brown fat cell. J. Biol. Chem. *276*, 1486–1493.

Barker, D.J.P. (1997). Maternal Nutrition, Fetal Nutrition, and Disease in Later Life. Nutrition. *13*, 807–813.

Bartelt, A., Bruns, O.T., Reimer, R., Hohenberg, H., Ittrich, H., Peldschus, K., Kaul, M.G., Tromsdorf, U.I., Weller, H., Waurisch, C., et al. (2011). Brown adipose tissue activity controls triglyceride clearance. Nat. Med. *17*, 200–205.

Beauchamp, B., Ghosh, S., Dysart, M., Kanaan, G.N., Chu, A., Blais, A., Rajamanickam, K., Tsai, E.C., Patti, M.-E., and Harper, M.-E. (2015a). Low birth weight is associated with adiposity,

impaired skeletal muscle energetics, and weight loss resistance in mice. Int. J. Obes. 2005 *39*, 702–711.

Beauchamp, B., Thrush, A.B., Quizi, J., Antoun, G., McIntosh, N., Al-Dirbashi, O.Y., Patti, M.-E., and Harper, M.-E. (2015b). Undernutrition during pregnancy in mice leads to dysfunctional cardiac muscle respiration in adult offspring. Biosci. Rep. *35*.

Beaudry, J.L., and McClelland, G.B. (2010). Thermogenesis in CD-1 mice after combined chronic hypoxia and cold acclimation. Comp. Biochem. Physiol. B Biochem. Mol. Biol. *157*, 301–309.

Bechmann, L.P., Hannivoort, R.A., Gerken, G., Hotamisligil, G.S., Trauner, M., and Canbay, A. (2012). The interaction of hepatic lipid and glucose metabolism in liver diseases. J. Hepatol. *56*, 952–964.

Bertholet, A.M., Kazak, L., Chouchani, E.T., Bogaczyńska, M.G., Paranjpe, I., Wainwright, G.L., Bétourné, A., Kajimura, S., Spiegelman, B.M., and Kirichok, Y. (2017). Mitochondrial Patch Clamp of Beige Adipocytes Reveals UCP1-Positive and UCP1-Negative Cells Both Exhibiting Futile Creatine Cycling. Cell Metab. *25*, 811-822.e4.

van der Bliek, A.M., Shen, Q., and Kawajiri, S. (2013). Mechanisms of mitochondrial fission and fusion. Cold Spring Harb. Perspect. Biol. *5*.

Bordicchia, M., Liu, D., Amri, E.-Z., Ailhaud, G., Dessì-Fulgheri, P., Zhang, C., Takahashi, N., Sarzani, R., and Collins, S. (2012). Cardiac natriuretic peptides act via p38 MAPK to induce the brown fat thermogenic program in mouse and human adipocytes. J. Clin. Invest. *122*, 1022–1036.

Boström, P., Wu, J., Jedrychowski, M.P., Korde, A., Ye, L., Lo, J.C., Rasbach, K.A., Boström, E.A., Choi, J.H., Long, J.Z., et al. (2012). A PGC1-α-dependent myokine that drives brown-fat-like development of white fat and thermogenesis. Nature. *481*, 463–468.

Bouchard, C. (1997). Genetics of Human Obesity: Recent Results from Linkage Studies. J. Nutr. *127*, 1887S-1890S.

Bougnères, P., Pantalone, L., Linglart, A., Rothenbühler, A., and Le Stunff, C. (2008). Endocrine Manifestations of the Rapid-Onset Obesity with Hypoventilation, Hypothalamic, Autonomic Dysregulation, and Neural Tumor Syndrome in Childhood. J. Clin. Endocrinol. Metab. *93*, 3971–3980.

Braun, K., Oeckl, J., Westermeier, J., Li, Y., and Klingenspor, M. (2018). Non-adrenergic control of lipolysis and thermogenesis in adipose tissues. J. Exp. Biol. *221*.

Bray, G.A., Frühbeck, G., Ryan, D.H., and Wilding, J.P.H. (2016). Management of obesity. Lancet Lond. Engl. *387*, 1947–1956.

Bray, G.A., Kim, K.K., Wilding, J.P.H., and World Obesity Federation (2017a). Obesity: a chronic relapsing progressive disease process. A position statement of the World Obesity Federation. Obes. Rev. Off. J. Int. Assoc. Study Obes. *18*, 715–723.

Bray, G.A., Kim, K.K., Wilding, J.P.H., and World Obesity Federation (2017b). Obesity: a chronic relapsing progressive disease process. A position statement of the World Obesity Federation. Obes. Rev. Off. J. Int. Assoc. Study Obes. *18*, 715–723.

Brent, G.A. (2012). Mechanisms of thyroid hormone action. J. Clin. Invest. *122*, 3035–3043.

Bronnikov, G., Houstěk, J., and Nedergaard, J. (1992). Beta-adrenergic, cAMP-mediated stimulation of proliferation of brown fat cells in primary culture. Mediation via beta 1 but not via beta 3 adrenoceptors. J. Biol. Chem. *267*, 2006–2013.

Bronnikov, G., Bengtsson, T., Kramarova, L., Golozoubova, V., Cannon, B., and Nedergaard, J. (1999). beta1 to beta3 switch in control of cyclic adenosine monophosphate during brown adipocyte development explains distinct beta-adrenoceptor subtype mediation of proliferation and differentiation. Endocrinology. *140*, 4185–4197.

Budisteanu, M., Barca, D., Chirieac, S.M., and Magureanu, S. (2010). Cohen syndrome – a rare genetic cause of hypotonia in children. Maedica. *5*, 56–61.

Bukowiecki, L., Collet, A.J., Follea, N., Guay, G., and Jahjah, L. (1982). Brown adipose tissue hyperplasia: a fundamental mechanism of adaptation to cold and hyperphagia. Am. J. Physiol. *242*, E353-359.

Burcelin, R. (2012). Regulation of metabolism: a cross talk between gut microbiota and its human host. Physiol. Bethesda Md. *27*, 300–307.

Busiello, R.A., Savarese, S., and Lombardi, A. (2015). Mitochondrial uncoupling proteins and energy metabolism. Front. Physiol. *6*.

Butler, M.G. (2011). Prader-Willi Syndrome: Obesity due to Genomic Imprinting. Curr. Genomics. *12*, 204–215.

Camps, J., Marsillach, J., and Joven, J. (2009). The paraoxonases: role in human diseases and methodological difficulties in measurement. Crit. Rev. Clin. Lab. Sci. *46*, 83–106.

Cannon, B., and Nedergaard, J. (2004). Brown Adipose Tissue: Function and Physiological Significance. Physiol. Rev. *84*, 277–359.

Carrillo, J.L.M., Campo, J.O.M.D., Coronado, O.G., Gutiérrez, P.T.V., Cordero, J.F.C., and Juárez, J.V. (2018). Adipose Tissue and Inflammation. Adipose Tissue.

Carwile, J.L., and Michels, K.B. (2011). Urinary bisphenol A and obesity: NHANES 2003-2006. Environ. Res. *111*, 825–830.

Cassard-Doulcier, A.M., Bouillaud, F., Chagnon, M., Gelly, C., Dionne, F.T., Oppert, J.M., Bouchard, C., Chagnon, Y., and Ricquier, D. (1996). The Bcl I polymorphism of the human uncoupling protein (ucp) gene is due to a point mutation in the 5'-flanking region. Int. J. Obes. Relat. Metab. Disord. J. Int. Assoc. Study Obes. *20*, 278–279.

Chakrabarti, P., Kim, J.Y., Singh, M., Shin, Y.-K., Kim, J., Kumbrink, J., Wu, Y., Lee, M.-J., Kirsch, K.H., Fried, S.K., et al. (2013). Insulin Inhibits Lipolysis in Adipocytes via the Evolutionarily Conserved mTORC1-Egr1-ATGL-Mediated Pathway. Mol. Cell. Biol. *33*, 3659–3666.

Chan, J.M., Rimm, E.B., Colditz, G.A., Stampfer, M.J., and Willett, W.C. (1994). Obesity, fat distribution, and weight gain as risk factors for clinical diabetes in men. Diabetes Care. *17*, 961–969.

Chen, X., Beydoun, M.A., and Wang, Y. (2008). Is sleep duration associated with childhood obesity? A systematic review and meta-analysis. Obes. Silver Spring Md. *16*, 265–274.

Chen, Y., Buyel, J.J., Hanssen, M.J.W., Siegel, F., Pan, R., Naumann, J., Schell, M., van der Lans, A., Schlein, C., Froehlich, H., et al. (2016). Exosomal microRNA miR-92a concentration in serum reflects human brown fat activity. Nat. Commun. *7*, 11420.

Chinkers, M., Garbers, D.L., Chang, M.S., Lowe, D.G., Chin, H.M., Goeddel, D.V., and Schulz, S. (1989). A membrane form of guanylate cyclase is an atrial natriuretic peptide receptor. Nature. *338*, 78–83.

Choe, S.S., Huh, J.Y., Hwang, I.J., Kim, J.I., and Kim, J.B. (2016). Adipose Tissue Remodeling: Its Role in Energy Metabolism and Metabolic Disorders. Front. Endocrinol. *7*.

Chouchani, E.T., Kazak, L., Jedrychowski, M.P., Lu, G.Z., Erickson, B.K., Szpyt, J., Pierce, K.A., Laznik-Bogoslavski, D., Vetrivelan, R., Clish, C.B., et al. (2016). Mitochondrial ROS regulate thermogenic energy expenditure and sulfenylation of UCP1. Nature. *532*, 112–116.

Chung, D., Dzal, Y.A., Seow, A., Milsom, W.K., and Pamenter, M.E. (2016). Naked mole rats exhibit metabolic but not ventilatory plasticity following chronic sustained hypoxia. Proc. R. Soc. B Biol. Sci. *283*, 20160216.

Cioffi, F., Gentile, A., Silvestri, E., Goglia, F., and Lombardi, A. (2018). Effect of Iodothyronines on Thermogenesis: Focus on Brown Adipose Tissue. Front. Endocrinol. *9*.

Claus, T.H., Lowe, D.B., Liang, Y.J., Salhanick, A.I., Lubeski, C.K., Yang, L., Lemoine, L.M., Zhu, J., and Clairmont, K.B. (2005). Specific inhibition of hormone-sensitive lipase improves lipid profile while reducing plasma glucose. J. Pharmacol. Exp. Ther. *315*, 1396–1402.

Colditz, G.A., Willett, W.C., Rotnitzky, A., and Manson, J.E. (1995). Weight gain as a risk factor for clinical diabetes mellitus in women. Ann. Intern. Med. *122*, 481–486.

Collins, S., Yehuda-Shnaidman, E., and Wang, H. (2010). Positive and negative control of Ucp1 gene transcription and the role of β-adrenergic signaling networks. Int. J. Obes. *34*, S28–S33.

Contreras, C., Gonzalez, F., Fernø, J., Diéguez, C., Rahmouni, K., Nogueiras, R., and López, M. (2015). The brain and brown fat. Ann. Med. *47*, 150–168.

Cooper, G.M. (2000). Mitochondria. Cell Mol. Approach 2nd Ed.

Cousin, B., Cinti, S., Morroni, M., Raimbault, S., Ricquier, D., Pénicaud, L., and Casteilla, L. (1992). Occurrence of brown adipocytes in rat white adipose tissue: molecular and morphological characterization. J. Cell Sci. *103*, 931–942.

Cypess, A.M., Lehman, S., Williams, G., Tal, I., Rodman, D., Goldfine, A.B., Kuo, F.C., Palmer, E.L., Tseng, Y.-H., Doria, A., et al. (2009). Identification and importance of brown adipose tissue in adult humans. N. Engl. J. Med. *360*, 1509–1517.

DeFronzo, R.A., Ferrannini, E., Groop, L., Henry, R.R., Herman, W.H., Holst, J.J., Hu, F.B., Kahn, C.R., Raz, I., Shulman, G.I., et al. (2015). Type 2 diabetes mellitus. Nat. Rev. Dis. Primer. *1*, 15019.

Demine, S., Renard, P., and Arnould, T. (2019). Mitochondrial Uncoupling: A Key Controller of Biological Processes in Physiology and Diseases. Cells. *8*, 795.

Dietz, W.H., and Gortmaker, S.L. (1985). Do we fatten our children at the television set? Obesity and television viewing in children and adolescents. Pediatrics. *75*, 807–812.

DiPasquale, D.M., Kolkhorst, F.W., and Buono, M.J. (2015). Acute normobaric hypoxia reduces body temperature in humans. High Alt. Med. Biol. *16*, 61–66.

Dube, N., Khan, K., Loehr, S., Chu, Y., and Veugelers, P. (2017). The use of entertainment and communication technologies before sleep could affect sleep and weight status: a population-based study among children. Int. J. Behav. Nutr. Phys. Act. *14*, 97.

Duchen, M.R. (2004). Roles of Mitochondria in Health and Disease. Diabetes. *53*, S96–S102.

Duffey, K.J., Gordon-Larsen, P., Jacobs, D.R., Williams, O.D., and Popkin, B.M. (2007). Differential associations of fast food and restaurant food consumption with 3-y change in body mass index: the Coronary Artery Risk Development in Young Adults Study. Am. J. Clin. Nutr. *85*, 201–208.

Dulloo, A.G., and Miller, D.S. (1984). Energy balance following sympathetic denervation of brown adipose tissue. Can. J. Physiol. Pharmacol. *62*, 235–240.

Eckel, R.H., Jakicic, J.M., Ard, J.D., de Jesus, J.M., Houston Miller, N., Hubbard, V.S., Lee, I.-M., Lichtenstein, A.H., Loria, C.M., Millen, B.E., et al. (2014). 2013 AHA/ACC Guideline on Lifestyle Management to Reduce Cardiovascular Risk: A Report of the American College of Cardiology/American Heart Association Task Force on Practice Guidelines. J. Am. Coll. Cardiol. *63*, 2960–2984.

Enerbäck, S., Jacobsson, A., Simpson, E.M., Guerra, C., Yamashita, H., Harper, M.-E., and Kozak, L.P. (1997). Mice lacking mitochondrial uncoupling protein are cold-sensitive but not obese. Nature *387*, 90–94.

von Essen, G., Lindsund, E., Cannon, B., and Nedergaard, J. (2017). Adaptive facultative diet-induced thermogenesis in wild-type but not in UCP1-ablated mice. Am. J. Physiol. Endocrinol. Metab. *313*, E515–E527.

Esteve Ràfols, M. (2014). Adipose tissue: Cell heterogeneity and functional diversity. Endocrinol. Nutr. Engl. Ed. *61*, 100–112.

Farmer, S.R. (2008). Brown Fat and Skeletal Muscle: Unlikely Cousins? Cell. *134*, 726–727.

Fedorenko, A., Lishko, P.V., and Kirichok, Y. (2012). Mechanism of fatty-acid-dependent UCP1 uncoupling in brown fat mitochondria. Cell. *151*, 400–413.

Felson, D.T. (1995). Weight and osteoarthritis. J. Rheumatol. Suppl. *43*, 7–9.

Fischer, A.W., Schlein, C., Cannon, B., Heeren, J., and Nedergaard, J. (2018). Intact innervation is essential for diet-induced recruitment of brown adipose tissue. Am. J. Physiol.-Endocrinol. Metab. *316*, E487–E503.

Fogelholm, M., Valve, R., Kukkonen-Harjula, K., Nenonen, A., Hakkarainen, V., Laakso, M., and Uusitupa, M. (1998). Additive effects of the mutations in the beta3-adrenergic receptor and uncoupling protein-1 genes on weight loss and weight maintenance in Finnish women. J. Clin. Endocrinol. Metab. *83*, 4246–4250.

Foster, D.O., and Frydman, M.L. (1978). Nonshivering thermogenesis in the rat. II. Measurements of blood flow with microspheres point to brown adipose tissue as the dominant site of the calorigenesis induced by noradrenaline. Can. J. Physiol. Pharmacol. *56*, 110–122.

Foster, D.O., and Frydman, M.L. (1979). Tissue distribution of cold-induced thermogenesis in conscious warm- or cold-acclimated rats reevaluated from changes in tissue blood flow: The dominant role of brown adipose tissue in the replacement of shivering by nonshivering thermogenesis. Can. J. Physiol. Pharmacol. *57*, 257–270.

French, S.A., Harnack, L., and Jeffery, R.W. (2000). Fast food restaurant use among women in the Pound of Prevention study: dietary, behavioral and demographic correlates. Int. J. Obes. Relat. Metab. Disord. J. Int. Assoc. Study Obes. *24*, 1353–1359.

Frey, T.G., Perkins, G.A., and Ellisman, M.H. (2006). Electron tomography of membrane-bound cellular organelles. Annu. Rev. Biophys. Biomol. Struct. *35*, 199–224.

Frezza, C., Cipolat, S., Martins de Brito, O., Micaroni, M., Beznoussenko, G.V., Rudka, T., Bartoli, D., Polishuck, R.S., Danial, N.N., De Strooper, B., et al. (2006). OPA1 controls apoptotic cristae remodeling independently from mitochondrial fusion. Cell. *126*, 177–189.

Frühbeck, G., Gómez-Ambrosi, J., Muruzábal, F.J., and Burrell, M.A. (2001). The adipocyte: a model for integration of endocrine and metabolic signaling in energy metabolism regulation. Am. J. Physiol. Endocrinol. Metab. *280*, E827-847.

Fuemmeler, B.F., Agurs-Collins, T.D., McClernon, F.J., Kollins, S.H., Kail, M.E., Bergen, A.W., and Ashley-Koch, A.E. (2008). Genes implicated in serotonergic and dopaminergic functioning predict BMI categories. Obes. Silver Spring Md. *16*, 348–355.

Fukano, K., Okamatsu-Ogura, Y., Tsubota, A., Nio-Kobayashi, J., and Kimura, K. (2016). Cold Exposure Induces Proliferation of Mature Brown Adipocyte in a ß3-Adrenergic Receptor-Mediated Pathway. PLoS ONE. *11*.

Fumeron, F., Durack-Bown, I., Betoulle, D., Cassard-Doulcier, A.M., Tuzet, S., Bouillaud, F., Melchior, J.C., Ricquier, D., and Apfelbaum, M. (1996). Polymorphisms of uncoupling protein (UCP) and beta 3 adrenoreceptor genes in obese people submitted to a low calorie diet. Int. J. Obes. Relat. Metab. Disord. J. Int. Assoc. Study Obes. *20*, 1051–1054.

Garfinkel, L. (1985). Overweight and cancer. Ann. Intern. Med. *103*, 1034–1036.

Garvey, W.T., Garber, A.J., Mechanick, J.I., Bray, G.A., Dagogo-Jack, S., Einhorn, D., Grunberger, G., Handelsman, Y., Hennekens, C.H., Hurley, D.L., et al. (2014). American association of clinical endocrinologists and american college of endocrinology position statement on the 2014 advanced framework for a new diagnosis of obesity as a chronic disease. Endocr. Pract. Off. J. Am. Coll. Endocrinol. Am. Assoc. Clin. Endocrinol. *20*, 977–989.

Gautier, H., Bonora, M., Schultz, S.A., and Remmers, J.E. (1987). Hypoxia-induced changes in shivering and body temperature. J. Appl. Physiol. Bethesda Md. *62*, 2477–2484.

Ghorbani, M., and Himms-Hagen, J. (1997). Appearance of brown adipocytes in white adipose tissue during CL 316,243-induced reversal of obesity and diabetes in Zucker fa/fa rats. Int. J. Obes. Relat. Metab. Disord. J. Int. Assoc. Study Obes. *21*, 465–475.

Global BMI Mortality Collaboration, null, Di Angelantonio, E., Bhupathiraju, S., Wormser, D., Gao, P., Kaptoge, S., Berrington de Gonzalez, A., Cairns, B., Huxley, R., Jackson, C., et al. (2016). Body-mass index and all-cause mortality: individual-participant-data meta-analysis of 239 prospective studies in four continents. Lancet Lond. Engl. *388*, 776–786.

Golozoubova, V., Hohtola, E., Matthias, A., Jacobsson, A., Cannon, B., and Nedergaard, J. (2001). Only UCP1 can mediate adaptive nonshivering thermogenesis in the cold. FASEB J. *15*, 2048–2050.

de Gonzalez, A.B., Hartge, P., Cerhan, J.R., Flint, A.J., Hannan, L., MacInnis, R.J., Moore, S.C., Tobias, G.S., Anton-Culver, H., Freeman, L.B., et al. (2010). Body-Mass Index and Mortality among 1.46 Million White Adults. N. Engl. J. Med. *363*, 2211–2219.

Gordillo, M., Evans, T., and Gouon-Evans, V. (2015). Orchestrating liver development. Dev. Camb. Engl. *142*, 2094–2108.

Gordon, C.J., and Fogelson, L. (1991). Comparative effects of hypoxia on behavioral thermoregulation in rats, hamsters, and mice. Am. J. Physiol. *260*, R120-125.

Granneman, J.G., Burnazi, M., Zhu, Z., and Schwamb, L.A. (2003). White adipose tissue contributes to UCP1-independent thermogenesis. Am. J. Physiol. Endocrinol. Metab. *285*, E1230-1236.

Grattan, D.R. (2008). Fetal Programming from Maternal Obesity: Eating Too Much for Two? Endocrinology. *149*, 5345–5347.

Gruden, G., Landi, A., and Bruno, G. (2014). Natriuretic Peptides, Heart, and Adipose Tissue: New Findings and Future Developments for Diabetes Research. Diabetes Care. *37*, 2899–2908.

Gruppuso, P.A., and Sanders, J.A. (2016). Regulation of liver development: implications for liver biology across the lifespan. J. Mol. Endocrinol. *56*, R115-125.

Guh, D.P., Zhang, W., Bansback, N., Amarsi, Z., Birmingham, C.L., and Anis, A.H. (2009). The incidence of co-morbidities related to obesity and overweight: a systematic review and meta-analysis. BMC Public Health. *9*, 88.

ten Hacken, N.H.T. (2009). Physical inactivity and obesity: relation to asthma and chronic obstructive pulmonary disease? Proc. Am. Thorac. Soc. *6*, 663–667.

Hall, K.D., Ayuketah, A., Brychta, R., Cai, H., Cassimatis, T., Chen, K.Y., Chung, S.T., Costa, E., Courville, A., Darcey, V., et al. (2019). Ultra-Processed Diets Cause Excess Calorie Intake and Weight Gain: An Inpatient Randomized Controlled Trial of Ad Libitum Food Intake. Cell Metab. *30*, 67-77.e3.

Hany, T.F., Gharehpapagh, E., Kamel, E.M., Buck, A., Himms-Hagen, J., and von Schulthess, G.K. (2002). Brown adipose tissue: a factor to consider in symmetrical tracer uptake in the neck and upper chest region. Eur. J. Nucl. Med. Mol. Imaging. *29*, 1393–1398.

Hao, Q., Yadav, R., Basse, A.L., Petersen, S., Sonne, S.B., Rasmussen, S., Zhu, Q., Lu, Z., Wang, J., Audouze, K., et al. (2015). Transcriptome profiling of brown adipose tissue during cold exposure reveals extensive regulation of glucose metabolism. Am. J. Physiol. Endocrinol. Metab. *308*, E380-392.

Harmelen, V.V., Lönnqvist, F., Thörne, A., Wennlund, A., Large, V., Reynisdottir, S., and Arner, P. (1997). Noradrenaline-induced lipolysis in isolated mesenteric, omental and subcutaneous adipocytes from obese subjects. Int. J. Obes. *21*, 972–979.

Harms, M.M., and Seale, P. (2013). Brown and beige fat: development, function and therapeutic potential. Nat. Med. *19*, 1252–1263.

Haslam, D.W., and James, W.P.T. (2005). Obesity. The Lancet. *366*, 1197–1209.

Herman, M.A., Peroni, O.D., Villoria, J., Schön, M.R., Abumrad, N.A., Blüher, M., Klein, S., and Kahn, B.B. (2012). A novel ChREBP isoform in adipose tissue regulates systemic glucose metabolism. Nature. *484*, 333–338.

Herrera, B.M., Keildson, S., and Lindgren, C.M. (2011). Genetics and epigenetics of obesity. Maturitas. *69*, 41–49.

Hijmans, B.S., Grefhorst, A., Oosterveer, M.H., and Groen, A.K. (2014). Zonation of glucose and fatty acid metabolism in the liver: mechanism and metabolic consequences. Biochimie. *96*, 121–129.

Hill, J.O., and Commerford, R. (1996). Physical activity, fat balance, and energy balance. Int. J. Sport Nutr. *6*, 80–92.

Hill, J.O., Wyatt, H.R., and Peters, J.C. (2012). Energy Balance and Obesity. Circulation. *126*, 126–132.

Hilse, K.E., Kalinovich, A.V., Rupprecht, A., Smorodchenko, A., Zeitz, U., Staniek, K., Erben, R.G., and Pohl, E.E. (2016). The expression of UCP3 directly correlates to UCP1 abundance in brown adipose tissue. Biochim. Biophys. Acta *1857*, 72–78.

Himms-Hagen, J. (1985). Brown Adipose Tissue Metabolism and Thermogenesis. Annu. Rev. Nutr. *5*, 69–94.

Himms-Hagen, J. (1990). Brown adipose tissue thermogenesis: interdisciplinary studies. FASEB J. Off. Publ. Fed. Am. Soc. Exp. Biol. *4*, 2890–2898.

Himms-Hagen, J., Melnyk, A., Zingaretti, M.C., Ceresi, E., Barbatelli, G., and Cinti, S. (2000). Multilocular fat cells in WAT of CL-316243-treated rats derive directly from white adipocytes. Am. J. Physiol. Cell Physiol. *279*, C670-681.

Hirschey, M.D., and Zhao, Y. (2015). Metabolic Regulation by Lysine Malonylation, Succinylation, and Glutarylation. Mol. Cell. Proteomics MCP. *14*, 2308–2315.

Hirschey, M.D., Shimazu, T., Goetzman, E., Jing, E., Schwer, B., Lombard, D.B., Grueter, C.A., Harris, C., Biddinger, S., Ilkayeva, O.R., et al. (2010). SIRT3 regulates fatty acid oxidation via reversible enzyme deacetylation. Nature. *464*, 121–125.

Hirschey, M.D., Shimazu, T., Huang, J.-Y., Schwer, B., and Verdin, E. (2011). SIRT3 Regulates Mitochondrial Protein Acetylation and Intermediary Metabolism. Cold Spring Harb. Symp. Quant. Biol. *76*, 267–277.

Hondares, E., Rosell, M., Gonzalez, F.J., Giralt, M., Iglesias, R., and Villarroya, F. (2010). Hepatic FGF21 Expression Is Induced at Birth via PPARα in Response to Milk Intake and Contributes to Thermogenic Activation of Neonatal Brown Fat. Cell Metab. *11*, 206–212.

Hondares, E., Iglesias, R., Giralt, A., Gonzalez, F.J., Giralt, M., Mampel, T., and Villarroya, F. (2011). Thermogenic activation induces FGF21 expression and release in brown adipose tissue. J. Biol. Chem. *286*, 12983–12990.

Hu, F. (2008). Obesity Epidemiology (Oxford University Press, USA).

Ikeda, K., Maretich, P., and Kajimura, S. (2018). The Common and Distinct Features of Brown and Beige Adipocytes. Trends Endocrinol. Metab. *29*, 191–200.

Jakobs, S. (2006). High resolution imaging of live mitochondria. Biochim. Biophys. Acta *1763*, 561–575.

James, W.P.T. (2008). WHO recognition of the global obesity epidemic. Int. J. Obes. 2005 *32 Suppl 7*, S120-126.

Jeffery, R.W., and French, S.A. (1998). Epidemic obesity in the United States: are fast foods and television viewing contributing? Am. J. Public Health. *88*, 277–280.

Jeffery, R.W., Baxter, J., McGuire, M., and Linde, J. (2006). Are fast food restaurants an environmental risk factor for obesity? Int. J. Behav. Nutr. Phys. Act. *3*, 2.

Jensen M. D., Ryan Donna H., Apovian Caroline M., Ard Jamy D., Comuzzie Anthony G., Donato Karen A., Hu Frank B., Hubbard Van S., Jakicic John M., Kushner Robert F., et al. (2014). 2013 AHA/ACC/TOS Guideline for the Management of Overweight and Obesity in Adults. Circulation. *129*, S102–S138.

Jess, T. (2014). Microbiota, antibiotics, and obesity. N. Engl. J. Med. *371*, 2526–2528.

Jiang, F., Zhu, S., Yan, C., Jin, X., Bandla, H., and Shen, X. (2009). Sleep and obesity in preschool children. J. Pediatr. *154*, 814–818.

Jing, E., O'Neill, B.T., Rardin, M.J., Kleinridders, A., Ilkeyeva, O.R., Ussar, S., Bain, J.R., Lee, K.Y., Verdin, E.M., Newgard, C.B., et al. (2013). Sirt3 Regulates Metabolic Flexibility of Skeletal Muscle Through Reversible Enzymatic Deacetylation. Diabetes. *62*, 3404–3417.

de Jong, J.M.A., Larsson, O., Cannon, B., and Nedergaard, J. (2015). A stringent validation of mouse adipose tissue identity markers. Am. J. Physiol. Endocrinol. Metab. *308*, E1085-1105.

Kadowaki, H., Yasuda, K., Iwamoto, K., Otabe, S., Shimokawa, K., Silver, K., Walston, J., Yoshinaga, H., Kosaka, K., and Yamada, N. (1995). A mutation in the beta 3-adrenergic receptor gene is associated with obesity and hyperinsulinemia in Japanese subjects. Biochem. Biophys. Res. Commun. *215*, 555–560.

Kajimura, S., Spiegelman, B.M., and Seale, P. (2015). Brown and Beige Fat: Physiological Roles beyond Heat Generation. Cell Metab. *22*, 546–559.

Katz, L.S., Xu, S., Ge, K., Scott, D.K., and Gershengorn, M.C. (2017). T3 and Glucose Coordinately Stimulate ChREBP-Mediated Ucp1 Expression in Brown Adipocytes From Male Mice. Endocrinology. *159*, 557–569.

Kazak, L., Chouchani, E.T., Jedrychowski, M.P., Erickson, B.K., Shinoda, K., Cohen, P., Vetrivelan, R., Lu, G.Z., Laznik-Bogoslavski, D., Hasenfuss, S.C., et al. (2015). A creatine-driven substrate cycle enhances energy expenditure and thermogenesis in beige fat. Cell. *163*, 643–655.

Kelly, T., Yang, W., Chen, C.-S., Reynolds, K., and He, J. (2008). Global burden of obesity in 2005 and projections to 2030. Int. J. Obes. 2005 *32*, 1431–1437.

Kershaw, E.E., and Flier, J.S. (2004). Adipose tissue as an endocrine organ. J. Clin. Endocrinol. Metab. *89*, 2548–2556.

Khaodhiar, L., McCowen, K.C., and Blackburn, G.L. (1999). Obesity and its comorbid conditions. Clin. Cornerstone. *2*, 17–31.

Kimm, S.Y., Glynn, N.W., Obarzanek, E., Kriska, A.M., Daniels, S.R., Barton, B.A., and Liu, K. (2005). Relation between the changes in physical activity and body-mass index during adolescence: a multicentre longitudinal study. The Lancet. *366*, 301–307.

Kim-Motoyama, H., Yasuda, K., Yamaguchi, T., Yamada, N., Katakura, T., Shuldiner, A.R., Akanuma, Y., Ohashi, Y., Yazaki, Y., and Kadowaki, T. (1997). A mutation of the beta 3-adrenergic receptor is associated with visceral obesity but decreased serum triglyceride. Diabetologia. *40*, 469–472.

Klop, B., Elte, J.W.F., and Cabezas, M.C. (2013). Dyslipidemia in obesity: mechanisms and potential targets. Nutrients. *5*, 1218–1240.

Kohlmeier, M. (2003). Nutrient metabolism. (1st Edition). London: Academic Press.

Kong, X., Yao, T., Zhou, P., Kazak, L., Tenen, D., Lyubetskaya, A., Dawes, B.A., Tsai, L., Kahn, B.B., Spiegelman, B.M., et al. (2018). Brown Adipose Tissue Controls Skeletal Muscle Function via the Secretion of Myostatin. Cell Metab. *28*, 631-643.e3.

Kottke, F.J., and Phalen, J.S. (1948). Effect of hypoxia upon temperature regulation of mice, dogs, and man. Am. J. Physiol. *153*, 10–15.

Kumar, S., and Lombard, D.B. (2018). Functions of the sirtuin deacylase SIRT5 in normal physiology and pathobiology. Crit. Rev. Biochem. Mol. Biol. *53*, 311–334.

Labbé, S.M., Caron, A., Bakan, I., Laplante, M., Carpentier, A.C., Lecomte, R., and Richard, D. (2015). In vivo measurement of energy substrate contribution to cold-induced brown adipose tissue thermogenesis. FASEB J. Off. Publ. Fed. Am. Soc. Exp. Biol. *29*, 2046–2058.

Lafontan, M., and Berlan, M. (1993). Fat cell adrenergic receptors and the control of white and brown fat cell function. J. Lipid Res. *34*, 1057–1091.

Lagercrantz, J., Farnebo, F., Larsson, C., Tvrdik, T., Weber, G., and Piehl, F. (1998). A comparative study of the expression patterns for vegf, vegf-b/vrf and vegf-c in the developing and adult mouse. Biochim. Biophys. Acta. *1398*, 157–163.

Lau, D.C.W., Douketis, J.D., Morrison, K.M., Hramiak, I.M., Sharma, A.M., and Ur, E. (2007). 2006 Canadian clinical practice guidelines on the management and prevention of obesity in adults and children [summary]. CMAJ. *176*, S1–S13.

Leblanc, J., Dussault, J., Lupien, D., and Richard, D. (1982). Effect of diet and exercise on norepinephrine-induced thermogenesis in male and female rats. J. Appl. Physiol. *52*, 556–561.

Lee, H.-S. (2015). Impact of Maternal Diet on the Epigenome during In Utero Life and the Developmental Programming of Diseases in Childhood and Adulthood. Nutrients. *7*, 9492–9507.

Lewis, C.E., Smith, D.E., Wallace, D.D., Williams, O.D., Bild, D.E., and Jacobs, D.R. (1997). Seven-year trends in body weight and associations with lifestyle and behavioral characteristics in black and white young adults: the CARDIA study. Am. J. Public Health. *87*, 635–642.

Lim, S., Honek, J., and Cao, Y. (2013). Blood Vessels in White and Brown Adipose Tissues. In Angiogenesis in Adipose Tissue, Y. Cao, ed. (New York, NY: Springer New York), pp. 77–102.

Liu, D., Bordicchia, M., Zhang, C., Fang, H., Wei, W., Li, J.-L., Guilherme, A., Guntur, K., Czech, M.P., and Collins, S. (2016). Activation of mTORC1 is essential for β-adrenergic stimulation of adipose browning. J. Clin. Invest. *126*, 1704–1716.

Liu, D., Ceddia, R.P., and Collins, S. (2018). Cardiac natriuretic peptides promote adipose 'browning' through mTOR complex-1. Mol. Metab. *9*, 192–198.

Lodish, H., Berk, A., Zipursky, S.L., Matsudaira, P., Baltimore, D., and Darnell, J. (2000). Electron Transport and Oxidative Phosphorylation. Mol. Cell Biol. 4th Ed.

Long, J.Z., Svensson, K.J., Tsai, L., Zeng, X., Roh, H.C., Kong, X., Rao, R.R., Lou, J., Lokurkar, I., Baur, W., et al. (2014). A smooth muscle-like origin for beige adipocytes. Cell Metab. *19*, 810–820.

Longo, M., Zatterale, F., Naderi, J., Parrillo, L., Formisano, P., Raciti, G.A., Beguinot, F., and Miele, C. (2019). Adipose Tissue Dysfunction as Determinant of Obesity-Associated Metabolic Complications. Int. J. Mol. Sci. *20*, 2358.

Loos, R.J. (2018). The genetics of adiposity. Current Opinion in Genetics & Development. *50*, 86–95.

López, M., Varela, L., Vázquez, M.J., Rodríguez-Cuenca, S., González, C.R., Velagapudi, V.R., Morgan, D.A., Schoenmakers, E., Agassandian, K., Lage, R., et al. (2010). Hypothalamic AMPK and fatty acid metabolism mediate thyroid regulation of energy balance. Nat. Med. *16*, 1001–1008.

Manson, J.E., Colditz, G.A., Stampfer, M.J., Willett, W.C., Rosner, B., Monson, R.R., Speizer, F.E., and Hennekens, C.H. (1990). A prospective study of obesity and risk of coronary heart disease in women. N. Engl. J. Med. *322*, 882–889.

Manson, J.E., Willett, W.C., Stampfer, M.J., Colditz, G.A., Hunter, D.J., Hankinson, S.E., Hennekens, C.H., and Speizer, F.E. (1995). Body weight and mortality among women. N. Engl. J. Med. *333*, 677–685.

Marín-García, J., and Goldenthal, M.J. (2002). The Mitochondrial Organelle and the Heart. Rev. Esp. Cardiol. Engl. Ed. *55*, 1293–1310.

van Marken Lichtenbelt, W.D., Vanhommerig, J.W., Smulders, N.M., Drossaerts, J.M.A.F.L., Kemerink, G.J., Bouvy, N.D., Schrauwen, P., and Teule, G.J.J. (2009). Cold-Activated Brown Adipose Tissue in Healthy Men. N Engl J Med. *360*,1500-1508.

Marshall, J.D., Maffei, P., Collin, G.B., and Naggert, J.K. (2011). Alström syndrome: genetics and clinical overview. Curr. Genomics. *12*, 225–235.

Martínez-Sánchez, N., Moreno-Navarrete, J.M., Contreras, C., Rial-Pensado, E., Fernø, J., Nogueiras, R., Diéguez, C., Fernández-Real, J.-M., and López, M. (2016). Thyroid hormones induce browning of white fat. J. Endocrinol. *232*, 351–362.

Martínez-Sánchez, N., Seoane-Collazo, P., Contreras, C., Varela, L., Villarroya, J., Rial-Pensado, E., Buqué, X., Aurrekoetxea, I., Delgado, T.C., Vázquez-Martínez, R., et al. (2017). Hypothalamic AMPK-ER Stress-JNK1 Axis Mediates the Central Actions of Thyroid Hormones on Energy Balance. Cell Metab. *26*, 212-229.e12.

McMurray, F., MacFarlane, M., Kim, K., Patten, D.A., Wei-LaPierre, L., Fullerton, M.D., and Harper, M.-E. (2019). Maternal diet–induced obesity alters muscle mitochondrial function in offspring without changing insulin sensitivity. FASEB J. *33*,13515-13526

Menke, A., Rust, K.F., Fradkin, J., Cheng, Y.J., and Cowie, C.C. (2014). Associations between trends in race/ethnicity, aging, and body mass index with diabetes prevalence in the United States: a series of cross-sectional studies. Ann. Intern. Med. *161*, 328–335.

Mileykovskaya, E., Zhang, M., and Dowhan, W. (2005). Cardiolipin in energy transducing membranes. Biochem. Biokhimiia. *70*, 154–158.

Mills, E.L., Pierce, K.A., Jedrychowski, M.P., Garrity, R., Winther, S., Vidoni, S., Yoneshiro, T., Spinelli, J.B., Lu, G.Z., Kazak, L., et al. (2018). Accumulation of succinate controls activation of adipose tissue thermogenesis. Nature. *560*, 102-106

Murphy, M.P. (2009). How mitochondria produce reactive oxygen species. Biochem. J. *417*, 1–13.

Nedergaard, J., Bengtsson, T., and Cannon, B. (2007). Unexpected evidence for active brown adipose tissue in adult humans. Am. J. Physiol. Endocrinol. Metab. *293*, E444-452.

Nedergaard, J., Bengtsson, T., and Cannon, B. (2011). New powers of brown fat: fighting the metabolic syndrome. Cell Metab. *13*, 238–240.

Ng, M., Fleming, T., Robinson, M., Thomson, B., Graetz, N., Margono, C., Mullany, E.C., Biryukov, S., Abbafati, C., Abera, S.F., et al. (2014). Global, regional, and national prevalence of overweight and obesity in children and adults during 1980-2013: a systematic analysis for the Global Burden of Disease Study 2013. Lancet Lond. Engl. *384*, 766–781.

Nicholls, D.G. (2006). The physiological regulation of uncoupling proteins. Biochim. Biophys. Acta BBA - Bioenerg. *1757*, 459–466.

Oetting, A., and Yen, P.M. (2007). New insights into thyroid hormone action. Best Pract. Res. Clin. Endocrinol. Metab. *21*, 193–208.

Ohta, K. (2014). The Role of Tsukushi as an Extracellular Signaling Coordinator. In New Principles in Developmental Processes, H. Kondoh, and A. Kuroiwa, eds. (Tokyo: Springer Japan), pp. 227–238.

Ohta, K., Lupo, G., Kuriyama, S., Keynes, R., Holt, C.E., Harris, W.A., Tanaka, H., and Ohnuma, S.-I. (2004). Tsukushi functions as an organizer inducer by inhibition of BMP activity in cooperation with chordin. Dev. Cell. *7*, 347–358.

Olsen, J.M., Sato, M., Dallner, O.S., Sandström, A.L., Pisani, D.F., Chambard, J.-C., Amri, E.-Z., Hutchinson, D.S., and Bengtsson, T. (2014). Glucose uptake in brown fat cells is dependent on mTOR complex 2-promoted GLUT1 translocation. J. Cell Biol. *207*, 365–374.

Oppert, J.M., Vohl, M.C., Chagnon, M., Dionne, F.T., Cassard-Doulcier, A.M., Ricquier, D., Pérusse, L., and Bouchard, C. (1994). DNA polymorphism in the uncoupling protein (UCP) gene and human body fat. Int. J. Obes. Relat. Metab. Disord. J. Int. Assoc. Study Obes. *18*, 526–531.

World Health Organization. (2014). Global status report on noncommunicable diseases 2014: attaining the nine global noncommunicable diseases targets; a shared responsibility. Accessed September22, 2019.

Ostrowski, M., Carmo, N.B., Krumeich, S., Fanget, I., Raposo, G., Savina, A., Moita, C.F., Schauer, K., Hume, A.N., Freitas, R.P., et al. (2010). Rab27a and Rab27b control different steps of the exosome secretion pathway. Nat. Cell Biol. *12*, 19–30.

Pallotti, F., and Lenaz, G. (2001). Chapter 1 Isolation and subfractionation of mitochondria from animal cells and tissue culture lines. In Methods in Cell Biology, (Academic Press), pp. 1–35.

Pamenter, M.E., Dzal, Y.A., and Milsom, W.K. (2015). Adenosine receptors mediate the hypoxic ventilatory response but not the hypoxic metabolic response in the naked mole rat during acute hypoxia. Proc. Biol. Sci. *282*, 20141722.

Pamenter, M.E., Lau, G.Y., Richards, J.G., and Milsom, W.K. (2018). Naked mole rat brain mitochondria electron transport system flux and H+ leak are reduced during acute hypoxia. J. Exp. Biol. *221*, jeb171397.

Park, A., Kim, W.K., and Bae, K.-H. (2014). Distinction of white, beige and brown adipocytes derived from mesenchymal stem cells. World J. Stem Cells. *6*, 33–42.

Park, H., He, A., Tan, M., Johnson, J.M., Dean, J.M., Pietka, T.A., Chen, Y., Zhang, X., Hsu, F.-F., Razani, B., et al. (2019). Peroxisome-derived lipids regulate adipose thermogenesis by mediating cold-induced mitochondrial fission. J. Clin. Invest. *129*, 694–711.

Park, J., Chen, Y., Tishkoff, D.X., Peng, C., Tan, M., Dai, L., Xie, Z., Zhang, Y., Zwaans, B.M.M., Skinner, M.E., et al. (2013). SIRT5-mediated lysine desuccinylation impacts diverse metabolic pathways. Mol. Cell. *50*, 919–930.

Park, T.J., Reznick, J., Peterson, B.L., Blass, G., Omerbašić, D., Bennett, N.C., Kuich, P.H.J.L., Zasada, C., Browe, B.M., Hamann, W., et al. (2017). Fructose-driven glycolysis supports anoxia resistance in the naked mole-rat. Science. *356*, 307–311.

Partinen, M. (1995). Epidemiology of obstructive sleep apnea syndrome. Curr. Opin. Pulm. Med. *1*, 482–487.

Patten, D.A., Wong, J., Khacho, M., Soubannier, V., Mailloux, R.J., Pilon-Larose, K., MacLaurin, J.G., Park, D.S., McBride, H.M., Trinkle-Mulcahy, L., et al. (2014). OPA1-dependent cristae modulation is essential for cellular adaptation to metabolic demand. EMBO J. *33*, 2676–2691.

Pereira, M.A., Kartashov, A.I., Ebbeling, C.B., Horn, L.V., Slattery, M.L., Jacobs, P.D.R., and Ludwig, D.S. (2005). Fast-food habits, weight gain, and insulin resistance (the CARDIA study): 15-year prospective analysis. Lancet. *365*, 36–42.

Pfanner, N., Laan, M. van der, Amati, P., Capaldi, R.A., Caudy, A.A., Chacinska, A., Darshi, M., Deckers, M., Hoppins, S., Icho, T., et al. (2014). Uniform nomenclature for the mitochondrial contact site and cristae organizing system. J. Cell Biol. *204*, 1083–1086.

Pietiläinen, K.H., Kaprio, J., Borg, P., Plasqui, G., Yki-Järvinen, H., Kujala, U.M., Rose, R.J., Westerterp, K.R., and Rissanen, A. (2008). Physical inactivity and obesity: a vicious circle. Obes. Silver Spring Md. *16*, 409–414.

Pollack A. (2013). AMA Recognizes Obesity as a Disease. NYT imescom. 2013 Available at: http://nyti.ms/1Guko03. Accessed November 20, 2019.

Rajala, M.W., and Scherer, P.E. (2003). Minireview: The adipocyte--at the crossroads of energy homeostasis, inflammation, and atherosclerosis. Endocrinology. *144*, 3765–3773.

Rao, R.R., Long, J.Z., White, J.P., Svensson, K.J., Lou, J., Lokurkar, I., Jedrychowski, M.P., Ruas, J.L., Wrann, C.D., Lo, J.C., et al. (2014). Meteorin-like Is a Hormone that Regulates Immune-Adipose Interactions to Increase Beige Fat Thermogenesis. Cell. *157*, 1279–1291.

Raposo, G., and Stoorvogel, W. (2013). Extracellular vesicles: exosomes, microvesicles, and friends. J. Cell Biol. *200*, 373–383.

Ravelli, A.C., van der Meulen, J.H., Osmond, C., Barker, D.J., and Bleker, O.P. (1999). Obesity at the age of 50 y in men and women exposed to famine prenatally. Am. J. Clin. Nutr. *70*, 811–816.

Reinehr, T., Hinney, A., de Sousa, G., Austrup, F., Hebebrand, J., and Andler, W. (2007). Definable somatic disorders in overweight children and adolescents. J. Pediatr. *150*, 618–622, 622.e1-5.

Roberts, L.D., Boström, P., O'Sullivan, J.F., Schinzel, R.T., Lewis, G.D., Dejam, A., Lee, Y.-K., Palma, M.J., Calhoun, S., Georgiadi, A., et al. (2014). β-Aminoisobutyric Acid Induces Browning of White Fat and Hepatic β-Oxidation and Is Inversely Correlated with Cardiometabolic Risk Factors. Cell Metab. *19*, 96–108.

Roseboom, T.J., van der Meulen, J.H.P., Ravelli, A.C.J., Osmond, C., Barker, D.J.P., and Bleker, O.P. (2001). Effects of prenatal exposure to the Dutch famine on adult disease in later life: an overview. Mol. Cell. Endocrinol. *185*, 93–98.

Rosen, E.D., and Spiegelman, B.M. (2014). What We Talk About When We Talk About Fat. Cell. *156*, 20–44.

Rothwell, N.J., and Stock, M.J. (1984). Effects of denervating brown adipose tissue on the responses to cold, hyperphagia and noradrenaline treatment in the rat. J. Physiol. *355*, 457–463.

Rich P. (2015) CMA recognizes obesity as a disease. www.cma.ca/En/Pages/cmarecognizes-obesity-as-a-disease.aspx2015. Accessed November 20, 2019.

Rui, L. (2014). Energy metabolism in the liver. Compr. Physiol. *4*, 177–197.

Sacks, H., and Symonds, M.E. (2013). Anatomical Locations of Human Brown Adipose Tissue. Diabetes. *62*, 1783–1790.

Saito, M. (2013). Brown Adipose Tissue as a Regulator of Energy Expenditure and Body Fat in Humans. Diabetes Metab. J. *37*, 22–29.

Sanchez-Gurmaches, J., Hung, C.-M., Sparks, C.A., Tang, Y., Li, H., and Guertin, D.A. (2012). PTEN loss in the Myf5 lineage redistributes body fat and reveals subsets of white adipocytes that arise from Myf5 precursors. Cell Metab. *16*, 348–362.

Sanchez-Gurmaches, J., Hung, C.-M., and Guertin, D.A. (2016). Emerging Complexities in Adipocyte Origins and Identity. Trends Cell Biol. *26*, 313–326.

Sarangarajan, R., Meera, S., Rukkumani, R., Sankar, P., and Anuradha, G. (2017). Antioxidants: Friend or foe? Asian Pac. J. Trop. Med. *10*, 1111–1116.

Scerif, M., Goldstone, A.P., and Korbonits, M. (2011). Ghrelin in obesity and endocrine diseases. Mol. Cell. Endocrinol. *340*, 15–25.

Scherer, P.E., Williams, S., Fogliano, M., Baldini, G., and Lodish, H.F. (1995). A novel serum protein similar to C1q, produced exclusively in adipocytes. J. Biol. Chem. *270*, 26746–26749.

Schweiger, M., Schreiber, R., Haemmerle, G., Lass, A., Fledelius, C., Jacobsen, P., Tornqvist, H., Zechner, R., and Zimmermann, R. (2006). Adipose Triglyceride Lipase and Hormone-sensitive Lipase Are the Major Enzymes in Adipose Tissue Triacylglycerol Catabolism. J. Biol. Chem. *281*, 40236–40241.

Seale, P., Bjork, B., Yang, W., Kajimura, S., Chin, S., Kuang, S., Scimè, A., Devarakonda, S., Conroe, H.M., Erdjument-Bromage, H., et al. (2008). PRDM16 controls a brown fat/skeletal muscle switch. Nature. *454*, 961–967.

Shabalina, I.G., Jacobsson, A., Cannon, B., and Nedergaard, J. (2004). Native UCP1 Displays Simple Competitive Kinetics between the Regulators Purine Nucleotides and Fatty Acids. J. Biol. Chem. *279*, 38236–38248.

Shaw, J.M., and Nunnari, J. (2002). Mitochondrial dynamics and division in budding yeast. Trends Cell Biol. *12*, 178–184.

Shi, F., and Collins, S. (2017). Second messenger signaling mechanisms of the brown adipocyte thermogenic program: an integrative perspective. Horm. Mol. Biol. Clin. Investig. *31*.

Shi, T., Wang, F., Stieren, E., and Tong, Q. (2005). SIRT3, a Mitochondrial Sirtuin Deacetylase, Regulates Mitochondrial Function and Thermogenesis in Brown Adipocytes. J. Biol. Chem. *280*, 13560–13567.

Shimizu, I., Aprahamian, T., Kikuchi, R., Shimizu, A., Papanicolaou, K.N., MacLauchlan, S., Maruyama, S., and Walsh, K. (2014). Vascular rarefaction mediates whitening of brown fat in obesity. J. Clin. Invest. *124*, 2099–2112.

Shimizu, Y., Satoh, S., Yano, H., Minokoshi, Y., Cushman, S.W., and Shimazu, T. (1998). Effects of noradrenaline on the cell-surface glucose transporters in cultured brown adipocytes: novel mechanism for selective activation of GLUT1 glucose transporters. Biochem. J. *330 ( Pt 1)*, 397–403.

Shin, H.D., Kim, K.S., Cha, M.H., and Yoon, Y. (2005). The effects of UCP-1 polymorphisms on obesity phenotypes among Korean female subjects. Biochem. Biophys. Res. Commun. *335*, 624–630.

Simbeni, R., Pon, L., Zinser, E., Paltauf, F., and Daum, G. (1991). Mitochondrial membrane contact sites of yeast. Characterization of lipid components and possible involvement in intramitochondrial translocation of phospholipids. J. Biol. Chem. *266*, 10047–10049.

Sipiläinen, R., Uusitupa, M., Heikkinen, S., Rissanen, A., and Laakso, M. (1997). Polymorphism of the beta3-adrenergic receptor gene affects basal metabolic rate in obese Finns. Diabetes. *46*, 77–80.

Smith, R.E., and Horwitz, B.A. (1969). Brown fat and thermogenesis. Physiol. Rev. *49*, 330–425.

Soo Kim, K., Cho, D.-Y., Joo Kim, Y., Choi, S.M., Kim, J.Y., Shin, S.U., and Yoon, Y.S. (2005). The finding of new genetic polymorphism of UCP-1 A-1766G and its effects on body fat accumulation. Biochim. Biophys. Acta BBA - Mol. Basis Dis. *1741*, 149–155.

Soulez, B., Dewailly, D., and Rosenfield, R.L. (1996). Polycystic Ovary Syndrome: A Multidisciplinary Challenge. The Endocrinologist. *6*, 19.

Spiegelman, B.M., and Flier, J.S. (2001). Obesity and the Regulation of Energy Balance. Cell. *104*, 531–543.

Spiegelman, B.M., Hu, E., Kim, J.B., and Brun, R. (1997). PPARγ and the control of adipogenesis. Biochimie. *79*, 111–112.

Statistics Canada. (2019). Overweight and obese adults, 2018. 82-625-X. Version released June 25th, 2019. Ottawa. ISSN: 1920-9118. https://www150.statcan.gc.ca/n1/pub/82-625-x/2019001/article/00005-eng.htm. Accessed December4, 2019.

Stanford, K.I., Lynes, M.D., Takahashi, H., Baer, L.A., Arts, P.J., May, F.J., Lehnig, A.C., Middelbeek, R.J.W., Richard, J.J., So, K., et al. (2018). 12,13-diHOME: An Exercise-Induced Lipokine that Increases Skeletal Muscle Fatty Acid Uptake. Cell Metab. *27*, 1111-1120.e3.

Strosberg, A.D. (1997). Association of β3-adrenoceptor polymorphism with obesity and diabetes: current status. Trends Pharmacol. Sci. *18*, 449–454.

Suspitsin, E.N., and Imyanitov, E.N. (2016). Bardet-Biedl Syndrome. Mol. Syndromol. *7*, 62–71.

Sustarsic, E.G., Ma, T., Lynes, M.D., Larsen, M., Karavaeva, I., Havelund, J.F., Nielsen, C.H., Jedrychowski, M.P., Moreno-Torres, M., Lundh, M., et al. (2018). Cardiolipin Synthesis in Brown and Beige Fat Mitochondria Is Essential for Systemic Energy Homeostasis. Cell Metab. *28*, 159-174.e11.

Taber, D.R., Chriqui, J.F., Powell, L., and Chaloupka, F.J. (2013). Association between state laws governing school meal nutrition content and student weight status: implications for new USDA school meal standards. JAMA Pediatr. *167*, 513–519.

Tammelin, T., Laitinen, J., and Näyhä, S. (2004). Change in the level of physical activity from adolescence into adulthood and obesity at the age of 31 years. Int. J. Obes. *28*, 775–782.

Tan, M., Peng, C., Anderson, K.A., Chhoy, P., Xie, Z., Dai, L., Park, J., Chen, Y., Huang, H., Zhang, Y., et al. (2014). Lysine glutarylation is a protein posttranslational modification regulated by SIRT5. Cell Metab. *19*, 605–617.

Tattersall, G.J., and Milsom, W.K. (2009). Hypoxia reduces the hypothalamic thermogenic threshold and thermosensitivity. J. Physiol. *587*, 5259–5274.

Théry, C., Witwer, K.W., Aikawa, E., Alcaraz, M.J., Anderson, J.D., Andriantsitohaina, R., Antoniou, A., Arab, T., Archer, F., Atkin-Smith, G.K., et al. (2018). Minimal information for studies of extracellular vesicles 2018 (MISEV2018): a position statement of the International Society for Extracellular Vesicles and update of the MISEV2014 guidelines. Journal of Extracellular Vesicles. *7*, 1535750.

Thomou, T., Mori, M.A., Dreyfuss, J.M., Konishi, M., Sakaguchi, M., Wolfrum, C., Rao, T.N., Winnay, J.N., Garcia-Martin, R., Grinspoon, S.K., et al. (2017). Adipose-derived circulating miRNAs regulate gene expression in other tissues. Nature. *542*, 450–455.

Trasande, L., Attina, T.M., and Blustein, J. (2012). Association between urinary bisphenol A concentration and obesity prevalence in children and adolescents. JAMA *308*, 1113–1121.

Trayhurn, P. (2005). Adipose Tissue in Obesity—An Inflammatory Issue. Endocrinology. *146*, 1003–1005.

Trayhurn, P., and Beattie, J.H. (2001). Physiological role of adipose tissue: white adipose tissue as an endocrine and secretory organ. Proc. Nutr. Soc. *60*, 329–339.

Trayhurn, P., and Wood, I.S. (2004). Adipokines: inflammation and the pleiotropic role of white adipose tissue. Br. J. Nutr. *92*, 347–355.

Trefts, E., Williams, A.S., and Wasserman, D.H. (2015). Exercise and the Regulation of Hepatic Metabolism. Prog. Mol. Biol. Transl. Sci. *135*, 203–225.

Trefts, E., Gannon, M., and Wasserman, D.H. (2017). The liver. Curr. Biol. *27*, R1147–R1151.

Tucker, L.A., and Friedman, G.M. (1989). Television viewing and obesity in adult males. Am. J. Public Health. *79*, 516–518.

Turta, O., and Rautava, S. (2016). Antibiotics, obesity and the link to microbes - what are we doing to our children? BMC Med. *14*, 57.

Tzameli, I. (2012). The evolving role of mitochondria in metabolism. Trends Endocrinol. Metab. *23*, 417–419.

Ukropec, J., Anunciado, R.P., Ravussin, Y., Hulver, M.W., and Kozak, L.P. (2006). UCP1-independent thermogenesis in white adipose tissue of cold-acclimated Ucp1-/- mice. J. Biol. Chem. *281*, 31894–31908.

Umekawa, T., Yoshida, T., Sakane, N., Kogure, A., Kondo, M., and Honjyo, H. (1999). Trp64Arg mutation of beta3-adrenoceptor gene deteriorates lipolysis induced by beta3-adrenoceptor agonist in human omental adipocytes. Diabetes. *48*, 117–120.

Vaughan, C.H., and Bartness, T.J. (2012). Anterograde transneuronal viral tract tracing reveals central sensory circuits from brown fat and sensory denervation alters its thermogenic responses. Am. J. Physiol. Regul. Integr. Comp. Physiol. *302*, R1049-1058.

Vickers, M.H., Breier, B.H., Cutfield, W.S., Hofman, P.L., and Gluckman, P.D. (2000). Fetal origins of hyperphagia, obesity, and hypertension and postnatal amplification by hypercaloric nutrition. Am. J. Physiol. Endocrinol. Metab. *279*, E83-87.

Villarroya, F., Cereijo, R., Villarroya, J., and Giralt, M. (2017). Brown adipose tissue as a secretory organ. Nat. Rev. Endocrinol. *13*, 26–35.

Virtanen, K.A., Lidell, M.E., Orava, J., Heglind, M., Westergren, R., Niemi, T., Taittonen, M., Laine, J., Savisto, N.-J., Enerbäck, S., et al. (2009). Functional brown adipose tissue in healthy adults. N. Engl. J. Med. *360*, 1518–1525.

Waldman, S.A., Rapoport, R.M., and Murad, F. (1984). Atrial natriuretic factor selectively activates particulate guanylate cyclase and elevates cyclic GMP in rat tissues. J. Biol. Chem. *259*, 14332–14334.

Walsh, J.A. (2013). Obesity & the First Law of Thermodynamics. Am. Biol. Teach. *75*, 413–415.

Walsh, C.T., Garneau-Tsodikova, S., and Gatto, G.J. (2005). Protein posttranslational modifications: the chemistry of proteome diversifications. Angew. Chem. Int. Ed Engl. *44*, 7342–7372.

Wang, Y. (2001). Cross-national comparison of childhood obesity: the epidemic and the relationship between obesity and socioeconomic status. Int. J. Epidemiol. *30*, 1129–1136.

Wang, H., and Eckel, R.H. (2009). Lipoprotein lipase: from gene to obesity. Am. J. Physiol.-Endocrinol. Metab. *297*, E271–E288.

Wang, G., Meyer, J.G., Cai, W., Softic, S., Li, M.E., Verdin, E., Newgard, C., Schilling, B., and Kahn, C.R. (2019a). Regulation of UCP1 and Mitochondrial Metabolism in Brown Adipose Tissue by Reversible Succinylation. Mol. Cell. *74*, 844-857.e7.

Wang, G.-X., Zhao, X.-Y., Meng, Z.-X., Kern, M., Dietrich, A., Chen, Z., Cozacov, Z., Zhou, D., Okunade, A.L., Su, X., et al. (2014). The brown fat-enriched secreted factor Nrg4 preserves metabolic homeostasis through attenuation of hepatic lipogenesis. Nat. Med. *20*, 1436–1443.

Wang, H., Zhang, Y., Yehuda-Shnaidman, E., Medvedev, A.V., Kumar, N., Daniel, K.W., Robidoux, J., Czech, M.P., Mangelsdorf, D.J., and Collins, S. (2008). Liver X Receptor α Is a Transcriptional Repressor of the Uncoupling Protein 1 Gene and the Brown Fat Phenotype. Mol Cell Biol. *28*, 2187–2200.

Wang, J., Adab, P., Liu, W., Chen, Y., Li, B., Lin, R., Liu, W., Cheng, K.K., and Pallan, M. (2017). Prevalence of adiposity and its association with sleep duration, quality, and timing among 9-12-year-old children in Guangzhou, China. J. Epidemiol. *27*, 531–537.

Wang, Q., Sharma, V.P., Shen, H., Xiao, Y., Zhu, Q., Xiong, X., Guo, L., Jiang, L., Ohta, K., Li, S., et al. (2019b). The hepatokine Tsukushi gates energy expenditure via brown fat sympathetic innervation. Nat. Metab. *1*, 251–260.

Wang, Y., Rimm, E.B., Stampfer, M.J., Willett, W.C., and Hu, F.B. (2005). Comparison of abdominal adiposity and overall obesity in predicting risk of type 2 diabetes among men. Am. J. Clin. Nutr. *81*, 555–563.

Warner, M., Wesselink, A., Harley, K.G., Bradman, A., Kogut, K., and Eskenazi, B. (2014). Prenatal exposure to dichlorodiphenyltrichloroethane and obesity at 9 years of age in the CHAMACOS study cohort. Am. J. Epidemiol. *179*, 1312–1322.

Weiner, J., Kranz, M., Klöting, N., Kunath, A., Steinhoff, K., Rijntjes, E., Köhrle, J., Zeisig, V., Hankir, M., Gebhardt, C., et al. (2016). Thyroid hormone status defines brown adipose tissue activity and browning of white adipose tissues in mice. Sci. Rep. *6*, 38124.

Weiner, J., Hankir, M., Heiker, J.T., Fenske, W., and Krause, K. (2017). Thyroid hormones and browning of adipose tissue. Mol. Cell. Endocrinol. *458*, 156–159.

Wicksteed, B., and Dickson, L.M. (2017). PKA Differentially Regulates Adipose Depots to Control Energy Expenditure. Endocrinology. *158*, 464–466.

Wikstrom, J.D., Mahdaviani, K., Liesa, M., Sereda, S.B., Si, Y., Las, G., Twig, G., Petrovic, N., Zingaretti, C., Graham, A., et al. (2014). Hormone-induced mitochondrial fission is utilized by brown adipocytes as an amplification pathway for energy expenditure. EMBO J. *33*, 418–436.

Willett, W.C., Manson, J.E., Stampfer, M.J., Colditz, G.A., Rosner, B., Speizer, F.E., and Hennekens, C.H. (1995). Weight, weight change, and coronary heart disease in women. Risk within the “normal” weight range. JAMA. *273*, 461–465.

Yang, R., and Barouch, L.A. (2007). Leptin signaling and obesity: cardiovascular consequences. Circ. Res. *101*, 545–559.

Young, P., Arch, J.R., and Ashwell, M. (1984). Brown adipose tissue in the parametrial fat pad of the mouse. FEBS Lett. *167*, 10–14.

Yu, X.X., Lewin, D.A., Forrest, W., and Adams, S.H. (2002). Cold elicits the simultaneous induction of fatty acid synthesis and β-oxidation in murine brown adipose tissue: prediction from differential gene expression and confirmation in vivo. FASEB J. *16*, 155–168.

Zhang, W., and Bi, S. (2015). Hypothalamic Regulation of Brown Adipose Tissue Thermogenesis and Energy Homeostasis. Front. Endocrinol. *6*.

Zhang, Y., Proenca, R., Maffei, M., Barone, M., Leopold, L., and Friedman, J.M. (1994). Positional cloning of the mouse obese gene and its human homologue. Nature. *372*, 425–432.

Zingaretti, M.C., Crosta, F., Vitali, A., Guerrieri, M., Frontini, A., Cannon, B., Nedergaard, J., and Cinti, S. (2009). The presence of UCP1 demonstrates that metabolically active adipose tissue in the neck of adult humans truly represents brown adipose tissue. FASEB J. Off. Publ. Fed. Am. Soc. Exp. Biol. *23*, 3113–3120.

de Zwaan, M. (2001). Binge eating disorder and obesity. Int. J. Obes. Relat. Metab. Disord. J. Int. Assoc. Study Obes. *25 Suppl 1*, S51-55.

## CHAPTER 2: SIRT3 CONTROLS BROWN FAT THERMOGENESIS BY DEACETYLATION REGULATION OF PATHWAYS UPSTREAM OF UCP1

Rajaa Sebaa[1,2,3], Jeff Johnson[4], Chantal Pileggi[1], Michaela Norgren[1], Jian Xuan[1], Yuka Sai[2,5], Qiang Tong[6], Izabella Krystkowiak[7], Emma Bondy-Chorney[2,5], Norman E. Davey[7,8], Nevan Krogan[4], Michael Downey[2,5]* and Mary-Ellen Harper[1,2]*

[1]Department of Biochemistry, Microbiology and Immunology, Faculty of Medicine, University of Ottawa, Ottawa, ON, Canada
[2]Ottawa Institute of Systems Biology, Faculty of Medicine, University of Ottawa, Ottawa, ON, Canada
[3]Department of Medical Laboratories, College of Applied Medical Sciences, University of Shaqra, Duwadimi, Saudi Arabia
[4]Department of Cellular and Molecular Pharmacology, University of California, San Francisco, San Francisco, CA, USA
[5]Department of Cellular and Molecular Medicine, Faculty of Medicine, University of Ottawa, Ottawa, ON, Canada
[6]USDA/ARS Children's Nutrition Research Center, Department of Pediatrics, Baylor College of Medicine, Houston, Texas, USA
[7]Conway Institute of Biomolecular & Biomedical Research, University College Dublin, Belfield, Dublin 4, Ireland
[8]Division of Cancer Biology, The Institute of Cancer Research, 237 Fulham Road, London SW3 6JB, UK

*** To whom correspondence should be addressed:**
Dr. Mary-Ellen Harper, PhD
Professor
Department of Biochemistry, Microbiology and Immunology
Ottawa Institute of Systems Biology
Faculty of Medicine, University of Ottawa
451 Smyth Road, Ottawa, ON Canada, ON K1H 8M5
Email: mharper@uottawa.ca
Tel: +1-613-562-5800 Ext 8235

Dr. Michael Downey**,** PhD
Assistant Professor
Department of Cellular and Molecular Medicine
Ottawa Institute of Systems Biology
Faculty of Medicine, University of Ottawa
451 Smyth Road, Ottawa, ON Canada, ON K1H 8M5
Email: mdowne2@uottawa.ca
Tel: +613-562-5800 Ext 8908

## 2.1 STATEMENT OF MANUSCRIPT STATUS AND CONTRIBUTIONS

### 2.1.1 STATEMENT OF MANUSCRIPT STATUS

The manuscript “SIRT3 controls brown fat thermogenesis by deacetylation regulation of pathways upstream of UCP1” has been published at the Journal of Molecular Metabolism on April 11, 2019.

### 2.1.2 CONTRIBUTION STATEMENT

RS, MD and MEH conceived the ideas for the project. RS conducted most of the experiments and analyzed most of the results. MD helped with mass spectrometry (MS) sample preparation, analyzed MS data and prepared MS related figures. JJ conducted mass spectrometry analysis. CP helped with many high resolution respirometry analyses of the electron transport chain complexes. MN helped with western blotting and histological analyses. JX helped with *in vivo* analyses of mice, genotyping and colony maintenance. YS helped with MS sample prep. EBC helped to design UCP1 constructs and contributed expertise for cell culture. QT provided *Sirt3*KO mice and expert advice. NK supervised the work of JJ. IK and NED carried out the acetylation annotation analysis. RS, MD and MEH drafted and wrote the paper. All authors read and approved the paper.

### 2.1.3 ACKNOWLEDGEMENTS AND FUNDING

Authors are very grateful for the expert advice of Dr. Martin Jastroch (Wenner-Gren Institute, Stockholm University) during the optimization of Seahorse analyses of UCP1 transfected HEK293T cells. We would like to thank the Newborn Screening group at the Children's Hospital of Eastern Ontario for their expert assistance with acylcarnitine analyses. We thank Alix Denoncourt for help with plasmid prep. We thank Ziyad El Hankouri for help with western blotting. This work was funded by grants from the Natural Sciences and Engineering Research Council (NSERC) of Canada (to MEH; RGPIN 04973); NSERC grant RGPIN 05015 (to MD), NIH grants: U19AI118610 and P01CA177322 to JRJ and P50 GM082250 to NK. RS is the recipient of a scholarship from the University of Shaqra, Duwadimi, Saudi Arabia. MN was funded by an NSERC Undergraduate Research Scholarship. CP is the recipient of a Mitacs postdoctoral fellowship.

### 2.1.4 CONFLICT OF INTEREST

None declared.

## 2.2 ABSTRACT

**Objective:** Brown adipose tissue (BAT) is important for thermoregulation in many mammals. Uncoupling protein 1 (UCP1) is the critical regulator of thermogenesis in BAT. Here we aimed to investigate the deacetylation control of BAT and to investigate a possible functional connection between UCP1 and sirtuin 3 (SIRT3), the master mitochondrial lysine deacetylase.

**Methods:** We carried out physiological, molecular, and proteomic analyses of BAT from wild-type and *Sirt3*KO mice when BAT is activated. Mice were either cold exposed for 2 days or were injected with the β3-adrenergic agonist, CL316,243 (1mg/kg; *i.p.*). Mutagenesis studies were conducted in a cellular model to assess the impact of acetylation lysine sites on UCP1 function. Cardiac punctures were collected for proteomic analysis of blood acylcarnitines. Isolated mitochondria were used for functional analysis of OXPHOS proteins.

**Results:** Our findings showed that SIRT3 absence in mice resulted in impaired BAT lipid use, whole body thermoregulation, and respiration in BAT mitochondria, without affecting UCP1 expression. Acetylome profiling of BAT mitochondria revealed that SIRT3 regulates acetylation status of many BAT mitochondrial proteins including UCP1 and crucial upstream proteins. Mutagenesis work in cells suggested that UCP1 activity was independent of direct SIRT3-regulated lysine acetylation. However, SIRT3 impacted BAT mitochondrial proteins activities of acylcarnitine metabolism and specific electron transport chain complexes, CI and CII.

**Conclusions:** Our data highlight that SIRT3 likely controls BAT thermogenesis indirectly by targeting pathways upstream of UCP1.

**Keywords:** Brown adipose tissue; Thermogenesis; Thermoregulation; Mitochondria; Uncoupling protein 1; Sirtuin 3; Acetylation; Oxidative phosphorylation; Fatty acid oxidation; Acylcarnitines

## 2.3 INTRODUCTION

Brown adipose tissue (BAT) helps many mammals, including humans, maintain body temperature in cold environments through a process called non-shivering thermogenesis (Blondin et al., 2014; Himms-Hagen, 1985; Nicholls and Locke, 1984; U Din et al., 2016). BAT thermogenesis can be stimulated by cold exposure and by pharmacological administration of adrenergic receptor agonists (Cannon and Nedergaard, 2004). BAT activation results in the uptake and oxidation of large amounts of glucose and fatty acids (FAs) in a process that can markedly increase whole body energy expenditure in mice (Bartelt et al., 2011; Yu et al., 2002).

BAT thermogenesis is dependent on the activity of uncoupling protein-1 (UCP1), an abundant protein in the mitochondrial inner membrane that induces proton leak-mediated respiration (Enerbäck et al., 1997; Heaton et al.). When BAT is activated, *UCP1* gene expression is increased by the action of multiple transcription factors including the peroxisome proliferator activated receptor (PPAR) and CCAAT/enhancer binding protein (C/EBP) families and cyclic AMP (cAMP) response binding protein (CREB), as well as thyroid hormone (Rabelo et al., 1995; Shore et al., 2013). These transcription factors are activated by p38 mitogen-activated protein kinase (MAPK), which is considered as the central mediator of the cAMP signaling pathway that induces brown adipocyte thermogenesis (Cao et al., 2004). UCP1-mediated thermogenesis falls under the regulation of the sympathetic nervous system via the activation of adrenergic receptors, and subsequently stimulation of lipolysis in BAT. The liberated FAs are then used for the allosteric activation of UCP1, and to support greatly increased rates of mitochondrial fatty acid oxidation (FAO). The latter provides reducing equivalents/electrons to drive the electron transport chain (ETC), which establishes the inner membrane protonmotive force that in turn drives the

protonophore activity of UCP1 (Cannon and Nedergaard, 2004; Nicholls and Rial, 1999; Shabalina et al., 2004).

BAT has high expression of sirtuin 3 (SIRT3), which is an $NAD^+$-dependent deacetylase in the mitochondria (Lombard et al., 2007). A previous study showed that cold increases the transcription of SIRT3 mRNA in BAT; however the impact on protein levels is unclear (Shi et al., 2005). SIRT3 is the master regulator of deacetylation in the mitochondria (Lombard et al., 2007) while the other mitochondrial sirtuins, SIRT4 and SIRT5 do not have significant roles in mitochondrial deacetylation (Du et al., 2011; Haigis et al., 2006; Lombard et al., 2007; Tan et al., 2014). Large-scale acetylome analyses from multiple studies demonstrate that mitochondrial proteins are frequently targets for lysine acetylation (Anderson and Hirschey, 2012; Hirschey et al., 2010, 2011; Jing et al., 2013). While lysine acetylation outside of the mitochondria is catalyzed by lysine acetyltransferase (KAT) enzymes, no mitochondrial KAT enzyme in BAT has been described to date. Overall mitochondrial acetylation levels are correlated with the level of acetyl-CoA (Weinert et al., 2014), and much of the acetylation that occurs in mitochondria is thought to occur non-enzymatically, owing in part to the high concentrations of acetyl-CoA as a product of FAO (Pougovkina et al., 2014). SIRT3 appears to play a critical role in reversing these such non-enzymatic acetylation, which are generally thought to have an inhibitory effect on enzymatic activities in mitochondria (Weinert et al., 2015).

Consistent with this, Hirschey *et al* showed that the absence of SIRT3 in fasting mice is associated with decreased FAO rates in various tissues, including BAT, and these mice are intolerant to acute cold stress (Hirschey et al., 2010). Altogether these findings are consistent

with the notion that SIRT3 could be a critical regulator of BAT thermogenesis, and that the underlying molecular mechanisms merit investigation.

To investigate the control of SIRT3-mediated deacetylation of BAT thermogenesis, we studied the metabolic phenotypes of BAT from *Sirt*3 knock-out (*Sirt3*KO) mice that were cold exposed for 2 days, or were held at thermoneutrality and injected with the β3-adrenergic agonist CL316,243. We report that mice deficient in SIRT3 display widespread defects in BAT lipid use/oxidation and in thermoregulation even in fed conditions. We also show that respiration is decreased in mitochondria isolated from BAT of *Sirt3*KO mice relative to wild-type controls. While SIRT3 impacted acetylation sites on UCP1 in room temperature housed mice, there were little SIRT3-dependent effects at these same sites after cold stress and mutation of these sites to prevent acetylation did not affect protein function in a cellular model. In contrast, the absence of SIRT3 impacted acetylation on diverse FAO/ acylcarnitine- related enzymes and ETC proteins in BAT mitochondria under both conditions. Functions controlled by these proteins are defective in *Sirt3*KO mice under conditions that activate BAT *in vivo*. Together, our findings suggest that SIRT3 indirectly controls BAT thermogenesis by deacetylating and promoting the function of pathways upstream of UCP1.

## 2.4 MATERIALS AND METHODS

### 2.4.1 ANIMALS

*Sirt3* whole body knock-out (KO) mice were described previously (Palacios et al., 2009). *Sirt3* knock-out was confirmed by PCR before experimentation. Mice were given *ad libitum*, a standard rodent chow (44.2% carbohydrates, 6.2% fat, and 18.6% crude protein; diet T.2018, Harlan

Teklad, Indianapolis IN) and water, and were housed with a 12/12 h light-dark cycle in ventilated cages. At an age of 5-8 weeks, male mice were used in two different experimental approaches to maximize the activity of BAT. Mice were kept either at room temperature (24°C), housed in groups of 2-3 mice, or were exposed to 4°C for 2 days, housed individually, with free access to water and food. Body weights were taken, as well as the weights of epididymal white adipose tissue (eWAT) and interscapular BAT (iBAT) after sacrificing mice by cervical dislocation. Tissues were used immediately for experiments or were flash frozen and stored at -80 °C for later analyses. In other experiments, mice were injected with the β3-adrenergic agonist**,** CL 316,243 (1 mg/kg *i.p*.) and were housed at 28 °C. All animal experimental procedures were in accordance with the guidelines and principles of the Canadian Council of Animal Care and after the approval of the Animal Care Committee of the University of Ottawa.

**2.4.2 BODY COMPOSITION AND COMPREHENSIVE METABOLIC PHENOTYPING**

EchoMRI (EchoMRI, Houston TX) was used to assess lean body mass, and fat mass of mice. To examine characteristics of metabolic phenotype we used a Comprehensive Lab Animal Monitoring System (CLAMS; Columbus Systems, Columbus OH). During CLAMS analyses, mice were housed individually at 28°C for at least 2 days for acclimation purposes and then were exposed to 4°C for two days in the CLAMS system. In other experiments to address BAT-specific thermogenic activity, mice were studied at thermoneutrality (28°C) before and after CL 316,243 injections. Mice were fasted 3 hours prior to, and following the 10:00 bolus i.p. injection of CL 316,243 (1mg/kg) to avoid food associated effects (*e.g.*, foraging activity; thermic effect of food). Pre-CL injection values were averaged (07:00-10:00). Post-CL injection values were those at 90-minute post-injection.

### 2.4.3 HISTOLOGICAL ANALYSES OF BAT

iBAT from mice that were housed at room temperature or exposed to the cold was dissected, cleaned to remove any white adipose, muscle or connective tissues, and then fixed in 10% formalin overnight. iBAT was then ethanol dehydrated and stored in 70% ethanol prior to paraffin embedding. Paraffin embedded tissue was sectioned to the largest surface area and used for Hematoxylin and Eosin (H&E) staining. After H&E staining, Mirax Viewer Image software (version 1.6) was used to analyze the sections in a ZEISS-MIRAX Midi Slide scanning system (Zeiss Microimaging, Oberkochen, Germany, and 3DTech, Budapest, Hungary) and digital images were acquired at 20x magnification. Images were extracted using Aperio ImageScope software (version 12.3.3; Leica Biosystems), and the extracted images were analyzed using FIJI (ImageJ; NIH) software (Schindelin et al., 2012). The range thresholding that was applied across all replicate images in all conditions was (200-255). Finally, the total image area was measured, and a percent lipid area was calculated.

### 2.4.4 CORE BODY TEMPERATURE MEASUREMENT

The core body temperature of mice was measured using an anal thermometer (Physitemp TH-8 Thermalert Monitoring Thermometer, Physitemp, USA) before and after cold exposure.

### 2.4.5 BAT MITOCHONDRIAL ISOLATION

Mitochondria were isolated from iBAT of WT and *Sirt3*KO mice as described previously (Shabalina et al., 2010). Briefly, on the day of the experiment, iBAT of 1-3 male mice from each genotype, was quickly dissected, cleaned and kept on ice. iBAT was then rapidly cut with scissors into small pieces, before being homogenizing in 0.25M sucrose using 4 to 5 strokes in a Potter Elvehjem

teflon–glass tissue grinder. The iBAT homogenate was subjected to differential centrifugation steps starting with a spin at 8500g for 10 min, to remove the fat layers. After removing the supernatant, the wall of the tubes was wiped to remove any residual amount of fat following by re-suspending pellets in the sucrose buffer (0.25M). To remove nuclei and cell debris, the suspension was then spun at 800g for 10 min. The mitochondria-containing supernatants were collected and were spun at 8500g for 10 min to pellet the mitochondria. Finally, the mitochondria were washed with 0.25M sucrose containing 0.3% fatty acid-free bovine serum albumin for 10 min at 8500g to remove endogenous fatty acids. The mitochondrial pellet was gently re-suspended in specific buffers depending on the downstream applications (see below).

**2.4.6 WESTERN BLOTTING**

Mitochondrial pellets were resuspended in 0.25M sucrose supplemented with 10mM sodium butyrate (Sigma Aldrich), 10mM nicotinamide (Sigma Aldrich) and protease inhibitor mixture (Complete Mini, Roche). Protein concentration was quantified using the Bradford method (Biorad). 10µg of mitochondrial proteins was loaded per lane onto a 12% SDS-polyacrylamide gel. After electrophoresis, proteins were transferred by electro-blotting to nitrocellulose membrane. Nitrocellulose membrane was used for all blots and was blocked with 5% BSA for 1 hour. After that, membranes were incubated with primary antibodies to examine the expression of SIRT3, UCP1, total mitochondrial acetylation levels, and oxidative phosphorylation (OXPHOS) complexes. Western blotting was performed with the following antibodies: anti-SIRT3 antibody (1: 1,500; Cell Signaling, #5490S); anti-UCP-1 antibody (1: 3,000; Sigma Aldrich, #U6382); anti-acetylated lysine antibody (1:1500; Calbiochem #ST1027); total OXPHOS rodent antibody cocktail (1:2000; Abcam, #Ab110413); and anti-cytochrome c oxidase antibody (1: 4,000; Invitrogen

#459600). Cytochrome c oxidase was used as a mitochondrial loading control. Western blots of UCP1 and total mitochondrial acetylation in Figures 2.2D and 2.3C were probed from the same membrane. Quantification was performed by using the ImageJ software (NIH).

### 2.4.7 LABEL FREE MASS SPECTROMETRY ACETYLOME PROFILING

Sample preparation for acetylome profiling followed a protocol originally developed for yeast *S. cerevisiae* (Downey et al., 2015), with appropriate modifications implemented for mouse BAT. For each treatment group (warm or cold), all samples were processed at the same time to ensure consistency. N=6 for each treatment group, where a single biological replicate is one mitochondrial protein prep from iBAT isolated from one mouse. **Generation of AcK peptides:** Mitochondrial protein samples were suspended in 1mL of AcK buffer (8M Urea, 0.1 M Tris-HCl pH 8.0, 150 mM NaCl, 10 mM sodium butyrate (Sigma Aldrich 303410), 10 mM nicotinamide (Sigma Aldrich 3376), with Roche protease inhibitor tablet (w/o EDTA). Resuspended samples were quantitated using a BCA assay. For each sample, 0.4 or 1.4 mg of mitochondrial protein from iBAT of room temperature housed or cold exposed mice, respectively, was reduced using TCEP (Sigma Aldrich C4706–2, 4 mM final concentration) prior to alkylation with iodoacetamide (Sigma Aldrich L1149–5G, 10 mM final concentration), and quenching with DTT (10 mM final concentration). Subsequently, samples were diluted to < 2M urea with 0.1 M Tris-HCl pH 8.0 and digested with trypsin (Pierce 90058, ~15µg/sample). Digestions were performed at room temperature overnight. Samples were acidified using 10 % TFA to a pH of <3, which was monitored by spotting on pH paper. Samples were clarified by centrifugation at 10,000g at room temperature to remove precipitate and loaded onto a Sep Pak tC18 column (Waters). Column activation was with 1 ml 80% ACN/0.1% TFA. Equilibration was with 3 × 1 ml 0.1% TFA. The

columns were washed with 5 × 1 ml 0.1% TFA. Bound peptides were eluted with 1 ml 40% ACN/0.1% TFA. **AcK enrichment:** The eluted peptides were frozen and lyophilized prior to resuspension in AcK IP buffer (0.1 M Tris-HCl pH 8, 50 mM NaCl, Roche protease inhibitor tablet w/o EDTA) and clarification by centrifugation (2 minutes at 10,000 rpm). Supernatant was incubated with 50 µL packed volume of ImmuneChem anti-AcK agarose beads (ICP0388) at 4 °C for 2 hours. Beads were washed twice with 1mL lysis buffer and twice with 1mL water. Two elutions of 60 µL of 0.15% TFA (10 minutes) were pooled. Peptides were purified on Pierce C18 spin tips (84850) according to manufacturer's instructions. Elutions were dried on a speed vac.

**Mass spectrometry analysis:** Mass spectrometry analysis was carried out on a Thermo Fisher Orbitrap Fusion with an Easy nLC 1200 ultra-high pressure liquid chromatography system interfaced via a Nanospray Flex nanoelectrospray source. Peptide samples were injected on a C18 reverse phase column (25 cm x 75 um packed with ReprosilPur C18 AQ 1.9 um particles). Peptides were separated via an organic gradient from 5% to 30% ACN in 0.1% formic acid (112 minutes, flow rate of 300 nl/min). All samples were analyzed in technical duplicate. **Data acquisition:** The mass spectrometer acquired the spectra in a data-dependent manner throughout the gradient, acquiring a full scan in the Orbitrap (at 120,000 resolutions with an AGC target of 200,000 and a maximum injection time of 100 ms). This was followed by as many MS/MS scans as could be acquired on the most abundant ions in 3s in the dual linear ion trap (rapid scan type, intensity threshold of 5000, HCD collision energy of 29%, AGC target of 10,000, a maximum injection time of 35 ms, and an isolation width of 1.6 m/z). For this dataset, singly and unassigned charge states were rejected. Dynamic exclusion was enabled with a repeat count of 1, an exclusion duration of 20 s, and an exclusion mass width of +/- 10 ppm. **Extraction:** Raw mass

spectrometry data were assigned to murine protein sequences. MS1 intensities extracted with the MaxQuant software package (version 1.5.5.1) (Cox and Mann, 2008). Data were searched against the SwissProt murine protein database (downloaded on January 11, 2016). In addition to lysine acetylation, variable modifications were allowed for N-terminal protein acetylation, methionine oxidation. A static modification was used for carbamidomethyl cysteine. **Data analysis:** The MaxQuant data were analyzed using our in-house computational pipeline for statistical analysis of relative quantification with fixed and/or mixed effect models, implemented in the MS stats Bioconductor package (version 3.3.10) (Choi et al., 2014). Contaminants, decoy hits, and peptides not containing acetyllysine residues were removed. Samples for each comparison (WT versus *Sirt3*KO in either warm or cold conditions) were normalized across fractions by median-centering the log2-transformed MS1-intensity distributions. MS stats group comparison functions were run with the following settings: no interaction terms for missing values, no interference, unequal intensity feature variance, restricted technical and biological scope of replication. Statistically significant changing sites between wild-type and *Sirt3*KO mice were selected by applying a log2-fold-change (>1.0) and an adjusted p-value (<0.05) corrected for multiple testing threshold. Warm and cold treatment conditions were analyzed separately since these groups were analyzed at different times. Peptides identified by MaxQuant that did not contain KAc sites were extracted from the data to compare KAc site changes to underlying protein abundance changes. The data were analyzed by MSstats in an identical fashion as the KAc site analysis. Protein L2FC values were normalized by median-centering to account for systematic sample loading errors and then were plotted against KAc site L2FC values where both protein and site values could be calculated. **GO term enrichment**: Analysis was performed using the

Metascape analysis tool (Tripathi et al., 2015). Proteins with KAc sites with L2FC *Sirt3*KO/WT > 1.0 or L2FC and with adjusted p-value < 0.05 were extracted as the gene set for enrichment. A custom background gene set was set as the full list of proteins detected in each experiment. The top term in each summary group are shown.

### 2.4.8 PLASMID DESIGN

Synthetic murine UCP1 constructs were ordered from ATUM (https://www.atum.bio). $UCP1^{(WT)}$ encodes the sequence dictated by Uniprot accession P12242. $UCP1^{(K\text{-}R)}$ and $UCP1^{(K\text{-}Q)}$ constructs contain mutations coding for appropriate changes to lysines 56 and 151. Constructs are expressed from the CMV promoter in vector pD2610-v10. The GFP control vector was also purchased from ATUM and encodes GFP under the control of the same vector, with the designation of pD2610-v10-03.

### 2.4.9 CULTURE AND TRANSFECTION OF HEK293T CELLS

HEK293T cells were cultured in high glucose DMEM medium (Gibco, ThermoFisher) provided with 10% FBS (Wisent) and 1% Antibiotics-Antimycotic (Gibco, ThermoFisher). HEK293T cells were passaged when they reached 90% confluency. For transfection, 70,000 cells were seeded per well in 24-well plates and left overnight. 24 hours after seeding, cells were transfected with the different plasmids (500ng/well) as described in the manufacturer's protocol (ThermoFisher, #15338100). After 8 hours of transfection, the cells were trypsinized and their viability was measured to be greater that 90% using Trypan blue staining. Transfected cells were seeded in 96-well Seahorse plates or 24-well dishes for western blot confirmation of UCP1 expression. After 24h, cells were analyzed using a Seahorse 96e XF Analyzer and a modified mitochondrial stress assay. The latter assay was conducted as follows.

### 2.4.10 SEAHORSE ANALYSIS OF UCP1-MEDIATED LEAK RESPIRATION IN TRANSFECTED CELLS

On the day of the assay, growth medium was changed to Seahorse medium for 1 h prior to the actual analyses; this medium consisted of phenol-free DMEM, including 10mM glucose, 10mM pyruvate, and 0.4% BSA. The mitochondrial stress test protocol was modified to examine UCP1-mediated proton leak, and the following reagents were used**: (**4-[(E)-2-(5,6,7,8-Tetrahydro-5,5,8,8-tetramethyl-2-naphthalenyl)-1-propenyl] benzoic acid**)** (TTNPB; 15 µM or 30 µM; Sigma, #T3757), 2µg/ml oligomycin (Sigma, #O4876), carbonilcyanide *p*-triflouromethoxyphenylhydrazone (FCCP; 3µM; Sigma, #C2920), 2µM rotenone (Sigma, #R8875) and 2µM antimycin A (Sigma, #A8674). The Seahorse protocol was as follows: Basal respiration (3 cycles; 3 min mix and 3 min measure), TTNPB injection (4 cycles; 3 min mix and 3 min measure); oligmycin (3 cycles; 3 min mix and 3 min measure); FCCP (3 cycles; 3 min mix and 3 min measure), and finally, injected together, rotenone and antimycin A (3 cycles; 3 min mix and 3 min measure). TTNPB was added as a first injection in order to activate UCP1, and then proton leak respiration was measured as that following the addition of oligomycin (to inhibit ATP synthase). To assess UCP1-dependent respiration, we compared OCR values in the presence of oligomycin from vehicle treated or TTNPB treated cells in each individual transfection condition (GFP-, $UCP1^{wt}$, $UCP1^{K\text{--}R}$ and $UCP1^{K\text{--}Q}$ transfected HEK 293 cells).

### 2.4.11 CLARK ELECTRODE BASED ANALYSES OF UCP-DEPENDENT RESPIRATION IN BAT MITOCHONDRIA

Mitochondria were re-suspended in a buffer containing (20mM TES (pH 7.2), 100mMKCl and 0.6% fatty-acid-free BSA). Respiration rates of iBAT mitochondria were determined in Oxytherm (HansaTech, Kings Lynn, UK) Clark electrode systems at 37°C, at 0.25 mg-0.35mg protein/mL

in100mM KCL, 20mM TES (pH 7.2), 4mM $KH_2PO_4$, 2mM $MgCl_2$, and 1mM EDTA and 0.3% fatty acid-free bovine serum albumin. Mitochondria were energized with 25 µM palmitoyl-L-carnitine (PLC; Sigma, #P1645) or 5mM glycerol-3-phosphate (G3P; Sigma, #G7886) plus 5mM malate (Sigma, #M1000). Malate was added to replenish TCA cycle intermediates lost during the isolation process. After stable rates of oxygen consumption were determined, 2mM guanosine 5'-diphosphate (GDP; Sigma, #G7127) was then added to determine UCP1-dependent respiration. Oxygen consumption rates were normalized to mitochondrial protein, as determined by Bradford assays.

### 2.4.12 HIGH RESOLUTION RESPIROMETERY OF THE ACTIVITIES OF ELECTRON TRANSPORT CHAIN COMPLEXES IN BAT MITOCHONDRIA

Respiration rates linked to each electron transport chain complex (CI, CII, CIII and CIV), were determined using high resolution respirometry (HRR) (Oxygraph-2k; Oroboros, Innsbruck, Austria). To rule out the possibility that these respiratory rates were confounded by effects of SIRT3 on UCP1 we began each experiment by uncoupling the mitochondria by adding 1.4 µM FCCP (Sigma, #C2920) prior to the addition of substrates and inhibitors. The Oxygraph-2k units were calibrated and all measurements were performed at 37°C. Rates were determined for 100 µg of mitochondrial protein in 2 ml of buffer (110mM sucrose, 60mM K-lactobionate, 20mM HEPES, 20mM taurine, 10mM $KH_2PO_4$, 3mM $MgCl_2$, 0.5mM EGTA, 1 g/l BSA, pH 7.1), in the presence of 5mM malate (Sigma, #M1000) and 1.4 µM FCCP. Rates specifically associated with each of the complexes were assessed as follows: Complex I [5mM pyruvate (Sigma, #P2256); followed with 0.5 µM rotenone (Sigma, #R8875) to inhibit CI], Complex II [10mM succinate (Sigma, #S2378); followed by 5mM malonate (Sigma, #M1296) to inhibit CII], Complex III [5mM

G3P (Sigma, #G7886); followed by 1 µM antimycin A (Sigma, #A8674) to inhibit CIII], and Complex IV [0.5mM TMPD (Sigma, #3134) and 2mM ascorbate (Sigma, #A4034); followed by 100mM azide (Sigma, #S2002) to inhibit CIV]. Oxygen consumption rates (OCR) were normalized to mitochondrial protein levels, as determined by Bradford assays.

### 2.4.13 PLASMA ACYLCARNITINE ANALYSES

To stimulate BAT thermogenesis, mice were injected with the β3-adrenergic agonist, CL316,243 (1mg/kg; *i.p.*). Ninety min later, mice were anaesthetized and blood was collected by cardiac puncture for plasma acylcarnitine measurements. Blood samples were dried on filter paper (Whatman ProteinSaver 903) and stored at −20°C. Measurements were done at the Newborn Screening lab at the Children's Hospital of Eastern Ontario (CHEO) using mass spectrometry. Methods are described in (Beauchamp et al., 2015).

### 2.4.14 STATISTICAL ANALYSIS

Data are represented as mean ± SEM. Two-tailed Student's t-tests, one-way ANOVA and two-way ANOVA with multi-comparison tests were used to determine statistical significance. Statistical significance, and Ns, are described in the figure legends.

### 2.4.15 ACETYLATION ANNOTATIONS

The annotation and associated analyses presented in Supplementary Table 3 were performed using the functionality of SLiMSearch tool as previously described (Krystkowiak and Davey, 2017). The identified acetylation sites were annotated with overlapping sequence annotation, including information describing protein modular architecture, post-translational modifications, any solved protein structures, SNPs and experimentally characterized functional regions.

### 2.4.16 DATA AVAILABILITY

The mass spectrometry proteomics data have been deposited to the ProteomeXchange Consortium via the PRIDE (Perez-Riverol et al., 2019) partner repository with the dataset identifier PXD013056. The cold stress dataset is annotated under the 'MD10' keys and the room temperature experiment is annotated under the 'OMDYS21-32' keys.

## 2.5 RESULTS

### 2.5.1 SIRT3 ABSENCE DOES NOT AFFECT METAMORPHIC CHARACTERISTICS OF MICE

To investigate the role of SIRT3 under cold stress, we began by comparing body weight, body composition and metabolic characteristics in *Sirt3*KO and wild type (WT) mice at the whole body level. Previous work in mice has established that during 1 day at 4°C, BAT is stimulated to such a high extent that shivering thermogenesis becomes minimal (Golozoubova et al., 2001; Nedergaard and Cannon, 2013; Stier et al., 2014). Therefore, to assess effects on BAT thermogenic processes, mice were challenged to the cold (4°C) for 2 days. Under these conditions, we found *Sirt3*KO mice showed no differences in total body weight, lean mass and fat mass as determined by Echo-MRI, relative to WT mice (Figure 2.1A-C). Both *Sirt3*KO and WT mice also showed no differences in epididymal white adipose tissue (eWAT) or interscapular brown adipose tissue (iBAT) mass before and after cold exposure (Figure 2.1D, E). To study the effect of the cold on the resting metabolic rate, oxygen consumption ($VO_2$) was assessed before and after cold exposure. Measurements normalized to lean body mass showed that WT and *Sirt3*KO mice had similarly increased metabolic rates upon cold exposure (Figure 2.1F).

### 2.5.2 SIRT3 ABSENCE RESULTS IN IMPAIRED BAT LIPID USE AND THERMOREGULATION IN MICE

While there were no changes to these phenotype characteristics of *Sirt3*KO mice upon cold exposure at the whole body level, we also examined the metabolic and morphologic changes within BAT itself. Since it has been reported that the mRNA level of SIRT3 is increased in BAT in response to the cold (Shi et al., 2005), we first tested the impact of cold on SIRT3 protein levels by isolating mitochondria from iBAT of room temperature housed or cold exposed mice. Surprisingly, SIRT3 protein level in WT mice was not increased upon cold exposure (Figure 2.1G, H).

While previous work demonstrates that FAs derived from white adipose tissue (WAT) support BAT thermogenesis (Schreiber et al., 2017; Shin et al., 2017), FAs are also supplied locally from BAT lipid droplets (Cannon and Nedergaard, 2004). Therefore, we measured lipid droplet content in BAT of WT and *Sirt3*KO mice using quantitative morphometry. WT mice showed a significant reduction in lipid droplet content in iBAT sections after 2 days of cold exposure, but this same significant decrease was not observed in *Sirt3*KO mice (Figure 2.1I, J). These data suggest decreased FA utilization in the absence of SIRT3. Moreover, unlike WT mice, there was no decrease in the RER of *Sirt3*KO mice after CL316,243 injection indicating a fatty acid oxidation defect upon BAT activation (Supplementary Figure 2.1C, D). Consistent with a functional impact on lipid use and fatty acid oxidation when BAT is activated, *Sirt3*KO mice had a significant reduction in their ability to maintain core body temperature in response to the cold (Figure 2.1K). Therefore, while *Sirt3*KO were outwardly phenotypically normal, they had defects consistent with a role for SIRT3 in thermoregulation. Next, we investigated the functional relationship between SIRT3 and BAT mitochondrial respiration.

### 2.5.3 IMPAIRED RESPIRATION IN BAT MITOCHONDRIA OF *SIRT3*KO MICE

To study UCP1-dependent proton leak respiration, isolated iBAT mitochondria from room temperature housed WT and *Sirt3*KO mice were energized by 25µM palmitoyl-L-carnitine (PLC) since long fatty acids are activators and substrates for BAT mitochondria (Cannon and Nedergaard, 2004; Silva et al., 2005). UCP1 activity was subsequently inhibited by adding 2mM guanosine diphosphate (GDP). Mitochondria isolated from BAT of *Sirt3*KO mice showed defective UCP1-dependent respiration relative to those from WT mice (Figure 2.2A). Moreover, *Sirt3*KO mitochondria function was examined glycerol-3-phosphate (G3P), which is an excellent substrate for BAT mitochondrial respiration (Shabalina et al., 2013) and provides reducing equivalents that enter the electron transport chain at Complex III. BAT mitochondria from either room temperature housed or cold exposed WT and *Sirt3*KO mice were energized by 5mM G3P and UCP1 activity was then inhibited by adding 2mM GDP. Under these conditions, UCP1-dependent respiration in *Sirt3*KO mitochondria was lower than that in WT mice (Figure 2.2B, C). UCP1 levels after cold exposure were increased by cold stress in both WT and *Sirt3*KO mice, but we found no observable difference between genotypes (Figure 2.2D, E). Thus, the absence of SIRT3 itself did not affect the expression of UCP1 protein, suggesting that the decrease in UCP1-dependent respiration in *Sirt3*KO mice might be due to changes in UCP1 activity.

### 2.5.4 COLD STRESS AND SIRT3 INDUCE ACETYLATION AND DEACETYLATION, RESPECTIVELY, OF BAT MITOCHONDRIAL PROTEINS

We reasoned that SIRT3 could impact UCP1 activity directly by regulating acetylation of UCP1 lysine residues, or indirectly by regulating critical pathways required for UCP1 function (*e.g.,* upstream oxidation reactions that supply electrons to the respiratory chain, or the respiratory

chain itself). To investigate these potential modes of regulation, we used label-free quantitative acetylome profiling to compare non-histone protein acetylation in iBAT mitochondria isolated from WT or *Sirt3*KO mice (Figure 2.3A). SIRT3 impacted the acetylation status of hundreds of sites (or site combinations) in separate experiments carried out for room temperature housed or cold stressed mice (Supplementary Table 1). There was a significant correlation between acetylome profiles in room temperature and cold stressed mice (Figure 2.3B & Supplementary Figure 2A). As expected based on the role of SIRT3 as a lysine deacetylase, the vast majority of impacted acetylation marks were upregulated rather than downregulated in *Sirt3KO* mice (Figure 2.3B & Supplementary Figure 2A). This was confirmed by western blotting experiments (Figure 2.3C, D). For most of the significantly upregulated acetylations, the observed fold change (log2FC *Sirt3*KO/WT) seemed to be more dramatic at room temperature than in the cold (Figure 2.3E & Supplementary Figure 2B). This may be explained in part by the intriguing observation that cold stress itself increases the baseline of acetylation in wild-type mice (Figure 2.3C, D). Since our room-temperature and cold-stressed samples were processed for mass spectrometry at different times, identification of those acetylations impacted by cold-stress independently of SIRT3 will require additional experiments. Notably, analysis of non-acetylated peptides recovered in our experiments suggested that changes in acetylation status could not be explained by changes in protein levels (Supplementary Figure 2.3A,B & Supplementary Table S2).

GO-term enrichment of statistically significant upregulated sites (log2FC Sirt3/KO = ≥ 1, adjusted P value ≤ 0.05) using Metascape indicated enrichment of proteins assigned to fatty acid metabolic processes and the mitochondrial matrix under room temperature and cold stressed conditions (Figure 2.3F & Supplementary Figure 2C). Cold stressed mice also showed preferential

SIRT3-regulation of proteins functioning in the tricarboxylic acid (TCA) cycle (Figure 2.3F & Supplementary Figure 2C). Altogether, our data point to a significant contribution for SIRT3 in the regulation of the BAT mitochondrial acetylome, with enrichment in pathways that are likely to intersect with UCP1 function. Functional annotation of acetylation sites uncovered in our work using the SLiMSearch tool uncovered many sites in close proximity to known regulatory regions, domains, motifs and other previously identified PTMs (Supplementary Table S3).

### 2.5.5 ACETYLATION OF LYSINES ON UCP1 DOES NOT AFFECT UCP1 LEAK RESPIRATION

In support of acetylation playing a direct role in UCP1 function within BAT mitochondria, we uncovered four acetylations on UCP1 in both room temperature and cold stressed mice (K56, K67, K73 and K151). K56 and K151 showed a significant increase in acetylation in samples from *Sirt3*KO mice, but only when housed at room temperature (~ 3-fold each, Figure 2.4A & Supplementary Table 1). Intriguingly, these residues are located in similar positions in the first two of the three matrix-side loops of the protein (Klingenberg et al., 1999), and theoretically would be accessible to matrix SIRT3 activity. To determine if acetylation of K56 and K151 are important for UCP1-dependent leak respiration, we established an *in vitro* assay expressing mouse UCP1 in HEK293T cells. UCP1 function has previously been examined in HEK293 (Jastroch et al., 2011, 2012; Oelkrug et al., 2013). Cells were transfected with plasmids expressing wild-type murine UCP1$^{(WT)}$ or mutant UCP1 variants in which these residues cannot be acetylated, *i.e.,* UCP1 $^{(K\rightarrow R)}$ or that mimic constitutive acetylation, *i.e.,* UCP1 $^{(K\rightarrow Q)}$. A plasmid expressing GFP from the same vector was used as a negative control. Importantly, since HEK293T cells do not express UCP1 endogenously, these constructs provided the only source of UCP1, and the UCP1 variants were expressed at similar levels (Figure 2.4B). Herein, we used the retinoic acid analogue ,

TTNPB, to activate UCP1 in intact HEK293T cells rather than long chain FAs. In brown adipocytes, unlike HEK293 cells, long chain FAs are rapidly taken up and then used for the activation of UCP1, and fueling of beta-oxidation. Previous work has demonstrated that the fatty acid transporter, CD36, is not expressed in HEK293 cell (Xu et al., 2013) as it is in brown adipocytes. Thus we used TTNPB, which is cell permeable, to induce UCP1 leak respiration, as used before in UCP1 expressing HEK293 cells in plate-based respirometry assays (Oelkrug et al., 2013; Rial et al., 1999; Tomás et al., 2004).

As expected, GFP transfected cells did not show TTNPB-induced respiration (Figure 2.4C, D). In contrast, $UCP1^{(WT)}$ transfected cells had increased UCP1-mediated leak respiration (Figure 2.4E, F). A similar effect on leak respiration was observed with acetyl-defective UCP1 (Figure 2.4G, H) and with acetyl-mimic forms of UCP1 (Figure 2.4I, J), suggesting that these lysines alone cannot account for the impact of SIRT3 on UCP1 dependent respiration. Therefore, we investigated if the lower rate of UCP1-dependent respiration in *Sirt3*KO mitochondria was instead due to SIRT3-mediated regulation of upstream proteins of UCP1 that are involved in vital pathways supporting UCP1-mediated thermogenesis. Specifically, we focused on the FAO and ETC pathways.

### 2.5.6 DECREASED PLASMA LEVELS OF MEDIUM AND LONG CHAIN ACYLCARNITINES IN *SIRT3*KO MICE

Beyond being an allosteric agonist of UCP1 activity, FAs are a major energy substrate for active BAT. To be taken up into mitochondrial for oxidation, long chain FAs are first converted to acylcarnitines and then are transported to mitochondria matrix via carnitine acylcarnitine translocase (CACT) (Houten and Wanders, 2010). Defective FAO can lead to increased circulating

levels of acylcarnitines, and fasted *Sirt3*KO mice have previously been shown to have a defect in liver mitochondrial FAO and an accumulation of long chain acylcarnitines in the plasma (Hirschey et al., 2010). In our study, our acetylome profiling data showed that SIRT3 negatively regulated lysine acetylations on many proteins involved in the uptake and oxidation of fatty acids and in the metabolism of acylcarnitines in BAT from both room temperature housed and cold exposed mice (Figure 2.5A & Supplementary Table 1). Many of the lysine residues with strongly-regulated acetylations are located in important functional regions of target proteins, as identified by our SlimSearch annotation (Figure 2.5A and Supplementary Table S3). Regulation of these acetylations may be particularly important for FAO and acetylcarnitine metabolism.

To examine the impact of SIRT3 absence on the level or the production of acylcarnitines when BAT is activated, mice were injected with a standard bolus of the β3-adrenergic receptor selective agonist CL 316,243 (1 mg/kg *i.p.*), to induce BAT activity. Blood samples were collected 90 min post-injection by cardiac puncture for MS/MS acylcarnitine analyses. These experiments revealed that *Sirt3*KO mice had no differences in short chain acylcarnitines (Figure 2.5B), but had decreased levels of select medium-chain (C12:1OH) and long-chain (C14OH, C16:1OH, C16OH, C18:1, C18:1OH, C18:2OH) acylcarnitines, compared to WT mice (Figure 2.5C, D).

### 2.5.7 IMPAIRED ACTIVITIES OF ETC PROTEIN COMPLEXES IN *SIRT3*KO BAT MITOCHONDRIA

ETC proteins have a fundamental role in UCP1-dependent respiration because their activities drive the production of protonmotive force, which is necessary for UCP1 activity. Our acetylome profiling showed that proteins from each of the ETC complexes have many SIRT3 regulated sites (Figure 2.6A). Many of these were located in defined domains, motifs or other regions of interest

(Figure 2.6A and Supplementary Table 3). Western blotting analysis showed that SIRT3 absence does not affect the expression levels of marker proteins for each of the ETC complexes between WT and *Sirt3*KO mice (Figure 2.6B & Supplementary Figure 4A-D). However, there was an effect of cold on the expression of the CIII marker protein, which reached statistical significance in WT mice, but not in *Sirt3*KO. To determine if there were functional differences in the activities of the complexes (CI, CII, CIII and CIV), we designed UCP1-independent respiration protocols in which we were able to examine each complex individually. Analyses of CI, CII, CIII and CIV activities were conducted using high resolution respirometry (O2K-Oroboros) in isolated mitochondria from BAT of WT or *Sirt3*KO room temperature housed (Figure 2.6C-F) and cold exposed mice (Figure 2.6G-J). The chemical uncoupler carbonylcyanide *p*-triflouromethoxyphenylhydrazone (FCCP), was added at the beginning of each respiration experiment to exclude any involvement of UCP1 function in the analyses. Relative to WT controls, CI was impaired in BAT mitochondria of *Sirt3*KO mice in room temperature [31% decreased versus WT; (Figure 2.6C)] and both CI and CII were decreased under cold stressed conditions [25% and 29%, respectively; (Figures 2.6G, H)]. Taken together, these results indicate that the absence of SIRT3 results in decreased activities of complexes I and II in BAT.

## 2.6 DISCUSSION

### 2.6.1 DEACETYLATION OF UPSTREAM PROTEINS OF UCP1 AS A REGULATOR OF BAT THERMOGENESIS

The control of BAT thermogenesis can be exerted at many levels: total amount of tissue; number of brown adipocytes in each depot; number of mitochondria in each cell; levels of UCP1 protein per mitochondrion; and finally the degree to which UCP1 is activated acutely by effectors such as FA upon adrenergic activation (Cannon and Nedergaard, 2004; Himms-Hagen, 1990). Work from the Spiegelman lab also provides evidence that UCP1-mediated thermogenesis is regulated by reactive oxygen spices (ROS) and cysteine sulfenylation of UCP1 (Chouchani et al., 2016). Recently, it has been reported that BAT thermogenesis can be regulated independently of adrenergic activation by unexpected metabolites such as succinate, and its oxidation by CII activates ROS induced thermogenesis (Mills et al., 2018). However, an unanswered question is whether deacetylation of UCP1 and/or the upstream pathways of UCP1, *i.e.,* the supply and flux of electrons from FA oxidative reactions, controls BAT thermogenesis.

Our work is the first to identify and elaborate the connections between SIRT3, the master deacetylase in the mitochondria, and BAT thermogenesis in mice. We provide evidence that the absence of SIRT3: (1) impairs use of BAT lipid content, (2) impairs thermoregulation in mice (3) increases BAT mitochondrial protein acetylation, (4) increases UCP1 lysine acetylation, but the mutation of these sites does not affect UCP1 leak respiration, (5) increases lysine acetylation in proteins that play key roles in FA uptake and oxidation, and that this is associated with decreases in circulating medium- and long- acylcarnitines, and finally, (6) increases the lysine acetylation of ETC complex subunits, which is associated with their impaired activities. Thus, we provide strong

evidence that SIRT3-mediated deacetylation is fundamentally important in driving BAT thermogenesis and SIRT3 is indirectly regulating UCP1 thermogenesis.

Previous work demonstrates that that non-enzymatic mitochondrial acetylation is driven by high levels of acetyl-CoA produced by FAO (Pougovkina et al., 2014). It has also been suggested that SIRT3 may play a critical role in promoting the reversal of non-enzymatic acetylations (Weinert et al., 2015). Altogether, our work is consistent with a model wherein a rise in acetyl CoA levels driven by cold stress results in increased non-enzymatic acetylations. Here, we propose that UCP1-mediated thermogenesis is compromised due to a failure to deacetylate substrate uptake and oxidation proteins that function upstream of UCP1 in *Sirt3*KO mice. This model does not lessen the centrality of UCP1 activation in the control of BAT thermogenesis, but demonstrates the importance of fatty acid uptake and oxidation reactions, and of subsequent redox reactions in the ETC, which collectively generate the heat when BAT is activated.

### 2.6.2 PHENOTYPES OF *SIRT3*KO MICE

While we ultimately defined SIRT3 as a critical regulator of BAT thermogenesis, we observed no differences in body composition, elevation of $VO_2$ upon cold exposure or CL316,243 injection, iBAT weight, mitochondrial content and UCP1 content between WT and *Sirt3*KO mice. Our results are supportive and consistent with previous findings that *Sirt3*KO mice show normal body weight (Lombard et al., 2007). However, *Sirt3*KO mice have impaired BAT lipid use upon cold exposure and do not show a significant decrease RER after BAT-specific activation as seen in WT mice, which could be an indicator of less activated BAT in *Sirt3*KO mice. Hirschey *et al.* previously showed that acute cold stress (6 hours) is associated with cold intolerance in *Sirt3*KO mice, but only when mice were fasted (Hirschey et al., 2010). Here we have demonstrated that *Sirt3*KO

mice under normal housing conditions with *ad libitum* access to food are cold-intolerant at 48h, a time at which BAT thermogenesis is normally the major thermoregulatory mechanism and shivering thermogenesis is normally minimal. Interestingly, $VO_2$ is not different between WT and *Sirt3*KO mice. This was unexpected, but given that these analyses were conducted in a whole body knockout mice, it was not entirely surprising since metabolic responses to cold are highly complex and represent an aggregated consequence of the effects of cold on many systems (*e.g.,* neural, muscular, circulatory). It is possible that the thermoregulatory phenotype of the whole body *Sirt3*KO mice is affected by the absence of SIRT3 in tissues other than BAT. In spite of the complexity of the study model, specific activation of BAT by a β3-adrenergic receptor agonist proved that the activity of BAT in *Sirt3*KO mice is impaired. It is also possible that *Sirt3*KOmice have defective regulation of heat loss as seen in other mouse models in which altered heat loss contributes to thermoregulation in mice (Fischer et al., 2016).

### 2.6.3 MECHANISM OF SIRT3 FUNCTION IN BAT THERMOGENESIS

UCP1 is essential for BAT thermogenesis, and induction of UCP1 in *Sirt3*KO mice was similar to that observed in WT mice. This observation contrasts with previous work *in vitro*. Specifically, Shi *et al* reported that overexpression of SIRT3 in the brown adipocyte cell line, HIB1B, resulted in increased expression of UCP1 mRNAs and that overexpression of dominant negative forms of SIRT3 leads to down-regulated expression of UCP1 (Shi et al., 2005). Instead, our observation is consistent with the *in vivo* findings of Lombard and colleagues who showed that the absence of SIRT3 does not affect the expression of UCP1 in mouse BAT (Lombard et al., 2007). Despite the wild-type expression level of UCP1, UCP1-mediated respiration in mitochondria from *Sirt3*KO mice was significantly decreased under cold stress. This was not observed in room

temperature housed animals. Cold stress may provide an optimal scenario under which to evaluate the function of UCP1 when it is fully activated, and it was in these conditions that we found defective UCP1-mediated respiration in *Sirt3*KO mice. Our acetylome work suggests that the functional relationship between UCP1 and SIRT3 stems from an impact of SIRT3 on upstream regulatory pathways.

### 2.6.4 REGULATED ACETYLATIONS DRIVING THERMOGENESIS

We identified four acetylation sites on UCP1 in mitochondria from mouse BAT (K56, K67, K73 and K151) and this is consistent with a previous study that identified three acetylation sites (K67, K73 and K151) in UCP1 in BAT homogenate from rat (Lundby et al., 2012). Mutation of the two SIRT3-regulated sites (K56 and K151) did not impact UCP1 function in a cell culture system**.** Yet, we cannot completely rule out a role for acetylation in the direct regulation of UCP1. Point mutants of UCP1 were assayed in a HEK293T cell line, which has previously been used to study the effects of novel activators of UCP1, such as TTNPB (Oelkrug et al., 2013). However, this system may not account for variables that normally play important roles in UCP1 function in brown adipocytes. For example, the HEK293T cell model clearly cannot fully recapitulate the effects of cold on signaling and metabolic processes that occur *in vivo*. We also focused exclusively on acetylation sites that face the mitochondrial matrix. Other acetylations that were not tested or that were not identified in our work could also be important for UCP1 function. Finally, UCP1 acetylation/deacetylation could function redundantly with other PTMs such as sulfenylation (Chouchani et al., 2016), or indirect modes of UCP1 regulation that we describe here. Notably, our observation that SIRT3 did not impact UCP1 acetylation sites in cold stress suggests that any such regulation is unlikely to account for the impact of SIRT3 on UCP1-dependent respiration.

BAT oxidizes a large amount of FAs from the circulation originating from white adipose tissue (WAT) or from the lipolysis of lipid droplets in BAT. Defects in FAO cause the release of acylcarnitines from mitochondria into the circulation (Aguer et al., 2014; McCoin et al., 2015), and given our mitochondrial acetylome results, we originally hypothesized that circulating acylcarnitines would be increased. However, our results show that the plasma levels of medium-chain and long-chain acylcarnitines in *Sirt3*KO mice were lower compared to WT mice. The following interpretations are possible: 1) decreased formation of acylcarnitines, which requires the uptake of FA by BAT mitochondria, and/or, 2) increased consumption of acylcarnitines by BAT mitochondria. We favor the former, given that our results show the acetylation of many of the enzymes involved in acylcarnitine/fatty acid metabolism in BAT mitochondria, which could result in a negative impact on enzymatic activity. For example, our acetylome profiling revealed that CACT, the main mitochondrial enzyme that regulates the entry of acylcarnitines to the mitochondria for FAO processes, was hyper-acetylated in *Sirt3*KO mitochondria and this could decrease its function. However, other interpretations are possible: there may be indirect effects of the activation of BAT thermogenesis by the use of CL compound, wherein increases in circulating free fatty acids from WAT or BAT result in genotype-specific differences in acylcarnitine metabolism in other tissues, such as the liver. Further research is needed to clarify the role of SIRT3 in acylcarnitine metabolism in activated BAT.

Multi-tissue quantitative acetylome work shows that SIRT3 expression varies between tissues such as liver, heart, kidney, brain, and skeletal muscle (Dittenhafer-Reed et al., 2015). Moreover, the mitochondrial regulation mediated by SIRT3 in various tissues is in a tissue-specific fashion and there are differences in the degree of how much SIRT3 regulates the metabolic

pathways in different tissues (Dittenhafer-Reed et al., 2015), suggesting the importance of studying the role of SIRT3 in regulating the metabolic pathways in BAT and in its activated status. Given the unique function and important physiological role of BAT, we studied the role of SIRT3 in regulating the ETC pathway in BAT mitochondria, which is not well-characterized. For the first time, we report that *Sirt3*KO mitochondria from iBAT of cold exposed mice have impaired activities of CI and CII during cold stress and this correlates with the increased acetylation observed on subunits from CI and CII proteins. These observations extend the work of other groups who show that CI and/or CII function are decreased in isolated mitochondria from liver of *Sirt3*KO mice (Ahn et al., 2008; Cimen et al., 2010). Finley et al. found a trend ($p = 0.07$) for decreased enzymatic activity of CII in BAT mitochondria from *Sirt3*KO mice, but these analyses were not carried out under conditions that activate BAT, and more importantly, they were spectrophotometric Vmax-type assays, rather than assays of its activity within the functioning respiratory chain (Finley et al., 2011). Although previous work identified SIRT3 regulated sites in Subunit A of CII in liver mitochondria (Cimen et al., 2010; Finley et al., 2011), here our acetylome profiling data identify SIRT3 regulated lysine acetylation sites in subunit A and subunit B of CII in BAT mitochondria from mice housed in room temperature and cold conditions, suggesting a mechanism for the impact of SIRT3 on CII function specifically in this tissue. While we show that CI and CII proteins are equally expressed in BAT mitochondria from WT and *Sirt3*KO mice, we cannot rule out the possibility that the functional defects described herein stem from decreased stability of some subunits of CI and CII that were not examined. Alternatively, hyper-acetylation in the absence of SIRT3 may impair complex functions without affecting overall protein levels. An unresolved question is the fraction of each target protein population that is acetylated in the

presence and absence of SIRT3. Previous efforts to quantify stoichiometry of individual acetylation sites suggests that even regulated acetylations often involve only a small fraction of the target population at any one time (Hansen et al., 2019; Weinert et al., 2015; Zhou et al., 2016). In the mitochondria, these low-level acetylations may represent a form of protein damage that disrupt critical functions only when a threshold is reached across many proteins in a given pathway (Weinert et al., 2015). On the other hand, acetylations impacting a larger fraction of a target population may be better situated to disrupt critical protein-protein interactions or directly inhibit important enzymatic activities.

## 2.7 CONCLUSION

Altogether, our results demonstrate for the first time that SIRT3-mediated deacetylation of an extensive array of mitochondrial proteins in BAT plays a fundamental role in thermogenesis. We propose a model wherein UCP1-mediated thermogenesis is indirectly regulated by deacetylation of many substrate uptake and oxidation pathways that are upstream of UCP1. Our proteomics findings provide an extensive resource for future investigations into these mechanisms, and others, in the context of the newly described functional connections between SIRT3 and UCP1.

## 2.8 REFERENCE


Aguer, C., McCoin, C.S., Knotts, T.A., Thrush, A.B., Ono-Moore, K., McPherson, R., Dent, R., Hwang, D.H., Adams, S.H., and Harper, M.-E. (2014). Acylcarnitines: potential implications for skeletal muscle insulin resistance. The FASEB Journal. *29*, 336–345.

Ahn, B.-H., Kim, H.-S., Song, S., Lee, I.H., Liu, J., Vassilopoulos, A., Deng, C.-X., and Finkel, T. (2008). A role for the mitochondrial deacetylase Sirt3 in regulating energy homeostasis. Proc Natl Acad Sci U S A. *105*, 14447–14452.

Anderson, K.A., and Hirschey, M.D. (2012). Mitochondrial protein acetylation regulates metabolism. Essays Biochem. *52*.

Bartelt, A., Bruns, O.T., Reimer, R., Hohenberg, H., Ittrich, H., Peldschus, K., Kaul, M.G., Tromsdorf, U.I., Weller, H., Waurisch, C., et al. (2011). Brown adipose tissue activity controls triglyceride clearance. Nature Medicine. *17*, 200–205.

Beauchamp, B., Thrush, A.B., Quizi, J., Antoun, G., McIntosh, N., Al-Dirbashi, O.Y., Patti, M.-E., and Harper, M.-E. (2015). Undernutrition during pregnancy in mice leads to dysfunctional cardiac muscle respiration in adult offspring. Biosci Rep. *35*.

Blondin, D.P., Labbé, S.M., Tingelstad, H.C., Noll, C., Kunach, M., Phoenix, S., Guérin, B., Turcotte, E.E., Carpentier, A.C., Richard, D., et al. (2014). Increased brown adipose tissue oxidative capacity in cold-acclimated humans. J. Clin. Endocrinol. Metab. *99*, E438-446.

Cannon, B., and Nedergaard, J. (2004). Brown Adipose Tissue: Function and Physiological Significance. Physiological Reviews. *84*, 277–359.

Cao, W., Daniel, K.W., Robidoux, J., Puigserver, P., Medvedev, A.V., Bai, X., Floering, L.M., Spiegelman, B.M., and Collins, S. (2004). p38 Mitogen-Activated Protein Kinase Is the Central Regulator of Cyclic AMP-Dependent Transcription of the Brown Fat Uncoupling Protein 1 Gene. Mol Cell Biol. *24*, 3057–3067.

Choi, M., Chang, C.-Y., Clough, T., Broudy, D., Killeen, T., MacLean, B., and Vitek, O. (2014). MSstats: an R package for statistical analysis of quantitative mass spectrometry-based proteomic experiments. Bioinformatics. *30*, 2524–2526.

Chouchani, E.T., Kazak, L., Jedrychowski, M.P., Lu, G.Z., Erickson, B.K., Szpyt, J., Pierce, K.A., Laznik-Bogoslavski, D., Vetrivelan, R., Clish, C.B., et al. (2016). Mitochondrial ROS regulate thermogenic energy expenditure and sulfenylation of UCP1. Nature. *532*, 112–116.

Cimen, H., Han, M.-J., Yang, Y., Tong, Q., Koc, H., and Koc, E.C. (2010). Regulation of Succinate Dehydrogenase Activity by SIRT3 in Mammalian Mitochondria. Biochemistry. *49*, 304–311.

Cox, J., and Mann, M. (2008). MaxQuant enables high peptide identification rates, individualized p.p.b.-range mass accuracies and proteome-wide protein quantification. Nat. Biotechnol. *26*, 1367–1372.

Dittenhafer-Reed, K.E., Richards, A.L., Fan, J., Smallegan, M.J., Siahpirani, A.F., Kemmerer, Z.A., Prolla, T.A., Roy, S., Coon, J.J., and Denu, J.M. (2015). SIRT3 mediates multi-tissue coupling for metabolic fuel switching. Cell Metab. *21*, 637–646.

Downey, M., Johnson, J.R., Davey, N.E., Newton, B.W., Johnson, T.L., Galaang, S., Seller, C.A., Krogan, N., and Toczyski, D.P. (2015). Acetylome profiling reveals overlap in the regulation of diverse processes by sirtuins, gcn5, and esa1. Mol. Cell Proteomics. *14*, 162–176.

Du, J., Zhou, Y., Su, X., Yu, J.J., Khan, S., Jiang, H., Kim, J., Woo, J., Kim, J.H., Choi, B.H., et al. (2011). Sirt5 Is an NAD-Dependent Protein Lysine Demalonylase and Desuccinylase. Science. *334*, 806–809.

Enerbäck, S., Jacobsson, A., Simpson, E.M., Guerra, C., Yamashita, H., Harper, M.-E., and Kozak, L.P. (1997). Mice lacking mitochondrial uncoupling protein are cold-sensitive but not obese. Nature. *387*, 90–94.

Finley, L.W.S., Haas, W., Desquiret-Dumas, V., Wallace, D.C., Procaccio, V., Gygi, S.P., and Haigis, M.C. (2011). Succinate Dehydrogenase Is a Direct Target of Sirtuin 3 Deacetylase Activity. PLoS One. *6*.

Fischer, A.W., Hoefig, C.S., Abreu-Vieira, G., de Jong, J.M.A., Petrovic, N., Mittag, J., Cannon, B., and Nedergaard, J. (2016). Leptin Raises Defended Body Temperature without Activating Thermogenesis. Cell Reports. *14*, 1621–1631.

Golozoubova, V., Hohtola, E., Matthias, A., Jacobsson, A., Cannon, B., and Nedergaard, J. (2001). Only UCP1 can mediate adaptive nonshivering thermogenesis in the cold. The FASEB Journal. *15*, 2048–2050.

Haigis, M.C., Mostoslavsky, R., Haigis, K.M., Fahie, K., Christodoulou, D.C., Murphy, A.J., Valenzuela, D.M., Yancopoulos, G.D., Karow, M., Blander, G., et al. (2006). SIRT4 Inhibits Glutamate Dehydrogenase and Opposes the Effects of Calorie Restriction in Pancreatic β Cells. Cell. *126*, 941–954.

Hansen, B.K., Gupta, R., Baldus, L., Lyon, D., Narita, T., Lammers, M., Choudhary, C., and Weinert, B.T. (2019). Analysis of human acetylation stoichiometry defines mechanistic constraints on protein regulation. Nat Commun. *10*.

Heaton, G.M., Wagenvoord, R.J., Kemp, A., and Nicholls, D.G. Brown-Adipose-Tissue Mitochondria: Photoaffinity Labelling of the Regulatory Site of Energy Dissipation. European Journal of Biochemistry. *82*, 515–521.

Himms-Hagen, J. (1985). Brown Adipose Tissue Metabolism and Thermogenesis. Annual Review of Nutrition. *5*, 69–94.

Himms-Hagen, J. (1990). Brown adipose tissue thermogenesis: interdisciplinary studies. FASEB J. *4*, 2890–2898.

Hirschey, M.D., Shimazu, T., Goetzman, E., Jing, E., Schwer, B., Lombard, D.B., Grueter, C.A., Harris, C., Biddinger, S., Ilkayeva, O.R., et al. (2010). SIRT3 regulates fatty acid oxidation via reversible enzyme deacetylation. Nature. *464*, 121–125.

Hirschey, M.D., Shimazu, T., Huang, J.-Y., Schwer, B., and Verdin, E. (2011). SIRT3 Regulates Mitochondrial Protein Acetylation and Intermediary Metabolism. Cold Spring Harb Symp Quant Biol. *76*, 267–277.

Houten, S.M., and Wanders, R.J.A. (2010). A general introduction to the biochemistry of mitochondrial fatty acid β-oxidation. J Inherit Metab Dis. *33*, 469–477.

Jastroch, M., Hirschberg, V., and Klingenspor, M. (2011). No mitochondrial uncoupling artefact is caused by expression of uncoupling protein 1 in a mammalian cell culture: A new system to study mitochondrial carrier proteins. The FASEB Journal. *25*, 1044.3-1044.3.

Jastroch, M., Hirschberg, V., and Klingenspor, M. (2012). Functional characterization of UCP1 in mammalian HEK293 cells excludes mitochondrial uncoupling artefacts and reveals no contribution to basal proton leak. Biochimica et Biophysica Acta (BBA) - Bioenergetics. *1817*, 1660–1670.

Jing, E., O'Neill, B.T., Rardin, M.J., Kleinridders, A., Ilkeyeva, O.R., Ussar, S., Bain, J.R., Lee, K.Y., Verdin, E.M., Newgard, C.B., et al. (2013). Sirt3 Regulates Metabolic Flexibility of Skeletal Muscle Through Reversible Enzymatic Deacetylation. Diabetes. *62*, 3404–3417.

Klingenberg, M., Echtay, K.S., Bienengraeber, M., Winkler, E., and Huang, S.G. (1999). Structure-function relationship in UCP1. Int. J. Obes. Relat. Metab. Disord. *23 Suppl 6*, S24-29.

Krystkowiak, I., and Davey, N.E. (2017). SLiMSearch: a framework for proteome-wide discovery and annotation of functional modules in intrinsically disordered regions. Nucleic Acids Res. *45*, W464–W469.

Lombard, D.B., Alt, F.W., Cheng, H.-L., Bunkenborg, J., Streeper, R.S., Mostoslavsky, R., Kim, J., Yancopoulos, G., Valenzuela, D., Murphy, A., et al. (2007). Mammalian Sir2 homolog SIRT3 regulates global mitochondrial lysine acetylation. Mol. Cell. Biol. *27*, 8807–8814.

Lundby, A., Lage, K., Weinert, B.T., Bekker-Jensen, D.B., Secher, A., Skovgaard, T., Kelstrup, C.D., Dmytriyev, A., Choudhary, C., Lundby, C., et al. (2012). Proteomic Analysis of Lysine Acetylation Sites in Rat Tissues Reveals Organ Specificity and Subcellular Patterns. Cell Rep. *2*, 419–431.

McCoin, C.S., Knotts, T.A., and Adams, S.H. (2015). Acylcarnitines—old actors auditioning for new roles in metabolic physiology. Nat Rev Endocrinol. *11*, 617–625.

Mills, E.L., Pierce, K.A., Jedrychowski, M.P., Garrity, R., Winther, S., Vidoni, S., Yoneshiro, T., Spinelli, J.B., Lu, G.Z., Kazak, L., et al. (2018). Accumulation of succinate controls activation of adipose tissue thermogenesis. Nature. *560*, 102-106.

Nedergaard, J., and Cannon, B. (2013). UCP1 mRNA does not produce heat. Biochimica et Biophysica Acta (BBA) - Molecular and Cell Biology of Lipids. *1831*, 943–949.
Nicholls, D.G., and Locke, R.M. (1984). Thermogenic mechanisms in brown fat. Physiological Reviews. *64*, 1–64.

Nicholls, D.G., and Rial, E. (1999). A history of the first uncoupling protein, UCP1. J. Bioenerg. Biomembr. *31*, 399–406.

Oelkrug, R., Goetze, N., Exner, C., Lee, Y., Ganjam, G.K., Kutschke, M., Müller, S., Stöhr, S., Tschöp, M.H., Crichton, P.G., et al. (2013). Brown fat in a protoendothermic mammal fuels eutherian evolution. Nature Communications. *4*, 2140.

Palacios, O.M., Carmona, J.J., Michan, S., Chen, K.Y., Manabe, Y., III, J.L.W., Goodyear, L.J., and Tong, Q. (2009). Diet and exercise signals regulate SIRT3 and activate AMPK and PGC-1α in skeletal muscle. Aging (Albany NY). *1*, 771–783.

Perez-Riverol, Y., Csordas, A., Bai, J., Bernal-Llinares, M., Hewapathirana, S., Kundu, D.J., Inuganti, A., Griss, J., Mayer, G., Eisenacher, M., et al. (2019). The PRIDE database and related tools and resources in 2019: improving support for quantification data. Nucleic Acids Res. *47*, D442–D450.

Pougovkina, O., te Brinke, H., Ofman, R., Cruchten, V., G, A., Kulik, W., Wanders, R.J.A., Houten, S.M., Boer, D., and C.j, V. (2014). Mitochondrial protein acetylation is driven by acetyl-CoA from fatty acid oxidation. Hum Mol Genet. *23*, 3513–3522.

Rabelo, R., Schifman, A., Rubio, A., Sheng, X., and Silva, J.E. (1995). Delineation of thyroid hormone-responsive sequences within a critical enhancer in the rat uncoupling protein gene. Endocrinology. *136*, 1003–1013.

Rial, E., González-Barroso, M., Fleury, C., Iturrizaga, S., Sanchis, D., Jiménez-Jiménez, J., Ricquier, D., Goubern, M., and Bouillaud, F. (1999). Retinoids activate proton transport by the uncoupling proteins UCP1 and UCP2. The EMBO Journal. *18*, 5827–5833.

Schindelin, J., Arganda-Carreras, I., Frise, E., Kaynig, V., Longair, M., Pietzsch, T., Preibisch, S., Rueden, C., Saalfeld, S., Schmid, B., et al. (2012). Fiji: an open-source platform for biological-image analysis. Nature Methods. *9*, 676–682.

Schreiber, R., Diwoky, C., Schoiswohl, G., Feiler, U., Wongsiriroj, N., Abdellatif, M., Kolb, D., Hoeks, J., Kershaw, E.E., Sedej, S., et al. (2017). Cold-Induced Thermogenesis Depends on ATGL-Mediated Lipolysis in Cardiac Muscle, but Not Brown Adipose Tissue. Cell Metab. *26*, 753-763.e7.

Shabalina, I.G., Jacobsson, A., Cannon, B., and Nedergaard, J. (2004). Native UCP1 Displays Simple Competitive Kinetics between the Regulators Purine Nucleotides and Fatty Acids. J. Biol. Chem. *279*, 38236–38248.

Shabalina, I.G., Ost, M., Petrovic, N., Vrbacky, M., Nedergaard, J., and Cannon, B. (2010). Uncoupling protein-1 is not leaky. Biochimica et Biophysica Acta (BBA) - Bioenergetics. *1797*, 773–784.

Shabalina, I.G., Petrovic, N., de Jong, J.M.A., Kalinovich, A.V., Cannon, B., and Nedergaard, J. (2013). UCP1 in Brite/Beige Adipose Tissue Mitochondria Is Functionally Thermogenic. Cell Reports. *5*, 1196–1203.

Shi, T., Wang, F., Stieren, E., and Tong, Q. (2005). SIRT3, a Mitochondrial Sirtuin Deacetylase, Regulates Mitochondrial Function and Thermogenesis in Brown Adipocytes. J. Biol. Chem. *280*, 13560–13567.

Shin, H., Ma, Y., Chanturiya, T., Cao, Q., Wang, Y., Kadegowda, A.K.G., Jackson, R., Rumore, D., Xue, B., Shi, H., et al. (2017). Lipolysis in Brown Adipocytes Is Not Essential for Cold-Induced Thermogenesis in Mice. Cell Metab. *26*, 764-777.e5.

Shore, A., Emes, R.D., Wessely, F., Kemp, P., Cillo, C., D'Armiento, M., Hoggard, N., and Lomax, M.A. (2013). A Comparative Approach to Understanding Tissue-Specific Expression of Uncoupling Protein 1 Expression in Adipose Tissue. Front. Genet. *3*, 304.

Silva, J.P., Shabalina, I.G., Dufour, E., Petrovic, N., Backlund, E.C., Hultenby, K., Wibom, R., Nedergaard, J., Cannon, B., and Larsson, N.-G. (2005). SOD2 overexpression: enhanced mitochondrial tolerance but absence of effect on UCP activity. EMBO J. *24*, 4061–4070.

Stier, A., Bize, P., Habold, C., Bouillaud, F., Massemin, S., and Criscuolo, F. (2014). Mitochondrial uncoupling prevents cold-induced oxidative stress: a case study using UCP1 knockout mice. Journal of Experimental Biology. *217*, 624–630.

Tan, M., Peng, C., Anderson, K.A., Chhoy, P., Xie, Z., Dai, L., Park, J.S., Chen, Y., Huang, H., Zhang, Y., et al. (2014). Lysine Glutarylation Is a Protein Post-Translational Modification Regulated by SIRT5. Cell Metab. *19*, 605–617.

Tomás, P., Jiménez-Jiménez, J., Zaragoza, P., Vuligonda, V., Chandraratna, R.A., and Rial, E. (2004). Activation by retinoids of the uncoupling protein UCP1. Biochim Biophys Acta. *1658*, 157–164.

Tripathi, S., Pohl, M.O., Zhou, Y., Rodriguez-Frandsen, A., Wang, G., Stein, D.A., Moulton, H.M., DeJesus, P., Che, J., Mulder, L.C.F., et al. (2015). Meta- and Orthogonal Integration of Influenza "OMICs" Data Defines a Role for UBR4 in Virus Budding. Cell Host Microbe. *18*, 723–735.

U Din, M., Raiko, J., Saari, T., Kudomi, N., Tolvanen, T., Oikonen, V., Teuho, J., Sipilä, H.T., Savisto, N., Parkkola, R., et al. (2016). Human brown adipose tissue [(15)O]O2 PET imaging in the presence and absence of cold stimulus. Eur. J. Nucl. Med. Mol. Imaging. *43*, 1878–1886.

Weinert, B.T., Iesmantavicius, V., Moustafa, T., Schölz, C., Wagner, S.A., Magnes, C., Zechner, R., and Choudhary, C. (2014). Acetylation dynamics and stoichiometry in Saccharomyces cerevisiae. Mol. Syst. Biol. *10*, 716.

Weinert, B.T., Moustafa, T., Iesmantavicius, V., Zechner, R., and Choudhary, C. (2015). Analysis of acetylation stoichiometry suggests that SIRT3 repairs nonenzymatic acetylation lesions. EMBO J. *34*, 2620–2632.

Xu, S., Jay, A., Brunaldi, K., Huang, N., and Hamilton, J.A. (2013). CD36 Enhances Fatty Acid Uptake by Increasing the Rate of Intracellular Esterification but Not Transport across the Plasma Membrane. Biochemistry. *52*, 7254–7261.

Yu, X.X., Lewin, D.A., Forrest, W., and Adams, S.H. (2002). Cold elicits the simultaneous induction of fatty acid synthesis and β-oxidation in murine brown adipose tissue: prediction from differential gene expression and confirmation in vivo. The FASEB Journal. *16*, 155–168.

Zhou, T., Chung, Y.-H., Chen, J., and Chen, Y. (2016). Site-Specific Identification of Lysine Acetylation Stoichiometries in Mammalian Cells. J. Proteome Res. *15*, 1103–1113.

## 2.9 FIGURES

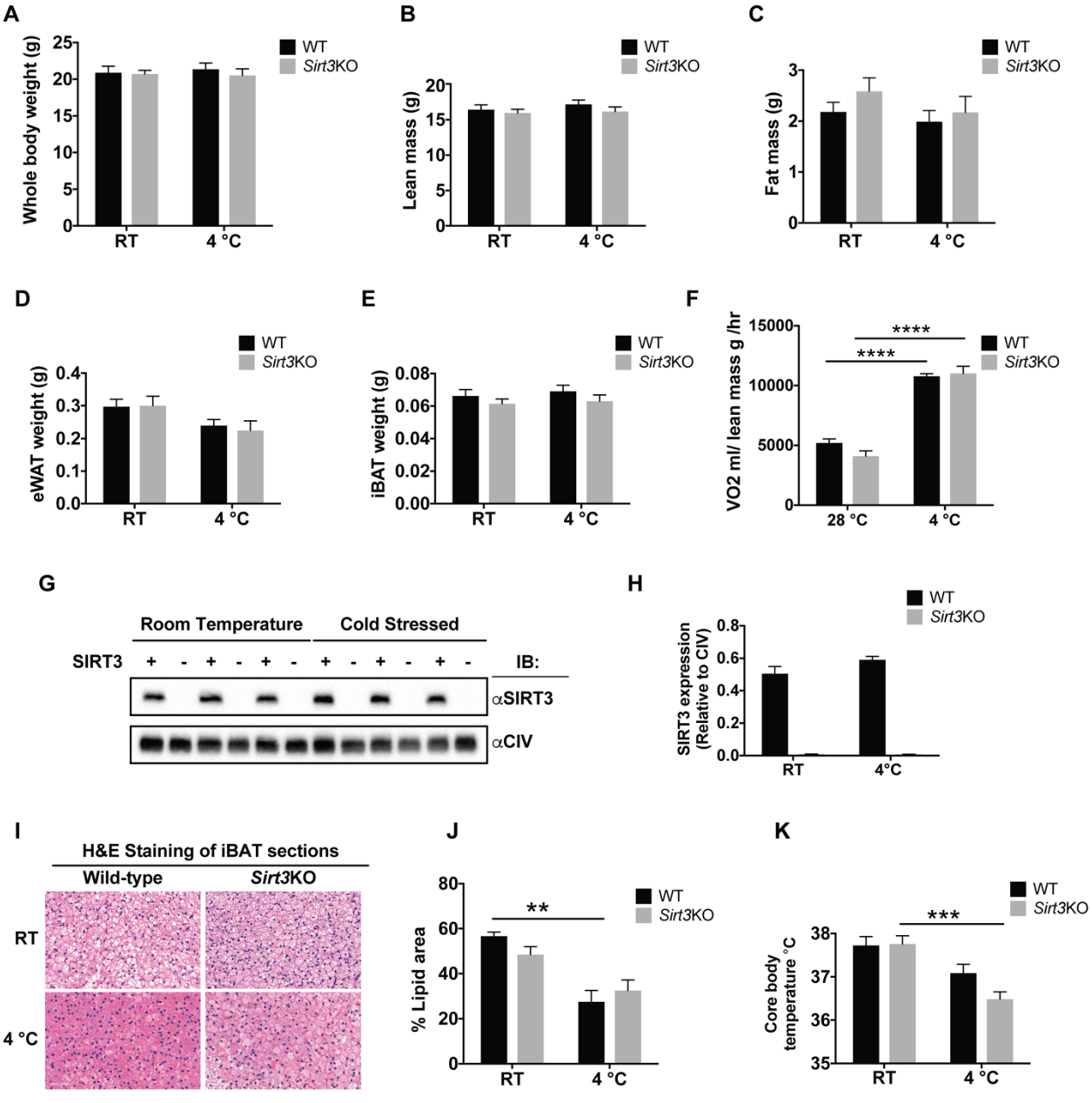
A
Whole body weight (g)
25
20
15
10
5
0
RT
4 °C
WT
Sirt3KO
B
Lean mass (g)
20
15
10
5
0
RT
4 °C
WT
Sirt3KO
C
Fat mass (g)
3
2
1
0
RT
4 °C
WT
Sirt3KO
D
eWAT weight (g)
0.4
0.3
0.2
0.1
0.0
RT
4 °C
WT
Sirt3KO
E
iBAT weight (g)
0.08
0.06
0.04
0.02
0.00
RT
4 °C
WT
Sirt3KO
F
VO2 ml/ lean mass g /hr
15000
10000
5000
0
****
****
28 °C
4 °C
WT
Sirt3KO
G
Room Temperature
Cold Stressed
SIRT3 + - + - + - + - + - + - IB:
αSIRT3
αCIV
H
SIRT3 expression (Relative to CIV)
0.8
0.6
0.4
0.2
0.0
RT
4°C
WT
Sirt3KO
I
H&E Staining of iBAT sections
Wild-type
Sirt3KO
RT
4 °C
J
% Lipid area
80
60
40
20
0
**
RT
4 °C
WT
Sirt3KO
K
Core body temperature °C
38
37
36
35
***
RT
4 °C
WT
Sirt3KO

**Figure 2.1: *Sirt3*KO mice have normal morphometrics but impaired use of lipid in BAT and impaired thermoregulation upon cold exposure.**

WT and *Sirt3*KO mice were housed at room temperature (23$^{o}$C) or were exposed to 4 °C for 2 days. A) Whole body weight, B) Lean mass, C) Fat mass, D) Epididymal white adipose tissues (eWAT), E) interscapular brown adipose tissues (iBAT) was measured, N=8-9/ group.

F) WT and *Sirt*3KO mice were kept either at 28 °C or 4 °C in CLAMS. $VO_2$ was measured and normalized to lean body mass, N=8-9/ group.

G) Western blotting analysis of SIRT3 expression in isolated mitochondria from iBAT of either room temperature housed or cold exposed WT and *Sirt3*KO mice. N=3/group

H) Quantification of SIRT3 western blotting.

I) H & E stained sections of iBAT of room temperature housed or cold stressed WT and *Sirt3*KO. N=4-6/group. Scale bar for all images: 50 µm.

J) Lipid droplet surface area percentage, as analyzed by quantitative morphometry. N=4-6/group.

K) Core body temperature, measured before and after cold exposure. N= 8/group.

Data are represented as mean ± SEM. Two-way ANOVA with Tukey's test, ***p<0.01, ***p<0.001, ****p<0.0001*.

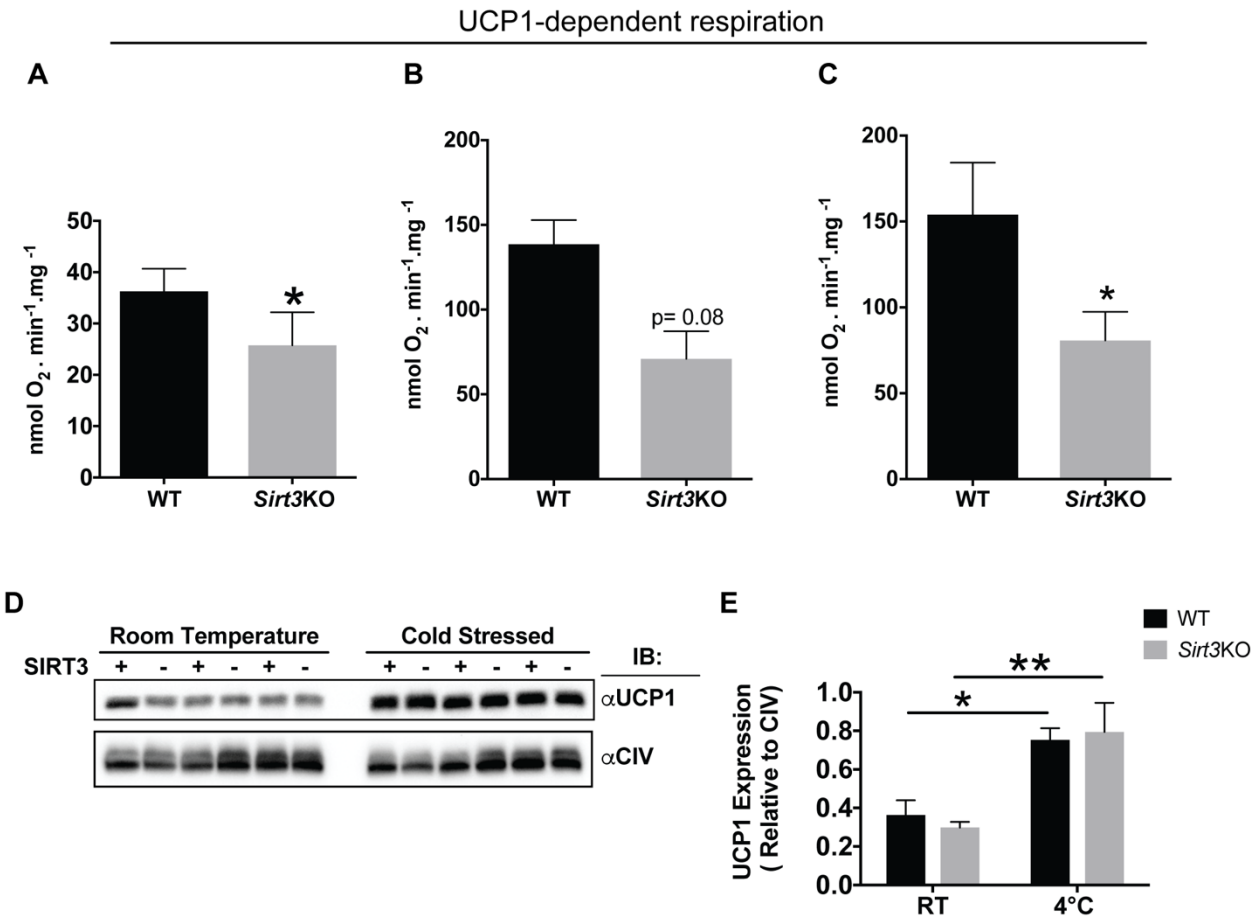
UCP1-dependent respiration
A
B
C
nmol O2 . min-1.mg -1
50
40
30
20
10
0
*
WT
Sirt3KO
200
150
100
50
0
p= 0.08
D
Room Temperature
Cold Stressed
SIRT3
+ - + - + -
+ - + - + -
IB:
αUCP1
αCIV
E
WT
Sirt3KO
**
*
UCP1 Expression
( Relative to CIV)
1.0
0.8
0.6
0.4
0.2
0.0
RT
4°C

**Figure 2.2: UCP1 dependent respiration is decreased in BAT of *Sirt3*KO mice.**
A) UCP1 dependent respiration was measured in isolated mitochondria from iBAT of room temperature housed WT and *Sirt*3KO mice. 0.35mg Mitochondria were energized with 25µM PLC and UCP1 dependent respiration was determined as that which was inhibited by 2mM GDP. N=6/group.
B) UCP1 dependent respiration was measured in isolated mitochondria from iBAT of room temperature housed WT and *Sirt*3KO mice. 0.25mg Mitochondria were energized with 5mM G3P and UCP1 dependent respiration was determined as that which was inhibited by 2mM GDP. N=4/group.
C) UCP1 dependent respiration were measured in isolated mitochondria from iBAT of cold exposed WT and *Sirt*3KO mice. 0.25mg Mitochondria were energized with 5mM G3P and UCP1 dependent respiration was determined as that inhibited by 2mM GDP. N=4/group.
D) Western blotting analysis of UCP1 expression. N=3/group.
E) Quantification of UCP1 western blotting.
Data are represented as mean ± SEM. Student's t-test; Two-tailed and two-way ANOVA with Sidak's test were used, **p<0.05 and **p<0.01.*

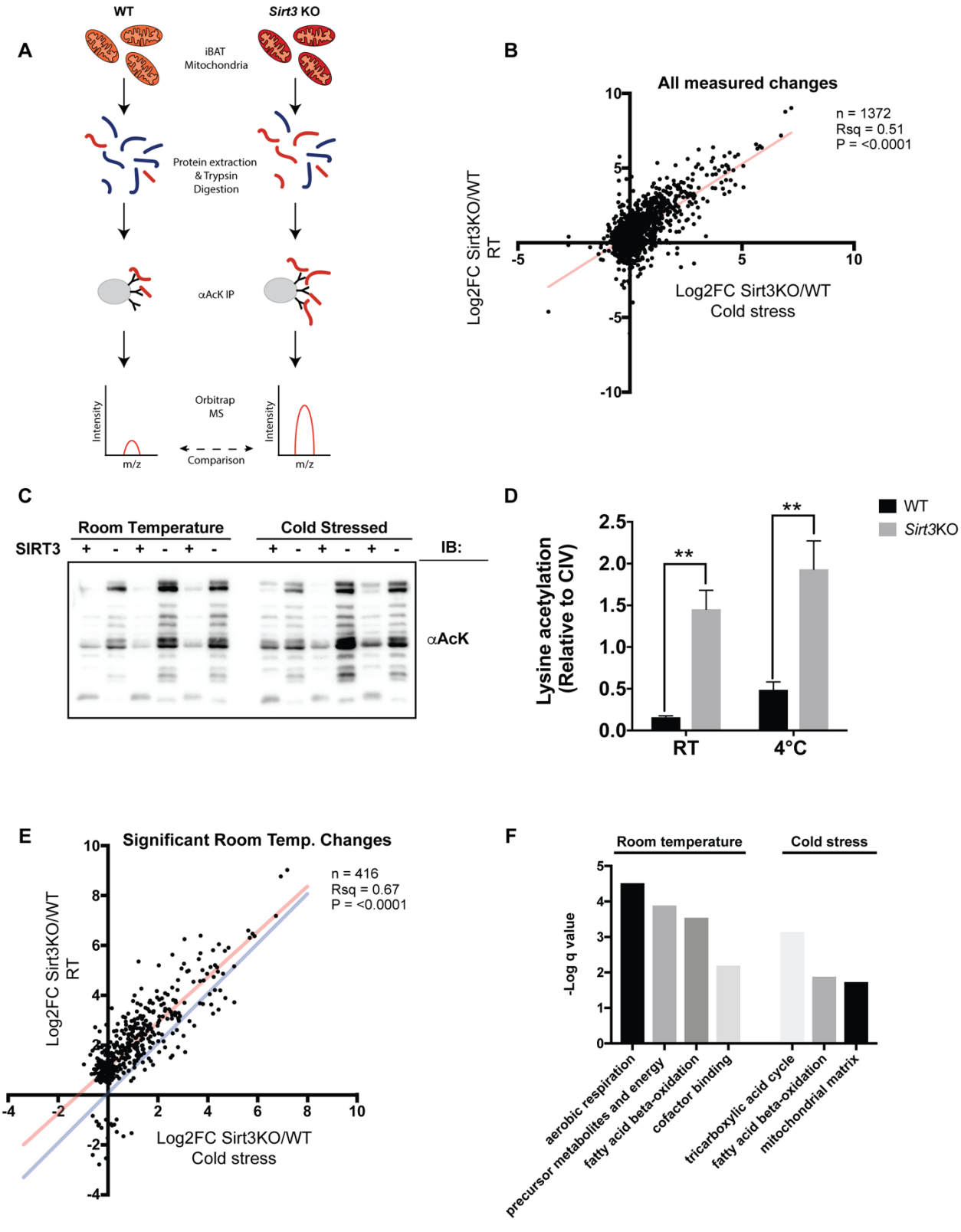
A
WT
Sirt3 KO
iBAT
Mitochondria
Protein extraction
& Trypsin
Digestion
αAcK IP
Orbitrap
MS
Intensity
m/z
Comparison
B
All measured changes
n = 1372
Rsq = 0.51
P = <0.0001
Log2FC Sirt3KO/WT
RT
Log2FC Sirt3KO/WT
Cold stress
C
Room Temperature
Cold Stressed
SIRT3
IB:
αAcK
D
WT
Sirt3KO
Lysine acetylation
(Relative to CIV)
RT
4°C
E
Significant Room Temp. Changes
n = 416
Rsq = 0.67
P = <0.0001
Log2FC Sirt3KO/WT
RT
Log2FC Sirt3KO/WT
Cold stress
F
Room temperature
Cold stress
-Log q value
aerobic respiration
precursor metabolites and energy
fatty acid beta-oxidation
cofactor binding
tricarboxylic acid cycle
fatty acid beta-oxidation
mitochondrial matrix

**Figure 2.3: Cold and the absence of SIRT3 increase mitochondrial acetylation.**

A) Schematic diagram of acetylome profiling of isolated BAT mitochondria. Proteins were extracted from iBAT mitochondria under denaturing conditions prior to trypsinization and immunopurification with anti-acetyllysine antibodies and analysis using Orbitrap MS, as described in the experimental procedures. Two distinct experiments were carried out comparing wild-type to *Sirt3*KO animals, housed at either room temperature (experiment 1) or at 4 °C for 2 days (experiment 2). N=6 BAT mitochondria samples for each genotype.

B) Measured Log2FC *Sirt3*KO/WT was plotted for acetylated lysines detected via MS for room temperature versus cold treated mice. Log2FC computed using MSStats, as described in the experimental procedures. Linear regression calculated using GraphPad Prism. This analysis includes significant and non-significant changes.

C) Total mitochondrial acetylation was assessed by western blotting from samples described in Figure 2.2D. N=3/group. **Note: same blots as Figure 2.2D were probed for mitochondrial acetylation. As such, the loading control of the acetylation blot is the same loading control in as Figure 2.2D.**

D) Quantification of mitochondrial acetylation western blotting.

Data are represented as mean ± SEM. Two-way ANOVA with Sidak's test was used, ***p<0.01.*

E) Greater measured impact of SIRT3 at room temperature relative to cold stressed animals. Measured Log2FC *Sirt3*KO/WT was plotted for acetylated lysines detected via MS for room temperature versus cold treated mice. Log2FC computed using MSStats, as described in the experimental procedures. Linear regression calculated using GraphPad Prism. Plotted are significantly-regulated sites detected in samples from room temperature housed animals, regardless of fold-change versus corresponding fold-change detected in cold stressed animals, regardless of significance. Red line indicates the best fit line of linear regression. The blue line represents slope = 1. The majority of data points above blue line suggests more dramatic changes in room temperature housed animals. The graph contains a subset of the data plotted in Figure 2.3B.

F) GO-term enrichment of SIRT3-regulated lysine acetylation sites calculated using Metascape for room-temperature and cold-regulated sites (log2 *Sirt3*KO/WT >1; adjusted *p*> 0.05). Only sites for which numerical p values should be calculated are shown. q values represent p values of GO-term analyses following adjustment for multiple-testing.

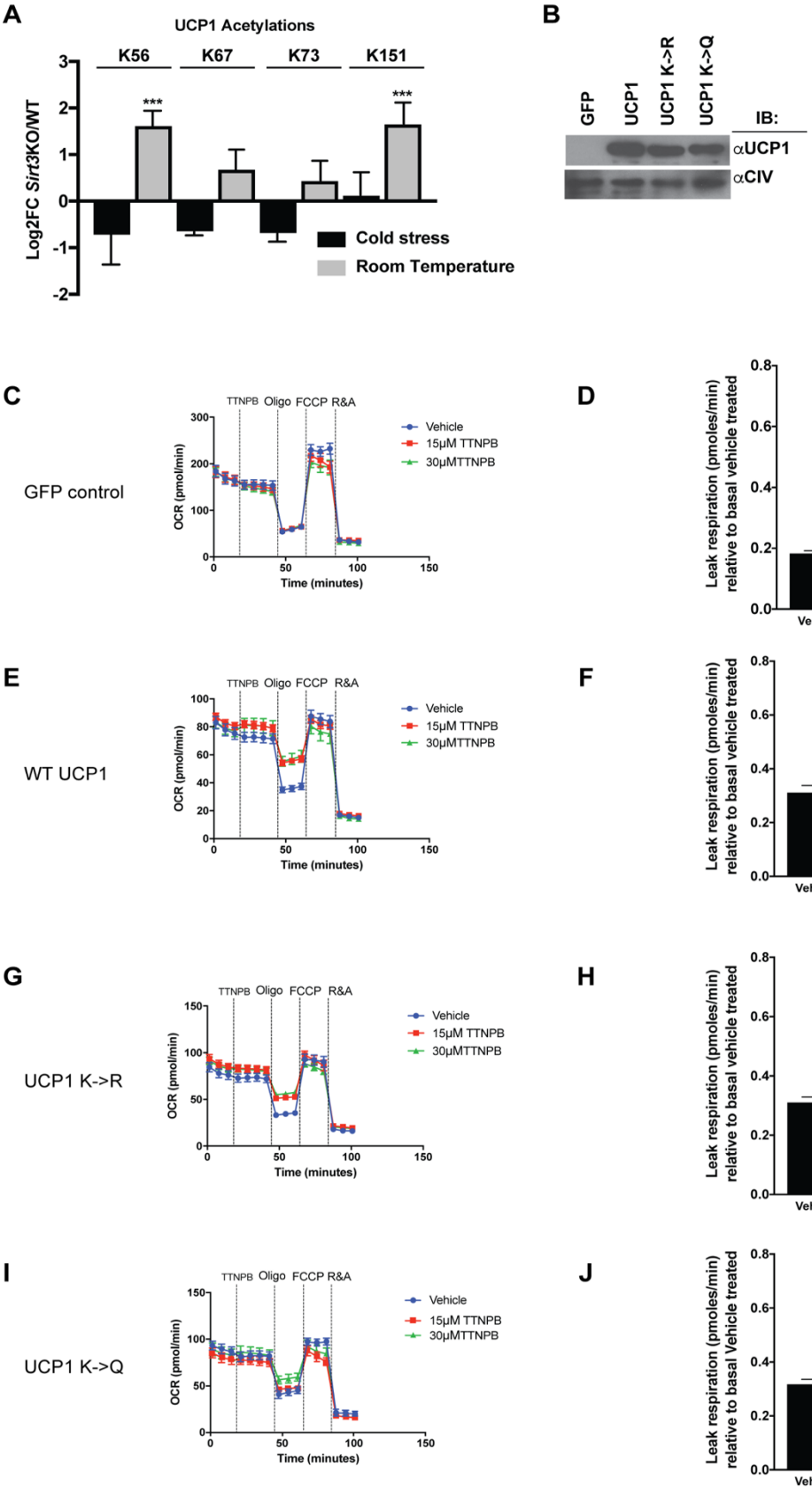
A
UCP1 Acetylations
K56
K67
K73
K151
***
***
Log2FC Sirt3KO/WT
Cold stress
Room Temperature
B
GFP
UCP1
UCP1 K->R
UCP1 K->Q
IB:
αUCP1
αCIV
C
GFP control
TTNPB Oligo FCCP R&A
OCR (pmol/min)
Time (minutes)
Vehicle
15μM TTNPB
30μMTTNPB
D
Leak respiration (pmoles/min) relative to basal vehicle treated
Vehicle
15μM TTNPB
30μM TTNPB
E
WT UCP1
F
G
UCP1 K->R
H
I
UCP1 K->Q
J
Leak respiration (pmoles/min) relative to basal Vehicle treated

**Figure 2.4: Acetylation of lysines on UCP1 does not affect UCP1 leak respiration.**

A) Regulated sites were detected in UCP1 from BAT mitochondria isolated from room temperature housed WT and *Sirt3*KO mice. Error bars represent standard error of the mean. Asterisks represent $p<0.01$. In corresponding cold stressed WT and *Sirt3*KO mice, no sites with statistically-significant changes were detected.

B) Western blotting of UCP1 expression in HEK293T cells that were transfected with GPF, $UCP1^{(wt)}$, $UCP1^{(K->R)}$ and $UCP1^{(K->Q)}$ plasmids.

C) A representative trace of functional analyses of GFP transfected cells that were injected with a vehicle control or injected with 15 µM or 30 µM TTNPB.

D) UCP1 leak respiration measurements of GFP transfected cells. N=4.

E) A representative trace of functional analyses of $UCP1^{(wt)}$ transfected cells that were injected with a vehicle control or injected with 15 µM or 30 µM TTNPB.

F) UCP1 leak respiration measurements of $UCP1^{(wt)}$ transfected cells. N=4.

G) A representative trace of functional analyses of $UCP1^{(K->R)}$ transfected cells that were injected with a vehicle control or injected with 15 µM or 30 µM TTNPB.

H) UCP1 leak respiration measurements of $UCP1^{(K->R)}$ transfected cells. N=4.

I) A representative trace of functional analyses of $UCP1^{(K->Q)}$ transfected cells that were injected with a vehicle control or injected with 15 µM or 30 µM TTNPB.

J) UCP1 leak respiration measurements of $UCP1^{(K->Q)}$ transfected cells. N=4.

All the trace graphs are representative of four independent experiments and UCP1 leak graphs are an average of the four independent experiments. Data are represented as mean ± SEM. One-way ANOVA with Bonferroni's test was used; *$*p<0.05$.*

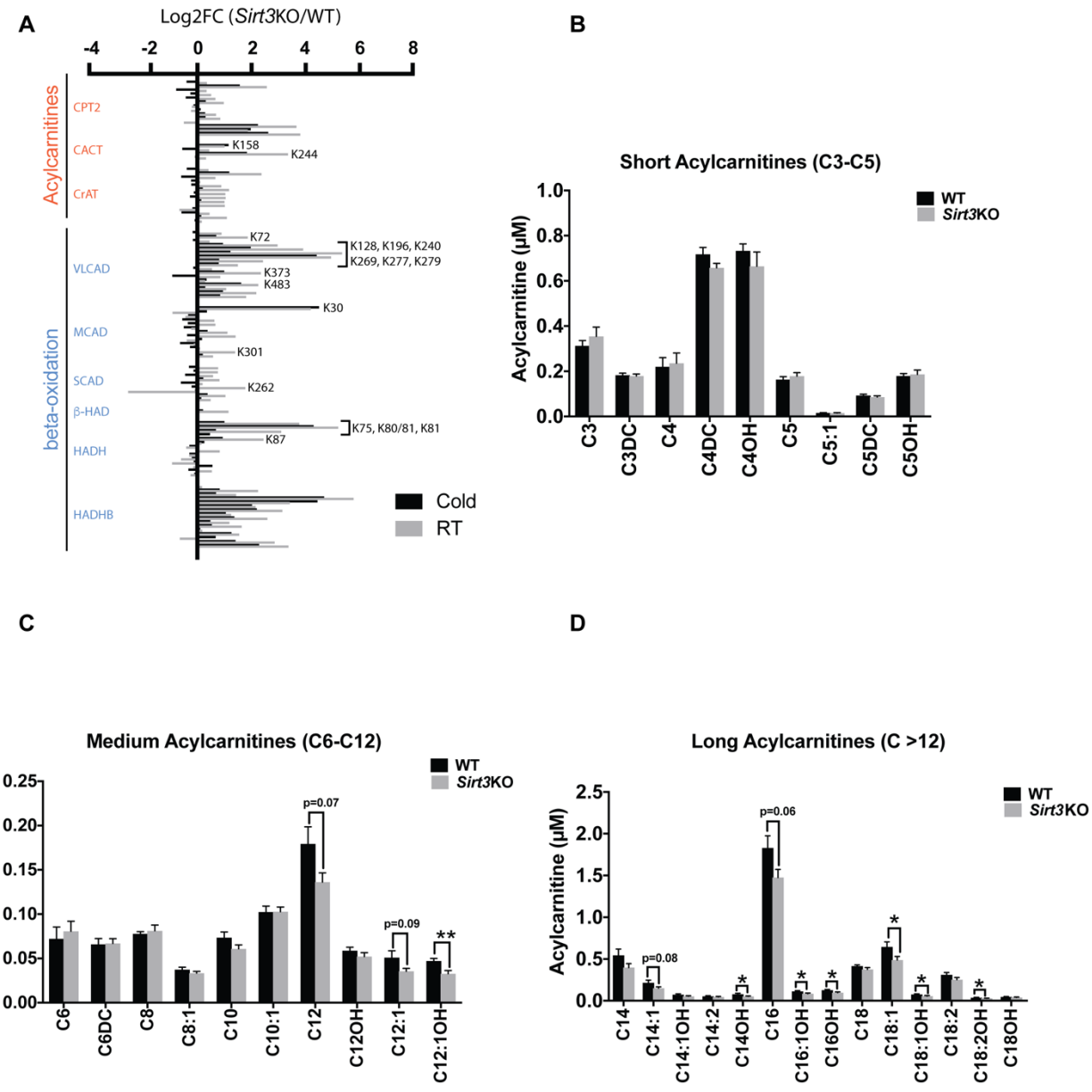
A
Log2FC (Sirt3KO/WT)
-4
-2
0
2
4
6
8
Acylcarnitines
CPT2
CACT
CrAT
beta-oxidation
VLCAD
MCAD
SCAD
β-HAD
HADH
HADHB
K158
K244
K72
K128, K196, K240
K269, K277, K279
K373
K483
K30
K301
K262
K75, K80/81, K81
K87
Cold
RT
B
Short Acylcarnitines (C3-C5)
Acylcarnitine (μM)
WT
Sirt3KO
C3
C3DC
C4
C4DC
C4OH
C5
C5:1
C5DC
C5OH
C
Medium Acylcarnitines (C6-C12)
Acylcarnitine (μM)
WT
Sirt3KO
p=0.07
p=0.09
**
C6
C6DC
C8
C8:1
C10
C10:1
C12
C12OH
C12:1
C12:1OH
D
Long Acylcarnitines (C >12)
Acylcarnitine (μM)
WT
Sirt3KO
p=0.06
p=0.08
*
C14
C14:1
C14:1OH
C14:2
C14OH
C16
C16:1OH
C16OH
C18
C18:1
C18:1OH
C18:2
C18:2OH
C18OH

**Figure 2.5: *Sirt3*KO mice have decreased levels of medium- and long-chain acylcarnitines.**
A) Measured Log2FCs of acetylation sites in selected proteins related to fatty acid oxidation or acylcarnitine metabolism from iBAT mitochondria isolated from room temperature or cold stressed WT and *Sirt3*KO mice. N=6/group. Indicated sites are those located in "regions of interest" from supplementary table 3 with ≥2 or great increase in *Sirt3KO* mice.
B-D) Plasma acylcarnitine analyses of WT and *Sirt3*KO mice that were injected with CL316.243 (1 mg/kg *i.p*.) to acutely activate BAT. Cardiac puncture blood samples were collected 90min-post injection used for MS/MS based acylcarnitines analysis.
B) Measurement of short-chain (C3-C5), C) medium-chain (C6-C12), D) long-chain acylcarnitines (C>12). N=8/group. Data are represented as mean ± SEM. Student's t-test; Two-tailed; **p<0.05, **p<0.01.*

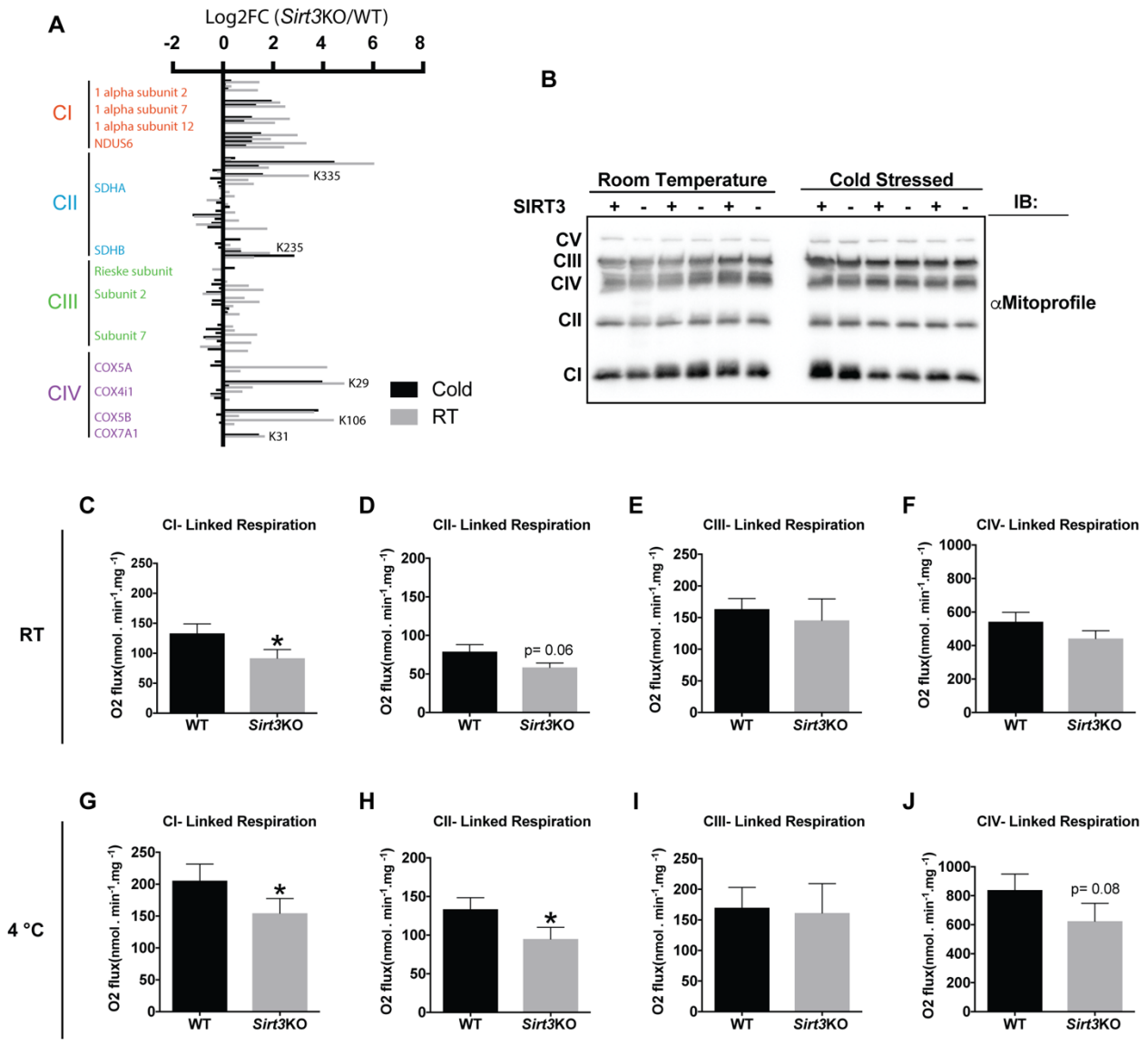
A
Log2FC (Sirt3KO/WT)
-2
0
2
4
6
8
CI
1 alpha subunit 2
1 alpha subunit 7
1 alpha subunit 12
NDUS6
CII
SDHA
SDHB
CIII
Rieske subunit
Subunit 2
Subunit 7
CIV
COX5A
COX4i1
COX5B
COX7A1
K335
K235
K29
K106
K31
Cold
RT
B
Room Temperature
Cold Stressed
SIRT3
+ - + - + - + - + - + -
IB:
CV
CIII
CIV
CII
CI
αMitoprofile
C
CI- Linked Respiration
D
CII- Linked Respiration
E
CIII- Linked Respiration
F
CIV- Linked Respiration
RT
O2 flux(nmol . min-1.mg -1)
WT
Sirt3KO
*
p= 0.06
G
CI- Linked Respiration
H
CII- Linked Respiration
I
CIII- Linked Respiration
J
CIV- Linked Respiration
4 °C
p= 0.08

**Figure 2.6: *Sirt3*KO mice have impaired ETC function.**
(A) Measured Log2FCs of lysine acetylation sites in selected proteins from ETC complexes CI-CIV from isolated mitochondria from iBAT of room temperature housed or cold exposed WT or *Sirt3*KO mice. N=6/group. Indicated sites are those located in "regions of interest" from supplementary table 3 with ≥2 or great increase in *Sirt3KO* mice.
(B) Western blotting analysis of OXPHOS protein expression in isolated BAT mitochondria. N=3/ group.
(C-F) High resolution respirometry functional analyses of ETC proteins in mitochondria isolated from BAT of room temperature housed WT and *Sirt3*KO mice.
(C) Complex I (CI) linked respiration; (D) Complex II (CII) linked respiration; (E) Complex III (CIII) linked respiration; (F) Complex IV (CIV) linked respiration. N= 6-14.
(G-J) High resolution respirometry functional analyses of ETC proteins in mitochondria isolated from BAT of cold exposed WT and *Sirt3*KO mice.
(G) Complex I (CI) linked respiration; (H) Complex II (CII) linked respiration; (I) Complex III (CIII) linked respiration; (J) Complex IV (CIV) linked respiration. N= 6-12. Data are presented as mean ± SEM. Student's t-test; Two-tailed; *$*p<0.05$.*

## CHAPTER 3: ACUTE HYPOXIA DIMINISHES BROWN FAT THERMOGENESIS IN NAKED MOLE-RAT BY DECREASING MITOCHONDRIAL CONTENT AND THERMOGENIC PROTEIN EXPRESSION

Matthew E Pamenter[1,2*†], Rajaa Sebaa[3,4,5†], Nikita Malholtra[1], Alexia Kirby[1], Hang Cheng[1], Nigel C Bennett[6], Barry van Jaarvsveld[6], Daniel W Hart[6], Glenn J Tattersall[7] and Mary-Ellen Harper[3,4]

[1]Department of Biology, University of Ottawa, Ottawa, ON, Canada
[2]University of Ottawa Brain and Mind Research Institute, Ottawa, ON, Canada
[3]Department of Biochemistry, Microbiology, and Immunology, Faculty of Medicine, University of Ottawa, Ottawa, ON, Canada
[4]Ottawa Institute of Systems Biology, University of Ottawa, Ottawa, ON, Canada
[5]Department of Medical Laboratories, College of Applied Medical Sciences, University of Shaqra, Duwadimi, Saudi Arabia
[6]Department of Zoology and Entomology, University of Pretoria, Pretoria, South Africa
[7]Department of Biological Sciences, Brock University, St. Catharines, ON, Canada

[†] **Co-first authors**

*** To whom correspondence should be addressed:**
Dr. Mary-Ellen Harper, PhD
Professor
Department of Biochemistry, Microbiology and Immunology
Ottawa Institute of Systems Biology
Faculty of Medicine, University of Ottawa
451 Smyth Road, Ottawa, ON Canada, ON K1H 8M5
Email: mharper@uottawa.ca
Tel: +1-613-562-5800 Ext 8458

Matthew Pamenter, PhD
Assistant professor
Department of Biology
Brain and Mind Research Institute
Faculty of Science, University of Ottawa
30 Marie Curie Pvt., Ottawa, ON, K1N 6N5, Canada.
Email: mpamenter@uottawa.ca
Tel: +1-613-562-5800 Ext. 6328

## 3.1 STATEMENT OF MANUSCRIPT STATUS AND CONTRIBUTIONS

### 3.1.1 STATEMENT OF MANUSCRIPT STATUS

The manuscript “Acute hypoxia diminishes brown fat thermogenesis in naked mole-rat by decreasing mitochondrial content and thermogenic protein expression” has been submitted for publication to the Journal of Nature Communications (NCOMMS-19-28577977-T) on December 2nd, 2019.

### 3.1.2 CONTRIBUTION STATEMENT

MP, GT, and MH conceived of and designed the study. BvJ and DH collected the South African animals with assistance from NB. RS performed the molecular biology experiments. HC and AK performed the physiology experiments and NM analyzed the physiological data. MP, RS, and GT conducted statistical analysis. MP, RS and MEH wrote the manuscript. All authors read and gave final approval of the published version and agree to be accountable for all content therein.

### 3.1.3 ACKNOWLEDGEMENTS AND FUNDING

We would like to thank the uOttawa and University of Pretoria animal care and veterinary services teams for their assistance in animal handling and husbandry. We would like to thank Dr. Ryan Russell, University of Ottawa for expert advice on electron micrograph analyses. This work was supported by an NSERC Discovery grant and a Canada Research Chair awarded to MEP. Supported by NSERC Discovery Grants to GJT and MEH and a University of Ottawa Research Chair to MEH. Collection and housing of mole-rats in Africa were funded by a SARChI grant (GUN 64576) to NCB.

### 3.1.4 COMPETING INTERESTS

We have no competing interests.

## 3.2 ABSTRACT

Eusocial naked mole-rats (NMRs) are among the most hypoxia-tolerant mammals. During hypoxia, body temperature ($T_b$) decreases to ambient temperature via unknown mechanisms. In small mammals, non-shivering thermogenesis in brown adipose tissue (BAT) is critical to $T_b$ regulation. We hypothesized that hypoxia decreases iBAT thermogenesis in NMRs. To test this, we held animals at 20, 30, or 36°C and measured changes in $T_b$ during normoxia and hypoxia (7% $O_2$; 1 hr). Interscapular thermogenesis was high in normoxia but heat production from this region ceased during hypoxia and $T_b$ decreased. In isolated iBAT from animals treated for 1 hr in normoxia or hypoxia we found that hypoxia: 1) rapidly decreased UCP1 and electron transport chain (ETC) complexes II-IV expression in iBAT, 2) increased ubiquitination of iBAT proteins, and 3) altered mitochondrial ultrastructural characteristics. In comparative experiments, UCP1 expression was decreased in hypoxia in 3 other social African mole-rats species but not a solitary species. These findings suggest that the ability to rapidly down-regulate thermogenesis to conserve energy in hypoxia may have evolved preferentially in social species.

**Keywords:** hypoxic metabolic response; thermoregulation; non-shivering thermogenesis; metabolic rate; passive cooling, uncoupling protein 1

## 3.3 INTRODUCTION

Animals that inhabit hypoxic environments have evolved elegant suites of physiological adaptations that enable them to thrive in low oxygen niches (Bickler and Buck, 2007; Buck and Pamenter, 2018; Dzal et al., 2015). The key to tolerating hypoxia is to match metabolic demand to reduced energy supply (Buck and Pamenter, 2006; Hochachka, 1986; Hochachka et al., 1996), and hypoxia-tolerant animals typically exhibit robust decreases in metabolic rate when oxygen is limited (Dzal et al., 2015; Guppy and Withers, 1999). Cold-induced thermogenesis is among the most energy-intensive processes in small mammals and many hypoxia-tolerant mammals employ thermoregulatory strategies to reduce body temperature ($T_b$) and facilitate reduced metabolic demand in hypoxia (Ramirez et al., 2007; Steiner and Branco, 2002). Naked mole-rats (*Heterocephalus glaber*) are among the most hypoxia-tolerant mammals identified and tolerate minutes of complete anoxia, hours at 3% $O_2$, and days to weeks at 8-10% $O_2$ (Chung et al., 2016; Pamenter et al., 2015, 2018; Park et al., 2017). In acute hypoxia, the rate of oxygen consumption (an indirect measure of metabolic rate) of adult naked mole-rats decreases by up to 85% (Pamenter et al., 2015, 2018), and $T_b$ decreases to near ambient levels (Dzal et al., 2019; Houlahan et al., 2018; Ilacqua et al., 2017; Kirby et al., 2018; Pamenter et al., 2019). Although this degree of metabolic rate and $T_b$ suppression is not remarkable among hypoxia-tolerant species (Guppy and Withers, 1999), it is important to note that other mammals that are capable of similar or more extreme metabolic rate suppression in severe hypoxia typically enter into a coma- or torpor-like state until $O_2$ levels are restored (Guppy and Withers, 1999; Hayden and Lindberg, 1970). Conversely, naked mole-rats remain conscious and active in hypoxia, albeit to a reduced degree (Houlahan et al., 2018; Ilacqua et al., 2017; Kirby et al., 2018).

Naked mole-rats have previously been described as the only poikilothermic mammal because their $T_b$ was found to conform closely to ambient temperature ($T_a$) across a wide range of experimental temperatures (Buffenstein and Yahav, 1991). However, in this earlier study, naked mole-rats were exposed to high air flow, which would enhance the rate of convective heat loss across their naked skin surface and potentially mask the ability of these animals to endogenously regulate $T_b$. Indeed, naked mole-rats are poor thermoregulators due to their lack of insulating fur and fat (DALY and BUFFENSTEIN, 1998), which allows for rapid loss of heat through convective mechanisms. However, the definition of poikilothermia stipulates that 1) $T_b$ is largely dependent on $T_a$, and 2) the organism be unable to endogenously regulate $T_b$ without external assistance (*e.g.*, through basking or huddling strategies). It is therefore important to note that several other studies have demonstrated that naked mole-rats maintain their $T_b$ well above $T_a$ in a range of temperatures and under conditions with low or no gas flow to experimentally dissipate heat via convective cooling across the skin surface. For example, Withers and Jarvis reported a $T_a$-$T_b$ differential ranging from 1.15 ± 0.07 to 13.2 ± 0.92°C in naked mole-rats exposed to $T_a$s ranging from 34-15°C (Withers and Jarvis, 1980), McNab reported a $T_a$-$T_b$ differential ranging from 0 to 8.2°C in $T_a$s ranging from 37-10°C (McNab, 1966), and Kirby et al. reported a $T_a$-$T_b$ differential ranging from 3-8°C in $T_a$s ranging from 30-20°C (Kirby et al., 2018). Concomitantly, metabolic rate is substantially elevated in cold temperatures, likely reflecting the high metabolic cost of thermogenesis (Kirby et al., 2018; Withers and Jarvis, 1980), particularly in this small, naked mammal (Sumbera, 2019). Taken together, these findings refute the classification of naked mole-rats as poikilothermic mammals; this species may be more

accurately considered heterothermy because they are weakly capable of thermogenesis, but are generally not very efficient thermoregulators (Kirby et al., 2018).

This ability to thermoregulate, even weakly, is likely important to the ecophysiology of this species as naked mole-rat burrow temperatures have a warm but variable thermal range, spanning < 25°C to < 45°C (Holtze et al., 2018).

Importantly, the metabolic cost that may be attributed to thermoregulation in the cold is substantial, and the metabolic rate of naked mole-rats held in cold temperatures is >2 to 4-fold greater than when they are held within the thermoneutral zone of this species (Kirby et al., 2018; Withers and Jarvis, 1980). However, the whole animal metabolic rate of naked mole-rats in acute hypoxia is not significantly different between cold and warm experimental conditions (Kirby et al., 2018). These observations suggest two intriguing hypotheses: specifically, that naked mole-rats: 1) employ active thermogenesis in cold, normoxic conditions, and 2) thermogenesis is reduced during acute hypoxia to conserve energy and support the robust hypoxic metabolic rate suppression previously reported in this species (Chung et al., 2016; Dzal et al., 2019; Kirby et al., 2018; Pamenter et al., 2015, 2018, 2019). The primary mechanism of cold-induced thermogenesis in small mammals is through uncoupling protein-1 (UCP1)-mediated mitochondrial uncoupling in brown adipose tissue (BAT) (*i.e.*, non-shivering thermogenesis (NST). Activation of UCP1 uncouples the mitochondrial proton gradient from ATP-synthesis, resulting in heat generation through futile cycling of the electron transport chain (ETC) (Argyropoulos and Harper, 2002; Nedergaard et al., 2001). Importantly, naked mole-rats express functional BAT (Daly et al., 1997; Hislop and Buffenstein, 1994; Woodley and Buffenstein, 2002); however, no study has directly examined thermogenic adaptations to hypoxia or the underlying mechanisms in this species.

Given the high cost of thermoregulation (particularly for a small and naked rodent) and the requisite need to lower metabolic demand in hypoxia, such an investigation is of pressing interest in the study of ecophysiological adaptations to life in hypoxia in this fascinating species. Therefore, in the present study we employ *in vivo* thermal imaging in combination with molecular biology and electron microscopy approaches to interrogate thermogenic adaptations to acute hypoxia in naked mole-rat interscapular BAT (iBAT). We also explore the underlying molecular mechanism in iBAT from naked mole-rats and several closely related hypoxia-tolerant African mole-rat species.

## 3.4 MATERIALS AND METHODOLOGY

### 3.4.1 ANIMALS

Naked mole-rats were bred at the University of Ottawa and group-housed in interconnected multi-cage systems at 30°C and 21% $O_2$ in 50% humidity with a 12L:12D light cycle. *Cryptomys hottentotus mahali* (CHM), *Cryptomys hottentotus pretoriae* (CHP), *Georychus capensis* (GC), and *Cryptomys hottentotus hottentotus* (CHH) were wild captured in South Africa and were individually housed at the University of Pretoria at ~27°C and 21% $O_2$ in 50% humidity with a 12L:12D light cycle. Animals were fed fresh tubers, vegetables, fruit and Pronutro cereal supplement (Bokomo Food Products, Namibia) *ad libitum*. Animals were not fasted prior to experimental trials.

All experimental procedures were approved by the University of Ottawa Animal Care Committee (protocol #2535), in accordance with the Animals for Research Act and by the Canadian Council on Animal Care. Trapping and experiments conducted in South Africa were conducted with

appropriate government permits and with experimental procedures approved by the animal ethics committee of the University of Pretoria (EC069-17). All experiments were performed during daylight working hours in the middle of the animals' 12L:12D light cycle. Naked mole-rats that are housed within colony systems do not exhibit circadian rhythmicity of general locomotor activity (Riccio and Goldman, 2000a), and exhibit inconsistent rhythmicity of $T_b$ and metabolic rate (Riccio and Goldman, 2000b); however, significant changes in these latter parameters were only reported in animals during the nocturnal phase of their circadian cycle with no significant changes observed during the daylight period of this cycle. Therefore, since we only ran experimental trials during the daylight period, we do not expect our results to be influenced by circadian rhythms. We did not conduct *in vivo* experiments in the other mole-rat species.

We examined physiological responses to environmental hypoxia and/or collected tissue from seventy-three male and female non-breeding subordinate adult (1-2-year-old) naked mole-rats weighing 48.3  4.9 g (mean ± SEM). Non-breeding (subordinate) naked mole-rats do not undergo sexual development or express sexual hormones and thus we did not take sex into consideration when evaluating our results (Holmes et al., 2009). We also collected tissues from 6-10 animals per species of CHM (109.1 ± 6.6 g), CHP (114.8 ± 12.3 g), GC (133.2 ± 19.0 g), and CHH (78.7 ± 5.5 g), following 3 hrs of normoxia or hypoxia (see below).

**3.4.2 EXPERIMENTAL DESIGN AND TISSUE COLLECTION**

Surface temperatures were measured via thermal imaging from forty-one animals divided into 5 experimental groups: (*i*) 20°C, 30°C, 30°C + sham saline injection, 30°C + isoproterenol injection, and 36°C. For all groups (and following saline or saline + drug injections where applicable), baseline recordings were obtained for 1 hr in normoxia (21% $O_2$, 0% $CO_2$, balance $N_2$) and then

the incurrent gas composition was switched to 7% ($O_2$, 0% $CO_2$, balance $N_2$) for 1 hr followed by 1 hr in normoxia (recovery). Following experimentation, animals were returned to their colonies. The temperature of the room in which the experiments were conducted was held at 20, 30, or 36°C and animals were acclimated for at least 2-3 hrs at the appropriate temperature prior to commencing experimentation. These temperatures were selected since an $T_a$ of 30°C is the housing temperature of our colonies, and is near the thermoneutral zone of naked mole-rats (which spans from ~30.5-34°C) (Yahav and Buffenstein, 1991); the 20°C experimental temperature was selected to increase the thermal scope within which the animals were able to respond through thermoregulatory adaptations to hypoxia; naked mole-rats have a higher metabolic rate in colder temperatures relative to near their thermoneutral zone (Kirby et al., 2018), and thus repeating our experiments in this temperature magnifies the impact of our treatments on metabolic rate and $T_b$ and therefore our ability to detect any physiological changes in this condition. The 36°C experimental temperature was selected to examine thermogenic responses in an $T_a$ at which naked mole-rats would likely not need to actively thermoregulate (*i.e.*, above their thermoneutral zone).

In other experiments, thirty-two naked mole-rats were exposed to either normoxia or 1 hr of acute hypoxia (7% $O_2$). All of these experiments were conducted at an $T_a$ of 30°C. Similarly, captured populations of CHM, CHP, GC, and CHH were divided into two treatment groups ($n$ = 3-6 per treatment per species) and exposed to 3 hrs of normoxia or hypoxia (5% $O_2$) at ~ 28°C. Note that these experiments were conducted in Pretoria, which is at mild altitude resulting in normoxic ambient oxygen level of 18 kPa. At the end of each exposure, animals were sacrificed as described

below, with tissue collected for molecular biology and electron microscopy approaches over ice and stored at -80 °C until analyzed.

### 3.4.3 COLLECTION AND ANALYSIS OF THERMOGRAPHIC DATA

FLIR thermal images were captured directly to radiometric video files using an infrared thermal imaging camera (Make: FLIR, Model: SC 660) connected to a computerized acquisition program (Thermacam Researcher Pro v 2.9). Images were captured every 10 seconds throughout the experimental period. Image analysis followed that described previously (Greenberg et al., 2012; McCafferty et al., 2013; Tattersall, 2016). Emissivity was assumed to be 0.96, air temperature and reflected environment temperatures were set to 20, 30 or 36°C, respectively, relative humidity set to 50%, the object distance set to 0.35 meters, and the transmittance of the Germanium IR window set to 0.95 (determined empirically). Image analysis was conducted every fifth minute during the experimental period, by drawing regions of interest (ROI) over the interscapular and hind back regions. Average temperatures across the entire ROI were extracted.

### 3.4.4 BODY TEMPERATURE MEASUREMENTS

Body temperature was measured using a handheld radio frequency identification (RFID) reader that scanned individual naked mole-rats instrumented with subcutaneous RFID microchips (Destron Fearing, Dallas, TX) every 10 mins, as described previously (Kirby et al., 2018).

### 3.4.5 WESTERN BLOTTING

Interscapular brown adipose tissue (iBAT) was dissected from naked mole-rats or different species of mole-rats that were kept either in normoxia (21% $O_2$) or hypoxia (5% $O_2$) for 1 or 3 hrs. After dissection, iBAT was snap-frozen and stored at -80 °C until it was used for the protein expression analysis. On the day of the experiment, the frozen tissue was thawed on ice, cleaned

from white fat, cut into small pieces, and subsequently homogenized in 500µl of homogenizing buffer, consisting of 0.25M sucrose supplemented with protease inhibitor mixture (Complete Mini, Roche). iBAT was manually homogenized on ice in a Potter Elvehjem Teflon–glass tissue grinder using 4 to 5 strokes. The homogenate was spun at 8500g for 10 mins at 4°C to remove lipid containing supernatant layer, which was discarded. Based on pellet size, 50 – 100 µl of 0.25M sucrose buffer was added to gently resuspend the pellet. Protein concentration was measured by a Bradford assay (Biorad). 10 µg of the homogenate protein was loaded per lane onto a 12% SDS-polyacrylamide gel, which in turn was run for 1-1.5 hrs at 130 volts. The separated proteins were transferred to a nitrocellulose membrane for 1 hr at 100 volts. Successful transfer was determined by Ponceau S staining. Membranes were then incubated with 5% bovine serum albumin for 30 mins to block non-specific binding sites. Levels of specific proteins were determined using the following primary antibodies: UCP1 antibody (1:3,000; Sigma Aldrich, #U6382); total oxidative phosphorylation (OXPHOS) rodent antibody cocktail (1:2000; Abcam, #Ab110413); and anti-ubiquitin antibody (1:2000; Abcam, #Ab7780). Quantification was performed by using the ImageJ software (NIH).

**3.4.6 TRANSMISSION ELECTRON MICROSCOPY (TEM)**

Naked mole-rats were anesthetized with Ketamine (200mg/kg) + Xylazine (10mg/kg) and then perfusion-fixed via cardiac puncture using 2% formaldehyde and 2.5% glutaraldehyde. Following fixation, iBAT was dissected and further fixed overnight at 4°C in 2.5% glutaraldehyde in 0.15M sodium cacodylate buffer, pH 7.4, and washed three times with washing buffer. Samples were post-fixed with 1% aqueous $OsO_4$ + 1.5% aqueous potassium ferrocyanide for 2 h and washed three times with washing buffer. Specimens were dehydrated in a graded ethanol-d$H_2O$ from 30,

50, 70, 80, 90 to 100% ethanol. The samples were infiltrated with a graded Epon-ethanol series (1:1, 3:1), embedded in 100% Epon and then polymerized in an oven at 60°C for 48 h. Ultra thin sections (90–100 nm thick) were prepared from the polymerized blocks with a Diatome diamond knife using a Leica Microsystems EM UC7 ultramicrotome, transferred onto 200-mesh copper grids, and stained with 4% uranyl acetate for 6 min and Reynold's lead for 5 min. The TEM grids were imaged by a FEI Tecnai $G^2$ Spirit 120 kV TEM equipped with a Gatan Ultrascan 4000 CCD Camera Model 895. The proprietary Digital Micrograph 16-bit images (DM3) were converted to unsigned 8-bit TIFF images.

### 3.4.7 DATA COLLECTION AND STATISTICAL ANALYSIS

One-factor repeated measure ANOVAs were used to examin the main effects of acute inspired $PO_2$ on surface temperature and $T_b$ data. Tukey post-tests were used, when appropriate, to assess changes in variables from normoxic/resting conditions. Western blot data were analysed by unpaired Student's t-tests. Values are reported as mean ± S.E.M. All statistical analyses were performed using GraphPad Prism 6 (GraphPad Prism, La Jolla, CA, USA), with a significance level of $P < 0.05$.

## 3.5 RESULTS

### 3.5.1 NAKED MOLE-RATS EMPLOY INTERSCAPULAR THERMOGENESIS IN NORMOXIA BUT NOT HYPOXIA

We first examined surface temperatures in awake and freely behaving naked mole-rats during 1 hr of normoxia and in 30°C, which is the $T_a$ at which our animals are housed. We observed evidence for robust heat production in normoxia, with a particularly high degree of heat production apparent in the interscapular region, and that the $T_b$ of naked mole-rats was ~ 3°C > $T_a$ (Figure 3.1A&C). Upon exposure to an acute hypoxic challenge (7% $O_2$) surface temperature rapidly fell such that the animal largely disappeared into the background in the thermal image (Figure 3.1B&C). In all experiments, the temperature measured from the interscapular region was greater than the dorsal surface skin temperature or the core $T_b$ in normoxia, but with the onset of hypoxia, all body temperature measurements (RFID chip and FLIR analysis), including in the interscapular region, collapsed to within 1°C of the $T_a$ (Figure 3.1D). Upon reoxygenation, all temperature measurements returned towards normoxic values following a lag-time of ~ 20-40 mins.

We then repeated this experimental protocol in a $T_a$ of 20°C to increase the thermal scope within which animals might respond to a hypoxic challenge (Figure S1A&B). In this colder temperature and under normoxia, the naked mole-rat $T_b$ was ~ 7-9°C > $T_a$, suggesting that these animals were actively attempting to thermoregulate in the cold $T_a$. However, with the onset of hypoxia, all body temperature measurements again collapsed towards the $T_a$, such that $T_b$ in hypoxia was ~ 1°C > $T_a$. Finally, we repeated this experimental protocol at an $T_a$ above the thermoneutral zone of naked mole-rats (36°C, Figure S1C&D). At this $T_a$, $T_b$ was not significantly different from $T_a$ and

the degree of thermogenesis, as measured by interscapular thermal imaging, was minimal. With the onset of hypoxia and subsequent reoxygenation, $T_b$ was unchanged.

### 3.5.2 ADRENERGIC STIMULATION OF INTERSCAPULAR THERMOGENESIS IN NORMOXIA BUT NOT HYPOXIA

In response to cold exposure, the mammalian sympathetic nervous system releases noradrenaline to stimulate β-adrenergic receptors, which are localized primarily within adipose tissues. Activation of these receptors coordinates the release of energy from triglyceride droplets in white adipose tissue (WAT) and BAT to support UCP1-driven thermogenesis (Cannon and Nedergaard, 2004). These properties of BAT and UCP1 led us to reinvestigate the ability of naked mole-rats to regulate their $T_b$ through BAT thermogenesis upon adrenergic activation *in vivo*. Specifically, we examined the regulation of BAT NST via the injection of saline (sham controls) or the general β-adrenergic agonist isoproterenol (dissolved in saline). Saline alone had no effect on $T_b$ or thermogenesis in normoxia or hypoxia (Figure S2A&B); however, injection of isoproterenol resulted in enhanced thermogenesis in the interscapular region such that surface temperatures from this region were ~ 2-3°C greater (Figure S2C&D) than in sham-treated controls. Intriguingly, with the subsequent onset of hypoxia, this enhanced activation of interscapular thermogenesis was nonetheless curtailed and all measurements of $T_b$ decreased to within ~ 1°C of the $T_a$ (30°C).

### 3.5.3 HYPOXIA DECREASES THE EXPRESSION OF UCP1 AND MITOCHONDRIAL OXPHOS PROTEINS IN NAKED MOLE-RAT iBAT

To understand the mechanism underlying the rapid change in interscapular thermogenesis, we next held naked mole-rats for 1 hr in normoxia or acute hypoxia (7% $O_2$) at 30°C, and then rapidly dissected iBAT. We then examined the expression of UCP1 protein as well as that of

mitochondrial OXPHOS complexes I-V. We found that, following 1 hr of acute hypoxia, UCP1 protein expression decreased by 98% (Figure 3.2A&B). Similarly, the expression of mitochondrial ETC complexes II, III, and IV proteins decreased by 61, 30, and 63%, respectively (Figure 3.2C&D).

### 3.5.4 HYPOXIA INCREASES PROTEIN UBIQUITINATION AND ALTERS MITOCHONDRIAL MORPHOLOGY IN NAKED MOLE-RAT iBAT

Our observation of rapid changes in iBAT mitochondrial protein expression prompted further investigation of the underlying mechanisms. Since hypoxia is a powerful regulator of ubiquitination and proteasomal degradation of proteins (Wade et al., 2018), we next examined the ubiquitination levels of iBAT proteins in naked mole-rats exposed to hypoxia *in vivo*. We found that the ubiquitination levels in hypoxic iBAT homogenates were significantly increased compared to homogenates from normoxic animals (Figure 3.3A&B). These protein changes hint at the potential for changes in the morphology or dynamics of BAT mitochondria. We therefore next used electron microscopy to examine the morphology and ultrastructure of iBAT mitochondria from naked mole-rats treated in normoxic or hypoxic conditions. We found that iBAT from normoxic naked mole-rats contained abundant mitochondria with dense cristae and intact inner membranes. Conversely, iBAT from hypoxic naked mole-rats had significant mitochondrial morphological abnormalities, including decreased and jagged cristae and undefined mitochondrial membranes, consistent with the possibility of mitochondrial degradation (Figure 3.3C&D). Importantly, there were also degradative, or lysosome-like vacuoles between iBAT mitochondria from hypoxic naked mole-rats (Figure 3.3C&D). Taken together, our electron microscopy analysis demonstrates hypoxia-induced abnormalities in the ultrastructure of iBAT mitochondria.

### 3.5.5 HYPOXIA DECREASES EXPRESSION OF UCP1, BUT NOT OXPHOS PROTEINS IN iBAT FROM RELATED AFRICAN MOLE-RATS

To examine whether hypoxia-induced degradation of thermogenic proteins observed in naked mole-rats occurs also in iBAT of other, closely related mole-rat species, we similarly examined the effect of hypoxia on the expression of UCP1 and OXPHOS proteins in iBAT dissected from CHH, CHM, CHP, and GC following *in vivo* treatment in either normoxic or hypoxic conditions (Figures 3.4&3.5). As in naked mole-rats, iBAT homogenates from CHH, CHM, and CHP also exhibited significant decreases or a strong trend towards decreasing UCP1 expression in hypoxia (Figure 3.4), although UCP1 expression was unchanged in GC. Conversely, the expression of OXPHOS proteins was generally unchanged by hypoxia, with the exception of complexes III and IV in CHH, which were significantly increased by acute hypoxia (Figure 3.5).

## 3.6 DISCUSSION

In the present study, we demonstrate for the first time that acute hypoxia diminishes interscapular thermogenesis in naked mole-rats, consistent with previous observations of substantial hypoxia-mediated suppression of whole body metabolic rate in this species (Houlahan et al., 2018; Ilacqua et al., 2017; Kirby et al., 2018). Specifically, our study provides evidence that in naked mole-rats, hypoxia: 1) decreases interscapular thermogenesis at temperatures near or below thermoneutrality, 2) causes a significant reduction in the expression of UCP1 and ETC proteins in iBAT, 3) increases the degree of protein ubiquitination of iBAT proteins, and 4) induces abnormal ultrastructural characteristics in iBAT mitochondria, such as reduced cristae density. Furthermore, acute hypoxia tends to decrease UCP1 expression in iBAT

from 3 out of 4 related African mole-rat species but does not modify iBAT OXPHOS protein expression. Taken together, our results demonstrate that hypoxia depresses iBAT thermogenesis in naked mole-rats via unique mechanisms that are mediated, at least in part, by targeted reductions in mitochondrial content and of key thermogenic proteins, including UCP1.

### 3.6.1 HYPOXIA-TOLERANT SPECIES DECREASE THERMOGENESIS IN HYPOXIA

In most small mammals, BAT thermogenesis is an energy-intensive process that can drastically impact whole-body energy homeostasis. BAT thermogenesis is activated largely by the sympathetic nervous system and is regulated through transcriptional and post-translational mechanisms (Cannon and Nedergaard, 2004; Cao et al., 2004; Chouchani et al., 2016; Oelkrug et al., 2015; Sebaa et al., 2019; Wang et al., 2019). Previous studies indicate the existence of functional iBAT in naked mole-rats, as demonstrated by pharmacological thermogenic activation (Daly et al., 1997; Hislop and Buffenstein, 1994; Woodley and Buffenstein, 2002). Indeed, when BAT is thus activated, whole animal oxygen consumption is greatly increased and this increase in thermogenic oxygen demand explains most of the increases in whole body oxygen consumption in naked mole-rats under these conditions (Goldman et al., 1999; Hislop and Buffenstein, 1994; Woodley and Buffenstein, 2002). Our study confirms and extends this knowledge; we show that naked mole-rats do actively thermoregulate and engage BAT thermogenesis at temperatures near or below thermoneutrality or following treatment with an adrenergic agonist.

Beyond normoxic conditions, our work is the first to demonstrate that hypoxia decreases BAT thermogenesis in naked mole-rats. Notably, we observed a hypoxia-induced decrease in BAT thermogenesis in animals that had received injections of either saline or isoproterenol. These results indicate that hypoxia diminishes BAT thermogenesis regardless of

the degree to which BAT is activated when hypoxia is encountered. Intriguingly, acute hypoxia also reduces thermogenesis in other mammalian models of hypoxia-tolerance, including hibernators and neonates (Mortola and Dotta, 1992; Rohlicek et al., 1998), although the underlying mechanisms are poorly understood. For example, studies conducted on neonatal dogs and cats and on adult ground squirrels have revealed that hypoxia decreases shivering thermogenesis in these models (Barros et al., 2001; Gautier et al., 1987; Tattersall and Milsom, 2003). Conversely, adult hypoxia-intolerant mammals may require far longer durations of hypoxic exposure to induce thermogenic remodeling. For example, adult mice held in chronic hypoxia significantly decrease oxygen consumption by almost 30% after a treatment with NE, compared to control mice (Beaudry and McClelland, 2010).

### 3.6.2 NAKED MOLE-RAT iBAT UCP1 EXPRESSION CHANGES MORE RAPIDLY THAN IN MICE

UCP1 is essential for BAT thermogenesis (Enerbäck et al., 1997; Himms-Hagen, 1985; Nicholls, 2006), is expressed in mitochondria from classical BAT and beige adipose tissue, and is located in the mitochondrial inner membrane (Argyropoulos and Harper, 2002; Nedergaard et al., 2001). It is estimated that UCP1 comprises approximately 10% of BAT mitochondrial protein content (Busiello et al., 2015). It is well established that defects in the activity of UCP1 resulting from post-translation modifications or the absence of UCP1 can impact BAT thermogenesis (Chouchani et al., 2016; Enerbäck et al., 1997; Sebaa et al., 2019; Wang et al., 2019); mice lacking UCP1 are cold intolerant(Enerbäck et al., 1997). Given this essential role for UCP1 in BAT thermogenesis, we examined the effect of acute hypoxia on UCP1 protein levels in iBAT and found that these are significantly decreased following only 1 hr of *in vivo* hypoxia. Our observation is consistent with a study conducted on mice in which 4 wks of chronic hypoxia (480 mmHg) decreases transcript

and protein levels of UCP1 (Beaudry and McClelland, 2010). The turnover of UCP1 depends on the metabolic status of BAT; in mouse brown adipocytes the turnover of UCP1 takes 3.7 ± 0.4 days in basal conditions and 8.4 ± 0.9 days upon chronic adrenergic stimulation (Moazed and Desautels, 2002). Intriguingly, Kim and colleagues report that naked mole-rat UCP1 has a unique gene sequence, compared to other mammals, which results in the loss of the tight regulation of UCP1 activity by purine nucleotides (Kim et al., 2011).

### 3.6.3 HYPOXIA INDUCES MITOCHONDRIAL REMODELING OF iBAT, POTENTIALLY THROUGH UBIQUITINATION AND MITOPHAGY

In addition to UCP1, hypoxia also decreases the levels of CII, CII, and CIV ETC proteins in naked mole-rat iBAT. The turnover of these complexes in mice can vary depending on the tissue or treatments that cause metabolic changes in mitochondria (Karunadharma et al., 2015), but are in general considerably slower than the rate that we observe in naked mole-rat iBAT. The rapid degradation of thermogenic proteins in iBAT of naked mole-rats could be mediated by two well-known and -characterized mechanisms: the ubiquitin-proteasome system (UPS) and mitophagy.

In UPS dependent pathways, targeted proteins are ligated with ubiquitin and then degraded by proteasomes. Importantly, protein ubiquitination is a post-translational modification that leads to the degradation of protein not only through proteolysis but also through mitophagy as in the Pink1/Parkin dependent mitophagy mechanism (Cairó et al., 2019; Harper et al., 2018; Pickles et al., 2018). Naked mole-rats have a very high rate of proteasome activity compared to other rodents (Pride et al., 2015). Furthermore, they have a unique proteasome and high level of cytosolic activators for proteasomes (Rodriguez et al., 2012, 2014), which could explain the rapid degradation of the thermogenic proteins observed in our study.

However, proteasome function has only been examined in normoxia in this species and the effects of hypoxic exposure on these energy-intensive systems remains to be determined. For example, naked mole-rats downregulate ATP-dependent heat-shock protein function in early hypoxia but not that of ATP-independent heat-shock proteins (Nguyen et al., 2019), highlighting the potential for plasticity in this system to conserve in hypoxia.

There is also a possibility that thermogenic proteins are degraded through mitophagy as naked mole-rats have a very high rate of mitophagy compared to other rodents (Zhao et al., 2014). It has been previously shown that hypoxia can induce mitophagy in different experimental models (Fuhrmann et al., 2013). Mitophagy may occur in hypoxia as a protective mechanism to remove damaged mitochondria for tissue/cell survival (Zhang et al., 2016). In hypoxia-tolerant organisms, low oxygen exposure can increase mitophagy regulators such as phosphoglycerate mutase family member 5 (PGAM5) (Sokolova et al., 2019). Recent studies in mice demonstrate that depolarized BAT mitochondria are degraded through Pink1/Parkin-dependent mitophagy, and one of the fundamental steps in this mechanism is the ubiquitination of proteins found in the mitochondrial outer membrane (Cairó et al., 2019). Mechanistically, Pink1 is recruited on the mitochondrial outer membrane of damaged or defective mitochondria. Then, Pink1 phosphorylates ubiquitin molecules that bind to Parkin, which is a ubiquitin ligase, resulting in its activation. After this, the activated from of Parkin ubiquitinates proteins (Cairó et al., 2019). Since protein ubiquitination is involved in both mechanisms, UPS and mitophagy, and also serves as a marker for protein degradation, we next examined the total level of protein ubiquitination in iBAT homogenates from normoxic and hypoxic naked mole-rats. We found that protein

ubiquitination is significantly increased by hypoxia in naked mole-rat iBAT, suggesting a potential for UPS or mitophagy events that may be induced in hypoxic conditions.

While the degree of thermogenic mitochondrial protein expression is important for BAT function, mitochondrial structure and ultrastructure can also be important (Wikstrom et al., 2014). Mitochondria have two sets of membranes: an outer and an inner. The highly permeable outer membrane separates mitochondria from the cytoplasm and the highly selectively impermeable inner membrane separates the matrix from the intermembrane space. The inner membrane has a much larger surface than the outer membrane and the inner membrane is folded to form cristae, where UCP1 and ETC proteins are located. Thus, we also examined the ultrastructure of BAT mitochondria in normoxia and hypoxia and found that hypoxia disrupts the ultrastructure of mitochondria, including decreased cristae density and apparent degradation of the outer membranes. Hypoxia also induces the formation of dense vacuole-like structures that require further analysis. Altogether our findings are consistent with increased proteolysis or mitophagy during hypoxia, which may lead to decreased levels of UCP1 and ETC proteins that we observed in hypoxia iBAT.

**3.6.4 THE RESPONSE OF NAKED MOLE-RAT iBAT TO HYPOXIA IS UNIQUE AMONG MOLE-RATS.**

Based on the results from our study and previously published work, it is clear that the turnover of UCP1 and ETC proteins occurs in an animal-, tissue-, and treatment- specific manner. Therefore, we expanded our investigation to examine the turnover of UCP1 and ETC proteins after hypoxia exposure in four other hypoxia-tolerant African mole-rat species related to naked mole-rats, including 3 social species (CHH, CHM, CHP) and on solitary species (GC). Hypoxia causes distinct patterns of thermogenic proteins in these 4 mole-rats that are divergent from the

pattern observed in naked mole-rats. Specifically, hypoxia decreases or tended to decrease the expression of UCP1 in the social but not the solitary mole-rat species but did not consistently modify ETC proteins.

These differences may be due to the social structure within which these species commonly live. For example, cooperatively breeding and eusocial African mole-rat species, which include naked and Damaraland mole-rat (*Fukomys damarensis*), have relatively large colony sizes (Bennett et al., 1993) and construct complex tunnel systems with a relatively warm but nonetheless variable temperature range (19.6 to 29.3°C) (Roper et al., 2001). The number of colony members within a burrow system likely plays a critical role in the respiratory gas concentrations and the temperatures individual mole-rats experience. For example, $CO_2$ concentrations in the burrow system of solitary GC mole-rats are ~ 1.2%, whereas eusocial Damaraland mole-rats, which live in colonies of up to 40 individuals, have $CO_2$ concentrations as high as 6.4% (Roper et al., 2001). Furthermore, even though the environmental temperatures experienced are similar between the solitary GC and eusocial Damaraland mole-rats (and also naked mol-rats), individual Damaraland and naked mole-rats likely experience a smaller true temperature range as they employ huddling in nest chamber (a portion of the burrow system which is expected to have the lowest $O_2$ concentration, especially during huddling) (Kotze et al., 2008). Along this gradient of the social organization lie several social species, such as the CHH, CHP, and CHM mole-rats investigated in this study. The maximum colony size for these species is ~ 20 individuals with a mean colony size of 7 (Bennett and Faulkes, 2000; Bennett et al., 1990; van Jaarsveld et al., 2019). Thus, the respiratory gas concentrations of their burrow systems are expected to fall in between the solitary and eusocial species; however, this has not been documented to date. Therefore, the

variation seen between naked mole-rats, CHH, CHP, and CHM, and GC, may reflect an inverse relationship between the severity of hypoxia and the thermal range experienced by an individual mole-rat, which is determined by the number of colony members within a burrow system. Taken together, these results suggest that the rapid cycling and downregulation of thermogenic proteins in naked mole-rat iBAT is a mechanism novel to this species that likely evolved independently and as a result of the unique social and environmental niches that this species occupies.

## 3.7 CONCLUSIONS

Our results support the overall conclusion that naked mole-rats are capable of adapting to acute hypoxia by diminishing iBAT thermogenesis and that this is partially achieved by acutely decreasing the levels of thermogenic proteins and altering mitochondrial ultrastructure. Further elucidation of adaptive mechanisms in iBAT of naked mole-rats will lead to a better understanding of potentially unique mechanisms within the biology of this tissue that allows these interesting animals to survive in extreme conditions. It is likely that decreases in iBAT activity (and the associated thermogenesis) occur as part of the larger adaptive mechanism during hypoxia, as uncoupling in BAT to facilitate NST is a highly costly metabolic process, requiring large amounts of oxygen. In addition, it is likely that these metabolic changes in iBAT mitochondria invoke reliance on anaerobic metabolic pathways such as glycolysis to survive (Pamenter et al., 2019). Further analyses of aerobic and anaerobic pathways in naked mole-rat iBAT during normoxia, hypoxia, and following reoxygenation are warranted.

## 3.8 REFERENCES


Argyropoulos, G., and Harper, M.-E. (2002). Uncoupling proteins and thermoregulation. J. Appl. Physiol. *92*, 2187–2198.

Barros, R.C., Zimmer, M.E., Branco, L.G., and Milsom, W.K. (2001). Hypoxic metabolic response of the golden-mantled ground squirrel. J. Appl. Physiol. *91*, 603–612.

Beaudry, J.L., and McClelland, G.B. (2010). Thermogenesis in CD-1 mice after combined chronic hypoxia and cold acclimation. Comp. Biochem. Physiol. B, Biochem. Mol. Biol. *157*, 301–309.

Bennett, N. C. & Faulkes, C. G. *African mole-rats: ecology and eusociality*. (Cambridge University Press, 2000).

Bennett, N.C., Jarvis, J.U.M., and Wallace, D.B. (1990). The relative age structure and body masses of complete wild-captured colonies of two social mole-rats, the common mole-rat, Cryptomys hottentotus hottentotus and the Damaraland mole-rat, Cryptomys damarensis. Journal of Zoology. *220*, 469–485.

Bennett, N.C., Jarvis, J.U., Faulkes, C.G., and Millar, R.P. (1993). LH responses to single doses of exogenous GnRH by freshly captured Damaraland mole-rats, Cryptomys damarensis. J. Reprod. Fertil. *99*, 81–86.

Bickler, P.E., and Buck, L.T. (2007). Hypoxia tolerance in reptiles, amphibians, and fishes: life with variable oxygen availability. Annu. Rev. Physiol. *69*, 145–170.

Buck, L.T., and Pamenter, M.E. (2006). Adaptive responses of vertebrate neurons to anoxia--matching supply to demand. Respir Physiol Neurobiol. *154*, 226–240.

Buck, L.T., and Pamenter, M.E. (2018). The hypoxia-tolerant vertebrate brain: Arresting synaptic activity. Comp. Biochem. Physiol. B, Biochem. Mol. Biol. *224*, 61–70.

Buffenstein, R., and Yahav, S. (1991). Is the naked mole-rat Hererocephalus glaber an endothermic yet poikilothermic mammal? Journal of Thermal Biology. *16*, 227–232.

Busiello, R.A., Savarese, S., and Lombardi, A. (2015). Mitochondrial uncoupling proteins and energy metabolism. Front. Physiol. *6*.

Cairó, M., Campderrós, L., Gavaldà-Navarro, A., Cereijo, R., Delgado-Anglés, A., Quesada-López, T., Giralt, M., Villarroya, J., and Villarroya, F. (2019). Parkin controls brown adipose tissue plasticity in response to adaptive thermogenesis. EMBO Reports. *20*, e46832.

Cannon, B., and Nedergaard, J. (2004). Brown Adipose Tissue: Function and Physiological Significance. Physiological Reviews. *84*, 277–359.

Cao, W., Daniel, K.W., Robidoux, J., Puigserver, P., Medvedev, A.V., Bai, X., Floering, L.M., Spiegelman, B.M., and Collins, S. (2004). p38 Mitogen-Activated Protein Kinase Is the Central Regulator of Cyclic AMP-Dependent Transcription of the Brown Fat Uncoupling Protein 1 Gene. Mol Cell Biol. *24*, 3057–3067.

Chouchani, E.T., Kazak, L., Jedrychowski, M.P., Lu, G.Z., Erickson, B.K., Szpyt, J., Pierce, K.A., Laznik-Bogoslavski, D., Vetrivelan, R., Clish, C.B., et al. (2016). Mitochondrial ROS regulate thermogenic energy expenditure and sulfenylation of UCP1. Nature. *532*, 112–116.

Chung, D., Dzal, Y.A., Seow, A., Milsom, W.K., and Pamenter, M.E. (2016). Naked mole rats exhibit metabolic but not ventilatory plasticity following chronic sustained hypoxia. Proceedings of the Royal Society B: Biological Sciences. *283*, 20160216.

DALY, T.J.M., and BUFFENSTEIN, R. (1998). Skin morphology and its role in thermoregulation in mole-rats, Heterocephalus glaber and Cryptomys hottentotus. J Anat. *193*, 495–502.

Daly, T.J., Williams, L.A., and Buffenstein, R. (1997). Catecholaminergic innervation of interscapular brown adipose tissue in the naked mole-rat (Heterocephalus glaber). J. Anat. *190 ( Pt 3)*, 321–326.

Dzal, Y.A., Jenkin, S.E.M., Lague, S.L., Reichert, M.N., York, J.M., and Pamenter, M.E. (2015). Oxygen in demand: How oxygen has shaped vertebrate physiology. Comp. Biochem. Physiol., Part A Mol. Integr. Physiol. *186*, 4–26.

Dzal, Y.A., Seow, A., Borecky, L.G., Chung, D., Gill, S.K.G., Milsom, W.K., and Pamenter, M.E. (2019). Glutamatergic Receptors Modulate Normoxic but Not Hypoxic Ventilation and Metabolism in Naked Mole Rats. Front. Physiol. *10*.

Enerbäck, S., Jacobsson, A., Simpson, E.M., Guerra, C., Yamashita, H., Harper, M.-E., and Kozak, L.P. (1997). Mice lacking mitochondrial uncoupling protein are cold-sensitive but not obese. Nature. *387*, 90–94.

Fuhrmann, D.C., Wittig, I., Heide, H., Dehne, N., and Brüne, B. (2013). Chronic hypoxia alters mitochondrial composition in human macrophages. Biochimica et Biophysica Acta (BBA) - Proteins and Proteomics. *1834*, 2750–2760.

Gautier, H., Bonora, M., Schultz, S.A., and Remmers, J.E. (1987). Hypoxia-induced changes in shivering and body temperature. J. Appl. Physiol. *62*, 2477–2484.

Goldman, B.D., Goldman, S.L., Lanz, T., Magaurin, A., and Maurice, A. (1999). Factors Influencing Metabolic Rate in Naked Mole-Rats (Heterocephalus glaber). Physiology & Behavior. *66*, 447–459.

Greenberg, R., Cadena, V., Danner, R.M., and Tattersall, G. (2012). Heat Loss May Explain Bill Size Differences between Birds Occupying Different Habitats. PLOS ONE. *7*, e40933.

Guppy, M., and Withers, P. (1999). Metabolic depression in animals: physiological perspectives and biochemical generalizations. Biol Rev Camb Philos Soc. *74*, 1–40.

Harper, J.W., Ordureau, A., and Heo, J.-M. (2018). Building and decoding ubiquitin chains for mitophagy. Nature Reviews Molecular Cell Biology. *19*, 93–108.

Hayden, P., and Lindberg, R.G. (1970). Hypoxia-induced torpor in pocket mice (genus: Perognathus). Comp. Biochem. Physiol. *33*, 167–179.

Himms-Hagen, J. (1985). Brown Adipose Tissue Metabolism and Thermogenesis. Annual Review of Nutrition. *5*, 69–94.

Hislop, M.S., and Buffenstein, R. (1994). Noradrenaline induces nonshivering thermogenesis in both the naked mole-rat (Heterocephalus glaber) and the Damara mole-rat (Cryptomys damarensis) despite very different modes of thermoregulation. Journal of Thermal Biology. *19*, 25–32.

Hochachka, P.W. (1986). Defense strategies against hypoxia and hypothermia. Science. *231*, 234–241.

Hochachka, P.W., Buck, L.T., Doll, C.J., and Land, S.C. (1996). Unifying theory of hypoxia tolerance: molecular/metabolic defense and rescue mechanisms for surviving oxygen lack. Proc. Natl. Acad. Sci. U.S.A. *93*, 9493–9498.

Holmes, M.M., Goldman, B.D., Goldman, S.L., Seney, M.L., and Forger, N.G. (2009). Neuroendocrinology and sexual differentiation in eusocial mammals. Front Neuroendocrinol. *30*, 519–533.

Holtze, S., Braude, S., Lemma, A., Koch, R., Morhart, M., Szafranski, K., Platzer, M., Alemayehu, F., Goeritz, F., and Hildebrandt, T.B. (2018). The microenvironment of naked mole-rat burrows in East Africa. African Journal of Ecology. *56*, 279–289.

Houlahan, C.R., Kirby, A.M., Dzal, Y.A., Fairman, G.D., and Pamenter, M.E. (2018). Divergent behavioural responses to acute hypoxia between individuals and groups of naked mole rats. Comp. Biochem. Physiol. B, Biochem. Mol. Biol. *224*, 38–44.

Ilacqua, A.N., Kirby, A.M., and Pamenter, M.E. (2017). Behavioural responses of naked mole rats to acute hypoxia and anoxia. Biol. Lett. *13*.

van Jaarsveld, B., Bennett, N.C., Hart, D.W., and Oosthuizen, M.K. (2019). Locomotor activity and body temperature rhythms in the Mahali mole-rat (C. h. mahali): The effect of light and ambient temperature variations. J. Therm. Biol. *79*, 24–32.

Karunadharma, P.P., Basisty, N., Chiao, Y.A., Dai, D.-F., Drake, R., Levy, N., Koh, W.J., Emond, M.J., Kruse, S., Marcinek, D., et al. (2015). Respiratory chain protein turnover rates in mice are highly heterogeneous but strikingly conserved across tissues, ages, and treatments. FASEB J. *29*, 3582–3592.

Kim, E.B., Fang, X., Fushan, A.A., Huang, Z., Lobanov, A.V., Han, L., Marino, S.M., Sun, X., Turanov, A.A., Yang, P., et al. (2011). Genome sequencing reveals insights into physiology and longevity of the naked mole rat. Nature. *479*, 223–227.

Kirby, A.M., Fairman, G.D., and Pamenter, M.E. (2018). Atypical behavioural, metabolic and thermoregulatory responses to hypoxia in the naked mole rat (Heterocephalus glaber). Journal of Zoology. *305*, 106–115.

Kotze, J., Bennett, N.C., and Scantlebury, M. (2008). The energetics of huddling in two species of mole-rat (Rodentia: Bathyergidae). Physiol. Behav. *93*, 215–221.

McCafferty, D.J., Gilbert, C., Thierry, A.-M., Currie, J., Le Maho, Y., and Ancel, A. (2013). Emperor penguin body surfaces cool below air temperature. Biology Letters *9*, 20121192.

McNab, B.K. (1966). The Metabolism of Fossorial Rodents: A Study of Convergence. Ecology. *47*, 712–733.

Moazed, B., and Desautels, M. (2002). Differentiation-dependent expression of cathepsin D and importance of lysosomal proteolysis in the degradation of UCP1 in brown adipocytes. Can. J. Physiol. Pharmacol. *80*, 515–525.

Mortola, J.P., and Dotta, A. (1992). Effects of hypoxia and ambient temperature on gaseous metabolism of newborn rats. Am. J. Physiol. *263*, R267-272.

Nedergaard, J., Golozoubova, V., Matthias, A., Asadi, A., Jacobsson, A., and Cannon, B. (2001). UCP1: the only protein able to mediate adaptive non-shivering thermogenesis and metabolic inefficiency. Biochim. Biophys. Acta *1504*, 82–106.

Nguyen, V.C., Deck, C.A., and Pamenter, M.E. (2019). Naked mole-rats reduce the expression of ATP-dependent but not ATP-independent heat shock proteins in acute hypoxia. Journal of Experimental Biology. *222*.

Nicholls, D.G. (2006). The physiological regulation of uncoupling proteins. Biochimica et Biophysica Acta (BBA) - Bioenergetics. *1757*, 459–466.

Oelkrug, R., Polymeropoulos, E.T., and Jastroch, M. (2015). Brown adipose tissue: physiological function and evolutionary significance. J. Comp. Physiol. B, Biochem. Syst. Environ. Physiol. *185*, 587–606.

Pamenter, M.E., Dzal, Y.A., and Milsom, W.K. (2015). Adenosine receptors mediate the hypoxic ventilatory response but not the hypoxic metabolic response in the naked mole rat during acute hypoxia. Proc. Biol. Sci. *282*, 20141722.

Pamenter, M.E., Lau, G.Y., Richards, J.G., and Milsom, W.K. (2018). Naked mole rat brain mitochondria electron transport system flux and H+ leak are reduced during acute hypoxia. Journal of Experimental Biology. *221*, jeb171397.

Pamenter, M.E., Dzal, Y.A., Thompson, W.A., and Milsom, W.K. (2019). Do naked mole rats accumulate a metabolic acidosis or an oxygen debt in severe hypoxia? Journal of Experimental Biology. *222*, jeb191197.

Park, T.J., Reznick, J., Peterson, B.L., Blass, G., Omerbašić, D., Bennett, N.C., Kuich, P.H.J.L., Zasada, C., Browe, B.M., Hamann, W., et al. (2017). Fructose-driven glycolysis supports anoxia resistance in the naked mole-rat. Science. *356*, 307–311.

Pickles, S., Vigié, P., and Youle, R.J. (2018). Mitophagy and Quality Control Mechanisms in Mitochondrial Maintenance. Current Biology. *28*, R170–R185.

Pride, H., Yu, Z., Sunchu, B., Mochnick, J., Coles, A., Zhang, Y., Buffenstein, R., Hornsby, P.J., Austad, S.N., and Pérez, V.I. (2015). Long-lived species have improved proteostasis compared to phylogenetically-related shorter-lived species. Biochem. Biophys. Res. Commun. *457*, 669–675.

Ramirez, J.-M., Folkow, L.P., and Blix, A.S. (2007). Hypoxia tolerance in mammals and birds: from the wilderness to the clinic. Annu. Rev. Physiol. *69*, 113–143.

Riccio, A.P., and Goldman, B.D. (2000a). Circadian rhythms of locomotor activity in naked mole-rats (Heterocephalus glaber). Physiol. Behav. *71*, 1–13.

Riccio, A.P., and Goldman, B.D. (2000b). Circadian rhythms of body temperature and metabolic rate in naked mole-rats. Physiol. Behav. *71*, 15–22.

Rodriguez, K.A., Edrey, Y.H., Osmulski, P., Gaczynska, M., and Buffenstein, R. (2012). Altered Composition of Liver Proteasome Assemblies Contributes to Enhanced Proteasome Activity in the Exceptionally Long-Lived Naked Mole-Rat. PLOS ONE. *7*, e35890.

Rodriguez, K.A., Osmulski, P.A., Pierce, A., Weintraub, S.T., Gaczynska, M., and Buffenstein, R. (2014). A cytosolic protein factor from the naked mole-rat activates proteasomes of other species and protects these from inhibition. Biochim. Biophys. Acta. *1842*, 2060–2072.

Rohlicek, C.V., Saiki, C., Matsuoka, T., and Mortola, J.P. (1998). Oxygen transport in conscious newborn dogs during hypoxic hypometabolism. J. Appl. Physiol. *84*, 763–768.

Roper, T.J., Bennett, N.C., Conradt, L., and Molteno, A.J. (2001). Environmental conditions in burrows of two species of African mole-rat, Georhychus capensis and Cryptomys damarensis. Journal of Zoology. *254*, 101–107.

Sebaa, R., Johnson, J., Pileggi, C., Norgren, M., Xuan, J., Sai, Y., Tong, Q., Krystkowiak, I., Bondy-Chorney, E., Davey, N.E., et al. (2019). SIRT3 controls brown fat thermogenesis by deacetylation regulation of pathways upstream of UCP1. Molecular Metabolism. 25, 35–49.

Sokolova, I.M., Sokolov, E.P., and Haider, F. (2019). Mitochondrial mechanisms underlying tolerance to fluctuating oxygen conditions: Lessons from hypoxia-tolerant organisms. Integr. Comp. Biol. *59*, 938-952.

Steiner, A.A., and Branco, L.G.S. (2002). Hypoxia-induced anapyrexia: implications and putative mediators. Annu. Rev. Physiol. *64*, 263–288.

Sumbera, R. (2019). Thermal biology of a strictly subterranean mammalian family, the African

mole-rats (Bathyergidae, Rodentia) - a review. J. Therm. Biol. *79*, 166–189.

Tattersall, G.J. (2016). Infrared thermography: A non-invasive window into thermal physiology. Comp. Biochem. Physiol., Part A Mol. Integr. Physiol. *202*, 78–98.

Tattersall, G.J., and Milsom, W.K. (2003). Transient peripheral warming accompanies the hypoxic metabolic response in the golden-mantled ground squirrel. J. Exp. Biol. *206*, 33–42.

Wade, B.E., Zhao, J., Ma, J., Hart, C.M., and Sutliff, R.L. (2018). Hypoxia-induced alterations in the lung ubiquitin proteasome system during pulmonary hypertension pathogenesis. Pulm Circ. *8*.

Wang, G., Meyer, J.G., Cai, W., Softic, S., Li, M.E., Verdin, E., Newgard, C., Schilling, B., and Kahn, C.R. (2019). Regulation of UCP1 and Mitochondrial Metabolism in Brown Adipose Tissue by Reversible Succinylation. Molecular Cell. *74*, 844-857.e7.

Wikstrom, J.D., Mahdaviani, K., Liesa, M., Sereda, S.B., Si, Y., Las, G., Twig, G., Petrovic, N., Zingaretti, C., Graham, A., et al. (2014). Hormone-induced mitochondrial fission is utilized by brown adipocytes as an amplification pathway for energy expenditure. EMBO J. *33*, 418–436.

Withers, P.C., and Jarvis, J.U.M. (1980). The effect of huddling on thermoregulation and oxygen consumption for the naked mole-rat. Comparative Biochemistry and Physiology Part A: Physiology. *66*, 215–219.

Woodley, R., and Buffenstein, R. (2002). Thermogenic changes with chronic cold exposure in the naked mole-rat (Heterocephalus glaber). Comparative Biochemistry and Physiology - Part A: Molecular & Integrative Physiology. *133*, 827–834.

Yahav, S., and Buffenstein, R. (1991). Huddling Behavior Facilitates Homeothermy in the Naked Mole Rat Heterocephalus glaber. Physiological Zoology. *64*, 871–884.

Zhang, W., Ren, H., Xu, C., Zhu, C., Wu, H., Liu, D., Wang, J., Liu, L., Li, W., Ma, Q., et al. (2016). Hypoxic mitophagy regulates mitochondrial quality and platelet activation and determines severity of I/R heart injury. ELife. *5*, e21407.

Zhao, S., Lin, L., Kan, G., Xu, C., Tang, Q., Yu, C., Sun, W., Cai, L., Xu, C., and Cui, S. (2014). High autophagy in the naked mole rat may play a significant role in maintaining good health. Cell. Physiol. Biochem. *33*, 321–332.

### 3.9 FIGURES

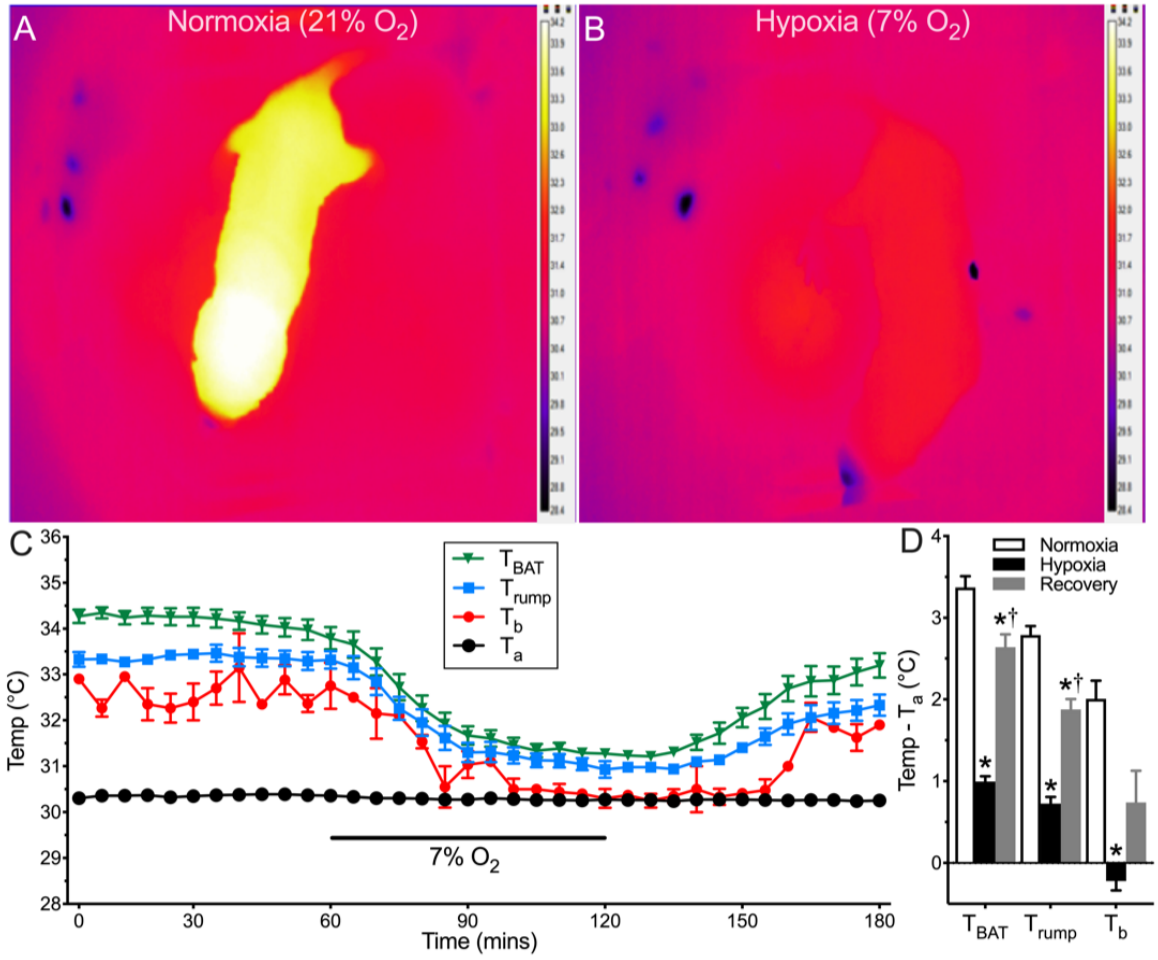
A
Normoxia (21% O2)
B
Hypoxia (7% O2)
C
TBAT
Trump
Tb
Ta
Temp (°C)
7% O2
Time (mins)
D
Normoxia
Hypoxia
Recovery
Temp - Ta (°C)
TBAT
Trump
Tb

**Figure 3.1: Naked mole-rat thermogenesis ceases in acute hypoxia and body temperature drops to ambient levels.** (A&B) FLIR thermal images of a naked mole-rat following 60 minutes of exposure to normoxia (A: 21% $O_2$) or hypoxia (B: 7% $O_2$). (C) Summaries of ambient temperature ($T_a$, black circles), core body temperature ($T_b$, red circles), interscapular brown adipose tissue temperature ($T_{BAT}$, green triangles), and dorsal skin surface temperature ($T_{rump}$, blue squares) from naked mole-rats exposed to a normoxia → hypoxia → recovery protocol in 30°C ($n$ = 10). (D) Summaries of temperature difference between physiological temperatures and $T_a$ in the final 10 mins of each treatment period. Data are mean ± SEM (repeated measures ANOVA with Tukey *post-test*). Asterisks indicate significant difference from normoxic controls ($p < 0.05$). Daggers indicate significant difference from hypoxia.

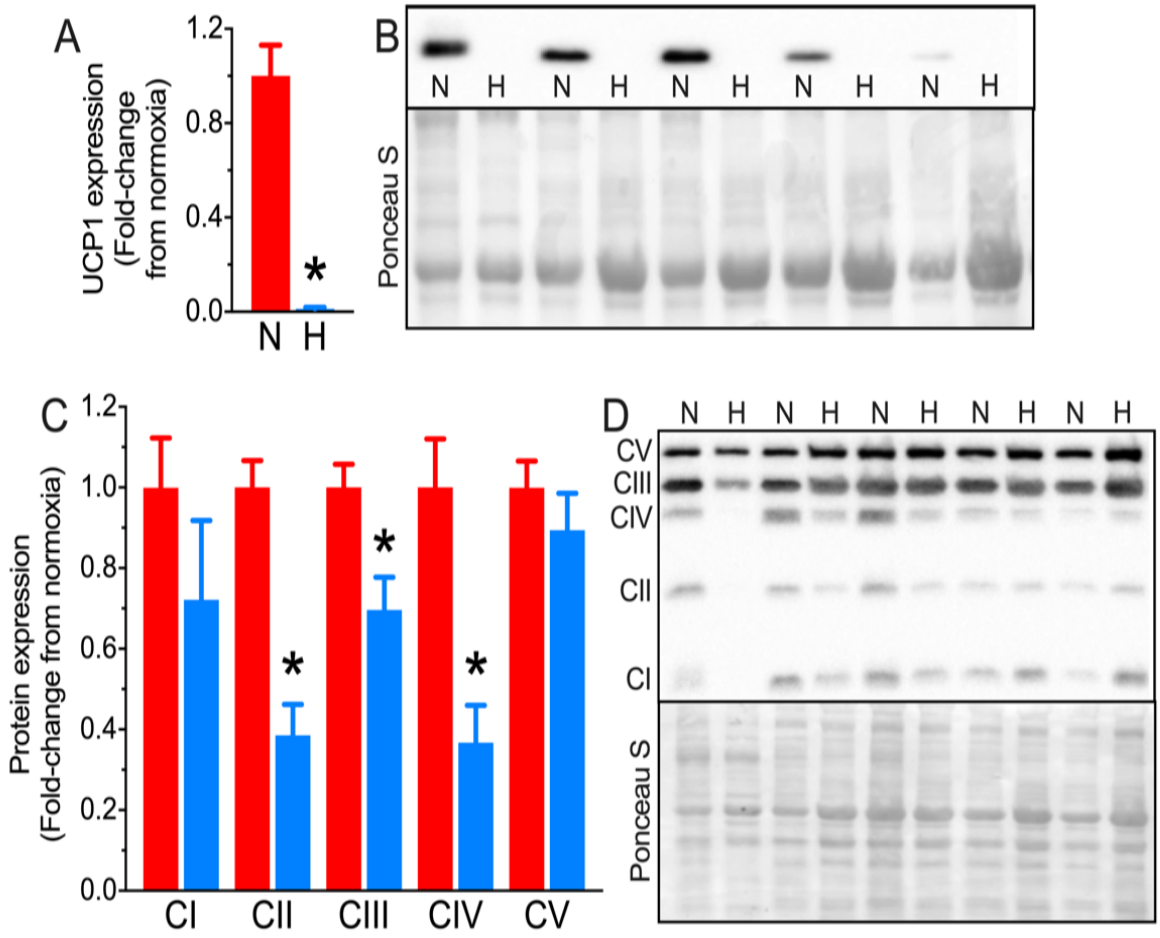
A
UCP1 expression
(Fold-change
from normoxia)
1.2
0.8
0.4
0.0
N H
*
B
N H N H N H N H N H
Ponceau S
C
Protein expression
(Fold-change from normoxia)
1.2
1.0
0.8
0.6
0.4
0.2
0.0
CI CII CIII CIV CV
*
*
*
D
N H N H N H N H N H
CV
CIII
CIV
CII
CI
Ponceau S

**Figure 3.2: Thermogenic protein expression decreases in acute hypoxia.** (A) Summary of UCP1 expression in interscapular BAT from naked mole-rats treated in normoxia (red bars, *n* = 13) or 1 hr of hypoxia (7% $O_2$, blue bars, *n* = 5). Data are mean ± SEM. (B) Western blot image of UCP1 protein bands and total protein quantified with ponceau S. (C) Summary of ETC complexes I-IV and $F_1F_o$ATPase protein expression in interscapular BAT from naked mole-rats treated as in A. Data are mean ± SEM. (D) Western blot image of oxidative phosphorylation protein bands and total protein gel expression quantified with ponceau S. Asterisks indicate significant difference from normoxic controls (unpaired students t-test; $p < 0.05$).

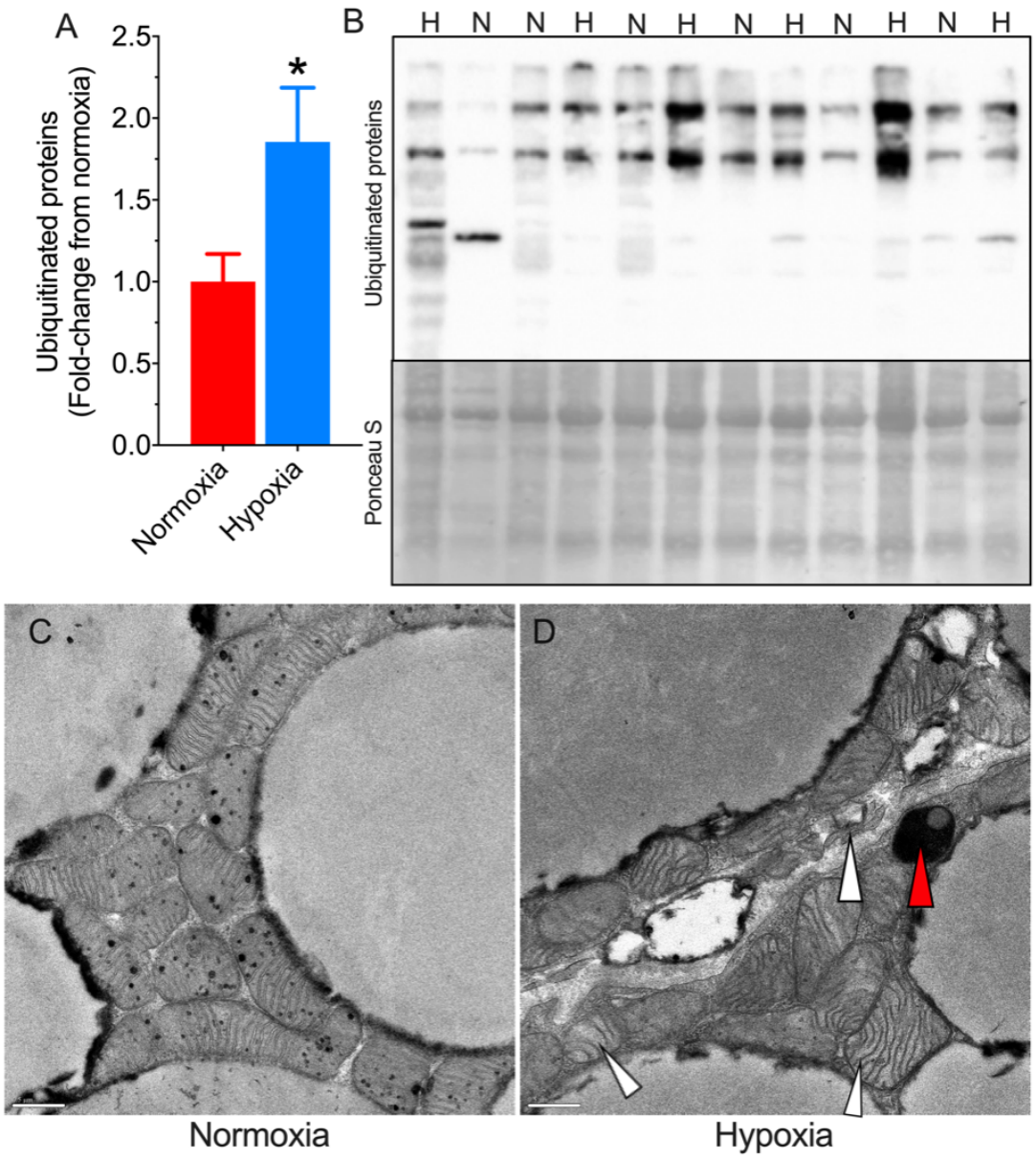
A
Ubiquitinated proteins
(Fold-change from normoxia)
2.5
2.0
1.5
1.0
0.5
0.0
*
Normoxia
Hypoxia
B
H N N H N H N H N H N H
Ubiquitinated proteins
Ponceau S
C
D
Normoxia
Hypoxia

**Figure 3.3: Acute hypoxia increases protein ubiquitination and induces abnormal mitochondrial morphology naked mole-rat BAT.** (A) Summary of western blot analysis of protein ubiquitination levels in interscapular BAT (iBAT) homogenates from naked mole-rats held at 30°C in normoxia (21% $O_2$, *n* = 6) or after 1 hr of hypoxia (7% $O_2$, *n* = 6). (B) Western blot image of ubiquitinated protein bands and total protein gel expression quantified with ponceau S. Data are mean ± SEM. Asterisks indicate significant difference from normoxic controls (unpaired students t-test; $p < 0.05$). (C&D) Representative electron micrographs of iBAT from naked mole-rats held at 30°C in normoxia (C) or hypoxia (D). White arrowheads indicate abnormal mitochondrial cristae and red arrowhead indicates degradative or lysosome-like vacuoles. Scale bars: 0.5 µm.

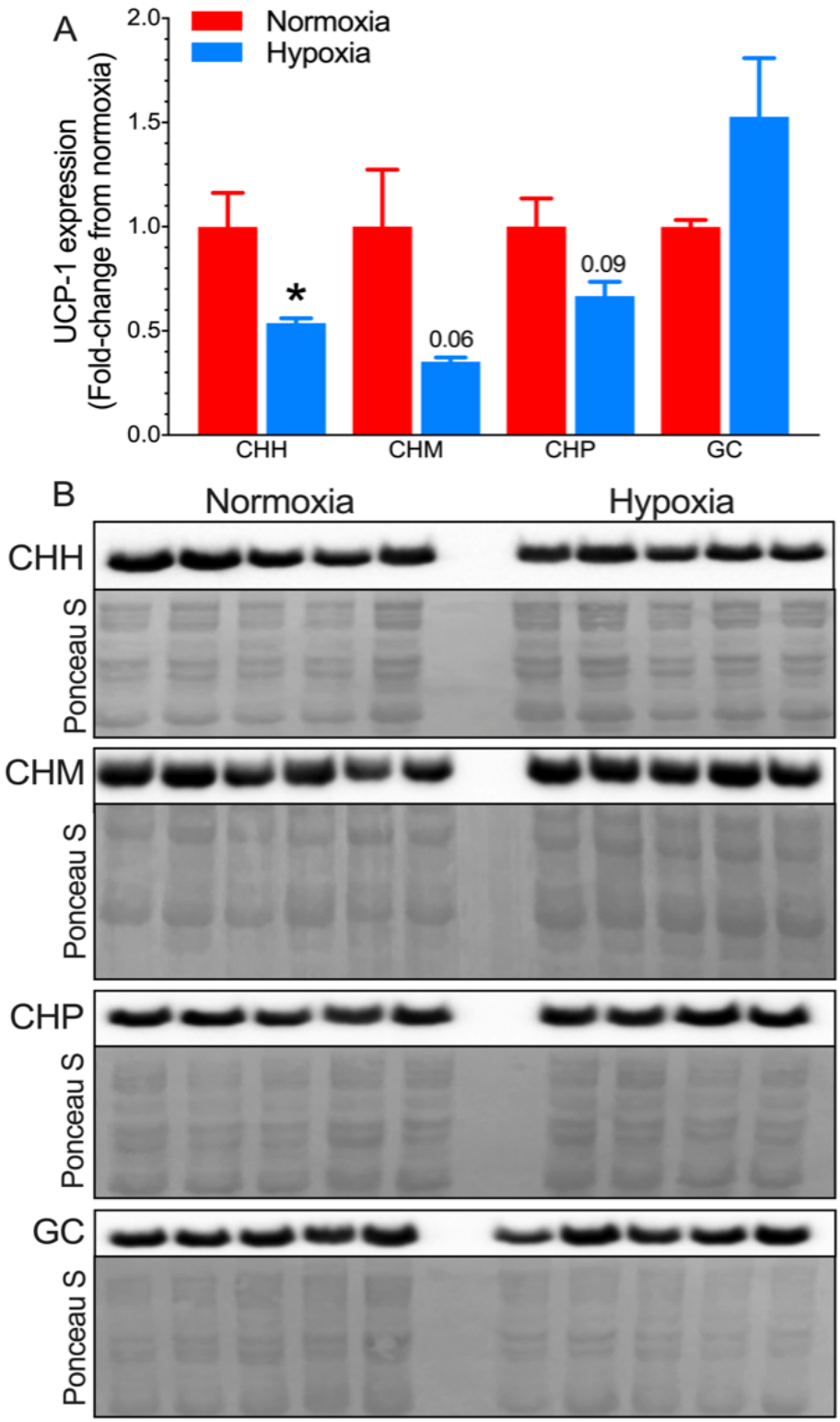
A
Normoxia
Hypoxia
UCP-1 expression
(Fold-change from normoxia)
2.0
1.5
1.0
0.5
0.0
*
0.06
0.09
CHH
CHM
CHP
GC
B
Normoxia
Hypoxia
CHH
Ponceau S
CHM
Ponceau S
CHP
Ponceau S
GC
Ponceau S

**Figure 3.4: Acute hypoxia generally reduces UCP1 expression in interscapular BAT from cousin species of African mole-rat.** (A) Summary of western blot analysis of UCP1 protein expression in interscapular BAT homogenates from 4 species of African mole-rats related to naked mole-rats (CHH: *Cryptomys hottentotus hottentotus*, CHM: *Cryptomys hottentotus mahali*, CHP: *Cryptomys hottentotus pretoriae*, GC: *Georychus capensis*) treated in 28°C in normoxia (18% $O_2$, *n* = 5-6 each) or after 3 hrs of hypoxia (5% $O_2$, *n* = 4-5 each). Data are mean ± SEM. Asterisks indicate significant difference from normoxic controls (unpaired students t-test; $p < 0.05$). (B) Western blot images of UCP1 protein expression from A, and total protein gel expression quantified with ponceau S.

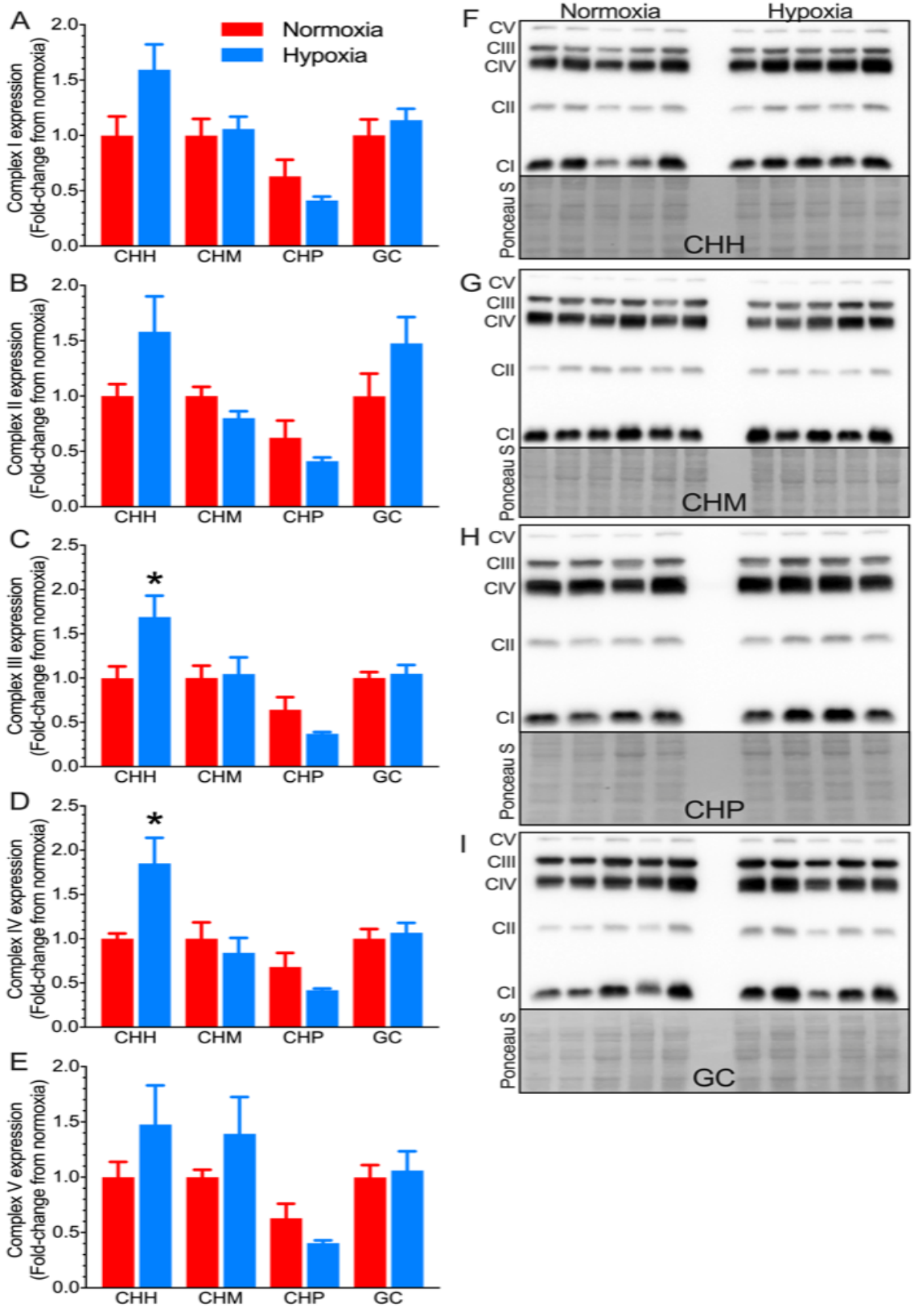
A
Normoxia
Hypoxia
Complex I expression (Fold-change from normoxia)
2.0
1.5
1.0
0.5
0.0
CHH
CHM
CHP
GC
B
Complex II expression (Fold-change from normoxia)
C
Complex III expression (Fold-change from normoxia)
2.5
*
D
Complex IV expression (Fold-change from normoxia)
E
Complex V expression (Fold-change from normoxia)
F
Normoxia
Hypoxia
CV
CIII
CIV
CII
CI
Ponceau S
CHH
G
CHM
H
CHP
I
GC

**Figure 3.5: Hypoxia does not consistently modify ETC protein expression in cousin species of African mole-rat.** (A-E) Summaries of western blot analysis of ETC protein expression in interscapular BAT homogenates from 4 species of African mole-rats related to naked mole-rats (CHH: *Cryptomys hottentotus hottentotus*, CHM: *Cryptomys hottentotus mahali*, CHP: *Cryptomys hottentotus pretoriae*, GC: *Georychus capensis*) treated in 28°C in normoxia (18% $O_2$, *n* = 4-6 each) or after 3 hrs of hypoxia (5% $O_2$, *n* = 4-5 each). Data are mean ± SEM. Asterisks indicate significant difference from normoxic controls (unpaired students t-test; $p < 0.05$). (F-I) Western blot images of ETC protein expression from CHH, CHM, CHP, and GC, and total protein gel expression quantified with ponceau S.

**CHAPTER 4: SMALL EXTRACELLULAR VESICLES RELEASED FROM ACUTELY ACTIVATED BROWN ADIPOSE TISSUE DO NOT IMPACT C2C12 MYOBLAST BIOENERGETICS**

Rajaa Sebaa[1,2,3], Ziyad El Hankouri[1], Jian Xuan[1], Derrick Gibbings[2,4] and Mary-Ellen Harper[1,2*]

[1]Department of Biochemistry, Microbiology and Immunology, Faculty of Medicine, University of Ottawa, Ottawa, ON, Canada
[2]Ottawa Institute of Systems Biology, Faculty of Medicine, University of Ottawa, Ottawa, ON, Canada
[3]Department of Medical Laboratories, College of Applied Medical Sciences, University of Shaqra, Duwadimi, Saudi Arabia
[4]Department of Cellular and Molecular Medicine, Faculty of Medicine, University of Ottawa, Ottawa, ON, Canada

*** To whom correspondence should be addressed:**
Dr. Mary-Ellen Harper, PhD
Professor
Department of Biochemistry, Microbiology and Immunology
Ottawa Institute of Systems Biology
Faculty of Medicine, University of Ottawa
451 Smyth Road, Ottawa, ON Canada, ON K1H 8M5
Email: mharper@uottawa.ca
Tel: +1-613-562-5800 Ext 8235

## 4.1 STATEMENT OF MANUSCRIPT STATUS AND CONTRIBUTIONS

### 4.1.1 STATEMENT OF MANUSCRIPT STATUS

The manuscript “Small extracellular vesicles released from acutely activated brown adipose tissue do not impact C2C12 myoblast bioenergetics” has been submitted for publication to the Journal of of *Applied Physiology, Nutrition, and Metabolism* (APNM-2019-0965) on December16$^{th}$, 2019.

### 4.1.2 CONTRIBUTION STATEMENT

RS and MEH conceived the ideas for the project. RS conducted most of the experiments including Zetaview analyses, Seahorse experiments and western blotting. ZE performed some of the Small extracellular vesicles isolations and analyses. RS and ZE analyzed data and RS prepared figures. RS and MEH drafted and wrote the paper.

### 4.1.3 ACKNOWLEDGEMENTS AND FUNDING

We would like to thank Ryan Reshke for his expert advice and help with the Zetaview analyses. We also thank Nidhi Kuksal for helping us with BAT dissections. This work was funded by a grant from the Natural Sciences and Engineering Research Council (NSERC) of Canada (MEH). RS is the recipient of a scholarship from the University of Shaqra, Duwadimi, Saudi Arabia.

### 4.1.4 CONFLICT OF INTEREST

None declared.

**4.2 ABSTRACT**

The physiological function of brown adipose tissue (BAT) is non-shivering thermogenesis (NST). How this unique tissue responds and signals to other tissues to allow integrative adaptive responses to a cold environment is complex and poorly understood. While NST occurs in BAT, shivering thermogenesis occurs in skeletal muscle (SkM). BAT releases signaling and regulatory molecules called BATokines, some of which are in small extracellular vesicles (sEV). We aimed to determine if sEV released from acutely activated BAT *in vivo* and *in vitro* had effects on SkM myoblast bioenergetics. Our results revealed that acute activation of BAT either *in vivo* or *in vitro* did not significantly affect the size and concentration of sEV released in mouse plasma or conditioned media, respectively. Unexpectedly, bioenergetics analyses demonstrated that sEV released from acutely activated BAT either *in vivo* or *in vitro* did not affect bioenergetics of C2C12 myoblasts following a 24h treatment. In conclusion, acutely activated BAT-derived sEV do not impact C2C12 myoblast bioenergetics under normal cellular and metabolic conditions. Future research should however examine how BAT-derived sEV could affect the energetics of SkM cells under additional conditions or different time-frames.

**Keywords:** extracellular vesicles, thermogenesis, skeletal muscle, mitochondria, β3-adrenergic receptor agonist, cellular respiration, glycolysis, metabolic flexibility

## 4.3 INTRODUCTION

Parenchymal cells in brown adipose tissue (BAT) and skeletal muscle (SkM) share common cellular origins and the tissues play essential roles in mammalian thermoregulation. Developmentally, brown adipocytes and myocytes are both derived from myogenic factor-5 (Myf5) expressing progenitors. The bidirectional fate switch of the progenitors is determined by the action of master regulators such as PRM16 and miRNA133 (An et al., 2017; Seale et al., 2008; Yin et al., 2013). Functionally, BAT is responsible for non-shivering thermogenesis (NST), and shivering thermogenesis is mediated by SkM (Cannon and Nedergaard, 2004; Enerbäck et al., 1997; Golozoubova et al., 2001). Shivering and NST are important for the survival of the organism in cold environments, and both processes require tremendous amounts of energy, thereby augmenting whole-body energy expenditure (Bal et al., 2017; Cannon and Nedergaard, 2011; Festuccia et al., 2011; Periasamy et al., 2017; Sepa-Kishi et al., 2017; Yu et al., 2002).

BAT and SkM are complementary in their thermoregulatory functions. Mouse studies demonstrate that during the first days of cold exposure, ST gradually decreases as NST is highly induced (Golozoubova et al., 2001; Nedergaard and Cannon, 2013; Stier et al., 2014). Moreover, when the production of heat in one of the tissues is defective, the other tissue increases its function to compensate for the defect in heat production in the other (Bal et al., 2017; Golozoubova et al., 2001). Thus there is functional cross-talk between BAT and SkM, some of which is thought to be mediated through the release of BATokines and myokines, respectively (Boström et al., 2012; Kong et al., 2018; Rao et al., 2014; Roberts et al., 2014; Stanford et al., 2018).

A potential mechanism that may facilitate functional links between BAT and SkM is through small extracellular vesicles (sEV). sEV are released by most cell types and can be found in different biological fluids, as well as in a conditioned media of cultured cells. They are characterized with a diameter less than 200 nm (Théry et al., 2018). They carry regulatory molecules that can be taken up by the recipient cells, and regulate their function (Gurunathan et al., 2019). Recent studies have reported that chronically activated BAT increases the release of sEV (Chen et al., 2016). Another study showed that miRNA-carrying sEV derived from BAT can regulate liver gene expression (Thomou et al., 2017). Many questions remain regarding the regulatory role of BAT-derived sEV in other tissues/cells. For example, it is unknown if sEV derived from activated BAT have regulatory effects on the bioenergetics of SkM tissue.

Given the strong links between BAT and SkM and the regulatory role of sEV, we speculated that activated BAT releases sEV that may modulate SkM myoblast bioenergetics. In order to study this, we collected sEV released from acutely activated BAT, *in vivo* and *in vitro,* and examined their metabolic effects in C2C12 myoblasts.

## 4.4 MATERIALS AND METHODS

### 4.4.1 ANIMALS

Male 129S1/SvlmJ mice, aged 5-7 weeks, were used for all experiments. They were housed at room temperature (24°C) and were kept in an individually ventilated cage system with a 12/12 light-dark cycle. They were given a standard rodent diet, *ad libitum,* composed of 44.2% carbohydrates, 6.2% fat, and 18.6% crude protein (diet T.2018, Harlan Teklad, Indianapolis IN) and water. All experimental animals were maintained under the guidelines and principles of the

Canadian Council of Animal Care and the approval of the Animal Care Committee of the University of Ottawa.

### 4.4.2 *IN VIVO* BAT ACTIVATION STUDIES AND PLASMA COLLECTION

Mice were housed individually at thermoneutrality (28°C) for 2 days for acclimation purposes, with free access to water and food. After 2 days of acclimation, mice were injected with either saline or the β3-adrenergic agonist CL 316,243 (1 mg/kg *i.p.*) to activate BAT *in vivo*. 90min post-injection, mice were anesthetized with 3% isoflurane to collect heparinized blood samples via cardiac puncture. For plasma collection, whole blood was spun at 1500 g for 20 min at 4°C. Plasma samples were frozen at -80°C until they were used for sEV extraction as done previously (Thrush et al., 2018).

### 4.4.3 *IN VITRO* BAT ACTIVATION STUDIES AND CONDITIONED MEDIA COLLECTION

For each experimental preparation, interscapular brown adipose tissue (iBAT) was dissected from five WT mice for subsequent pooling (this number of mice was necessary in order to collect sufficient vesicles from the conditioned media of the incubated tissue). Tissue was transferred into ice-chilled 0.25M sucrose buffer, and any white adipose and muscle tissues were removed. iBAT was then minced and weighed. All steps were done on ice. Immediately after mincing, iBAT was treated either with saline or CL 316,243 (100nM) in 10 ml of high glucose DMEM media (Gibco, Thermo Fisher Scientific) with 1% Antibiotics-Antimycotic (Gibco, Thermo Fisher Scientific). 90 min post-treatment, the conditioned media of treated iBAT was collected and filtered through cell strainers (pore size, 70µm) to remove minced BAT. The filtered conditioned media samples were stored at 4°C until the following day for sEV extraction.

### 4.4.4 sEV EXTRACTION

sEV were extracted by differential centrifugation, as previously described (Guo et al., 2017) with minor modifications. sEV extraction began with equal volumes of plasma sample or conditioned media from experimental groups. First, large cell debris and contaminating particles were removed by spinning the samples at 4°C: 300 x g for 10min; 2,000 x g for 10min; and 10,000 x g for 30 minutes. To pellet the sEV, the supernatant was then spun in an ultracentrifuge at 100,000 x g for 2 hours at 4°C. sEV were washed by resuspending in PBS and spinning again at 100,000 x g for 30 minutes at 4°C. The final sEV pellet was resuspended in 30 µL of PBS for the next analyses. Of note, the PBS used here and in the Zetaview analysis had previously been spun at 100,000 x g for 2 hours to remove any particles of sEV size. Extracted sEV were stored at 4°C for cell treatment within a week or western blotting analyses.

### 4.4.5 WESTERN BLOTTING

sEV pellets were mixed with loading dye, consisting of 1M Tris/HCL (pH=6.8), 8% SDS, 40% glycerol, 5% β-mercaptoethanol, 0.25M EDTA (pH=8), 0.2% bromophenol blue. The sEV samples were denatured for 5 min at 95°C and stored at -20°C for western blotting analyses. Samples were run on a 12% SDS- polyacrylamide gel for 1-1.5 h at 130 volts and were then transferred onto a nitrocellulose membrane for 1 h at 100 volts. The membrane was blocked with 5% BSA for 1 hour at room temperature. To check for sEV markers, the blocked membrane was incubated overnight at 4°C with primary antibodies: anti-alix (1:1000, BD Transduction Laboratories, #611621), anti-flotillin-2 (1:1000, Cell Signaling, #42A3) and calnexin (1:1000, Cell Signaling, #2679). The membrane was then washed three times for 10 min each at room temperature and incubated with secondary antibody (goat anti-mouse IgG, 1:5000) or (goat anti-rabbit IgG,

1:10000) for 1 hour at room temperature. The membrane was then washed again three times for 10 min each at room temperature. To visually detect the bands, membrane was covered with HRP detection reagent (Pierce ECL Western Blotting Substrate, Thermo Fisher Scientific, #32106) and exposed to x-ray film for protein band detection. Note: western blots in Figure 1A were from the same membrane.

#### 4.4.6 ZETAVIEW NANOPARTICLE TRACKING ANALYSIS

sEV samples first were diluted in PBS that was pre-spun to remove any sEV-sized particles. Nanoparticle tracking analyzer, (ZetaView PMX-110, ParticleMetrix), was used to characterize the sEV samples. Setting used for measuring sEV by Nanoparticle Tracking as follows: for pre-acquisition parameters (Sensitivity 85, Shutter Speed 40, Frame Rate (fps) 30, Resolution Highest, Camera Gain 770, Positions Measured 11) and for post-acquisition parameters (Minimum Brightness 15, Minimum Size (pixels) 10, Maximum Size (pixels) 500). The analyzer was first calibrated with polystyrene beads with known diameter size of 102nm (Microtrac, #900383) prior to sample readings**.** After calibration, the diluted samples were loaded into the cell of the analyzer and the dilution factor was entered in the Zetaview software for corrections before starting the analyses. The analyzer measures each sample at eleven different positions throughout the Zetaview cell. After automated analysis of all the eleven positions and removal any of outlier positions, the size (nm) and concentration (particles/ml) of the sEV were calculated. Corresponding software, ZetaView analyzer (8.02.31), was used to export the measurements of the sEV samples.

### 4.4.7 BIOENERGETIC ANALYSIS OF C2C12 MYOBLASTS

C2C12 myoblasts were cultured in high glucose DMEM media (Gibco, Thermo Fisher Scientific) supplemented with 10% FBS (Wisent Bioproducts) and 1% Antibiotics-Antimycotic (Gibco, Thermo Fisher Scientific). C2C12 myoblasts were split when their confluency reached 80%. For bioenergetic analyses, 10,000 C2C12 myoblasts were seeded per well in the Seahorse 96-well plates (Agilent) and were incubated in sEV-depleted growth media. Eight hours following cell seeding, myoblasts were treated with an equal plasma/conditioned media volume (5 µl) of sEV from each experimental condition. These were as follows: plasma sEV absolute numbers were $2.200 \pm 0.257 \times 10^7$ and $3.167 \pm 0.534 \times 10^7$ for saline and CL treated mice, respectively (mean± SEM). For the *in vitro* studies, they were $1.606 \pm 0.202 \times 10^7$ and $2.772 \pm 0.557 \times 10^7$ for saline and CL treated BAT explants, respectively (mean±SEM). This equivalent plasma/medium volume approach was used to model physiological effects of sEV released *in vivo* into the circulation. After 24 hours, sEV-containing medium medium was replaced with Seahorse medium, which consists of (DMEM, 25mM glucose, 1mM pyruvate, and 4mM glutamine, pH=7.4). Immediately prior to analysis, the plate was kept in a $CO_2$-free incubator for 45 minutes. During analysis in the Seahorse XFe96 system (Agilent), the following injections were included in the protocol: 2µg/ml oligomycin (3 cycles; 3 min mix and 3 min measure) to determine leak respiration; 2.4µM FCCP (3 cycles; 3 min mix and 3 min measure) to induce maximal respiration; 5.5µM antimycin A and 7.7µM rotenone (3 cycles; 3 min mix and 3 min measure) to inhibit mitochondrial respiration; and 20µM monensin (3 cycles; 3 min mix and 3 min measure) to induce the maximal glycolytic rate.

### 4.4.8 STATISTICAL ANALYSIS

Data are presented as mean± SEM. A Student's unpaired two-tailed t-test was used and statistical significance was determined using Graph Pad Prism 7 (GraphPad Prism, La Jolla, CA, USA). P values were considered as significant at $P < 0.05$.

## 4.5 RESULTS

### 4.5.1 ACUTE ACTIVATION OF BAT WITH CL316,243 DID NOT IMPACT PLASMA sEV SIZE OR CONCENTRATION

Even in the basal (non-activated) state, BAT has been shown to release sEV into the circulation, and is considered as one of the major sites of miRNA-containing sEV in mice (Thomou et al., 2017). However, the effect of acute activation of BAT on the release of circulatory sEV has not yet been reported. According to a previously published study (Hankir et al., 2017), acute BAT activation *in vivo* was performed with the injection of CL316,243 in mice and post-injection, BAT activity was assessed for 1h by infrared thermal imaging. In our study, we followed the same protocol with minor modifications. Mice were injected with either saline (controls) or CL316,243 (1 mg/kg) and 90 min post-injection, blood samples were collected for sEV extraction. Then, extracted sEV were used to check for sEV markers. Western blotting results showed the existence of positive sEV markers including alix and flotillin-2 and a negative sEV marker calnexin in the extracts of sEV from different groups (Figure 4.1A). Also, we investigated the effect of CL316,243 treatment on the characteristics of plasma sEV. The size distribution analyses of plasma sEV demonstrated successful extraction of sEV in each group (Figure 4.1B&1C). Zetaview analyses indicated that the median size of sEV extracted from plasma of CL316243 injected mice was not

different compared with those extracted form control mice. The median size of sEV in both groups is around 150nm (Figure 4.1D). Moreover, acute activation of BAT *in vivo* did not significantly affect the concentration of sEV in plasma, as seen in (Figure 4.1E).

### 4.5.2 PLASMA sEV RELEASED UPON ACUTE ACTIVATION OF BAT *IN VIVO* DID NOT AFFECT BIOENERGETICS OF C2C12 MYOBLASTS

Although the median size and concentration of plasma sEV were not impacted by the acute activation of BAT *in vivo*, we next examined the metabolic effects of BAT-derived sEV on C2C12 myoblasts. To examine this, we treated C2C12 myoblasts with sEV from plasma of saline-injected or CL316,243-injected mice. Based on our previously published sEV treatment protocol (Thrush et al., 2018), C2C12 myoblasts were treated with sEV for 24h. Then, oxygen consumption rate (OCR) and extracellular acidification rate (ECAR) measurements were assessed in the sEV -treated C2C12 myoblasts. Surprisingly, sEV collected from plasma of CL316,243-injected mice had no effects on mitochondrial respiration of C2C12 myoblasts, including basal, leak, maximal, ATP-linked, and spare capacity respiration rates, compared to the controls (Figure 4.2A). Then we examined ECAR, a proxy measure of glycolysis, at all of the same conditions used for OCR determinations. There were no differences in ECAR between groups under any of the conditions (Figure 4.2B). We then determined if there were differences in metabolic flexibility of the sEV treated C2C12 myoblasts. Results demonstrate that C2C12 myoblasts treated with plasma sEV from CL316,243-injected mice showed a slight decrease in their metabolic flexibility compared to the controls (Figure 4.2C). Thus, based on these findings, we conclude that sEV collected from

plasma of CL316,243-injected mice do not significantly impact the bioenergetics of C2C12 myoblasts under these experimental conditions.

### 4.5.3 ACUTE ACTIVATION OF BAT *IN VITRO* DID NOT IMPACT THE SIZE OR CONCENTRATION OF RELEASED sEV

As the activation of BAT *in vivo* affects metabolic activity in other tissues, *e.g.*, increased cardiac output due to increased metabolic demands of NST, and as our aim was to specifically examine sEV from BAT, we next conducted *in vitro* studies of sEV released exclusively from BAT. It has been reported that chronic cold exposure in mice can increase the release of sEV from BAT that was cultured *ex vivo* (Chen et al., 2016). However, it remained unknown whether acute activation of BAT *ex vivo* increases the release of sEV. Here, we studied sEV released from BAT that was acutely activated with CL316,243 and examined the characteristics of released sEV. In each experiment, BAT was dissected from 5 mice, cultured *ex vivo*, and treated with either saline or CL316,243 for 90min. Then, we characterized the sEV collected from the conditioned media in each group. The size distribution analyses of sEV collected from conditioned media demonstrated successful extraction of sEV in each group (Figure 4.3A&3B). However, there were no statistical differences in the median sizes of sEV between groups which is $\sim$ 150nm (Figure 4.3C). In addition, the concentration of sEV showed a strong trend for an increase in the number of BAT-derived sEV after CL316,243 treatment ($P = 0.07$) (Figure 4.3D).

### 4.5.4 sEV RELEASED FROM ACUTELY ACTIVATED BAT *IN VITRO* DID NOT AFFECT BIOENERGETICS OF C2C12 MYOBLASTS

Next, we investigated the effects of sEV that were exclusively derived from BAT explants on the bioenergetic characteristics of C2C12 myoblasts. Therefore, sEV released in the conditioned

media of saline-treated BAT or CL316,243-treated BAT were used for C2C12 myoblast treatments. Consistent with *in vivo* observations, bioenergetics analysis of the sEV-treated myoblasts demonstrated that sEV released from *in vitro* activated BAT did not impact OCR and ECAR in C2C12 myoblasts in any of the tested conditions (Figure 4.4A&B). We then again considered aspects of metabolic flexibility. Our results clearly demonstrated no differences in the metabolic flexibility between different groups of the sEV-treated C2C12 myoblasts (Figure 4.4C). Taken together, *in vitro* results indicated that sEV released from acutely activated BAT did not impact the bioenergetics of C2C12 myoblasts.

## 4.6 DISCUSSION

While BAT plays a fundamental role in whole-body energy metabolism and thermogenesis, it is also known that BAT acts as an active secretory organ of signaling and regulatory molecules, which can be packaged in sEV (Cannon and Nedergaard, 2004; Chen et al., 2016; Thomou et al., 2017; Villarroya and Giralt, 2015). sEV are found in many different biological fluids and contain regulatory molecules such as lipids, proteins, and nucleic acids; they can target recipient cells or tissues through various specific mechanisms (Zhang et al., 2015, 2019). It has been shown that adipose tissues including BAT are major sources of miRNAs packaged in sEV and the ablation of these tissues in mice leads to marked decreases in circulating levels of sEV-packaged miRNAs (Thomou et al., 2017). 3T3-L1 derived white adipocytes have been shown to release miRNAs in sEV, which can regulate gene expression in C2C12 myotubes. Ying's group showed that miRNA-130b released in the conditioned medium of TGF-β-treated white adipocytes was taken up by C2C12 myotubes. When they transfected miRNA-130b in C2C12 myotubes, the level of

peroxisome proliferator-activated receptor-γ coactivator 1 alpha (PGC1α) in C2C12 myotubes was decreased (Wang et al., 2013). Another study reported that obese mouse white adipose tissue (WAT) that was cultured *ex vivo* can release sEV into the culture medium. When WAT-derived fluorescently labelled sEV were injected intravenously into mice, sEV were shown to be taken up by blood monocytes, regulating their activation (Deng et al., 2009).

Indeed, there is increased interest in BAT-derived sEV and their biological roles. To our knowledge, there have only been two studies that investigated the impact of BAT activation on the characteristics of circulating sEV, *i.e.,* changes in the miRNA content of sEV (Chen et al., 2016) or the effects of sEV on distant tissues (Thomou et al., 2017). In 2016, Chen *et al.* demonstrated that chronic activation of BAT induces the release of BAT-derived sEV and they concluded that miRNA-92a packaged in sEV can be used as a biomarker of the activity of BAT in mice and humans (Chen et al., 2016). Another study conducted by Thomou *et al*. showed that BAT-derived miRNAs released in sEV can regulate gene expression of fibroblast growth factor 21 (FGF21) in the liver (Thomou et al., 2017).

BAT and SkM have essential and interrelated functions in mammalian thermoregulation. In cold environments, ST and NST in SkM and BAT, respectively, allow adaptation and survival. Because it is not known whether BAT-derived sEV contain molecules that can modulate SkM metabolism, the goal of this study was to investigate whether sEV released from acutely activated BAT can modulate the bioenergetics of C2C12 myoblasts following a 24h treatment. Our results clearly demonstrate that: 1) BAT does release sEV, 2) acute activation of BAT does not significantly impact the characteristics of released sEV (although there is a trend for increased

numbers), and 3) sEV derived from acutely activated BAT *in vivo* or *in vitro* do not affect the bioenergetics of C2C12 myoblasts under commonly used cell culture conditions.

Yet, there are a number of limitations in our study that warrant against overinterpretation. sEV can affect target cell functions through receptor activation, and through protein delivery to mediate acute effects, as well as through miRNA delivery, which may be needed to mediate longer term effects (*i.e*., days). Chen *et al.* showed that chronic activation of BAT in mice, that were either kept at 18 °C for 7 days followed by 4 °C for 7 days or injected daily with CL316,243 for 7 days, causes distinct patterns of circulating miRNA-containing sEVs (Chen et al., 2016). Some of the latter miRNAs were previously reported by others to affect mitochondrial metabolism in C2C12 myoblasts during differentiation through decreased expression of subunits of CI and CIV of the electron transport chain (Siengdee et al., 2015). In our study, we examined BAT-derived sEV and their metabolic effects on C2C12 myoblasts; further research is needed to look for any metabolic effects of BAT-derived sEV on C2C12 myoblasts during or following differentiation into myotubes. Furthermore, it is possible that the cargo of acutely activated BAT-derived sEV targets certain mitochondrial pathways that were not examined in this study, *e.g.,* fatty acid oxidation.

Notably, OCR measurements of C2C12 myoblasts treated with plasma sEV are lower than OCR measurements of C2C12 myoblasts treated with sEV from conditioned media, suggesting that distinct sEV are released in mouse plasma vs conditioned media. It could be that plasma sEV contain inhibitory molecules, that may reduce the maximal respiratory capacity of C2C12 myoblasts. In our study, plasma sEV were collected from mice kept at thermoneutrality (28°C) for more than 2 days, and it has been previously shown that mice kept at thermoneutrality

for a week have high serum levels of myostatin (a muscle inhibitor) (Kong et al., 2018). In another study, it was shown that myostatin can be released in isolated sEV (Kim et al., 2018). Thus, it could be that myostatin and/or other potential inhibitory molecules such as miRNAs reduce the maximal respiration characteristics of C2C12 myoblasts.

Considering the integrative thermogenic responses of SkM and BAT during cold exposure, with BAT thermogenesis augmenting, as ST in SkM diminishes (Nedergaard and Cannon, 2013), the sEV signaling from SkM to BAT may actually be more important than signaling from BAT to SkM. Indeed, ST is energetically very costly, and interferes with an animal's capacity to perform regular activities (*e.g.,* foraging), and it would make sense that SkM signaling to BAT 'furnaces' occurs under these conditions. Of note are the studies demonstrating that exercise induces WAT browning, through the release of myokines such as irisin, β-aminoisobutyric acid and Metrnl (Boström et al., 2012; Rao et al., 2014; Roberts et al., 2014), indicating communication from SkM to BAT. However, the idea that SkM ST specifically induces BAT NST through an sEV-mediated mechanism needs investigation.

In summary, our findings show that sEV released from acutely activated BAT do not impact standard bioenergetic characteristics of C2C12 myoblasts under normal metabolic conditions. Further research is needed to examine the potential impact of BAT-derived sEV under different metabolic conditions or time-frames.

## 4.7 REFERENCES


An, Y., Wang, G., Diao, Y., Long, Y., Fu, X., Weng, M., Zhou, L., Sun, K., Cheung, T.H., Ip, N.Y., et al. (2017). A Molecular Switch Regulating Cell Fate Choice between Muscle Progenitor Cells and Brown Adipocytes. Dev. Cell. *41*, 382-391.e5.

Bal, N.C., Singh, S., Reis, F.C.G., Maurya, S.K., Pani, S., Rowland, L.A., and Periasamy, M. (2017). Both brown adipose tissue and skeletal muscle thermogenesis processes are activated during mild to severe cold adaptation in mice. J. Biol. Chem. *292*, 16616–16625.

Boström, P., Wu, J., Jedrychowski, M.P., Korde, A., Ye, L., Lo, J.C., Rasbach, K.A., Boström, E.A., Choi, J.H., Long, J.Z., et al. (2012). A PGC1-α-dependent myokine that drives brown-fat-like development of white fat and thermogenesis. Nature. *481*, 463–468.

Cannon, B., and Nedergaard, J. (2004). Brown Adipose Tissue: Function and Physiological Significance. Physiol. Rev. *84*, 277–359.

Cannon, B., and Nedergaard, J. (2011). Nonshivering thermogenesis and its adequate measurement in metabolic studies. J. Exp. Biol. *214*, 242–253.

Chen, Y., Buyel, J.J., Hanssen, M.J.W., Siegel, F., Pan, R., Naumann, J., Schell, M., van der Lans, A., Schlein, C., Froehlich, H., et al. (2016). Exosomal microRNA miR-92a concentration in serum reflects human brown fat activity. Nat. Commun. *7*, 11420.

Deng, Z., Poliakov, A., Hardy, R.W., Clements, R., Liu, C., Liu, Y., Wang, J., Xiang, X., Zhang, S., Zhuang, X., et al. (2009). Adipose Tissue Exosome-Like Vesicles Mediate Activation of Macrophage-Induced Insulin Resistance. Diabetes. *58*, 2498–2505.

Enerbäck, S., Jacobsson, A., Simpson, E.M., Guerra, C., Yamashita, H., Harper, M.-E., and Kozak, L.P. (1997). Mice lacking mitochondrial uncoupling protein are cold-sensitive but not obese. Nature. *387*, 90–94.

Festuccia, W.T., Blanchard, P.-G., and Deshaies, Y. (2011). Control of Brown Adipose Tissue Glucose and Lipid Metabolism by PPARγ. Front. Endocrinol. *2*.

Golozoubova, V., Hohtola, E., Matthias, A., Jacobsson, A., Cannon, B., and Nedergaard, J. (2001). Only UCP1 can mediate adaptive nonshivering thermogenesis in the cold. FASEB J. *15*, 2048–2050.

Guo, H., Chitiprolu, M., Roncevic, L., Javalet, C., Hemming, F.J., Trung, M.T., Meng, L., Latreille, E., Tanese de Souza, C., McCulloch, D., et al. (2017). Atg5 Disassociates the V1V0-ATPase to Promote

Exosome Production and Tumor Metastasis Independent of Canonical Macroautophagy. Dev. Cell. *43*, 716-730.e7.

Gurunathan, S., Kang, M.-H., Jeyaraj, M., Qasim, M., and Kim, J.-H. (2019). Review of the Isolation, Characterization, Biological Function, and Multifarious Therapeutic Approaches of Exosomes. Cells. *8*(4), 307.

Hankir, M.K., Kranz, M., Keipert, S., Weiner, J., Andreasen, S.G., Kern, M., Patt, M., Klöting, N., Heiker, J.T., Brust, P., et al. (2017). Dissociation Between Brown Adipose Tissue 18F-FDG Uptake and Thermogenesis in Uncoupling Protein 1-Deficient Mice. J. Nucl. Med. Off. Publ. Soc. Nucl. Med. *58*, 1100–1103.

Kim, S., Lee, M.-J., Choi, J.-Y., Park, D.-H., Kwak, H.-B., Moon, S., Koh, J.-W., Shin, H.-K., Ryu, J.-K., Park, C.-S., et al. (2018). Roles of Exosome-Like Vesicles Released from Inflammatory C2C12 Myotubes: Regulation of Myocyte Differentiation and Myokine Expression. CPB. *48*, 1829–1842.

Kong, X., Yao, T., Zhou, P., Kazak, L., Tenen, D., Lyubetskaya, A., Dawes, B.A., Tsai, L., Kahn, B.B., Spiegelman, B.M., et al. (2018). Brown Adipose Tissue Controls Skeletal Muscle Function via the Secretion of Myostatin. Cell Metab. *28*, 631-643.e3.

Nedergaard, J., and Cannon, B. (2013). UCP1 mRNA does not produce heat. Biochim. Biophys. Acta BBA - Mol. Cell Biol. Lipids. *1831*, 943–949.

Periasamy, M., Herrera, J.L., and Reis, F.C.G. (2017). Skeletal Muscle Thermogenesis and Its Role in Whole Body Energy Metabolism. Diabetes Metab. J. *41*, 327–336.

Rao, R.R., Long, J.Z., White, J.P., Svensson, K.J., Lou, J., Lokurkar, I., Jedrychowski, M.P., Ruas, J.L., Wrann, C.D., Lo, J.C., et al. (2014). Meteorin-like Is a Hormone that Regulates Immune-Adipose Interactions to Increase Beige Fat Thermogenesis. Cell. *157*, 1279–1291.

Roberts, L.D., Boström, P., O'Sullivan, J.F., Schinzel, R.T., Lewis, G.D., Dejam, A., Lee, Y.-K., Palma, M.J., Calhoun, S., Georgiadi, A., et al. (2014). β-Aminoisobutyric Acid Induces Browning of White Fat and Hepatic β-Oxidation and Is Inversely Correlated with Cardiometabolic Risk Factors. Cell Metab. *19*, 96–108.

Seale, P., Bjork, B., Yang, W., Kajimura, S., Chin, S., Kuang, S., Scimè, A., Devarakonda, S., Conroe, H.M., Erdjument-Bromage, H., et al. (2008). PRDM16 controls a brown fat/skeletal muscle switch. Nature. *454*, 961–967.

Sepa-Kishi, D.M., Sotoudeh-Nia, Y., Iqbal, A., Bikopoulos, G., and Ceddia, R.B. (2017). Cold acclimation causes fiber type-specific responses in glucose and fat metabolism in rat skeletal muscles. Sci. Rep. *7* (1), 15430.

Siengdee, P., Trakooljul, N., Murani, E., Schwerin, M., Wimmers, K., and Ponsuksili, S. (2015). MicroRNAs Regulate Cellular ATP Levels by Targeting Mitochondrial Energy Metabolism Genes during C2C12 Myoblast Differentiation. PLOS ONE. *10*, e0127850.

Stanford, K.I., Lynes, M.D., Takahashi, H., Baer, L.A., Arts, P.J., May, F.J., Lehnig, A.C., Middelbeek, R.J.W., Richard, J.J., So, K., et al. (2018). 12,13-diHOME: An Exercise-Induced Lipokine that Increases Skeletal Muscle Fatty Acid Uptake. Cell Metab. *27*, 1111-1120.e3.

Stier, A., Bize, P., Habold, C., Bouillaud, F., Massemin, S., and Criscuolo, F. (2014). Mitochondrial uncoupling prevents cold-induced oxidative stress: a case study using UCP1 knockout mice. J. Exp. Biol. *217*, 624–630.

Théry, C., Witwer, K.W., Aikawa, E., Alcaraz, M.J., Anderson, J.D., Andriantsitohaina, R., Antoniou, A., Arab, T., Archer, F., Atkin-Smith, G.K., et al. (2018). Minimal information for studies of extracellular vesicles 2018 (MISEV2018): a position statement of the International Society for Extracellular Vesicles and update of the MISEV2014 guidelines. Journal of Extracellular Vesicles. *7*, 1535750.

Thomou, T., Mori, M.A., Dreyfuss, J.M., Konishi, M., Sakaguchi, M., Wolfrum, C., Rao, T.N., Winnay, J.N., Garcia-Martin, R., Grinspoon, S.K., et al. (2017). Adipose-derived circulating miRNAs regulate gene expression in other tissues. Nature. *542*, 450–455.

Thrush, A.B., Antoun, G., Nikpay, M., Patten, D.A., DeVlugt, C., Mauger, J.-F., Beauchamp, B.L., Lau, P., Reshke, R., Doucet, É., et al. (2018). Diet-resistant obesity is characterized by a distinct plasma proteomic signature and impaired muscle fiber metabolism. Int. J. Obes. *42*, 353–362.

Villarroya, F., and Giralt, M. (2015). The Beneficial Effects of Brown Fat Transplantation: Further Evidence of an Endocrine Role of Brown Adipose Tissue. Endocrinology. *156*, 2368–2370.

Yin, H., Pasut, A., Soleimani, V.D., Bentzinger, C.F., Antoun, G., Thorn, S., Seale, P., Fernando, P., van Ijcken, W., Grosveld, F., et al. (2013). MicroRNA-133 controls brown adipose determination in skeletal muscle satellite cells by targeting Prdm16. Cell Metab. *17*, 210–224.

Yu, X.X., Lewin, D.A., Forrest, W., and Adams, S.H. (2002). Cold elicits the simultaneous induction of fatty acid synthesis and β-oxidation in murine brown adipose tissue: prediction from differential gene expression and confirmation in vivo. FASEB J. *16*, 155–168.

Zhang, J., Li, S., Li, L., Li, M., Guo, C., Yao, J., and Mi, S. (2015). Exosome and exosomal microRNA: trafficking, sorting, and function. Genomics Proteomics Bioinformatics. *13*, 17–24.

Zhang, Q., Higginbotham, J.N., Jeppesen, D.K., Yang, Y.-P., Li, W., McKinley, E.T., Graves-Deal, R., Ping, J., Britain, C.M., Dorsett, K.A., et al. (2019). Transfer of Functional Cargo in Exomeres. Cell Rep. *27*, 940-954.e6.

**4.8 FIGURES**

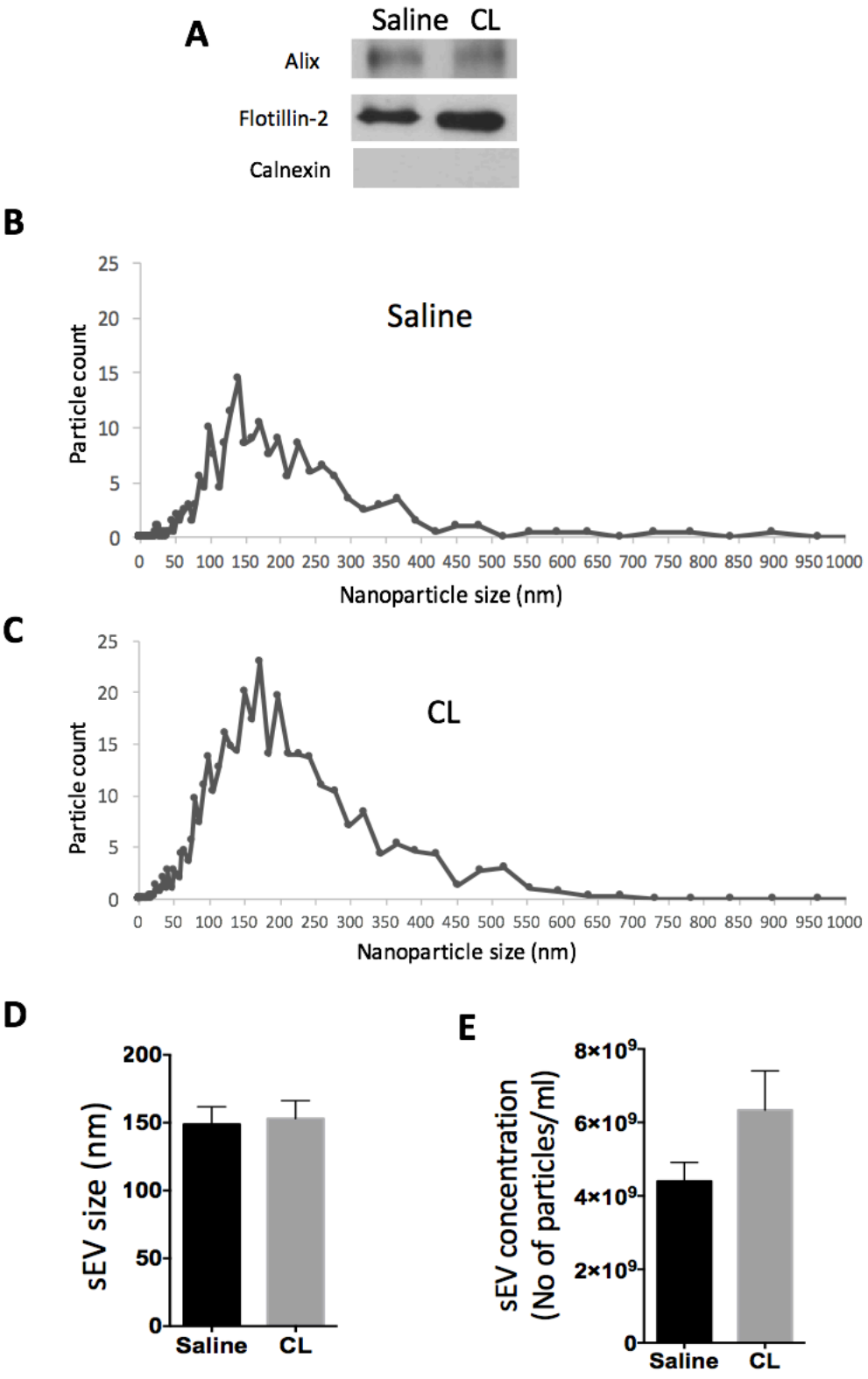
A
Saline
CL
Alix
Flotillin-2
Calnexin
B
Saline
Particle count
Nanoparticle size (nm)
C
CL
Particle count
Nanoparticle size (nm)
D
sEV size (nm)
Saline
CL
E
sEV concentration (No of particles/ml)
Saline
CL

**Figure 4.1: Characterization of plasma sEV from mice injected with saline or CL316,243.**

A) Western blots of the positive sEV markers (alix and flotillin-2) and negative sEV marker, calnexin. Representative particle size distribution graphs of sEV collected from plasma of B) saline-injected mice and C) CL316,243-injected from three different experiments. D) The median size and E) concentration of sEV collected from plasma of mice injected with saline or CL316,243. N=3/group. Data are represented as mean ± SEM. Student's t-test.

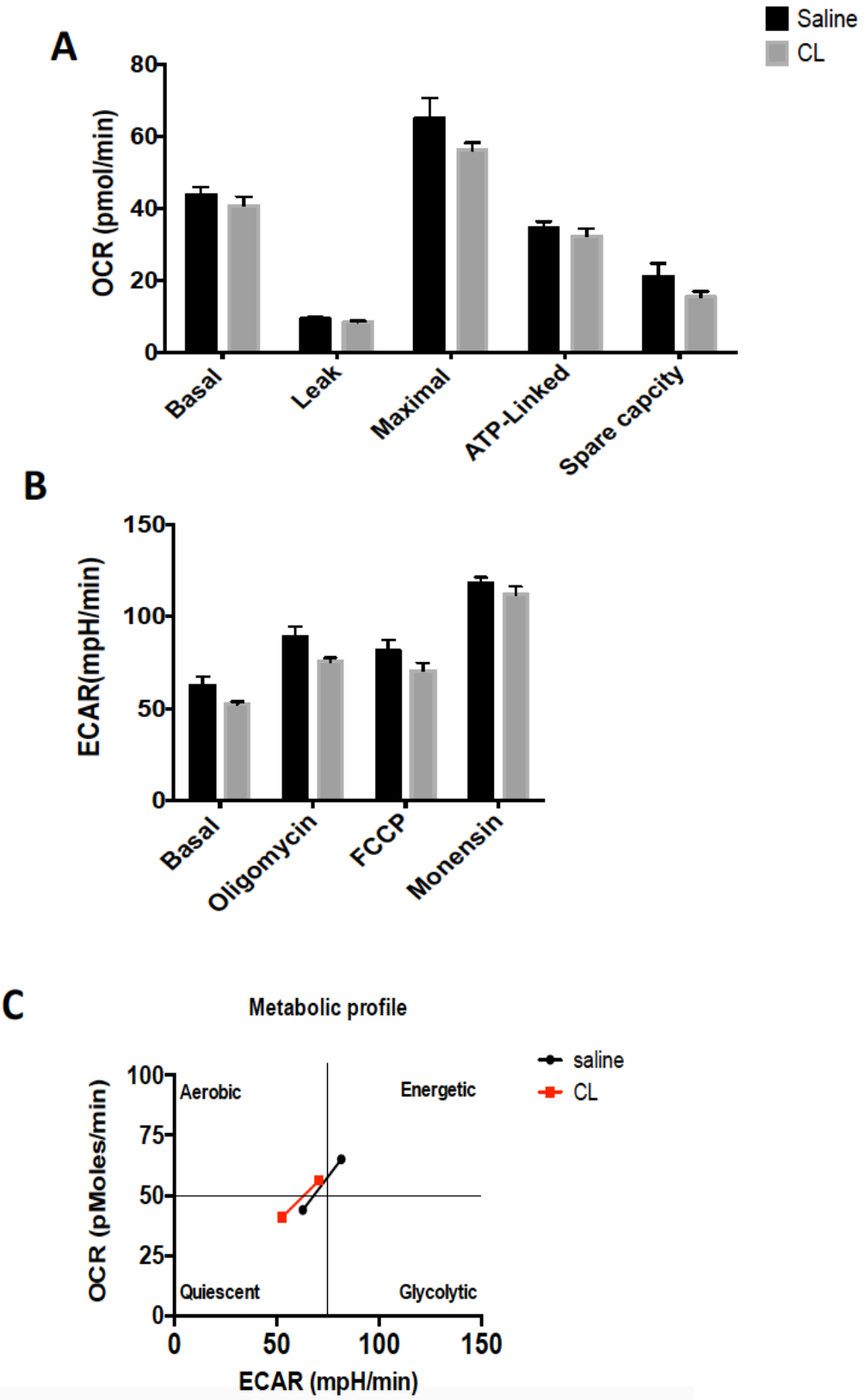
A
Saline
CL
OCR (pmol/min)
80
60
40
20
0
Basal
Leak
Maximal
ATP-Linked
Spare capcity
B
ECAR(mpH/min)
150
100
50
0
Basal
Oligomycin
FCCP
Monensin
C
Metabolic profile
saline
CL
OCR (pMoles/min)
100
75
50
25
0
Aerobic
Energetic
Quiescent
Glycolytic
0
50
100
150
ECAR (mpH/min)

**Figure 4.2: Plasma sEV from mice injected with CL316,243 do not impact bioenergetics of C2C12 myoblasts.** A) Oxygen consumption rate (OCR) and B) extracellular acidification rate (ECAR) were measured in C2C12 myoblasts that were treated with sEV collected from plasma of mice injected with saline or CL316,243. C) Metabolic profile; values used were those from OCR and ECAR at basal and FCCP-induced maximal respiration conditions. N=3/group. Data are represented as mean ± SEM. Student's t-test**.**

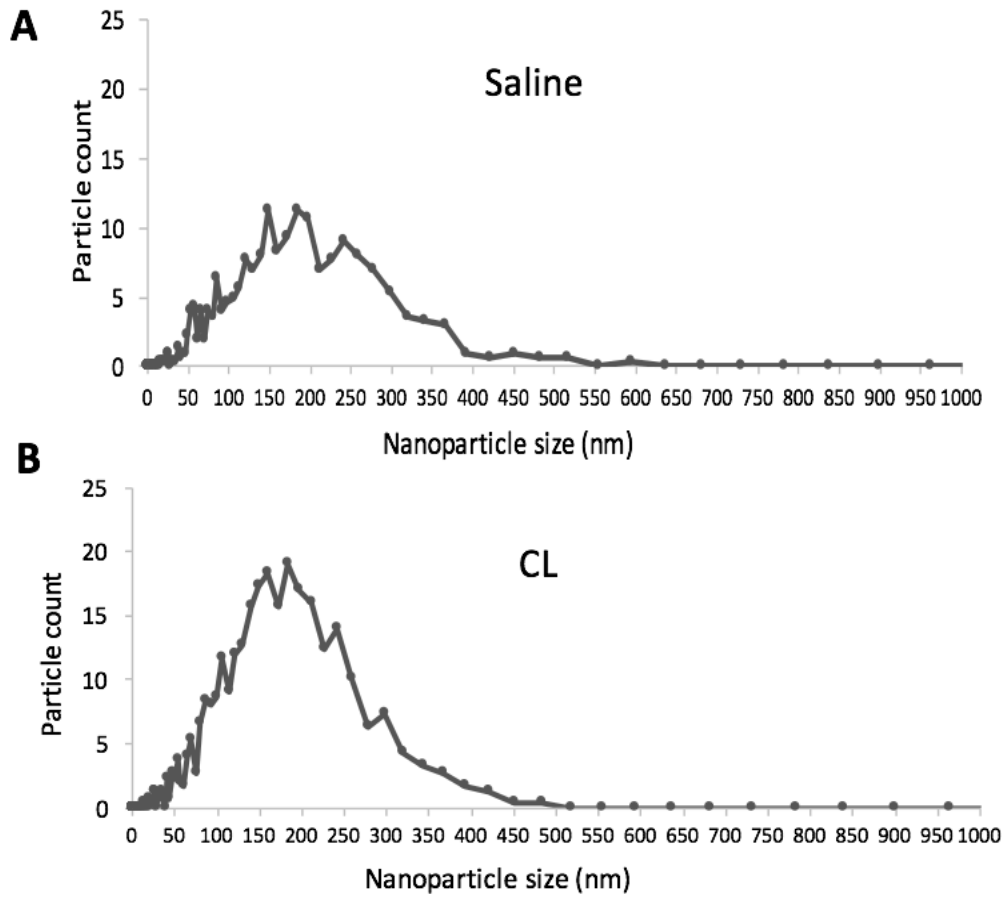
A
Saline
Particle count
Nanoparticle size (nm)
B
CL
Particle count
Nanoparticle size (nm)

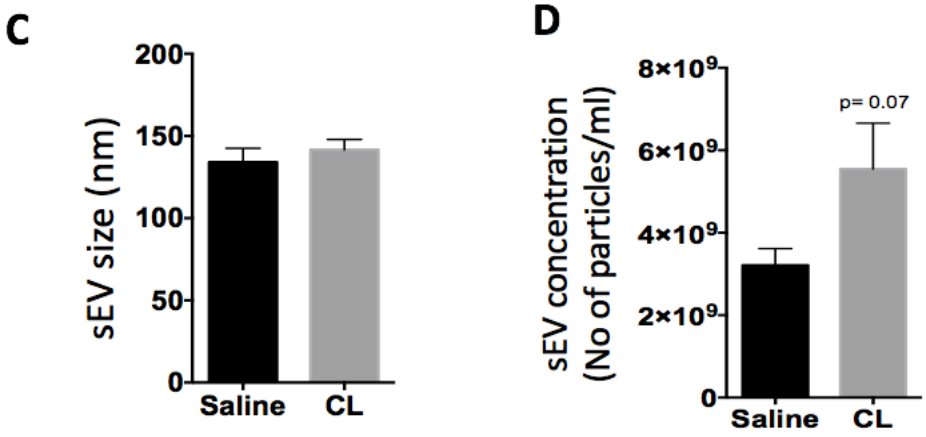
C
sEV size (nm)
Saline
CL
D
sEV concentration (No of particles/ml)
p= 0.07
Saline
CL

**Figure 4.3: Characterization of sEV collected from conditioned media of BAT explants treated with either saline or CL316,243.** Representative particle size distribution graphs of sEV collected from conditioned media of A) saline-treated BAT and B) CL316,243-treated BAT, from three different experiments. C) The median size and D) concentration of sEV collected from conditioned media of BAT treated with either saline or CL316,243. N=9/group. Data are represented as mean ± SEM. Student's t-test.

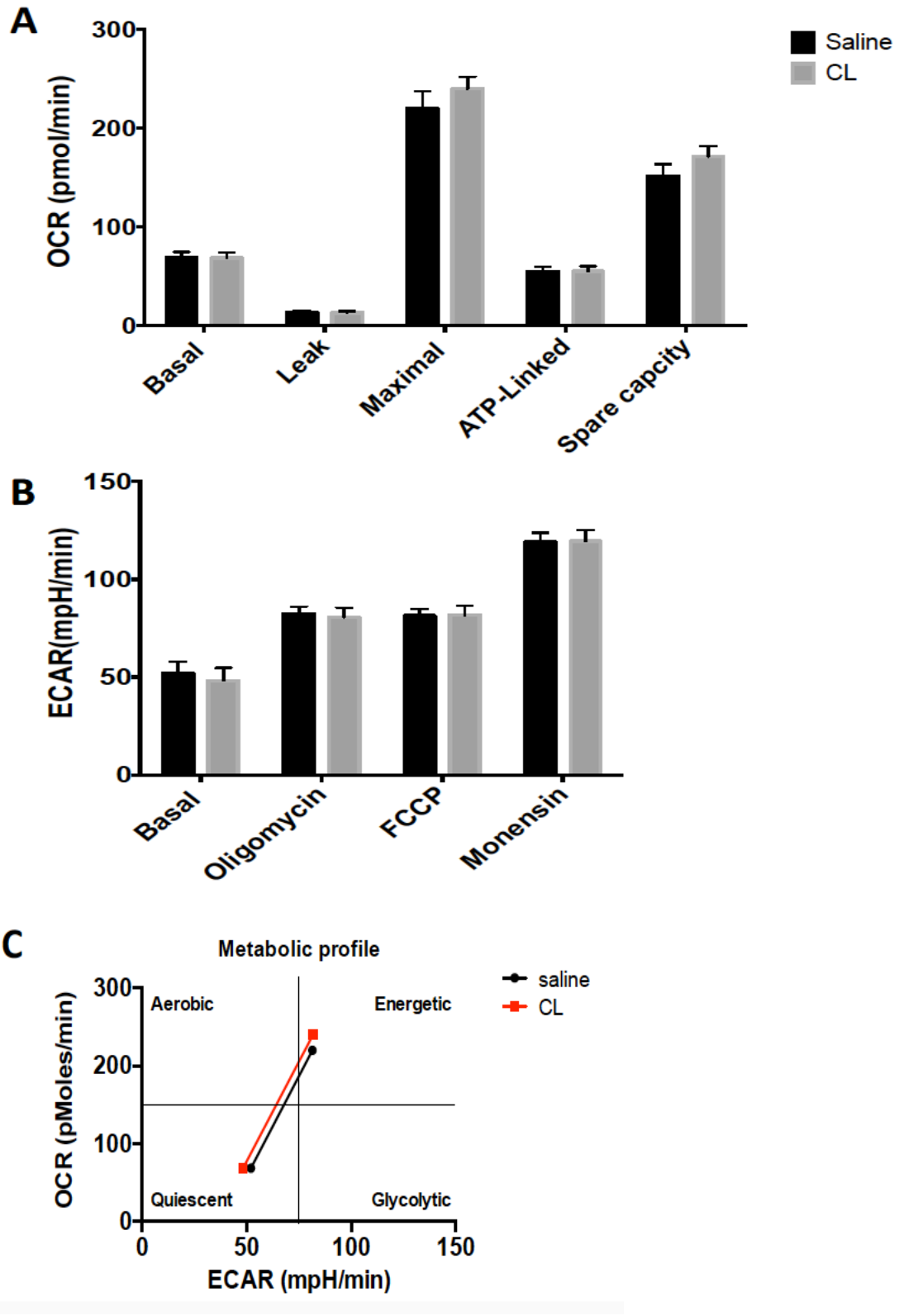
A
300
200
100
0
OCR (pmol/min)
Saline
CL
Basal
Leak
Maximal
ATP-Linked
Spare capcity
B
150
100
50
0
ECAR(mpH/min)
Basal
Oligomycin
FCCP
Monensin
C
Metabolic profile
300
200
100
0
OCR (pMoles/min)
Aerobic
Energetic
Quiescent
Glycolytic
saline
CL
0
50
100
150
ECAR (mpH/min)

**Figure 4.4: sEV released from BAT explants treated with CL316,243 do not impact the bioenergetics of C2C12 myoblasts.** A) Oxygen consumption rate (OCR) and B) extracellular acidification rate (ECAR) were measured in C2C12 myoblasts that were treated with sEV collected from conditioned media of saline-treated and CL316,243-treated BAT. C) Metabolic profile; values used were those from OCR and ECAR at basal and FCCP-induced maximal respiration conditions. N=9/group. Data are represented as mean ± SEM. Student's t-test.

## CHAPTER 5: GENERAL DISCUSSION

Over the past decades, BAT has gained great attention due to its therapeutic potential of being targeted to combat metabolic diseases, such as obesity. When it is activated, BAT oxidizes tremendous amounts of lipids and glucose to match its metabolic demands. Initially, BAT was thought to only be present in human infants and small rodents. Later on, BAT was confirmed to be present in adult humans (Cypess et al., 2009; Hany et al., 2002; van Marken Lichtenbelt et al., 2009). These facts about BAT have propelled researchers to conduct studies on different experimental models, including hibernating and non-hibernating species, to broaden our understanding of the regulation and physiological functions of BAT. These comparative physiological studies of BAT have clarified the differences between these experimental models in adapting to environmental conditions, which turn on/off BAT function. In addition to its thermogenic function, BAT releases regulatory molecules, such as batokines and sEV, which have recently become a focus of BAT research. In the same vein, this Ph.D. thesis will further extend our understanding of the regulation and function of BAT from different experimental models and physiological aspects.

The goal of Chapter 2 was to investigate the regulation of BAT thermogenesis by the master mitochondrial deacetylase, SIRT3, in mice. BAT thermogenesis is mainly under the control of the sympathetic nervous system, which releases NE to bind its receptors on brown adipocytes. The latter induces signaling cascades that eventually lead to the release of FFAs from lipid droplets to activate UCP1 (Cannon and Nedergaard, 2004; Nicholls, 2006). When UCP1 is activated, it uncouples the activity of the ETC system from the synthesis of ATP to produce heat. In addition to the above decribed mechanisms, BAT thermogenesis is controlled at the post-

translation level. Recent studies have shown that BAT thermogenesis can be controlled by the sulfenylation of UCP1 cysteine residues, and the succinylation of UCP1 and other mitochondrial proteins (Chouchani et al., 2016; Wang et al., 2019). Along these lines, we examined the possibility that mitochondrial protein deacetylation mediated by SIRT3 controls BAT thermogenesis. This notion is based on two observations in the literature, which suggested a role for SIRT3 in BAT thermogenesis. First, Shi *et al*. showed that cold exposure increases the transcript level of SIRT3 in BAT of mice (Shi et al., 2005). Second, Hirschey *et al.* demonstrated that fasted mice lacking SIRT3 are cold-intolerant when exposed to acute cold (Hirschey et al., 2010). However, it was not known by which mechanism SIRT3 controls BAT thermogenesis. In our study described in Chapter 2, we elucidated that SIRT3 indirectly controls BAT thermogenesis by deacetylating and promoting the function of mitochondrial proteins involved in acylcarnitine metabolism, FAO and the ETC pathway, which are upstream of UCP1.

In detail, after 2 days of cold exposure, we demonstrate that *Sirt3*KO mice have normal phenotypes, and exhibit no differences in the weights of the whole-body, eWAT and iBAT, compared to WT mice. Our observations are consistent with a study reporting that *Sirt3*KO mice had normal body weight (Lombard et al., 2007). While *Sirt3*KO mice have a generally normal phenotype, BAT of *Sirt3*KO mice exhibits defects in its morphology and activation. It is well known that BAT activation requires the utilization of FFAs derived from lipid droplets in BAT or WAT (Cannon and Nedergaard, 2004; Schreiber et al., 2017; Shin et al., 2017). Our results revealed that *Sirt3*KO mice do not show a significant decrease in BAT lipid content after cold exposure as seen in WT mice. Consistently, *Sirt3*KO mice do not show a significant decrease in RER after CL316,243 injection, as observed in WT mice. These results are indicative of less activated BAT in

*Sirt3*KO mice. Given the important role of BAT in thermoregulation, we examined the ability of *Sirt3KO* mice to maintain their body temperature after 2 days of cold exposure when BAT thermogenesis is the main thermoregulatory mechanism (Golozoubova et al., 2001; Nedergaard and Cannon, 2013; Stier et al., 2014). Our findings show that *Sirt3*KO mice have impaired thermoregulation following 2 days of cold exposure. However, since the absence of SIRT3 is at the whole-body level, we should acknowledge the fact that thermoregulatory defects seen in *Sirt3*KO mice might be also due to aggregated responses from different tissues known to play important roles in thermogenesis such as brain, muscle, and heart. Thus, we next performed *in vitro* experiments to confirm whether the absence of SIRT3 has an effect on the thermogenic respiration of BAT mitochondria.

Because UCP1 is the mediator of thermogenesis in BAT, we studied UCP1-dependent respiration in BAT mitochondria from *Sirt3*KO mice. We showed that UCP1-dependent respiration is significantly decreased in BAT mitochondria from *Sirt3*KO mice. Importantly, a defect in UCP1-dependent respiration is independent of the level of UCP1. Our results show that BAT of *Sirt3*KO mice has levels of UCP1 that are similar to those in WT mice, which is consistent with previous findings showing that the absence of SIRT3 does not affect the level of UCP1 (Lombard et al., 2007). Moreover, the level of UCP1 after cold exposure is significantly increased in BAT of both WT and *Sirt3*KO mice. Thus, we speculated that the decrease in UCP1-dependent respiration may be due to defects in the activity of UCP1 and/or its upstream proteins. Our speculation was based on previous published studies conducted in the liver and skeletal muscle of *Sirt3*KO mice, which demonstrated the negative effects of the absence of SIRT3 on the activity of some mitochondrial proteins (Hirschey et al., 2010; Jing et al., 2013).

Therefore, we performed label-free quantitative acetylome profiling on isolated mitochondria from WT and *Sirt3*KO mice kept in warm or cold conditions. Our acetylome profiling results confirm that SIRT3 is a major acetylation regulator in BAT mitochondria, and deacetylases an extensive number of mitochondrial proteins. Consistently, our acetylation blots show a major increase in mitochondrial protein acetylation in the absence of SIRT3. Interestingly, our acetylation blots illustrate that cold exposure itself can increase protein acetylation levels in BAT mitochondria, which could be related to the increased level of acetyl-CoA produced from FAO, which in turn can lead to non-enzymatic acetylation events (Pougovkina et al., 2014). Furthermore, our acetylome profiling indicates that UCP1 and its upstream proteins, involved in crucial pathways, are directly targeted by SIRT3.

We identified four lysine acetylation sites on UCP1 (K56, K67, K73 and K151), which is consistent with a previous study that showed three acetylation sites (K67, K73 and K151) on UCP1 in BAT homogenate from rats (Lundby et al., 2012). We found two direct SIRT3-regulated lysine sites on UCP1 (K56 and K151) and demonstrated that mutations of these sites in a HEK293T cellular model do not impact leak respiration following UCP1 activation with TTNPB, used previously as a UCP1 activator (Oelkrug et al., 2013; Tomás et al., 2004). These results suggest that the two lysine sites (K56 and K151) are not required for UCP1 activity. However, we cannot completely rule out the possibility of direct deacetylation control of UCP1 for several reasons. First, HEK293 cells have been previously used to study the activity of ectopically expressed UCP1 (Oelkrug et al., 2013), and our analyses were conducted in HEK293T cells, and it is possible that these cells do not possess all of the factors or mechanisms required for the control of UCP1. For instance, HEK293T cells are not physiologically capable to respond to cold stress as brown

adipocytes can do *in vivo*. Moreover, we only focused on the two acetylation sites regulated by SIRT3 (K56 and K151), while the other sites might play important roles for BAT thermogenesis. Furthermore, lysine deacetylation of UCP1 may share a redundant role with other PTMs, such as cysteine sulfenylation, or may function indirectly with the deacetylation of proteins upstream of UCP1 (to be discussed below).

As FAO is essential for BAT thermogenesis, we then examined the impact of the absence of SIRT3 on proteins involved in acylcarnitine metabolism and FAO. Defects in FAO lead to an accumulation of acylcarnitines in the circulation (Aguer et al., 2014; McCoin et al., 2015). Based on our acetylome profiling, we thought that there would be an increase in the level of acylcarnitines in the circulation of *Sirt3*KO mice after BAT activation. In contrast to this, our acylcarnitines analyses showed that circulatory levels of selected medium-chain and long-chain acylcarnitines were decreased in *Sirt3*KO mice. There are a few ways to interpret these unexpected findings. Potentially, the formation of acylcarnitines is decreased in BAT mitochondria due to a decrease in the uptake or entry of FA into the mitochondria of *Sirt3*KO BAT. Given our proteomics results, several enzymes involved in FAO and acylcarnitines metabolism are hyperacetylated in *Sirt3*KO BAT mitochondria and could have decreased functions. An example is carnitine acylcarnitine translocase (CACT), which is responsible for the entry and oxidation of acylcarnitines. Another possibility is that BAT activation achieved by CL316,243 injection might lead to secondary effects on acylcarnitine metabolism in other tissues, such as liver. As a result, it may contribute to distinct patterns of acylcarnitines in a genotype-specific manner. Future research should be conducted in order to obtain a better understanding of the role of SIRT3 in the metabolism of acylcarnitines in BAT.

While UCP1 is the main controller of BAT thermogenesis, ETC proteins are involved in the generation of proton motive force, which drives protons back to the mitochondrial matrix through UCP1. Therefore, we examined the effect of the absence of SIRT3 on the activity of ETC proteins, which has not been previously examined in intact BAT mitochondria. Importantly, we examined the activity of each of the complexes of the ETC pathway, independent of the activity of UCP1. For the first time, our functional analyses indicated that the activities of CI and CII in BAT mitochondria from cold exposed *Sirt3KO* mice were significantly decreased. These defects are associated with the hyperacetylation of lysine sites found on CI and CII subunits. Importantly, the absence of SIRT3 does not impact the level of these proteins. Our results are consistent with previously published work, which showed that the activities of CI and CII were decreased in isolated liver mitochondria from Sirt3KO mice (Ahn et al., 2008; Cimen et al., 2010). Moreover, a study conducted by Finley *et al.* showed a strong trend ($p=0.07$) for decreased enzymatic activity of CII in BAT mitochondria when BAT was not activated (Finley et al., 2011). Importantly, we demonstrated a significant defect in CII when BAT is maximally activated. Furthermore, while other studies identified lysine sites in subunit A of CII in liver mitochondria (Cimen et al., 2010; Finley et al., 2011), we found SIRT3-regulated lysine sites in both subunits A and B of CII in BAT mitochondria. This could suggest that SIRT3 deacetylases lysine sites on mitochondrial proteins in a tissue-specific manner.

Altogether, our findings in Chapter 2 illustrate that SIRT3 indirectly regulates BAT thermogenesis by targeting pathways upstream of UCP1. Our work does not lessen the requirement of UCP1 in BAT thermogenesis, but delineates the importance of SIRT3 in controlling substrate uptake/oxidation pathways upstream of UCP1, including FAO and ETC pathways. Also,

our mass spectrometry-based acetylome analysis provides an extensive resource for future investigations of fundamental metabolic pathways in BAT.

In Chapter 3, we investigated the effect of acute hypoxia on BAT thermogenesis in NMRs, and elucidated some of the adaptive mechanisms involved. As mentioned earlier, BAT is a highly metabolic tissue that requires high amounts of energy supplies and sufficient sympathetic control. For that reason, it is highly innervated and vascularized (Contreras et al., 2015; Lim et al., 2013). When BAT thermogenesis is induced, sympathetic signaling and oxygen consumption are increased. Several studies have shown the importance of sympathetic signaling in BAT thermogenesis, and that denervation of BAT leads to defective BAT thermogenesis and decreased whole-body energy expenditure (Dulloo and Miller, 1984; Fischer et al., 2018; Rothwell and Stock, 1984; Vaughan and Bartness, 2012). The effects of acute hypoxia on BAT thermogenesis are not well understood. However, it is known that hypoxia decreases body temperature in mammals (Ramirez et al., 2007; Steiner and Branco, 2002). Moreover, previous studies have demonstrated that hypoxia diminished shivering thermogenesis in cats and ground squirrels (Barros et al., 2001; Gautier et al., 1987), and that chronic hypoxia decreased whole-body oxygen consumption in mice after a treatment with NE (Beaudry and McClelland, 2010). Here, we studied the effect of acute hypoxia on BAT in the NMR, which is widely recognized as the most hypoxia-tolerant mammal (Buck and Pamenter, 2018; Chung et al., 2016; Park et al., 2017). It has been previously been shown that NMRs have functional BAT that can be induced by thermogenic stimuli (Daly et al., 1997; Hislop and Buffenstein, 1994; Woodley and Buffenstein, 2002). Upon acute hypoxia, NMRs have decreased oxygen consumption and body temperatures

that approximate ambient temperatures (Kirby et al., 2018). Thus, we hypothesized that acute hypoxia decreases BAT thermogenesis in NMRs.

For the first time, our findings elucidated that acute hypoxia diminishes BAT thermogenesis in NMRs supporting the survival of NMRs in extreme conditions. We demonstrated that hypoxia causes 1) decreased heat production in the interscapular area of NMRs, regardless of the extent to which BAT is activated, 2) decreased levels of selected thermogenic proteins, including UCP1, 3) decreased levels of UCP1 in some African mole rats, 4) increased protein ubiquitination levels in BAT of NMRs, and 5) abnormal ultrastructures of BAT mitochondria of NMRs. To our knowledge, our work is the first to investigate the direct effect of acute hypoxia on BAT thermogenesis in NMRs, and thereby contribute to an improved understanding of the adaptive mechanisms involved. Moreover our work investigated the molecular mechanisms involved in NMR adaptaion to acute hypoxia.

As previously mentioned, UCP1 is the main regulator of BAT thermogenesis and accounts for ~10% of BAT mitochondrial proteins (Busiello et al., 2015). Our findings show that following just one hour of hypoxia there are significantly decreased levels of UCP1 protein. Previous work showed that chronic hypoxia decreased the transcript and protein levels of UCP1 in BAT of mice (Beaudry and McClelland, 2010). Given the crucial involvement of the ETC system in BAT thermogenesis, we also examined the level of OXPHOS proteins in BAT of normoxic and hypoxic NMRs. We found that the levels of selected OXPHOS proteins including CII, CIII, CIV are significantly decreased after one hour of hypoxia. Beyond the rapid degradation of various BAT mitochondrial proteins, we also examined the effect of hypoxia on BAT of different African mole rat species. It is clear that African mole rats have distinct patterns of protein degradation where

some species had significant decreases or trends for decreases in the levels of UCP1 in response to acute hypoxia. However, the levels of OXPHOS proteins in hypoxic African mole rats were not changed, except for CIII, and CIV, which were increased in CHH. Others have shown that the turnover rates of OXPHOS proteins are highly variable in different mouse tissues and vary depending on the treatments that cause changes in the metabolic status of mitochondria (Karunadharma et al., 2015). Thus, our findings are consistent with the notion that the degradation of UCP1 and OXPHOS proteins occurs in a tissue-, and animal- dependent manner.

It is not clear how these thermogenic proteins in BAT of hypoxic NMRs are rapidly degraded. Two well-known mechanisms involved in mitochondrial protein degradation are the ubiquitination proteasome system (UPS) and the mitophagy system (Harper et al., 2018; Lavie et al., 2018; Pickles et al., 2018). Both mechanisms facilitate the turnover of proteins by ubiquitinating proteins that are targeted for degradation. We found that the total level of protein ubiquitination in BAT from hypoxic NMRs is significantly increased compared to BAT from normoxic NMRs, consistent with the idea of the induction of protein degradation mechanisms during hypoxia. However, future investigations are needed to assess the role of UPS or mitophagy mechanisms in BAT of hypoxic NMRs. Our results are consistent with previous studies demonstrating how NMRs have very high rates of proteolysis and autophagy compared to mice (Rodriguez et al., 2012, 2014; Zhao et al., 2014). As the levels of thermogenic proteins are important for BAT thermogenesis, the integrity and ultrastructure of BAT mitochondria are also fundmental (Wikstrom et al., 2014). As described above, mitochondria are composed of two membranes, the outer and inner membranes. The inner membrane has a larger membrane surface area, and is extensively folded to form cristae, where thermogenic proteins are located

(Cooper, 2000). Ultrastructure analysis of BAT mitochondria demonstrated that hypoxia caused mitochondrial abnormalities, such as degradation of mitochondrial outer membrane and decreased cristae density. Our ultrastructure findings are consistent with our western blotting results, which demonstated that hypoxia leads to decreases in the level of thermogenic proteins.

In summary, our observations in Chapter 3 show that BAT of NMR responds to acute hypoxia by decreasing its thermogenic function, which is achieved, at least in part, by decreasing the level of UCP1 and selected thermogenic proteins and by altering the morphology of BAT mitochondria. More research focusing on the understanding of the adaptive mechanisms evolved in hypoxic NMR will allow us to have a broader understanding about the physiology of this tissue in these species.

The research conducted in Chapter 4 was carried out to expand our understanding of the secretory role of BAT, and to examine the effects of BAT-derived sEV on SkM cell bioenergetics. While BAT is the major site of NST thermogenesis, BAT is recognized as an endocrine organ releasing regulatory molecules called batokines, which can control the function of other tissues (Pfeifer, 2015; Villarroya and Giralt, 2015). Recently, it has been shown that BAT can release sEV, and that its activation leads to an increase in the release of sEV (Chen et al., 2016; Thomou et al., 2017). However, the regulatory roles of sEV released from activated BAT are not well investigated. In general, sEV are released by most cell types and promote a means for tissue cross-talk. sEV can target the fuction of the recipient cells through their content (cargo) (Gurunathan et al., 2019). During cold exposure, BAT and SkM are responsible for NST and shivering thermogenesis, respectively, and if one of the tissue has defects in the production of heat, the other tissue compensates for the heat production defects in the other (Bal et al., 2017;

Golozoubova et al. 2001), sugessting a cross-talk mechanism induced between the two tissues. We questioned whether sEV released from activated BAT regulate bioenergetics of SkM myoblasts. Our findings demonstrate that BAT can release sEV and its acute activation does not significantly effect the size and concentration of released sEV. In contrast to what we speculated, our bioenergetics results demonstrate that BAT-derived sEV do not affect the cellular bioenergetics of C2C12 myoblasts following a 24h treatment. However, we cannot completely rule out a role for activated BAT-derived sEV in regulating the cellular bioenergetics of muscle cells for various reasons. The metabolic effects of sEV on C2C12 myoblasts might be pronounced with shorter or longer treatments. For instance, sEV may modulate the function of recipient cells through receptor activation or protein delivery to mediate short effects or through miRNA delivery to mediate longer effects. Also, previous published work of Chen *et al*. demonstrated that chronic activation of BAT causes distinct patterns of miRNAs packaged in sEV (Chen et al., 2016). Other research groups illustrated that some of these miRNAs regulate mitochondrial energy metabolism in C2C12 during differentiation by targeting genes encoding subunits of CI and CIV of the ETC system (Siengdee et al., 2015). Therefore, further investigation needs to be conducted to examine the effects of activated BAT-derived sEV on C2C12 myoblasts during or after differentiation into myotubes. Also, it is possible that these sEV might target cellular pathways that were not examined in our study (*e.g*., when cells are oxidizing fatty acids).

Of note, the maximal respiration of C2C12 myoblasts treated with plasma sEV is lesser than those treated with sEV from conditioned medium, suggesting distinct sEV released in plasma *vs* conditioned medium. Possibly, plasma sEV may contain inhibitory molecules that decrease the maximal respiration of C2C12 myoblasts. Notably, plasma used for sEV extraction was collected

from mice kept at thermoneutrality for 2 days and it was recently reported that mice kept at thermoneutrality for 7 days have elevated serum levels of myostatin, known as a muscle function inhibitor (Kong et al., 2018). Another study showed that myostatin can be released in sEV (Kim et al., 2018). Therefore, we speculate that plasma sEV might contain inhibitory molecules such as myostatin and/or miRNAs, which may decrease the maximal respiration of C2C12 myoblasts.

Altogether, our results show that sEV from acutely activated BAT *in vivo* and *in vitro* do not affect the bioenergetics of C2C12 myoblasts maintained under normal cell culture conditions. However, it would be of interest to examine the effects of these sEV on C2C12 myoblasts maintained under different metabolic conditions or under time-frames of treatments.

Overall, my Ph.D. research has expanded our understanding of the biology of BAT in different experimental models. We demonstrate that BAT thermogenesis is negatively regulated by mitochondrial acetylation resulting from the absence of SIRT3, and by acute hypoxia. Furthermore, we investigated the effects of BAT-derived sEV on the bioenergetics of SkM myoblasts to provide a basis for future investigations. Further studies are needed to advance our understanding of the physiology of BAT, which is required for designing therapeutic strategies targeting this tissue.

## 5.1 REFERENCES


Aguer, C., McCoin, C.S., Knotts, T.A., Thrush, A.B., Ono-Moore, K., McPherson, R., Dent, R., Hwang, D.H., Adams, S.H., and Harper, M.-E. (2014). Acylcarnitines: potential implications for skeletal muscle insulin resistance. The FASEB Journal. *29*, 336–345.

Ahn, B.-H., Kim, H.-S., Song, S., Lee, I.H., Liu, J., Vassilopoulos, A., Deng, C.-X., and Finkel, T. (2008). A role for the mitochondrial deacetylase Sirt3 in regulating energy homeostasis. Proc Natl Acad Sci U S A. *105*, 14447–14452.

Bal, N.C., Singh, S., Reis, F.C.G., Maurya, S.K., Pani, S., Rowland, L.A., and Periasamy, M. (2017). Both brown adipose tissue and skeletal muscle thermogenesis processes are activated during mild to severe cold adaptation in mice. J. Biol. Chem. *292*, 16616–16625.

Barros, R.C., Zimmer, M.E., Branco, L.G., and Milsom, W.K. (2001). Hypoxic metabolic response of the golden-mantled ground squirrel. J. Appl. Physiol. *91*, 603–612.

Beaudry, J.L., and McClelland, G.B. (2010). Thermogenesis in CD-1 mice after combined chronic hypoxia and cold acclimation. Comp. Biochem. Physiol. B, Biochem. Mol. Biol. *157*, 301–309.

Buck, L.T., and Pamenter, M.E. (2018). The hypoxia-tolerant vertebrate brain: Arresting synaptic activity. Comp. Biochem. Physiol. B, Biochem. Mol. Biol. *224*, 61–70.

Busiello, R.A., Savarese, S., and Lombardi, A. (2015). Mitochondrial uncoupling proteins and energy metabolism. Front. Physiol. *6*.

Cannon, B., and Nedergaard, J. (2004). Brown Adipose Tissue: Function and Physiological Significance. Physiological Reviews. *84*, 277–359.

Chen, Y., Buyel, J.J., Hanssen, M.J.W., Siegel, F., Pan, R., Naumann, J., Schell, M., van der Lans, A., Schlein, C., Froehlich, H., et al. (2016). Exosomal microRNA miR-92a concentration in serum reflects human brown fat activity. Nat Commun *7*, 11420.

Chouchani, E.T., Kazak, L., Jedrychowski, M.P., Lu, G.Z., Erickson, B.K., Szpyt, J., Pierce, K.A., Laznik-Bogoslavski, D., Vetrivelan, R., Clish, C.B., et al. (2016). Mitochondrial ROS regulate thermogenic energy expenditure and sulfenylation of UCP1. Nature. *532*, 112–116.

Chung, D., Dzal, Y.A., Seow, A., Milsom, W.K., and Pamenter, M.E. (2016). Naked mole rats exhibit metabolic but not ventilatory plasticity following chronic sustained hypoxia. Proceedings of the Royal Society B: Biological Sciences. *283*, 20160216.

Cimen, H., Han, M.-J., Yang, Y., Tong, Q., Koc, H., and Koc, E.C. (2010). Regulation of Succinate Dehydrogenase Activity by SIRT3 in Mammalian Mitochondria. Biochemistry. *49*, 304–311.

Cypess, A.M., Lehman, S., Williams, G., Tal, I., Rodman, D., Goldfine, A.B., Kuo, F.C., Palmer, E.L., Tseng, Y.-H., Doria, A., et al. (2009). Identification and importance of brown adipose tissue in adult humans. N. Engl. J. Med. *360*, 1509–1517.

Contreras, C., Gonzalez, F., Fernø, J., Diéguez, C., Rahmouni, K., Nogueiras, R., and López, M. (2015). The brain and brown fat. Ann. Med. *47*, 150–168.

Cooper, G.M. (2000). Mitochondria. The Cell: A Molecular Approach. 2nd Edition.

Daly, T.J., Williams, L.A., and Buffenstein, R. (1997). Catecholaminergic innervation of interscapular brown adipose tissue in the naked mole-rat (Heterocephalus glaber). J. Anat. *190 ( Pt 3)*, 321–326.

Dulloo, A.G., and Miller, D.S. (1984). Energy balance following sympathetic denervation of brown adipose tissue. Can. J. Physiol. Pharmacol. *62*, 235–240.

Finley, L.W.S., Haas, W., Desquiret-Dumas, V., Wallace, D.C., Procaccio, V., Gygi, S.P., and Haigis, M.C. (2011). Succinate Dehydrogenase Is a Direct Target of Sirtuin 3 Deacetylase Activity. PLoS One *6*.

Fischer, A.W., Schlein, C., Cannon, B., Heeren, J., and Nedergaard, J. (2018). Intact innervation is essential for diet-induced recruitment of brown adipose tissue. American Journal of Physiology-Endocrinology and Metabolism. *316*, E487–E503.

Gautier, H., Bonora, M., Schultz, S.A., and Remmers, J.E. (1987). Hypoxia-induced changes in shivering and body temperature. J. Appl. Physiol. *62*, 2477–2484.

Golozoubova, V., Hohtola, E., Matthias, A., Jacobsson, A., Cannon, B., and Nedergaard, J. (2001). Only UCP1 can mediate adaptive nonshivering thermogenesis in the cold. The FASEB Journal. *15*, 2048–2050.

Gurunathan, S., Kang, M.-H., Jeyaraj, M., Qasim, M., and Kim, J.-H. (2019). Review of the Isolation, Characterization, Biological Function, and Multifarious Therapeutic Approaches of Exosomes. Cells. *8*(4), 307.

Hany, T.F., Gharehpapagh, E., Kamel, E.M., Buck, A., Himms-Hagen, J., and von Schulthess, G.K. (2002). Brown adipose tissue: a factor to consider in symmetrical tracer uptake in the neck and upper chest region. Eur. J. Nucl. Med. Mol. Imaging. *29*, 1393–1398.

Harper, J.W., Ordureau, A., and Heo, J.-M. (2018). Building and decoding ubiquitin chains for mitophagy. Nature Reviews Molecular Cell Biology. *19*, 93–108.

Hirschey, M.D., Shimazu, T., Goetzman, E., Jing, E., Schwer, B., Lombard, D.B., Grueter, C.A., Harris, C., Biddinger, S., Ilkayeva, O.R., et al. (2010). SIRT3 regulates fatty acid oxidation via reversible enzyme deacetylation. Nature. *464*, 121–125.

Hislop, M.S., and Buffenstein, R. (1994). Noradrenaline induces nonshivering thermogenesis in both the naked mole-rat (Heterocephalus glaber) and the Damara mole-rat (Cryptomys damarensis) despite very different modes of thermoregulation. Journal of Thermal Biology. *19*, 25–32.

Jing, E., O'Neill, B.T., Rardin, M.J., Kleinridders, A., Ilkeyeva, O.R., Ussar, S., Bain, J.R., Lee, K.Y., Verdin, E.M., Newgard, C.B., et al. (2013). Sirt3 Regulates Metabolic Flexibility of Skeletal Muscle Through Reversible Enzymatic Deacetylation. Diabetes. *62*, 3404–3417.

Karunadharma, P.P., Basisty, N., Chiao, Y.A., Dai, D.-F., Drake, R., Levy, N., Koh, W.J., Emond, M.J., Kruse, S., Marcinek, D., et al. (2015). Respiratory chain protein turnover rates in mice are highly heterogeneous but strikingly conserved across tissues, ages, and treatments. FASEB J. *29*, 3582–3592.

Kim, S., Lee, M.-J., Choi, J.-Y., Park, D.-H., Kwak, H.-B., Moon, S., Koh, J.-W., Shin, H.-K., Ryu, J.-K., Park, C.-S., et al. (2018). Roles of Exosome-Like Vesicles Released from Inflammatory C2C12 Myotubes: Regulation of Myocyte Differentiation and Myokine Expression. CPB. *48*, 1829–1842.

Kirby, A.M., Fairman, G.D., and Pamenter, M.E. (2018). Atypical behavioural, metabolic and thermoregulatory responses to hypoxia in the naked mole rat (Heterocephalus glaber). Journal of Zoology. *305*, 106–115.

Kong, X., Yao, T., Zhou, P., Kazak, L., Tenen, D., Lyubetskaya, A., Dawes, B.A., Tsai, L., Kahn, B.B., Spiegelman, B.M., et al. (2018). Brown Adipose Tissue Controls Skeletal Muscle Function via the Secretion of Myostatin. Cell Metab. *28*, 631-643.e3.

Lavie, J., De Belvalet, H., Sonon, S., Ion, A.M., Dumon, E., Melser, S., Lacombe, D., Dupuy, J.-W., Lalou, C., and Bénard, G. (2018). Ubiquitin-Dependent Degradation of Mitochondrial Proteins Regulates Energy Metabolism. Cell Reports. *23*, 2852–2863.

Lim, S., Honek, J., and Cao, Y. (2013). Blood Vessels in White and Brown Adipose Tissues. In Angiogenesis in Adipose Tissue, Y. Cao, ed. (New York, NY: Springer New York), pp. 77–102.

Lombard, D.B., Alt, F.W., Cheng, H.-L., Bunkenborg, J., Streeper, R.S., Mostoslavsky, R., Kim, J., Yancopoulos, G., Valenzuela, D., Murphy, A., et al. (2007). Mammalian Sir2 homolog SIRT3 regulates global mitochondrial lysine acetylation. Mol. Cell. Biol. *27*, 8807–8814.

Lundby, A., Lage, K., Weinert, B.T., Bekker-Jensen, D.B., Secher, A., Skovgaard, T., Kelstrup, C.D., Dmytriyev, A., Choudhary, C., Lundby, C., et al. (2012). Proteomic Analysis of Lysine Acetylation Sites in Rat Tissues Reveals Organ Specificity and Subcellular Patterns. Cell Rep. *2*, 419–431.

McCoin, C.S., Knotts, T.A., and Adams, S.H. (2015). Acylcarnitines—old actors auditioning for new roles in metabolic physiology. Nat Rev Endocrinol. *11*, 617–625.

Nedergaard, J., and Cannon, B. (2013). UCP1 mRNA does not produce heat. Biochimica et Biophysica Acta (BBA) - Molecular and Cell Biology of Lipids. *1831*, 943–949.

Nicholls, D.G. (2006). The physiological regulation of uncoupling proteins. Biochimica et Biophysica Acta (BBA) - Bioenergetics. *1757*, 459–466.

Oelkrug, R., Goetze, N., Exner, C., Lee, Y., Ganjam, G.K., Kutschke, M., Müller, S., Stöhr, S., Tschöp, M.H., Crichton, P.G., et al. (2013). Brown fat in a protoendothermic mammal fuels eutherian evolution. Nature Communications. *4*, 2140.

Park, T.J., Reznick, J., Peterson, B.L., Blass, G., Omerbašić, D., Bennett, N.C., Kuich, P.H.J.L., Zasada, C., Browe, B.M., Hamann, W., et al. (2017). Fructose-driven glycolysis supports anoxia resistance in the naked mole-rat. Science. *356*, 307–311.

Pfeifer, A. (2015). NRG4: an endocrine link between brown adipose tissue and liver. Cell Metab. *21*, 13–14.

Pickles, S., Vigié, P., and Youle, R.J. (2018). Mitophagy and Quality Control Mechanisms in Mitochondrial Maintenance. Current Biology. *28*, R170–R185.

Pougovkina, O., te Brinke, H., Ofman, R., Cruchten, V., G, A., Kulik, W., Wanders, R.J.A., Houten, S.M., Boer, D., and C.j, V. (2014). Mitochondrial protein acetylation is driven by acetyl-CoA from fatty acid oxidation. Hum Mol Genet. *23*, 3513–3522.

Ramirez, J.-M., Folkow, L.P., and Blix, A.S. (2007). Hypoxia tolerance in mammals and birds: from the wilderness to the clinic. Annu. Rev. Physiol. *69*, 113–143.

Rodriguez, K.A., Edrey, Y.H., Osmulski, P., Gaczynska, M., and Buffenstein, R. (2012). Altered Composition of Liver Proteasome Assemblies Contributes to Enhanced Proteasome Activity in the Exceptionally Long-Lived Naked Mole-Rat. PLOS ONE. *7*, e35890.

Rodriguez, K.A., Osmulski, P.A., Pierce, A., Weintraub, S.T., Gaczynska, M., and Buffenstein, R. (2014). A cytosolic protein factor from the naked mole-rat activates proteasomes of other species and protects these from inhibition. Biochim. Biophys. Acta. *1842*, 2060–2072.

Rothwell, N.J., and Stock, M.J. (1984). Effects of denervating brown adipose tissue on the responses to cold, hyperphagia and noradrenaline treatment in the rat. The Journal of Physiology. *355*, 457–463.

Schreiber, R., Diwoky, C., Schoiswohl, G., Feiler, U., Wongsiriroj, N., Abdellatif, M., Kolb, D., Hoeks, J., Kershaw, E.E., Sedej, S., et al. (2017). Cold-Induced Thermogenesis Depends on ATGL-Mediated Lipolysis in Cardiac Muscle, but Not Brown Adipose Tissue. Cell Metab. *26*, 753-763.e7.

Shi, T., Wang, F., Stieren, E., and Tong, Q. (2005). SIRT3, a Mitochondrial Sirtuin Deacetylase, Regulates Mitochondrial Function and Thermogenesis in Brown Adipocytes. J. Biol. Chem. *280*, 13560–13567.

Shin, H., Ma, Y., Chanturiya, T., Cao, Q., Wang, Y., Kadegowda, A.K.G., Jackson, R., Rumore, D., Xue, B., Shi, H., et al. (2017). Lipolysis in Brown Adipocytes Is Not Essential for Cold-Induced Thermogenesis in Mice. Cell Metab. *26*, 764-777.e5.

Siengdee, P., Trakooljul, N., Murani, E., Schwerin, M., Wimmers, K., and Ponsuksili, S. (2015). MicroRNAs Regulate Cellular ATP Levels by Targeting Mitochondrial Energy Metabolism Genes during C2C12 Myoblast Differentiation. PLOS ONE. *10*, e0127850.

Steiner, A.A., and Branco, L.G.S. (2002). Hypoxia-induced anapyrexia: implications and putative mediators. Annu. Rev. Physiol. *64*, 263–288.

Stier, A., Bize, P., Habold, C., Bouillaud, F., Massemin, S., and Criscuolo, F. (2014). Mitochondrial uncoupling prevents cold-induced oxidative stress: a case study using UCP1 knockout mice. Journal of Experimental Biology. *217*, 624–630.

Thomou, T., Mori, M.A., Dreyfuss, J.M., Konishi, M., Sakaguchi, M., Wolfrum, C., Rao, T.N., Winnay, J.N., Garcia-Martin, R., Grinspoon, S.K., et al. (2017). Adipose-derived circulating miRNAs regulate gene expression in other tissues. Nature. *542*, 450–455.

Tomás, P., Jiménez-Jiménez, J., Zaragoza, P., Vuligonda, V., Chandraratna, R.A., and Rial, E. (2004). Activation by retinoids of the uncoupling protein UCP1. Biochim Biophys Acta. *1658*, 157–164.

van Marken Lichtenbelt, W.D., Vanhommerig, J.W., Smulders, N.M., Drossaerts, J.M.A.F.L., Kemerink, G.J., Bouvy, N.D., Schrauwen, P., and Teule, G.J.J. (2009). Cold-Activated Brown Adipose Tissue in Healthy Men. N Engl J Med. 360,1500-1508

Vaughan, C.H., and Bartness, T.J. (2012). Anterograde transneuronal viral tract tracing reveals central sensory circuits from brown fat and sensory denervation alters its thermogenic responses. Am. J. Physiol. Regul. Integr. Comp. Physiol. *302*, R1049-1058.

Villarroya, F., and Giralt, M. (2015). The Beneficial Effects of Brown Fat Transplantation: Further Evidence of an Endocrine Role of Brown Adipose Tissue. Endocrinology. *156*, 2368–2370.

Wang, G., Meyer, J.G., Cai, W., Softic, S., Li, M.E., Verdin, E., Newgard, C., Schilling, B., and Kahn, C.R. (2019). Regulation of UCP1 and Mitochondrial Metabolism in Brown Adipose Tissue by Reversible Succinylation. Molecular Cell. *74*, 844-857.e7.

Wikstrom, J.D., Mahdaviani, K., Liesa, M., Sereda, S.B., Si, Y., Las, G., Twig, G., Petrovic, N., Zingaretti, C., Graham, A., et al. (2014). Hormone-induced mitochondrial fission is utilized by brown adipocytes as an amplification pathway for energy expenditure. EMBO J. *33*, 418–436.

Woodley, R., and Buffenstein, R. (2002). Thermogenic changes with chronic cold exposure in the naked mole-rat (Heterocephalus glaber). Comparative Biochemistry and Physiology - Part A: Molecular & Integrative Physiology. *133*, 827–834.

Zhao, S., Lin, L., Kan, G., Xu, C., Tang, Q., Yu, C., Sun, W., Cai, L., Xu, C., and Cui, S. (2014). High autophagy in the naked mole rat may play a significant role in maintaining good health. Cell. Physiol. Biochem. *33*, 321–332.

## CHAPTER 6: APPENDIX

## 6.1 SUPPLEMENTARY FIGURES FOR CHAPTER 2

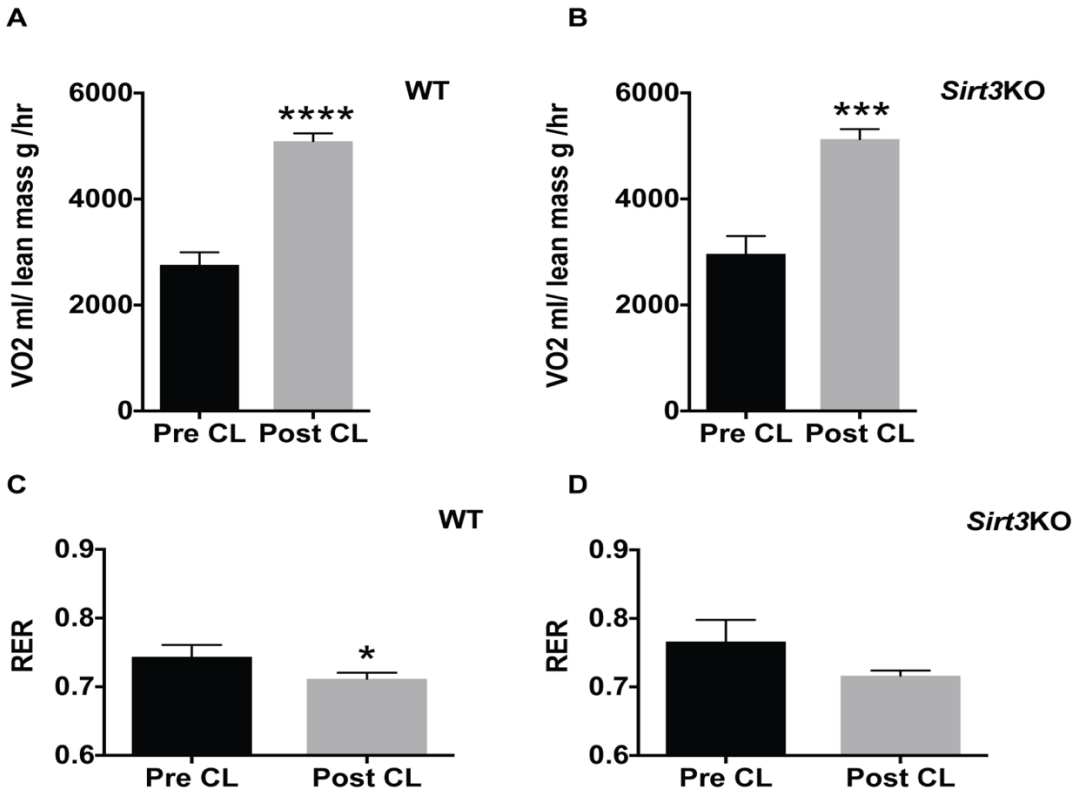

**Supplementary Figure 1 related to Figure 2.1**

$VO_2$ was assessed in (A) WT mice and (B) *Sirt3*KO mice that were kept at 28 °C and were injected with CL316,243 (1mg/kg; *i.p.*). $VO_2$ values were assessed before and after CL316, 243 injection. N=6/group. RER values associated with the selected $VO_2$ values were assessed in (C) WT mice and (D) *Sirt3*KO mice. N=6/group. Data are represented as mean ± SEM. Student's t-test; Two-tailed, **p<0.05, ***p<0.001, ****p<0.0001*.

A

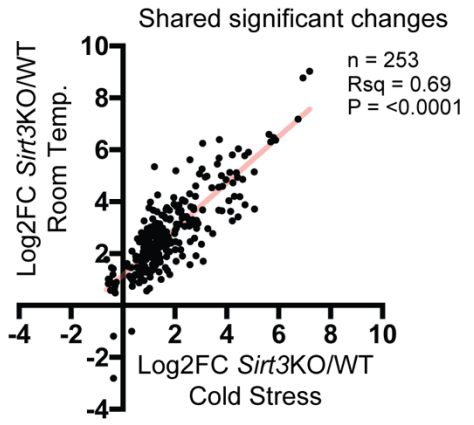
Shared significant changes
n = 253
Rsq = 0.69
P = <0.0001
Log2FC Sirt3KO/WT Room Temp.
Log2FC Sirt3KO/WT Cold Stress
10
8
6
4
2
-2
-4
-4
-2
2
4
6
8
10

B

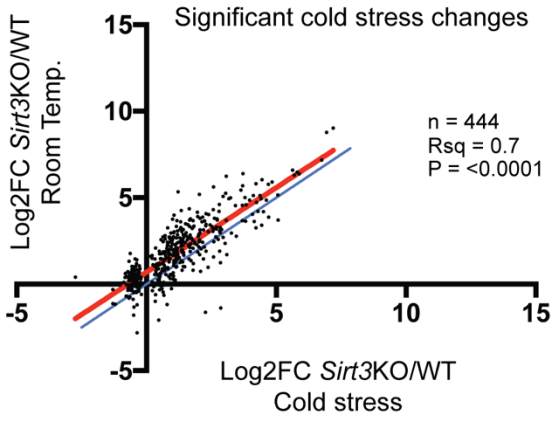
Significant cold stress changes
n = 444
Rsq = 0.7
P = <0.0001
Log2FC Sirt3KO/WT Room Temp.
Log2FC Sirt3KO/WT Cold stress
15
10
5
-5
-5
5
10
15

C

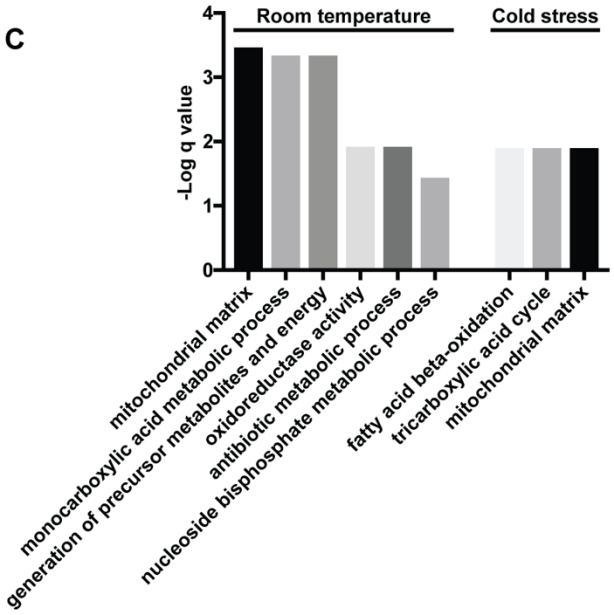
Room temperature
Cold stress
-Log q value
4
3
2
1
0
mitochondrial matrix
monocarboxylic acid metabolic process
generation of precursor metabolites and energy
oxidoreductase activity
antibiotic metabolic process
nucleoside bisphosphate metabolic process
fatty acid beta-oxidation
tricarboxylic acid cycle
mitochondrial matrix

**Supplementary Figure 2 related to Figure 2.3**

A) Measured Log2FC *Sirt3*KO/WT was plotted for acetylated lysines detected via MS for room temperature versus cold treated mice. Log2FC computed using MSStats as described in the experimental procedures. Linear regression calculated using GraphPad Prism. This analysis includes only measured changes that were deemed to be statistically significant (adjusted p value < 0.05) in both room temperature and cold stressed conditions. This graphs contains a subset of the data plotted in Figure 3B.

B) Plotted are significantly-regulated sites detected in samples from cold stressed animals, regardless of fold-change versus corresponding fold-change detected in room temperature animals, regardless of significance. Red line indicates the best fit line of linear regression. The blue line represents slope = 1. The majority of datapoints above blue line suggests more dramatic changes in room temperature housed animals. This analysis is complementary to that descried in Figure 3E and contains a subset of the data plotted in Figure 3B.

C) GO-term enrichment of SIRT3-regulated lysine acetylations sites calculated using Metascape for room temperature and cold regulated sites (log2 *Sirt3*KO/WT >1; adjusted *p*> 0.05). Included as regulated sites were those detected in 6 biological replicates of *Sirt3*KO and not detected in any WT samples, for which no p value could be calculated. q values shown represent p values of GO-term analyses following adjustment for multiple-testing.

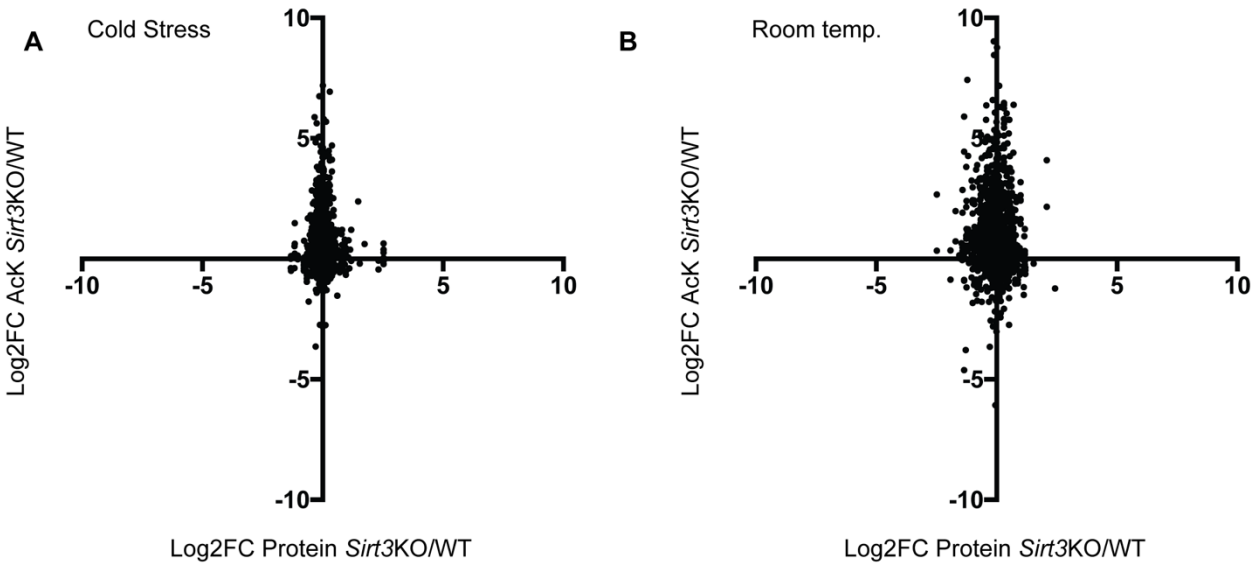


**Supplementary Figure 3 related to Figure 2.3**

Comparison of Log2FC (*Sirt3*KO/WT) for acetylated peptides versus estimated protein abundance Log2FC (*Sirt3 KO*/WT) for mice housed under cold stress (A) or room-temperature (B) conditions. Protein abundance is based on intensities of non-acetylated peptides bound to beads used in anti-acetyllysine immunoprecipitations.

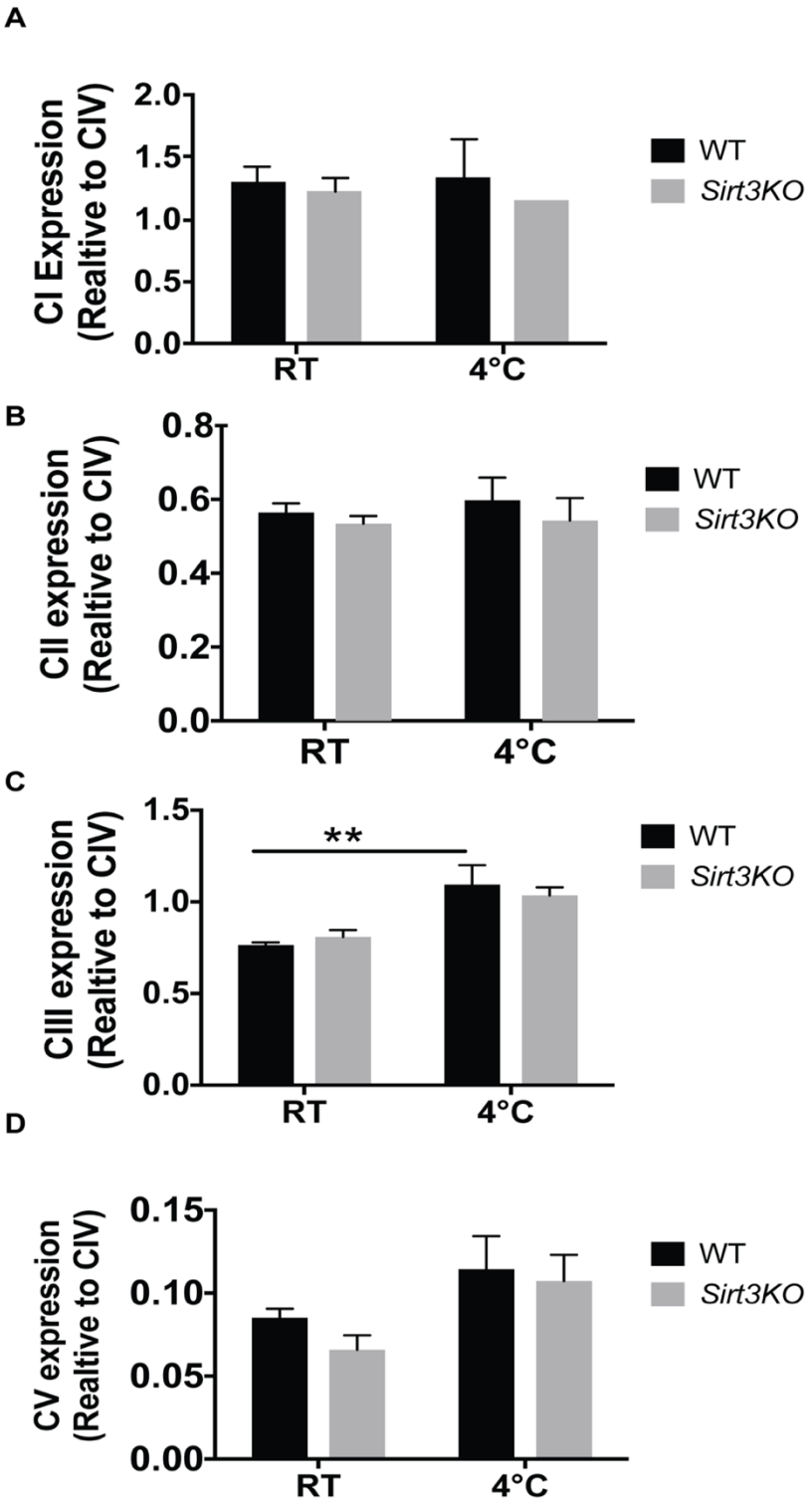
A
CI Expression (Realtive to CIV)
2.0
1.5
1.0
0.5
0.0
RT
4°C
WT
Sirt3KO
B
CII expression (Realtive to CIV)
0.8
0.6
0.4
0.2
0.0
RT
4°C
WT
Sirt3KO
C
CIII expression (Realtive to CIV)
1.5
1.0
0.5
0.0
**
RT
4°C
WT
Sirt3KO
D
CV expression (Realtive to CIV)
0.15
0.10
0.05
0.00
RT
4°C
WT
Sirt3KO

**Supplementary Figure 4 related to Figure 2.6**

Quantification of western blotting analysis of OXPHOS protein expression in isolated mitochondria from BAT of room temperature housed or cold exposed WT and *Sirt3*KO mice. N=3/group. A) Quantification results of CI expression, B) Quantification results of CII expression, C) Quantification results of CIII expression, and D) Quantification results of CV expression. Data are represented as mean ± SEM. Two-way ANOVA with Sidak's test was used, ***p<0.01.*

## 6.2 SUPPLEMENTARY TABLES FOR CHAPTER 2

Since the size and content of the supplementary tables for Chapter 2 are very huge, we would like to ask the examiners please to look at the online-avaliable supllementary tables found in the paper entitled: SIRT3 controls brown fat thermogenesis by deacetylation regulation of pathways upstream of UCP1.

Here is also the online link that takes you to the all supplementary tables.

Please use this link:

https://www.ncbi.nlm.nih.gov/pmc/articles/PMC6601363/

## 6.3 SUPPLEMENTARY FIGURES FOR CHAPTER 3

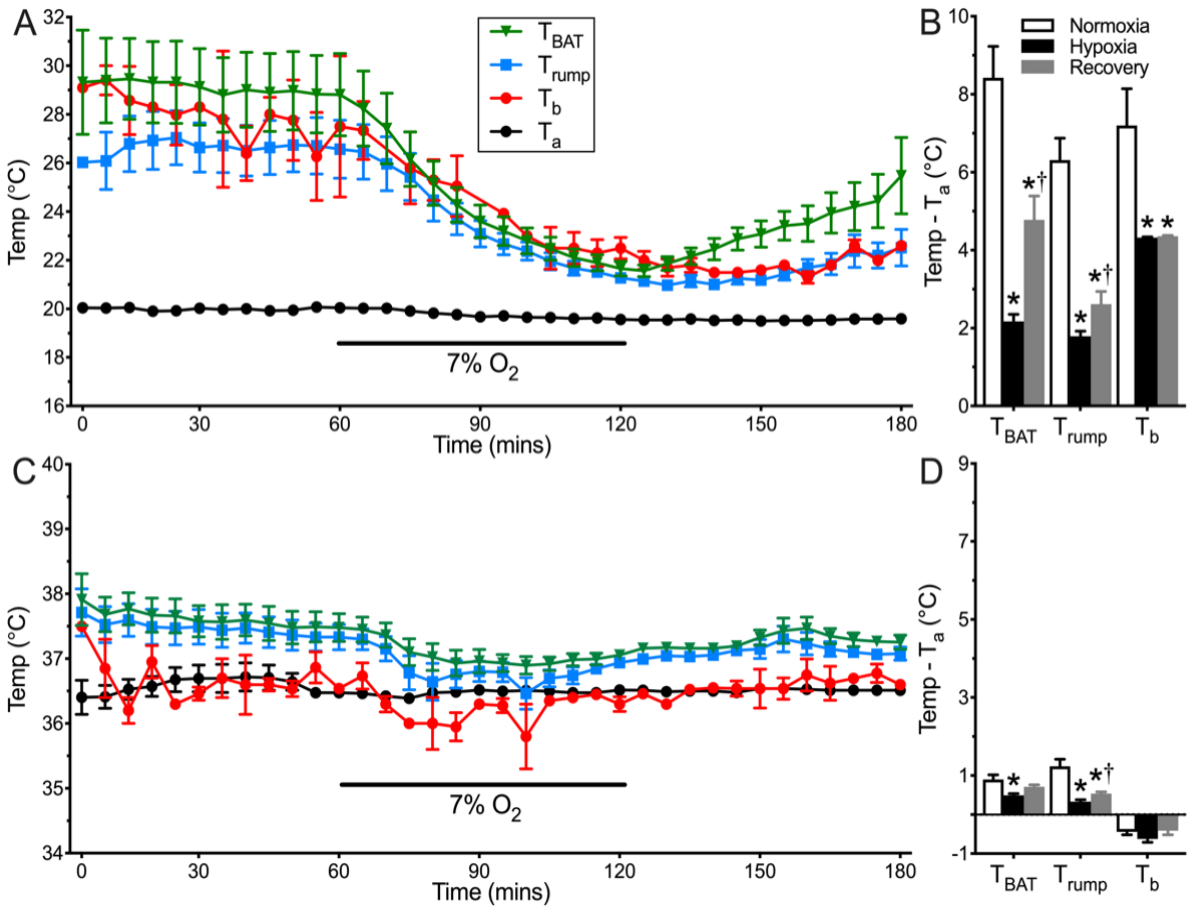

**Supplementary Figure 1 related to Figure 3.1**

Naked mole-rat actively thermoregulate in cold but not hot temperatures**.** (A&C) Summaries of ambient temperature ($T_a$, black circles), core body temperature ($T_b$, red circles), interscapular brown adipose tissue temperature ($T_{BAT}$, green triangles), and dorsal skin surface temperature ($T_{rump}$, blue squares) from naked mole-rats exposed to a normoxia → hypoxia → recovery protocol in 20ºC (A: *n* = 6), or 36ºC (C: *n* = 10). (B&D) Summaries of temperature difference between physiological temperatures and $T_a$ at 20ºC (B), or 36ºC (D). Data are mean ± SEM (repeated measures ANOVA with Turkey *post-test*). Asterisks indicate significant difference from normoxic controls. Daggers indicate significant difference from hypoxia.

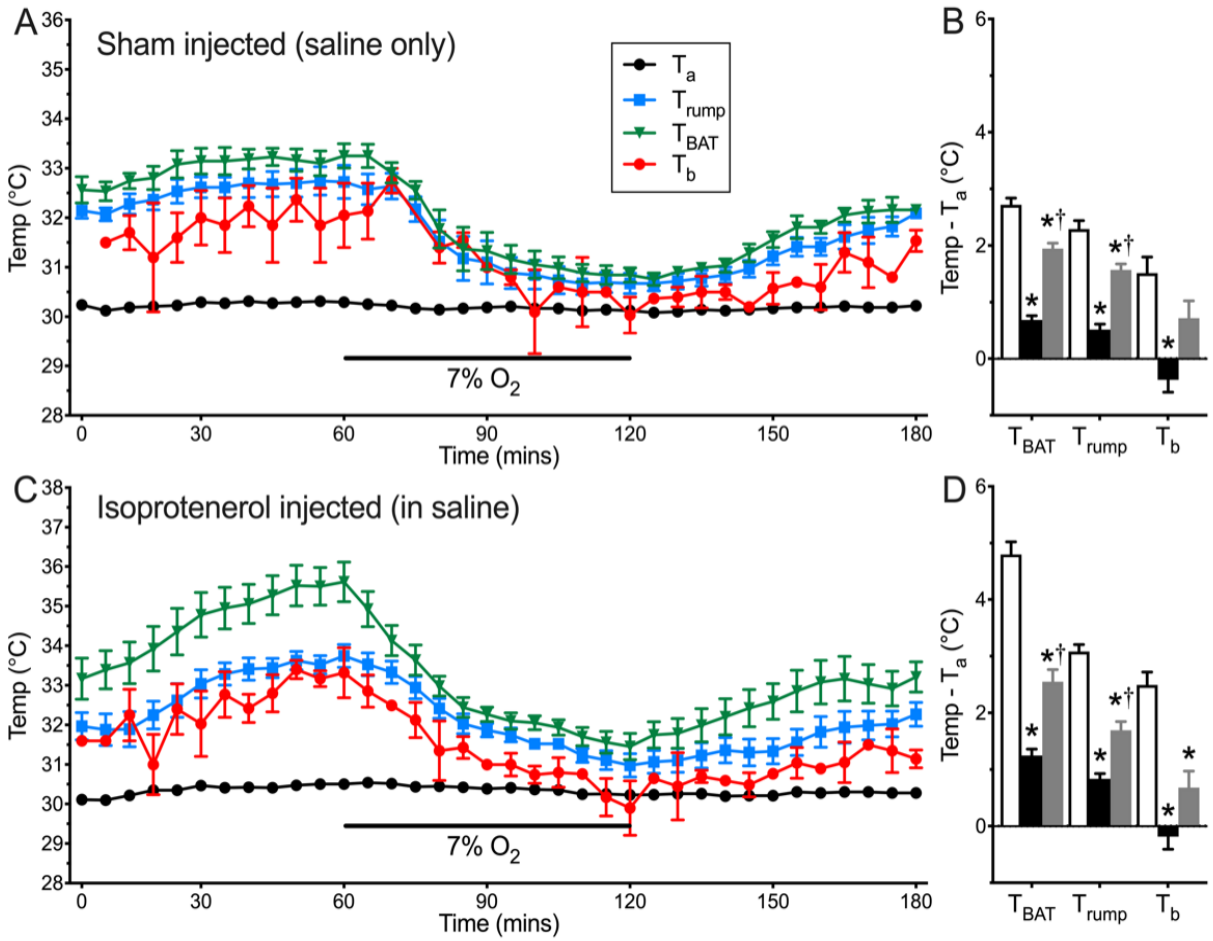
A
Sham injected (saline only)
Ta
Trump
TBAT
Tb
Temp (°C)
7% O2
Time (mins)
B
Temp - Ta (°C)
TBAT
Trump
Tb
C
Isoprotenerol injected (in saline)
Temp (°C)
7% O2
Time (mins)
D
Temp - Ta (°C)
TBAT
Trump
Tb

**Supplementary Figure 2 related to Figure 3.1**

Adrenergic stimulation enhances non-shivering thermogenesis in normoxia. (A&C) Summaries of ambient temperature ($T_a$, black circles), core body temperature ($T_b$, red circles), interscapular brown adipose tissue temperature ($T_{BAT}$, green triangles), and dorsal skin surface temperature ($T_{rump}$, blue squares) from naked mole-rats exposed to a normoxia → hypoxia → recovery protocol in 30ºC following injection of saline (A: *n* = 10), or isoproterenol (C: *n* = 10). (B&D) Summaries of temperature difference between physiological temperatures and $T_a$ for the same animals as in A&C. Data are mean ± SEM (repeated measures ANOVA with Turkey *post-test*). Asterisks indicate significant difference from normoxic controls. Daggers indicate significant difference from hypoxia.

## 6.4 PERMISSIONS AND COPYRIGHTS

**From Elsevier publishing group's website:**

https://www.elsevier.com/about/policies/copyright/permissions

Can I use material from my Elsevier journal article within my thesis/dissertation?

As an Elsevier journal author, you have the right to Include the article in a thesis or dissertation (provided that this is not to be published commercially) whether in full or in part, subject to proper acknowledgment; see the copyright page for more information. No written permission from Elsevier is necessary.

**From Elsevier publishing group's website:**

https://www.elsevier.com/about/our-business/policies/copyright

"**Authors sign an exclusive license agreement, where authors have copyright but license exclusive rights in their article to the publisher**. In this case authors have the right to:**

- Share their article in the same ways permitted to third parties under the relevant user license (together with **Personal Use** rights) so long as it contains a CrossMark logo, the end user license, and a DOI link to the version of record on ScienceDirect.
- **Personal Use**: Authors can use their articles, in full or in part, for a wide range of scholarly, non-commercial purposes as outlined below:
  - Use by an author in the author's classroom teaching (including distribution of copies, paper or electronic)
  - Distribution of copies (including through e-mail) to known research colleagues for their personal use (but not for Commercial Use)
  - **Inclusion in a thesis or dissertation (provided that this is not to be published commercially)**
  - Use in a subsequent compilation of the author's works
  - Extending the Article to book-length form
  - Preparation of other derivative works (but not for Commercial Use)
  - Otherwise using or re-using portions or excerpts in other works"
- Retain patent, trademark and other intellectual property rights (including research data).
- Proper attribution and credit for the published work.

## 6.5 CURRICULUM VITAE

Name: Rajaa Sebaa
Title: International Ph.D. candidate
PhD supervisor: Mary-Ellen Harper
Program: Biochemistry
Communication language: English- Arabic

**Education:**

| | | |
|---|---|---|
| **2009:** | BS | Biochemistry, University of King Abdulaziz, Jeddah, SA |
| **2011:** | MSc | Biochemistry, University of King Abdulaziz, Jeddah, SA |
| **2013- present:** | Ph.D | Biochemistry, University of Ottawa, Ottawa, CA |

**Job position:**

**2011-To date:** Biochemistry lecturer, Department of Medical Laboratories, College of Applied Medical Sciences, University of Shaqra, Duwadimi, SA

**Teaching experience:**

**2011-2012:** Teaching Biochemistry course. (1st year undergraduate students).
University of Shaqra

**Scholarship:**
Ph.D scholarship from the University of Shaqra, Duwadimi, Saudi Arabia.

**Research interests:**

- Expanding our understanding of the biology of brown adipose tissues in mammals.
- Investigating mechanisms that control the activity of brown adipose tissues.
- Understanding the physiological responses of brown adipose tissues to metabolic stressors.
- Studying the regulatory role of BAT derived sEV in skeletal muscle cell bioenergetics.

**Conferences, scientific meetings and symposiums attended:**

- Canadian Nutrition Society 2016 Annual Conference, May 5-7,2016, Ottawa- Gatineau, CA. (Presented a poster).
- Canadian Society of Molecular Biosciences 60th Annual conference, May 16-20, 2017, Ottawa, Ontario, CA. (Presented a poster).
- Translation and Therapeutic Perspectives of Brown Adipose Conference, May 2-4, 2017, Copenhagen, Denmark. (Presented a poster).
- Keystone Bioenergetics and Metabolic Disease Conference, January 21-25, 2018, Keystone Resort, Keystone, Colorado. (Presented a poster).
- Biochemistry, Microbiology and Immunology Scientific Symposium, May 17-18, 2018, Montebello, Quebec, CA. (Presented a Poster)
- Ottawa Institute for System Biology 2019 Scientific Symposium, May 6-7, 2019, Cornwall, Ontario, CA. (Presented a short talk).

**Manuscript published or submitted**

- Rajaa Sebaa, Jeff Johnson, Chantal Pileggi, Michaela Norgren, Jian Xuan, Yuka Sai, Qiang Tong, Izabella Krystkowiak, Emma Bondy-Chorney, Norman E. Davey, Nevan Krogan, Michael Downey* and Mary-Ellen Harper*. (2019). SIRT3 controls brown fat thermogenesis by deacetylation regulation of pathways upstream of UCP1. *Molecular Metabolism.* 25, 35–49.

- Matthew E Pamenter* †, Rajaa Sebaa †, Nikita Malholtra, Alexia Kirby, Hang Cheng, Nigel C Bennett, Barry van Jaarvsveld, Daniel W Hart, Glenn J Tattersall and Mary-Ellen Harper* .(2019). Submitted to the journal of *Nature Communications* for publication (NCOMMS-19-28577977-T) on December 2nd, 2019.

- Rajaa Sebaa, Ziyad El Hankouri, Jian Xuan, Derrick Gibbings and Mary-Ellen Harper* (2019). Submitted to the journal of *Applied Physiology, Nutrition, and Metabolism* for publication (APNM-2019-0965) on December 16th, 2019.